TEMPORARILY REACTIVE POLYELECTROLYTES TO IMPROVE LONG TERM CELL ENCAPSULATION

By CASANDRA MEGAN GARDNER, B.Sc.

A Thesis Submitted to the School of Graduate Studies in Partial Fulfillment of the Requirements for the Degree Doctor of Philosophy of Science

McMaster University

DOCTOR OF PHILOSOPHY OF SCIENCE (2012) McMaster University

(Chemistry and Chemical Biology) Hamilton, Ontario

TITLE: Temporarily Reactive Polyelectrolytes to Improve Long Term Cell Encapsulation

AUTHOR: Casandra Megan Gardner, B.Sc. (McMaster University)

SUPERVISOR: Professor Harald D.H. Stöver

NUMBER OF PAGES: xx, 147

Abstract

Coated calcium-alginate beads are the basis of many encapsulation methods used in pursuit of cell-based enzyme and hormone replacement therapies. The standard alginate - poly-L-lysine - alginate (APA) capsules consist of a calcium-alginate hydrogel core containing cells designed to express a therapeutic product, coated with permeability controlling poly-L-lysine (PLL, a polycation) followed by an exterior layer of polyanionic alginate. Although this approach is promising, the required long-term survival of the implanted cells has remained largely elusive as the current APA capsules suffer from several biocompatibility and mechanical strength issues, one of which is the weakening of ionic crosslinks over time, exposing the encapsulated cells to the host.

This thesis aims to replace the exterior layer of alginate with a Temporarily Reactive Polyelectrolyte (TPR) to reinforce AP capsules by forming covalently crosslinked shells. TRPs are polyanions that possess reactive electrophilic groups capable of forming permanent covalent crosslinks with the underlying polyamine (such as PLL), and subsequently hydrolyze, increasing the net negative charge of the polyanion. TRPs are thought to improve the biocompatibility and strength of the microcapsules by forming stable inert amide bonds, as well as increasing the net negative charge of the capsule through the liberation of carboxylates. This thesis will focus primarily on two TRPs: 50% hydrolyzed poly(methyl vinyl ether-*alt*-maleic anhydride), PMM_{50}, and poly(methacrylic acid-*co*-2-vinyl-4,4-dimethylazlactone) with a 50:50 co-monomer ratio, PMV_{50}. Their synthesis, rates of hydrolysis and capsule formation around encapsulated C2C12 cells for *in-vitro* and *in-vivo* studies will be described. Additionally the synthesis and rates of hydrolysis of other 2-vinyl-4,4-dimethylazlactone (VDMA)-copolymers are presented as potential candidates for future TRPs.

Acknowledgements

First and foremost I would like to thank my supervisor, Dr. Harald D.H. Stöver. He has been a wonderful supervisor, who has allowed me to follow my research interests while providing me unprecedented guidance. He allowed and supported me to be more involved with the biomedical side of my project, expanding my area of expertise greatly. I am grateful for the numerous collaborations that I got to be involved in, because of his strong initiative to work with experts in different fields. More than just a supervisor, Dr. Stöver has been an amazing role model and mentor for me. I truly believe that I would not have been as successful as I have been, if it wasn't for him.

I would also like to thank Dr. Nicholas A.D. Burke, or Dr. "Google" as we call him. Nick was enormous help to me throughout my Ph.D. He was never too busy to listen to my experimental problems, and then go on to solve them almost immediately. His continual guidance in the lab and his limitless knowledge was invaluable to me. I would also like to thank my group members; Janice Hickey, Jeffery Li, Jafar Mazumder, Rachelle Kleinberger, Sara Mohajeri, Padraic Foley, and Alison Stewart, for their support and friendship over the years. As well, I would like to thank my committee for their guidance with my project, Dr. Alex Adronov for his polymer knowledge, and Dr. Heather Sheardown for her biomedical knowledge and use of her biomedical facilities to allow me to develop my cell culturing 'skills', and explore more biomedical aspects of my project. I would also like to thank Dr. Murray A. Potter for his guidance, collaborations and use of facilities.

I would like to give special thanks Dr. Bob Berno for his enormous help with characterizing my polymers using NMR spectroscopy. His knowledge and wiliness to help was greatly appreciated. I would also like to thank the late Dr. Don Hughes for his NMR help, as well as Dr. Steve Kornic for his help with numerous other polymer characterizations.

Finally I would like to thank my family and friends. My husband Joshua Gardner for being so supportive, driving me to and picking me up from the lab on the weekends and late nights, listening to and helping me prefect my chemistry presentations, and for doing everything with a smile on his face. A special thanks goes out to my parents, Nancy and Tom Mills, for always encouraging me to get a higher education, for financial support over the years, and for attempting to read all of my published papers. Thanks to my sister, Jessica Mills, for listening to me vent and providing a good outlet when I was stressed. Finally, thanks to my good friend Amanda Fawcett, for listening to and letting me vent about all of my graduate problems (research and other).

Table of Contents

List of Figures

List of Tables

List of Scheme

List of Abbreviations and Symbols

AA	Acrylic acid
AAm	Acrylamide
ACN	Acetonitrile
AIBN	Azobisisobutyronitrile
AP	Calcium-Alginate-Poly-L-Lysine
APA	Calcium-Alginate-Poly-L-Lysine-Alginate
AF	5-Aminofluorescein
BSA	Bovine Serum Albumin
DMAA	Dimethylacrylamide
DMSO	Dimethyl sulfoxide
GPC	Gel Permeation Chromatography
HEMA	Hydroxyethyl methacrylate
MAA	Methacrylic acid
MPC	2-Methacryloyloxyethyl phosphorylcholine
$MPEG_{300}MA$	Methoxy poly(ethylene glycol) metacrylate
NMR	Nuclear Magnetic Resonance
PEG	Poly(ethylene glycol)
PLL	Poly-L-lysine
PMM_{50}	50% hydrolyzed poly(methyl vinyl ether-*alt*-maleic anhydride)
PMV_{50}	Poly(methacrylic acid-*co*-2-vinyl-4,4-dimethylazlactone) 50:50
THF	Tetrahydrofuran
TRITC	Tetramethylrhodamine isothiocyanate
TRP	Temporarily Reactive Polyelectrolyte
VDMA	2-Vinyl-4,4-dimethylazlactone or 4,4-dimethyl-2-vinyl-2-oxazoline-5-one

Declaration of Academic Achievement

A declaration of my research contributions is also given at the beginning of each chapter in this thesis.

CHAPTER 2

I performed all experiments except the fluorescent labeling of PLL, which was performed by Dr. Burke. Experiments I performed included; synthesis of PMM_{50}, measurement of rate of hydrolysis, coating optimization, covalent crosslinking experiments, kinetic permeability measurements, and initial protein binding studies. I also wrote the manuscript, with edits and guidance from Dr. Burke and Dr. Stöver.

CHAPTER 3

I performed the following experiments: determination of reactivity ratios, synthesis of PMV_{50} and higher VDMA content copolymers, analysis of the copolymers using ^{1}H NMR, quantitative ^{13}C NMR and GPC, model studies to highlight the transhydration reaction, measurement of PMV_{50}'s hydrolysis in buffer and coating of PMV_{50} onto AP capsules. Dr. Berno helped me set up the saturation-recovery experiment, to measure the T1 values of PMV_{50} for subsequent quantitative ^{13}C NMR analysis. Dr. Kornic performed elemental analysis and FT-IR on my PMV_{50} copolymer. I wrote the manuscript, with edits and guidance from Dr. Stover.

CHAPTER 4

Dr. Harald Stöver, Dr. Murray Potter and I designed the experiments presented in this paper. I synthesized the two TRPs, performed *in-vitro* cell viability analysis, cellular overgrowth analysis using optical as well as scanning electron microscope, mechanical strength tests, statistical analysis and wrote the paper. Anna Li performed implantations and explantations of capsules in mice, and both Anna Li and Zahra Isfahani performed flow cytometry on the blood samples. Dr. Harald Stöver and Dr. Murray Potter helped edit the paper.

CHAPTER 5

I designed and performed all experiments except for elemental analysis of the VDMA copolymers. Experiments I performed include: reactivity ratio determination, synthesis and characterization of all VDMA copolymers using GPC, ^{1}H NMR and quantitative ^{13}C NMR and measurements of the VDMA copolymer's hydrolysis. I also wrote the manuscript with edits and guidance from Dr. Stover. Carla Brown initially developed the pH titration program that I used to perform the hydrolysis measurements.

Chapter 1: Introduction to Cell Encapsulation

1.1 History of Cell Encapsulation

In 1964, Chang[1] was the first to present the idea of an "artificial cell," when he described the technique of encapsulating cells for immunoprotection. Sixteen years later Lim and Sun[2] (1980) reported the first successful immune-isolation of islets in a calcium-alginate – poly-L-lysine (PLL) – alginate, or APA, microcapsule to act as a bioartifical pancreas. The encapsulated islets were implanted into diabetic rats where they successfully secreted insulin in response to the blood glucose levels for two weeks.

Coated calcium-alginate capsules are the basis of many encapsulations used in pursuit of cell-based enzyme and hormone replacement therapies. APA capsules consist of a calcium-alginate hydrogel core containing cells designed to express the therapeutic product, coated with permeability controlling PLL (a polycation), followed by an exterior layer of polyanionic alginate (Figure 1.1). Although this system offered great potential for treating enzyme or hormone deficiency disorders (diabetes, hypoparathyroidism,[3] lysosomal storage disorder (LSD)[4], dwarfism[5], hemophilia B[6]), central nervous system disorders[7,8,9] (Parkinson's, Alzheimers, ALS, Huntington's) as well as some cancers,[10,11,12,13] and heart disease,[14] to date successful long-term treatment using immunoisolated cells has not been achieved in humans.[15,16,17]

Creating a successful microencapsulation system for cells is no easy task. For successful immunoisolation, the permeability of the microcapsules must be chosen to protect the encapsulated cells from the host's immune system, acting as a protective barrier to harmful host antibodies, and immune cells. At the same time, the capsule must allow for the indiffusion of oxygen and nutrients to the encapsulated cells and out-diffusion of expressed therapeutic products to the host (Figure 1.1).

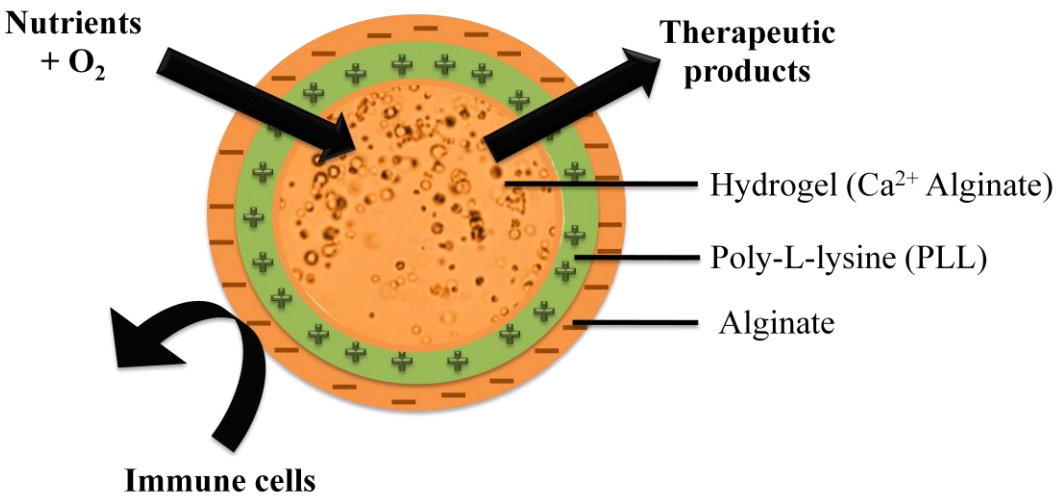

Figure 1.1 *Structure and permeability requirements for immunoisolation of cells in an APA capsule.*

The encapsulation material must be compatible[18] with the encapsulated cells, as well as the host. Poor compatibility towards the host ultimately presents as cellular overgrowth around capsules, leading to impaired oxygen and nutrient diffusion and subsequent necrosis of encapsulated cells. Poor compatibility with the encapsulated cells results in reduced cell viability and decreases secretion of the therapeutic products. One major obstacle to overcome in cell encapsulation systems is that the permeability required to let in oxygen and small nutrients, also permits the in-diffusion of small cytokines and reactive oxygen species (ROS), which can damage the encapsulated cells.[19,20]

Other important requirements for effective immunoisolation is that the encapsulation material must have sufficient mechanical strength to maintain the integrity of the capsules for extended periods of time *in-vivo*.[21,22] That is, it must resist deformation, fracture and chemical stresses, and not be biodegradable. The membrane morphology is also important for good biocompatibility, as surface roughness usually induces immunological and fibrotic reactions, compared to smooth surfaces.[23]

Other important factors to consider include microcapsule size. Microcapsules range from 100-800 µm depending on the need of the encapsulated cells. Smaller capsules allow for better oxygen and nutrient diffusion, promoting better cell viability, important for cells that can often suffer from necrosis such as Islets of Langerhans. In larger capsules hypoxia of the cells in the center of the capsules is more likely. Capsule size is also an important factor when choosing the appropriate transplantation site. The two most common sites of implantation for treating endocrine disorders are the peritoneal cavity,[24,25] which allows for a large graft volume but is poorly vascularized, and the liver portal vein,[26,27] which offers the opposite (an oxygen and nutrient rich environment, but a small graft volume).

For about 25 years after Lim and Sun[2] (1980) introduced the APA system, research has been directed towards optimizing[28,29,30] this system with only minor improvements. A review of the literature shows varying degrees of success for alginate based systems. While some studies have reported minimal fibrotic overgrowth and short term treatment of Type 1 Diabetes,[24,31] many report poor and inconsistent results due to poor biocompatibility[32] and lack of long-term mechanical strength.[33,34] These inconsistencies can largely be attributed to the lack of standardization of alginate purity and composition, and to the immunogenic properties of PLL. In general the APA system is limited to shorter term applications, as its ionically crosslinked network shows poor mechanical strength over long term periods.

1.2 Alginate

Alginate is a natural anionic polysaccharide primarily extracted from brown algae (*Phaeophyta*). It consists of 1,4-linked α-L-guluronate (G) and β-D-mannuronate (M) units, which can be arranged in homopolymeric (GGG blocks and MMM blocks) or heteropolymeric (MGM blocks).[35] Alginate has the ability to form hydrogels quickly under conditions that are compatible with living cells, in the presence of divalent cations such as calcium, barium or strontium.[36] Although other synthetic and natural polymers are under investigation for cell encapsulation, e.g., agarose,[37] cellulose sulfate[38], hyaluronic acid[39], poly(hydroxyethylmetacrylate-methyl methacrylate) (HEMA-MMA)[40], and functionalized poly(ethylene glycol) (PEG)[41], none have reached the same level of performance and popularity as alginate.

The chemical properties and purity of alginate vary greatly depending on where and when the algae are harvested, as well as on the extraction processes. Different batches of alginate will have different intrinsic viscosities, M:G compositions and distributions, as well as different levels of biocontaminates such as endotoxins, polyphenols, fucoidans and proteins. These impurities can result in fibrotic overgrowth, inflammatory reactions and cell necrosis,[42] if not properly removed. Medical grade alginate suppliers carry out extensive purifications, however residual contaminants can still remain.[43,44] Many groups further purify their alginate using different in-house techniques,[42,44,45,46,47] that can reduce the amounts of endotoxins and polyphenols, however relatively high residual amounts of biocontaminates still remain.[44] Although these in-house purification techniques have been shown to improve biocompatibility,[48] they have also been shown to induce changes in the intrinsic viscosity of alginate,[43,44] providing an additional factor that needs to be considered for consistent performance of alginate microcapsules.

Gelation of alginate to form microcapsules, has been shown to be primarily the result of G blocks selectively binding divalent cations, inducing chain-chain association forming a structure known as the ‘egg box model’[49] (Figure 1.2). Since G blocks bind

calcium ions strongly in a cooperative manner, M residues have been shown to have a higher binding affinity towards PLL in the APA capsule.[50]

Over the years, there has been a great debate over the optimal G:M ratio required to achieve the best strength and biocompatibility. In terms of biocompatibility, some groups have reported that M residues are the primary active cytokine inducers in alginate, stimulating human monocytes to produce tumor necrosis factor-alpha, interleukin-6, and interleukin-1[32], resulting in capsules with more cellular overgrowth[51]. Others have reported that guluronic acids were associated with more severe cellular overgrowth.[52,53] Subsequent studies found that this discrepancy had more to do with the contamination (impurities) in the alginates than with the alginate composition (G:M ratio).[54] More recently Tam[55] (2011) found that the main factors contributing to biocompatibility of highly purified alginate microcapsules are the G:M ratio and/or the intrinsic viscosity. More specifically, lower G content alginate capsules showed less fibrotic overgrowth compared to higher G content alginates, but lower G content capsules were also weaker, showing fragmentation *in-vivo*. It is plausible that lower G contents simply leads to higher degrees of hydration, which will reduce tissue reaction but at the cost of lower strength.

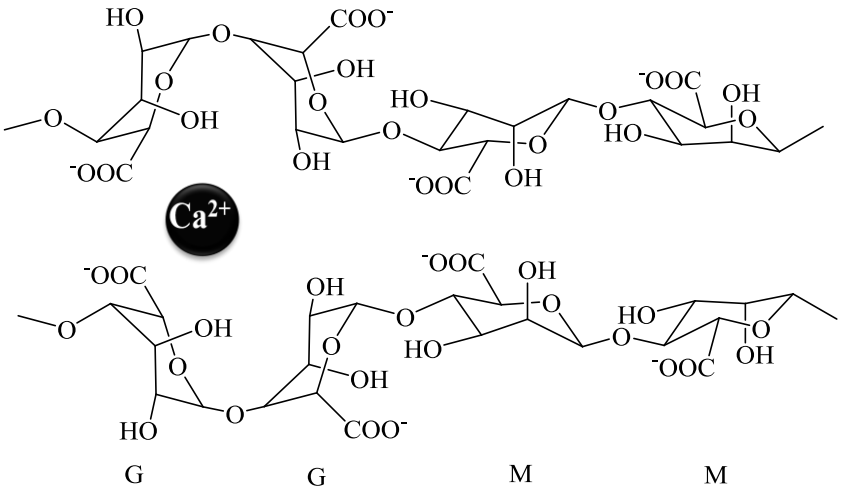

Figure 1.2 *Egg box model of two GG blocks electrostatically bound with calcium, on two GGMM alginate chains.*

It is clear that a fine balance is required for the G:M ratio and intrinsic viscosity, to achieve optimal capsule performance. Although the large diversity of chemical composition and purity of alginates can result in inconsistencies in the reported success of alginate based systems, some groups have managed to achieve a balance of properties good enough to justify clinical trials of encapsulated islets of Langerhans.[3,15,56]

1.3 Alginate-PLL microcapsules

Alginate microcapsules are made by dispersing a cell pellet in a sodium-alginate solution and extruding it through a needle several hundred micrometers in diameter into a ~100 millimolar solution of, e.g., calcium chloride. Rapid in-diffusion of calcium shrinks and gels the alginate into a transparent, smooth and spherical hydrogel bead, trapping the cells. The encapsulation can be carried out at room temperature or 4°C, physiological pH and in isotonic solution, making for an easy method for cell encapsulation. Although it has been reported that alginate capsules can provide a microenvironment which facilitates functional survival of islets,[57,58] some adherent cells require anchorage points inside the hydrogel for optimal viability. In the latter case, alginate can be covalently modified with arginine glycine aspartic acid (RGD), an adhesion peptide sequence, to provide the cells anchorage points inside the hydrogel.[14,59]

Under physiological conditions, calcium alginate capsules are sensitive towards ion exchange with sodium and magnesium, which results in osmotic swelling of the beads leading to an increase in permeability, destabilization and rupture of the gel.[34] To improve the mechanical strength and decrease the permeability of calcium-alginate capsules, barium as well as strontium has been used instead of calcium as they have a higher affinity for alginate.[36]

Alternatively, the anionic alginate capsules can be coated with a polycation, PLL being the most popular,[60] however poly-L-ornithine (PLO)[61,62] and chitosan,[63] are also used. It is widely known that like most polycations,[64] charged PLL is immunogenic,[65] so a final layer of alginate is coated over PLL in an attempt to 'hide' it from the immune system. However several studies have shown that this coating is not effective in masking or neutralizing the immunogenic PLL.[66,67] In 2011 Tam[61] used X-ray Photoelectron Spectroscopy (XPS) to show that APA and AP microcapsules had the same amount of polycation at their surface, and that the final alginate coating did not improve the host compatibility of the microcapsules. After comparing APA to A-PLO-A microcapsules, Tam concluded that the alginate-polycation interactions are more important for host compatibility then either the quantity of the polycation at the surface or the alginate coating. Thus, an alternative polyanionic coating that interacts more efficiently with PLL could be used to improve the biocompatibility of AP capsules.

An alternative approach to improve PLL's biocompatibility was demonstrated by Sawhney[68] (1992), who sought to decrease the charge density of PLL by pre-grafting it with PEG. The presence of PEG improved the biocompatibility of the capsules, but hindered PLL's electrostatic interaction with alginate during coating, resulting in a decrease in mechanical strength of the resulting capsules. Recently, Wilson (2011) used a similar approach to form conformal coatings of alginate / PLL-*graft*-PEG on individual islets.[69]

1.4 Improving APA capsules

Although APA capsules have entered the clinical trial phase, the large inconsistency in their performance reported in the literature will hinder their translation into large scale therapies. This thesis focuses on improving this capsule system, by replacing the exterior layer of alginate with a synthetic polyanion that is able to form covalent crosslinks with underlying PLL. Replacing the exterior alginate with a reactive synthetic polyanion, is expected to resolve the following problems associated with the conventional APA system:

1. As synthetic polymers do not contain biological impurities, there should be no biocontaminates present on the surface of the capsules, improving their host compatibility.

2. Properties of synthetic polymers can be easily modified to improve the microcapsules' mechanical strength, permeability, and compatibility with cells and host.

3. The weak ionic interactions of APA capsules that dissipate over time exposing the encapsulated cells will be reinforced with covalent crosslinks, improving the long term strength of the capsules.

4. The covalent crosslinking between PLL and reactive polyanions consumes a primary amine, and for anhydride-functional polyanions, generates an additional carboxyl anion. This will increase the net anionic charge density at the surface of the capsules, and further improve host compatibility.

5. The reactive polyanions may be functionalized with molecules that facilitate cell attachment, reduce inflammation, sequester or even convert inflammatory cytotoxins.[70]

1.5 Covalently Crosslinked Capsules

Covalent crosslinking of hydrogels in presence of cells requires cell-compatible chemistry. Two approaches are primarily used; photo-crosslinking and 'click' type chemical reactions, both of which can be carried out at room temperature in aqueous conditions at physiological pH, in a reasonable amount of time, and with no cytotoxic byproducts, initiators, or catalysts.

The majority of covalently crosslinked microcapsules reported use photo-initiated free radical crosslinking polymerization. Anseth's group has focused on preparing crosslinked PEG hydrogels by photo-initiated polymerization of diacrylated PEG around islet cells. These processes typically use cytocompatible photoinitiators,[71,72] or redox initiation using radicals generated from the reaction of glucose with glucose oxidase at

the hydrogel surface.[73] To improve the capsules' host compatibility, capsules have been functionalized to actively modulate the local immune environment. Examples include incorporation of antibodies and peptides to sequester damaging cytokines,[70] enzymes to break down reactive oxygen species (ROS)[74], and local anti-inflammatory agents.[75]

Numerous other photo-crosslinked systems have been reported over the years. In 2000, Lu[76] used photo-induced 2+2 coupling to crosslink α-phenoxycinnamylidene-modified poly(allylamine) around calcium alginate capsules. In the same year Wang[77] reported the analogous reaction involving PLL instead of poly(allylamine). In 2006, Rokstad[78] formed covalently crosslinked capsules by photo-polymerizing methacrylated alginate. A similar idea was presented by Reza[79] in 2010, who photo-polymerized methacrylated carboxymethylcellulose around encapsulated cells. In 2011 Lin[80] formed crosslinked PEG hydrogels using thiol-ene photo-click chemistry. Another approach was presented by Hall[81] (2011), who used Staudinger ligation between azide-functionalized alginate, and phosphine-functionalized PEG, to form a crosslinked network. Finally, Mironi-Harpaz[82] (2012) moved away from alginate based systems and photo-polymerized diacrylated PEG and PEG-fibrinogen. Although photo-crosslinking has been extensively explored, close attention must be paid to cytotoxic effects of the wavelength and duration of irradiation, free radicals generated and initiators and monomers used.[82] Fedorovich (2009) showed that presence of macromonomers protects cells during UV photo-initiated polymerization, likely by rendering the radicals generated less mobile.[83] Bahney (2011) compared UV and white light initiators based on Eosin.[84]

Considering these challenges, covalent crosslinking by click-type reactions might prove a more robust approach to cell encapsulation. Cellesi[85] (2002) used a tandem approach, combining the thermal gelation of linear poly(*N*-isopropylacrylamide) with covalent crosslinking using Michael-type addition between the thiols and acrylate end groups, to prepare covalently crosslinked capsules. In 2011, Klouda[86] combined thermal gellation of (meth)acrylated *N*-isopropylacrylamide with covalent crosslinking by redox initiated free radical polymerization in water. Mahou[87] (2010) used a vinyl sulfone-terminated 8-arm PEG and a thiol crosslinker to form covalently crosslinked calcium-alginate-PEG hybrid microcapsules. In a slightly more elaborate approach, Davidovich-Pinhas[88] (2011) also used Michael-type addition to covalently crosslink acrylated-PEG-alginate hydrogels using the acrylate end group of PEG and the sulfide end groups of mucus type glycoproteins that had been covalently bound to alginate. Ranganath[89] (2011) used genipin, a reactive aglycone derived from gardenia, to covalently crosslink the chitosan in calcium-alginate-chitosan capsules. Finally, Nimmo[90] (2011) reported a novel crosslinked hydrogel system formed using Diels-Alder coupling between a furan-modified HA and a dimaleimide-modified PEG.

Encapsulating cells in covalently crosslinking hydrogels is thus not new, but the challenge still exists to design a system that is fundamentally cell and host compatible, easily scalable in terms of materials and processes, and that can be tuned to meet often competing demands. This thesis is based on developing temporarily reactive polyanions

as a new, platform approach, to cell and host compatible hydrogels. It is based on a plug-in modification to the widely used APA system, retaining many of its inherent advantages while mitigating its shortcomings.

1.6 Reactive Polyanions

Our group uses the electrostatic interactions between two oppositely charged polyelectrolytes to facilitate covalent crosslink formation. In 2008 Mazumder[91,92] described the use of a reactive polyanion, composed of sodium methacrylate and the electrophilic comonomer methacryloyloxy ethylacetoacetate (MEAA), which can form covalent crosslinks with surface-bound PLL and other polyamines. While this system, as well as the above mentioned crosslinking systems, show promise for improving the mechanical strength and long term function of encapsulation systems, residual reactive groups can lead to undesirable protein binding during incubation or transplantation, unless the described chemistry is bio-orthogonal. However, cell compatible bio-orthogonal reactions often result from covalent bond formation between very hydrophobic chemical groups, which may also cause protein binding or other unwanted interactions.

This thesis aims to improve upon the previously described covalent systems by using Temporarily Reactive Polyelectrolytes (TRPs) to reinforce AP capsules by forming covalently crosslinked shells (Figure 1.3). TRPs are polyanions that possess reactive electrophilic groups capable of forming permanent covalent crosslinks with the polyamine (such as PLL) present on the capsule surface. The name refers to the fact that the residual electrophilic groups not consumed in this crosslinking reaction will hydrolyze to form carboxylate anions shortly after network formation. TRPs are hypothesized to improve capsule longevity and host compatibility by forming networks with permanent amide crosslinks and a net negative charge.

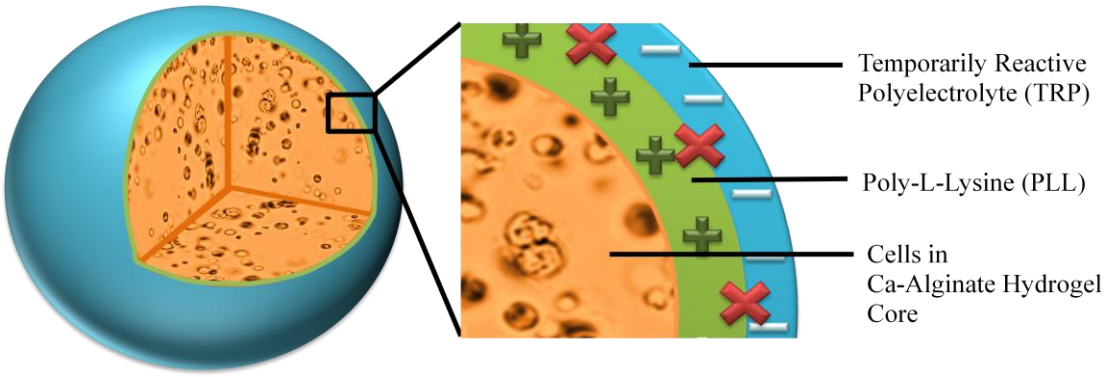

Figure 1.3 *Cells immobilized in AP capsule coated with a TRP which has formed covalent crosslinks with PLL present in the shell (seen as red x's)*

The thesis will focus primarily on two types of TRPs: 50% hydrolyzed poly(methyl vinyl ether-*alt*-maleic anhydride), PMM_{50}, and poly(methacrylic acid-*co*-2-vinyl-4,4-dimethylazlactone) with a 50:50 co-monomer ratio, PMV_{50} (Scheme 1.1). These two TRPs are distinguished by different formation (alternating copolymerization followed by partial hydrolysis, and semi-batch copolymerization, respectively) and different half-life times under physiological conditions (about 2.5 and 30 minutes, respectively). The rate of hydrolysis of their reactive groups will limit the amount of time available for crosslinking, as well as for any post-functionalization with bioactive molecules, such as antibodies, peptides or enzymes to sequester damaging cytokines or breakdown ROS, as described by Anseth.[70,74]

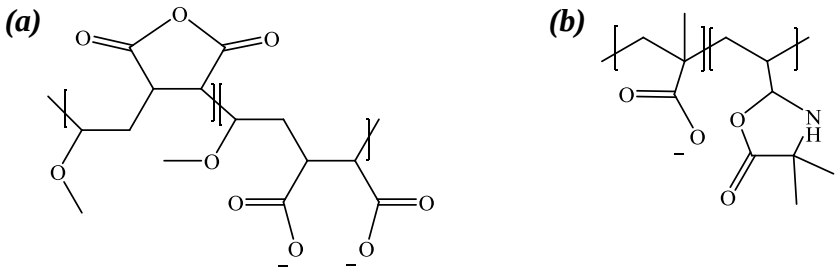

Scheme 1.1 *Chemical structures of* ***(a)*** *PMM_{50}* ***(b)*** *PMV_{50}*

Reported in this thesis are the synthesis and the rates of hydrolysis for both PMM_{50} and PMV_{50}. An in-depth study of the effects of molecular weights and coating solution concentrations of PLL and PMM_{50} on crosslinking and permeability of AP-PMM_{50} capsules was performed. The PMV_{50} system shows an interesting but undesirable transhydration side reaction between adjacent azlactone and methacrylic acid groups that can be suppressed through choice of composition or low temperature copolymerization.

A six week *in-vitro* and *in-vivo* mouse study is described, comparing AP-PMM_{50} and AP-PMV_{50} capsules to conventional APA capsules. The cell and host compatibilities of these capsules were assessed by measuring the viability of encapsulated C2C12 murine myoblast cells, quantifying the fibrotic overgrowth around explanted capsules, as well as measuring blood cytokine levels. These measurements not only allow for a comparison between APA and AP-TRP capsules, but also provide a baseline for future studies on AP-TRP capsules that have been functionalized with bioactive molecules to further improve their host and cell compatibility. The chemical resistance of the explanted *in-vivo* capsules was also assessed.

Finally, a more detailed study was carried out to understand how different comonomers affect the rate of hydrolysis of the azlactone groups. First, the reactivity ratios for 2-vinyl-4,4-dimethylazlactone and a number of ionic and polar neutral comonomers were determined. Then, a suite of corresponding no-drift copolymers was prepared by semi-batch processes. Their solubilities and rates of hydrolysis were analyzed, helping to identify promising candidates for future encapsulation cycles.

1.7 References

[1] T.M.S. Chang. *Science* **1964**, *146*, 524-525.
[2] F. Lim; A.M. Sun. *Science* **1980**, *210*, 908–909.
[3] C. Hasse; G. Klöck; A. Schlosser; U. Zimmermann; M. Rothmund. *Lancet* **1997**, *350*, 1296-197.
[4] C.J.D. Rose; L. Bastedo; S.A. Maier, P.L. Chang. *Hum. Gene Ther*. **2000**, *11*, 2117-2127.
[5] A.A. Hendy; G. Hortelano; G.S. Tannenbaum; P.L. Chang. *Hum. Gene Ther*. **1995**, *6*, 165-175.
[6] J.M. Van Raamsdonk; C.J.D. Ross; M.A. Potter; S. Kurachi; K. Kurachi; D.W. Stafford; P.L. Chang. *L. Lab. Clin. Med*. **2002**, *139*, 35-42.
[7] D.F Emerich; S.R. Winn. *Crit. Rev. Ther. Drug Carrier Syst*. **2001**, *18*, 265-298.
[8] C.J. Ross; M. Ralph, P.L. Chang. *Hum. Gene Ther*. **1999**, *10*, 49-59.
[9] Y.T. Kim; R. Hitchcock; K.W. Broadhead; D.J. Messina; P.A. Tresco. *J. Controlled Release* **2005**, *102*,101–111.
[10] T. Visted; M. Lund-Johansen. *Expert Opin. Biol. Ther.* **2003**, *3*, 551-561.
[11] S. Hao; L. Su; X. Guo; T. Mayana; J. Xiang. *Exp. Oncol*. **2005**, *27*, 56-60.
[12] B. Salmons; E.M. Brandtner; K. Hettrich; W. Wagenknecht; B. Volkert; S. Fischer; J.A. Dangerfield; W.H. Gunzburg. *Curr. Opin. Mol. Ther*. **2010**, *4*, 450-460.
[13] B. Salmons; W.H. Gunzburg. *Adv. Exp. Med. Biol*. **2010**, *670*, 92–103.
[14] J. Yu; K.T. Du; Q. Fang; Y. Gu; S.S. Mihardja; R.E. Sievers; J.C. Wu; R.J. Lee. *Biomaterials* **2010**, *31*, 7012-7020.
[15] B.E. Tuch; G.W. Keogh; L.J. Williams; W. Wu; J.L. Foster; V. Vaithilingam; R. Philips. *Diabetes Care* **2009**, *32*, 1887-1889.
[16] E.A. Ryan; J.R. Lkey; R.V. Rajotte; G.S. Korbutt, T. Kin, S. Imes, A. Rabinovitch; J.F. Elliott; D. Bigam, N.M. Kneteman; G.L. Warnock; I. Larsen; A.M. Shapiro. *Diabetes* **2001**, *50*, 710-719.
[17] E.A. Ryan; B.W. Paty; P.A Senior; D. Bigam; E. Alfadhi; N.M. Kneteman; J.R. Lakey; A.M. Shapiro. *Diabetes* **2005**, *54*, 2060-2069.
[18] D.F. Williams, European Society for Biomaterials, Definitions in Biomaterials : Proceedings of a Consensus Conference of the European Society for Biomaterials, Chester, England, Elsevier, Amsterdam, New York, 1987, March 3–5, 1986.
[19] B. Kulseng; B. Thu; T. Espevik; G. Skåk-Bræk. *Cell Transplant.* **1997**, *4*, 387-394.
[20] J.Y. Jang; D.Y. Lee; S.J. Park; Y. Byun. *Biomaterials* **2004**, *17*, 3663-3669.
[21] J.J. Schmidt; J. Rowley; H.J. Kong. *J Biomed. Mater. Res. A* **2008**, *87*, 1113–1122.
[22] I. Lacik. *Aust. J. Chem.* **2006**, *59*, 508–524.
[23] H. Zimmermann; F. Ehrhart; D. Zimmermann; K. Muller; A. Katsen-Globa; M. Behringer; P.J. Feilen, P. Gessner; G. Zimmermann; S.G. Shirley; M.M. Weber; J. Metze; U. Zimmermann. *Appl. Phys. A*, **2007**, *89*, 909–922.
[24] P. Soon-Shiong; R.E. Heintz; N. Merideth; Q.X. Yao; Z. Yao; T. Zheng; M. Murphy; M.K Moloney; M. Schmehl; M. Harris; R. Mendez; R. Mendz; P.A. Sandford. *Lancet* **1994**, *343*, 950-951.

[25] R.B. Elliott; L. Escobar; P.L. Tan; O. Garkavenko; R. Calafior; P. Basta; A.V. Vasconcellos; D.F. Emerich; C. Thanos; C. Bambra. *Transpl. Proc*. **2005**, *37*, 3505-3508.
[26]M.D. Brendel; A.O. Schultz, R.G. Bretzel. *Int. Islet. Transpl. Regist*. **1999**, *8*, 5-18.
[27] R.P. Robertson. *N. Engl. J. Med*. **2004**, *350*, 694-705.
[28] M.F.A. Goosen; G.M. O'Shea; H.M. Gharapetian; S. Chou; A.M. Sun. *Biotechnol. Bioeng.* **1985**, *27*, 146-150.
[29]A. King; S. Sandler; A. Andersson. *J. Biomed. Mater. Res*. **2001**, *57*, 374-383.
[30] G. Orive; S.K. Tam; J.L. Pedraz; J.P. Hallé. *Biomaterials* **2006**, *27*, 3691-3700.
[31] P. De Vos; J.F. Van Straaten; A.G. Nieuwenhuizen; M. de Groot; R.J. Ploeg; B.J. De Haan; R. Van Schilfgaarde. *Diabetes* **1999**, *48*, 1381-1388.
[32] M. Otterlei; K. Ostgaard, G. Skåk-Bræk; O. Smidsrød; P. Soon-Shiong; T. Espevik. *J. Immunother*. **1991**, *10*, 286-291.
[33] H. Wong; T.M.S. Chang. *Biomat. Art. Cells Immob. Biotech*. **1991**, *19*, 675-686.
[34] B. Thu; P. Bruheim; T. Espevik; O. Smidsrød; P. Soon-Shiong; G. Skjåk-Bræk. *Biomaterials* **1996**, *17*, 1069-1079.
[35] H. Zimmermann; S.G. Shirley; U. Zimmermann. *Current Diabetes Reports*. **2007**, *7*, 314-320.
[36] Ý.A. Mørch; I. Donati; B.L. Strand; G. Skjåk-Bræk. *Biomacromolecules* **2006**, *7*, 1471-1480.
[37] S. Sakai; K. Kawabata; T. Ono; H. Ijima; K. Kawakami. *Biomaterials* **2005**, *26*, 4786-4792.
[38] S. Schaffellner; V. Stadlbauer, P. Stiegler; O. Hauser; G. Halwachs; C. Lackner; F. Iberer; K.H. Tscheliessnigg. *Transplant. Proc*. **2005**, *37*, 248-252.
[39] C. Chung; I.E. Erickson; R.L. Mauck; J.A. Burdick. *Tissue. Eng. A* **2008**, *14*, 1121–1131.
[40] R.M. Dawson; R. Broughton; W.T. Stevenson; M.V. Sefton. *Biomaterials* **1987**, *8*, 360-366.
[41] F. Cellesi; W. Weber; M. Fussenegger; J.A. Hubbel; N. Tirelli. *Biotechnol. Bioeng*. **2004**, *6*, 740-749.
[42] G. Langlois; J. Dusseault; S. Bilodeau; S.K. Tam; D. Magassouba; J.P. Hallé. *Acta Biomater.* **2009**, *5*, 3433-3440.
[43] S.K. Tam; J. Dusseault; S. Polizu; M. Ménard; J.P. Hallé; L. Yahia. *Biomaterials* **2006**, *27*, 1296-1305.
[44] J. Dusseault; S.K. Tam; M. Ménard; S. Polizu; G. Jourdan; L. Yahia; J.P. Hallé. *J. Biomed. Mater. Res. A.* **2006**, *76*, 243-251.
[45] U. Zimmermann; G. Klöck; K. Federlin; K. Haning; M. Kowaslski; R.G. Bretzel; A. Horcher; H. Entenmann; U. Sieber; T. Zekorn. *Electrophoresis* **1992**, *13*, 269-274.
[46] G. Klöck; H. Frank; R. Houben; T. Zekorn; A. Horcher; U. Siebers; M. Wöhrle; K. Federlin; U. Zimmermann. *Appl. Microbiol. Biotechnol*. **1994**, *40*, 638-643.
[47] P. De Vos; B.J. De Haan; G.H. Wolters; J.H. Strubbe; R. Van Schilfgaarde. *Diabetologia*, **1997**, *40*, 262-270.

[48] M. Ménard; J. Dusseault; G. Langlois; W.E. Baille; S.K. Tam; L. Yhia; X.X Zhu; J.P. Hallé. *J. Biomed. Mater. Res. B: Applied Biomater.* **2010**, *93B*, 333-340.
[49] I. Braccini; S. Pérez. *Biomacromolecules* **2001**, *2*, 1089-1096.
[50] B. Thu; P. Bruheim; T. Espevik; O. Smidsrød; P. Soon-Shiong; G. Skåk-Bræk. *Biomaterials* **1996**, *17*, 1031-1040.
[51] P. Soon-Shiong; M. Otterlei; G. Skjåk-Bræk; O. Smidsrød; R. Heintz; R.P. Lanza; T. Espevik. *Transplant. Proc*. **1991**, *23*, 758-759.
[52] H.A. Clayton; N.J. London; P.S. Colloby; P.R. Bell; R.F. James. *J. Microencapsul.* **1991**, *8*, 221-233.
[53] P. De Vos; B. De Haan, R. Van Schifaarde. *Biomaterials* **1997**, *18*, 273-278.
[54] G. Orive; S. Ponce, R.M. Hernández; A.R. Gascón; M. Igartua; J.L. Pedraz. *Biomaterials* **2002**, *23*, 3825-3831.
[55] S.K. Tam; J. Busseault, S. Bilodeau; G. Langlois; J.P. Hallé; L. Yahia. *J. Biomed. Mater. Res. A* **2011**, *98*, 40-52.
[56] R.B. Elliott; L. Escobar; P.L.J. Tan; M. Muzina; S. Zwain; C. Buchanan. *Xenotransplantation* **2007**, *14*, 157–161.
[57] S. Sandler; A. Andersson; D.L. Eizirik; C. Hellerstrom; T. Espevik; B. Kulseng; B. Thu; D.G. Pipeleer; G. Skjåk-Bræk. *Transplantation* **1997**, *63*, 1712-1718.
[58] M.D. Lopez-Avalos, K. Tatarkiewicz; A. Sharma; S. Bonner-Weir; G.C Weir. *Transplantation* **2001**, *71*, 1154-1162.
[59] G. Orive; M. De Castro; H.J. Kong; R. M. Hernández; S. Ponce; D.J. Mooney; J. L. Pedraz. *J. Control. Release* **2008**, *135*, 203-210.
[60] D. Hunkeler. *Trends Polym. Sci*. **1999**, *5*, 286-293.
[61] R. Calafiore; G. Basta; G. Luca; A. Lemmi; M.P. Montanucci; G. Calabrese; L. Racanicchi; F. Mancuso; P. Brunetti. *Diabetic Care*, **2006**, *29*, 137-138.
[62] S.K. Tam; S. Bilodeau; J. Dusseault; G. Langlois, J.P. Hallé; L.H. Yahia. *Acta Biomater.* **2011**, *7*, 1683-1692.
[63] B.A. Zielinkski; P. Aebischer. *Biomaterials* 1994, 13, 1049-1-56.
[64] A. Prokop; D. Hunkeler; S. DiMari; A.A. Haralson; T.G. Wang. *Adv. Poly. Sci*. **1998**, *136*, 1-51.
[65] B.L. Strand; L. Ryan: P. In't Veld; B. Kulseng; A.M. Rokstad; G. Skják-Bræk; T. Espevik. *Cell Transplant*. **2001**, *10*, 263-275.
[66] B.L. Strand, Y. A. Mørch, T. Espevik, G. Skjåk-Bræk. *Biotechnol. Bioeng*. **2003**, *20*, 389-394.
[67] S. Juste; M. Lessard; N. Henley; M. Ménard; J.P. Hallé. *J. Biomed. Mater. Res.* **2005**, *72*, 389-398.
[68] A.S. Sawhney; J.A. Hubbell. *Biomaterials* **1992**, *13*, 863-870.
[69] J.T. Wilson; W. Cui; V. Kozovskaya; E. Kharlampieva; D. Pan; Z. Qu; V.R. Krishnamurthy; J. Mets; V. Kumar; J. Wen; Y. Song; V.V. Tsukruk; E.L. Chaikof. *J. Am. Chem. Soc.* **2011**, *133*, 7054-7064.
[70] C.C. Lin; A.T. Metter; K.S. Anseth. *Biomaterials* **2009**, *28*, 4907-4914.
[71] L.M. Weber; C.Y. Cheung; K.S. Anseth. *Cell Transplant.* **2008**, *16*, 1049-1057

[72] B.D. Fairbanks; M.P. Schwartz; C.N. Bowman; K.S. Anseth. *Biomaterials* **2009**, *30*, 6702-6707.
[73] P. S. Hume; C.N. Bowman; K.S. Anseth. *Biomaterials* **2011**, *32*, 6204-6212.
[74] P.S. Hume; K.S. Anseth. *J. Biomed. Mater. Res. A* **2011**, *99*, 29-37.
[75] A.A. Aimetti; M.W. Tibbitt; K.S. Anseth. *Biomacromolecules* **2009**, *10*, 1484-1489.
[76] M.Z. Lu; H.L. Lan; F.F. Wang; C.Y.J Wang. *Biotechnol. Bioeng*. **2000**, *70*, 179-483.
[77] Y.J. Wang. Development of new polycations for cell encapsulation with alginate, *Mat. Sci. Eng. C* **2000**, *13*, 59-63.
[78] A.M. Rokstad; I. Donati; M. Borgogna; J. Oberholzer; B.L. Strand; T. Espevik; G. Skjåk-Bræk. *Biomaterials* **2006**, *27*, 4726-4737.
[79] A.T. Reza; S.B. Nicoll. *Acta Biomater.* **2010**, *6*, 179-186.
[80] C. Lin; A. Raza; H. Shih. *Biomaterials* **2011**, 32, 9685-9695.
[81] K.K. Hall; K.M. Gattás-Asfura; C.L. Stabler. *Acta Biomater.* **2011**, *7*, 614-624.
[82] I. Mironi-Harpaz; D.Y. Wang; S. Venkatraman; D. Seliktar. *Acta Biomater.* **2012**, *8*, 1838-1848.
[83] N.E. Fedorovich; M.H. Oudshoorn; D. van Geemen; W.E. Hennink; J. Alblas; W.J.A. Dhert. *Biomaterials* **2009**, *30*, 344-353.
[84] C.S. Bahney; T.J. Lugan; C.W. Hsu; M. Bottlang; J.L. West; B. Johnstone. *Euro. Cell. Mater.* **2011**, 22, 43-55.
[85] F. Cellesi; N. Tirelli; J.A. Hubbell. *Macromol. Chem. Phys.* **2002**, *203*, 1466-1472.
[86] L. Klouda; K.R. Perkins; B.M. Watson; M.C. Hacker; S.J. Bryant; R.M. Raphael; F.K. Kasper; A.G. Mikos. *Acta Biomater.* **2011**, *7*, 1460-1467.
[87] R. Mahou; C. Wandrey. *Macromolecules* **2010**, *43*, 1371-1378.
[88] M. Davidovich-Pinhas; H. Bianco-Peled. *Acta Biomater.* **2011**, *7*, 2817-2825.
[89] S.H. Ranganath; A.L. Tan; F. He; C.H. Wang; W.B. Krantz. *AlChE Journal* **2011**, *57*, 3052-3062.
[90] C.M. Nimmo; S.C. Owen; M.S. Shoichet. *Biomacromolecules* **2011**, *12*, 824-830.
[91] M.A.J Mazumder; F. Shen, N.A.D. Burke, M.A.P. Potter, H.D.H Stover. *Biomacromolecules* **2008,** *9*, 2292-2300.
[92] F. Shen; M.A.J. Mazumder; N.A.D. Burke; H.D.H. Stöver; M.A. Potter. *J. Biomed. Mater. Res. B Appl. Biomater.* **2009,** *90*, 350-361.

CHAPTER 2: Crosslinked Microcapsules Formed From Self-deactivating Reactive Polyelectrolytes

Casandra M. Gardner, Nicholas A.D. Burke, Harald D.H. Stöver

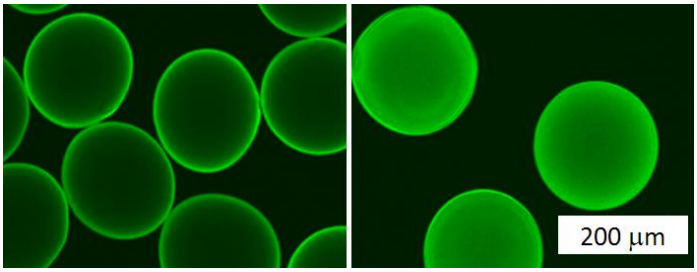

Published in *Langmuir*, **2010**, *26*, 4916-4924.

Contributions:
I performed all experiments except the fluorescent labeling of PLL, which was performed by Dr. Burke. Experiments I performed included: synthesis of PMM_{50}, measurement of rate of hydrolysis, coating optimization, covalent crosslinking experiments, kinetic permeability measurements, and initial protein binding studies. I also wrote the manuscript, with edits and guidance from Dr. Burke and Dr. Stöver.

2.1 Abstract

Poly(methyl vinyl ether-*alt*-maleic anhydride) (PMM_0) was partially hydrolyzed in a 9/1 ACN-d_3/D_2O mixture, then diluted with an aqueous buffer and coated onto poly-L-lysine (PLL)-coated calcium alginate capsules. The resulting 50% hydrolyzed polymer (PMM_{50}) is bound to the surface-immobilized PLL through both electrostatic and covalent interactions, resulting in a shell-crosslinked hydrogel capsule resistant to chemical challenges. Further hydrolysis of PMM_{50} in aqueous buffer was monitored by potentiometry, and found to proceed with a half-life time of about 2.5 minutes at 20°C such that residual anhydride groups not consumed by crosslinking with PLL would be deactivated by hydrolysis within several minutes of shell formation, removing potential sites for undesired protein binding. Initial protein binding tests involving incubation of the capsules in bovine serum albumin solutions for 24 hrs showed no indication of protein binding. The effects of coating temperature, PLL concentration and molecular weight, PMM_{50} molecular weight, and multiple PLL-PMM_{50} coatings on shell morphology and behavior were studied using confocal fluorescence microscopy as well as chemical challenges involving sodium citrate and sodium hydroxide. The resilience of the crosslinked shell improved with increasing concentrations of PLL and decreasing molecular weights of PMM_{50} as both resulted in more polyelectrolyte being bound to the capsule. The permeability of these covalently crosslinked capsules was studied using fluorescently labeled dextrans, and found to be comparable to standard APA capsules.

2.2 Introduction

This thesis describes a new approach to the formation of biocompatible crosslinked membranes, based on covalent reaction between reactive polyelectrolytes that subsequently undergo conversion of their crosslinking electrophilic groups into more desirable carboxylate anions. This approach was designed to reduce the level of inadvertent protein absorption to these membranes, a concept of importance to both industrial anti-fouling approaches and to the design of biomaterials, such as artificial tissues and capsules.

Immunoisolation by microencapsulation of primary or genetically engineered cells of allo- or xenogeneic origin holds great potential for treating many hormone and enzyme deficiency disorders. Principal targets of this approach are a variety of endocrine disorders,[1] including diabetes mellitus[2], hypoparathyroidism, dwarfism[3], central nervous system diseases[4,5,6] including Parkinson's, Alzheimer's, ALS, other genetic disorders including lysosomal storage disorders (LSDs)[7], hemophilia[8] as well as certain types of kidney[9,10] and liver[11] failure.

The basic idea of microencapsulation is to entrap such therapeutic cells in a semi-permeable polymeric hydrogel before implantation into the host such that they remain undetected by the immune system. Where the hydrogel itself is too permeable to immune markers, it can be coated with a permeability-controlling shell. The most common type of such microcapsule is the alginate - poly-L-lysine (PLL) – alginate, or APA capsule,

originally described by Lim and Sun.[2] APA capsules consist of calcium crosslinked alginate hydrogel cores, surrounded by PLL (a polycation) and an outer coating of alginate (a polyanion). Alginate is used for the exterior coating as it provides a non-toxic, negatively charged surface that hides the positively charged PLL from the host.

However, the properties of alginate, a naturally occurring polysaccharide composed of ß-D-mannuronic (M) and α-L-guluronic (G) acids, vary considerably depending upon the source and purification procedures,[12] posing a significant challenge to its use. Alginate has been shown to contain variable amounts of allergenic or immunogenic proteins, polyphenols and endotoxins[13] and require extensive purification to avoid immune responses. APA capsule failure after transplantation has been attributed to gradual weakening of the electrostatically bound alginate coating over time, exposing the underlying PLL to the immune system.[14] As well, alginate has recently been reported to degrade by oxidative-reductive and hydrolytic processes in the body, raising further concerns about long-term applications.[15]

Synthetic polymers have been utilized with varying degrees of success to improve on the mechanical and chemical stability, permeability, and biocompatibility of APA microcapsules.[16,17] The use of synthetic polymers can in principle facilitate tuning of the materials properties, while avoiding the biological impurities found in naturally occurring polymers.

Conventional APA capsules are held together by ionic interactions, and their resistance to different mechanical and chemical challenges can be substantially increased by covalent crosslinking.[18] This approach has led to a variety of chemical and photochemical crosslinking reactions, all carried out under physiological conditions. Concerns here include cytotoxic effects of crosslinking reagents, monomers, photochemical or thermal initiators, catalysts or by-products, the need for extreme pH or temperature, and slow crosslinking reactions leading to residual reactive groups.

An approach that avoids some of these problems is to use polymer-bound reactive groups which are typically less toxic because of lower bioavailability. Hubbell[19] has formed covalent crosslinks throughout a hydrogel core consisting of linear Pluronics polymers, using Michael-type addition between chains having thiol and acrylate end groups. Wang[20,21] has prepared microcapsules that form covalent bonds through photodimerization of modified poly(allylamine) or PLL in the capsular membrane. They have also explored the use of reactive poly(vinyl alcohol) to crosslink PLL at the capsule surface.[21] Photo-crosslinking of macromonomers and modified polymers[22] has also become a significant approach.[23]

We recently described the use of reactive polyanions bearing acetoacetate groups that can form covalent crosslinks with surface-bound poly-L-lysine and other polyamines.[24,25] This approach combines electrostatic attraction and preconcentration between the reactive polyelectrolytes, with subsequent spontaneous covalent crosslinking. While the resulting capsules proved more durable than APA capsules, there was evidence

that the residual acetoacetate groups in the reactive polyanion caused some undesirable protein binding during incubation or post-transplantation.[25]

The fully hydrolyzed poly(methyl vinyl ether-*alt*-maleic anhydride), or PMM_{100}, has been used to replace sodium alginate as the final outer coating material used in APA-type capsules,[26] resulting in improved mechanical strength compared to conventional APA capsules, while maintaining similar permeability.

The present work describes the use of partially (50%) hydrolyzed poly(methyl vinyl ether-*alt*-maleic anhydride), PMM_{50}, as transiently reactive water-soluble polyanions that permit covalent crosslinking with PLL surface layers. The high reactivity of the anhydride groups should ensure both a rapid reaction with the side-chain amines of PLL, as well as fast subsequent hydrolysis of residual anhydride units to form carboxylates. The absence of residual reactive groups during incubation and implantation should minimize protein binding as outlined in Scheme 2.1. This should lead to a diminished immune response compared to the acetoacetate-containing polyanion.

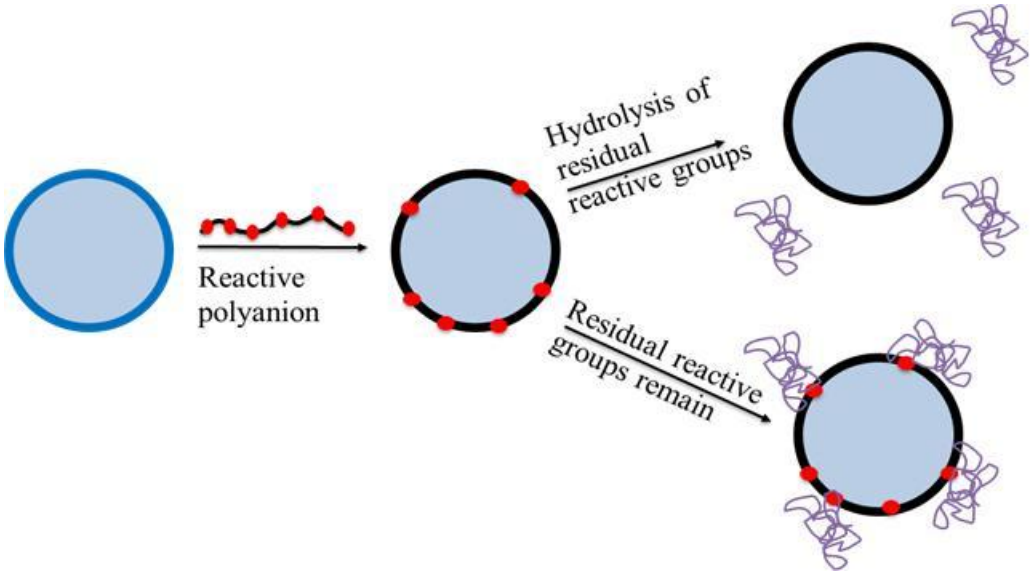

Scheme 2.1 *Schematic representation of coating an AP capsule with reactive polyanions. In PMM_{50} (top path) this is followed by rapid hydrolysis of residual reactive groups. The presence of residual reactive groups may lead to undesirable protein binding during subsequent incubation, or post-transplantation (bottom path).*

2.3 Experimental

2.3.1 Materials

Poly(methyl vinyl ether-*alt*-maleic anhydride) (PMM), as purchased (20 kDa from Scientific Polymer Products, Ontario, NY; 1080 kDa from Sigma-Aldrich, Oakville, ON) was found to be already partly hydrolyzed, and was hence heated in a vacuum oven at

140°C for 5 days to reform the completely anhydridic forms, PMM_0, containing less than 0.5% hydrolysis as determined by ^{1}H-NMR. The fully hydrolyzed analog, PMM_{100}(216 kDa), 5-aminofluorescein (AF), poly(L-lysine hydrobromide) (PLL, 15-30 kDa and 40-60 kDa), tetramethylrhodamine isothiocyanate-conjugated bovine serum albumin (BSA*r*, 66 kDa, 1 mol TRITC per mol albumin), fluorescein isothiocyanate-conjugated dextran (dextran-*f*, 10, 70, 150, 250 and 500 kDa), HEPES sodium salt, acetonitrile-d_3 (99.96 atom% D, ACN-d_3), D_2O (99.99 atom% D) and trypan blue stain (0.4% in 0.81% aqueous NaCl) were purchased from Sigma-Aldrich, Oakville, ON, and used as received. Sodium alginate (Pronova UP MVG, batch no. FP-610-03) was purchased from Novamatrix, Norway. Sodium chloride (Caledon Laboratories Ltd, ON), and calcium chloride (minimum 96% powder, anhydrous, Sigma-Aldrich, ON) were used as received. Sodium hydroxide and hydrochloric acid solutions were prepared from concentrates (Anachemia Chemical, Rouses Point, NY) by diluting to 0.100 M or 1.000 M with deionized water.

2.3.2 Preparation of PMM_{50} and $PMMf_{50}$ by Controlled Hydrolysis of PMM_0

PMM_0 (100 mg) was dissolved in 1.0 mL of an ACN-d_3/ D_2O (9:1 v/v) mixture in a screw-cap glass vial, forming a 10 w/v% solution. The vial was placed in an oven set to 60°C for either 14.5 hrs (20 kDa PMM_0) or 17 hrs (1080 kDa PMM_0), reaction times determined by ^{1}H-NMR to result in 50% hydrolysis, forming PMM_{50} of 20 kDa or 1080 kDa, respectively. After cooling to room temperature, 0.2 mL of the reaction mixture was then diluted to 10 mL with 35 mM HEPES pH 7.8 buffered saline. The resulting slightly turbid solution was immediately agitated on a vortex mixer for 10-30 s to give a clear solution, and then quickly filtered (0.45 μm) to give a final aqueous coating solution containing 0.2 wt% PMM_{50}. The complete dilution/agitation/filtration sequence is completed within one minute in order to minimize hydrolysis, and the solution is immediately used for coating. Coating solutions containing the fluorescently labeled analog $PMMf_{50}$, were prepared in the same way, except that 2 mol% AF (relative to total anhydride) was added at the beginning of the PMM_0 hydrolysis in acetonitrile.

The degree of labeling for $PMMf_{50}$ (20 and 1080 kDa) was determined by dialyzing $PMMf_{50}$ coating solution against deionized water for five days, with daily water changes, using cellulose dialysis tubing with a molecular weight cut-off of 3.5 kDa (Spectra/Por®, VWR Scientific, Mississauga, ON) and 14 kDa (Membra-cel, Viskase, Darien, IL), respectively. The polymer solution was concentrated using a rotary evaporator and isolated by freeze-drying. UV-visible spectroscopy was used to determine the degree of labeling; 1.03% and 0.88% for $PMMf_{50}$ of 20 and 1080 kDa, respectively.

2.3.3 Preparation of FITC-labelled Poly(L-Lysine) (15-30 and 40-60 kDa).

FITC-labelled poly(L-lysine), PLL*f*, was prepared as described earlier.[27] For example, PLL (15-30 kDa, 100 mg, 0.48 mmol lysine HBr units) was dissolved in 10 mL of 0.1 M $NaHCO_3$ buffer (pH 9) in a 20 mL glass vial. FITC (2.0 mg, 0.005 mmol)

dissolved in 0.2 mL DMF was added to the PLL solution and the mixture was stirred for 90 min at 20 °C. The resulting solution was adjusted to pH 7 with 1 M HCl and then dialysed for 5 days in deionized water using cellulose tubing (Spectrum Laboratories, 3.5 kDa MW cut-off) with daily water changes until the dialysate showed no absorbances for DMF or fluorescein. PLL*f* (15-30 kDa) was isolated by freeze-drying. Yield: 68.5 mg. The labelling degree was determined to be 1.05 mol% by UV-visible spectroscopy (73000 $M^{-1}cm^{-1}$) in 35 mM HEPES buffer (pH 7.4).

PLL*f* (40-60 kDa) was prepared in a similar manner from PLL (40-60 kDa, 202.8 mg, 0.97 mmol) in 18 mL of 0.1M $NaHCO_3$ buffer (pH 9) and FITC (3.7 mg, 0.0095 mmol) in 0.37 mL DMF except that dialysis tubing with a 14 kDa MW cut-off (Membra-Cel, Viskase Corp., Darien, IL) was used. Yield: 148.2 mg. Labelling degree: 0.85%.

2.3.4 Standard Procedure for Formation of Alginate-PLL-PMM_{50} (AP-PMM_{50}) and APA Capsules

All capsules were prepared by a procedure, derived from Sun[28] that has been described previously.[24] Briefly, a 1.0 wt% sodium alginate solution in aqueous saline was filtered (0.45 μm) and extruded through a 27 gauge needle at a liquid flow rate of 0.5 mL/min into a gelling bath containing 1.1 wt% calcium chloride and 0.45 wt% sodium chloride. The resulting calcium alginate beads were washed once with fresh gelling bath solution, followed by a saline wash. The alginate beads were then coated with PLL (15-30 or 40-60 kDa, both at 0.05 and 0.25 wt%) for 6 min. The resulting AP capsules were washed twice with saline, and coated with a 0.2% PMM_{50} (20 or 1080 kDa) solution for 6 min at 10°C, followed by a saline wash. Standard APA capsules where coated using PLL(0.05%, 15-30 kDa) and a 0.03% alginate solution for 6 mins. All coating and washing steps involved a 3:10 volume ratio of concentrated bead suspension to coating or saline wash solution.

2.3.5 Standard Procedure for Formation of Alginate-[PLL-PMM_{50}]$_2$ (A[P-PMM_{50}]$_2$) four-layer Capsules

Analogous four-layer capsules were prepared by coating Ca-Alg cores with, in sequence, PLL (0.05%, 15-30 kDa) for 6 min, PMM_{50} (0.2%, 1080 kDa) solution for 4 min, PLL (0.05%, 15-30 kDa) solution for 6 mins, and PMM_{50} (0.2%, 1080 kDa) solution for 6 min, with two saline washes after each PLL coating and after the final PMM_{50} coating, and one saline wash after the first PMM_{50} coating.

2.3.6 PMM hydrolysis calibration curve

Appropriate amounts of fully hydrolyzed poly(methyl vinyl ether-*alt*-maleic anhydride), $PMM_{100,}$ were dissolved in 35 mM HEPES pH 7.8 buffered saline, to mimic the amount of carboxylic acid groups present in a 0.2% PMM solution with degrees of

hydrolysis of approximately 20, 40, 50, 60, 80 and 100%. The pH of these solutions were measured and used to generate a pH vs. % hydrolysis calibration curve.

2.3.7 Characterization

Proton NMR spectra were obtained on a Bruker AV200 spectrometer. The pH of aqueous solutions was measured on a Corning 440 pH meter. Rates of hydrolysis in aqueous saline were determined by monitoring pH with time using a PC-Titrate (Mandel Scientific) automatic titrator.

Capsules were examined by optical and fluorescence microscopy with an Olympus BX51 optical microscope fitted with a Q-Imaging Retiga EXi digital camera and ImagePro software. Capsules were also examined using a ZEISS LSM 510 confocal laser scanning microscope (CLSM) fitted with air-cooled Argon and HeNe lasers (LASOS; LGK 7628-1), and running LSM Image browser software (version 3.5). Images were further analyzed with ImageJ software to generate 10 pixel wide line profiles.

2.3.8 Kinetic Permeability Study

Capsule permeability was evaluated using dextran-*f* samples of 10, 70, 150, 250 and 500 kDa. For each dextran, approximately 20 AP-PMM_{50} capsules were placed on a microscope slide in the centre of a Teflon washer (1.5 cm diameter, 300 μm high), exposed to 200 μL of 0.1% dextran-*f* in saline, promptly covered with a glass cover slip and examined by fluorescence microscopy. This procedure, described recently,[26] flattens and seals the top and bottom surfaces of the beads, transforming them into rounded cylinders that permit observation of lateral in-diffusion of the dextran-*f*. Images were taken every minute for 20 min and the fluorescence intensities from the central ca. 20% of the beads, as well as from the surrounding continuous phase, were obtained using the ImagePro software. Reported are the ratios of intensities of the bead centre and the continuous phase, in order to compensate for photobleaching. These permeability measurements were carried out in triplicate for each dextran-*f* MW.

2.3.9 Test for Covalent Crosslinking

Capsules made with a fluorescently-labeled PMM*f* were tested for crosslinking by placing one drop of a concentrated capsule suspension containing about 30 capsules on a microscope slide mounted on a fluorescence microscope. The supernatant was removed and immediately replaced with 2 drops of 1M sodium citrate, a good calcium chelator, and the capsules were gently mixed. This process was repeated once. Subsequently, the supernatant was replaced with two drops of 0.1 M sodium hydroxide under gentle agitation, and the integrity of any remaining shells assessed qualitatively by fluorescence microscopy.

2.3.10 Protein Binding study

This procedure was carried out as described by Shen (2009).[25] Briefly, 0.1 mL of concentrated bead suspension was added to 1 mL of a 0.05% solution of rhodamine-labelled BSA (BSA*r*) in saline. After 24 hrs at room temperature, the capsules were washed five times with 1 mL saline for 2 min before examination by confocal microscopy for the presence and distribution of any residual BSA*r*.

2.4 Results and discussion

This work investigates the use of a polyanion bearing short-lived reactive groups for cell encapsulation within polyamine-coated alginate beads. The polymer should allow electrostatic preconcentration by complexation to surface-bound PLL, followed by rapid formation of a covalently crosslinked shell, and subsequent hydrolysis of residual reactive electrophilic groups to prevent inadvertent covalent protein binding. The polymer chosen for investigation was an alternating copolymer of methyl vinyl ether and maleic anhydride (PMM_0 or Gantrez AN) that is commercially available in a variety of molecular weights.

One challenge in using PMM-type copolymers as coatings for AP capsules is that the all-anhydride material, PMM_0, is insoluble in the aqueous solutions required for coating hydrogel capsules. It was thus necessary to develop a method for controlled partial hydrolysis of PMM_0 to the point where the polymer was water-soluble but still carried sufficient anhydride groups for effective crosslinking. This partial hydrolysis should be carried out in homogeneous solution to ensure a consistent degree of hydrolysis across all chains. This required a water-miscible solvent that readily dissolves both PMM_0 and its partially hydrolyzed forms. The solvent should also have low cytotoxicity since it will be present in the aqueous coating solution following dilution of the hydrolysis mixture with buffered saline. It was also desirable to be able to use deuterated versions of the organic solvent, in order to follow the hydrolysis by ^{1}H-NMR.

Dimethyl sulfoxide (DMSO), a solvent initially targeted for its good solvency properties and good cell compatibility, had to be rejected as it showed a persistent pink colour upon dissolution of PMM_0 that was attributed to reaction between the anhydride groups and DMSO.[29,30] Acetonitrile (ACN), a solvent with acceptable cell compatibility given the short exposure (≤10 min) to about 2% ACN in saline,[31] was eventually selected. In particular, a 9/1 v/v mixture of ACN-d_3/D_2O was found to easily dissolve 10 wt% PMM_0 at room temperature and to give controlled partial hydrolysis at 60^{o}C leading to PMM_{50} as monitored by ^{1}H NMR. The reaction remained visually homogeneous throughout the reaction, ensuring consistent degrees of hydrolysis across all chains.

Figure 2.1 shows ^{1}H NMR spectra of a 10 wt% PMM(1080 kDa) solution during such a hydrolysis. The CH signal of the anhydride units of PMM moves upfield during hydrolysis, from 3.2 ppm for the anhydride to 2.8 ppm for the dicarboxylic acid. Comparison of the areas under the peaks at 2.8 ppm and 2.1 ppm (CH_2 of MVE) gave the

degree of hydrolysis. PMM(1080 kDa) solutions stayed homogeneous upon dilution with a 50 fold excess of saline after 17 hrs at 60°C when this PMM was 50% hydrolyzed (PMM_{50}). The lower molecular weight PMM(20 kDa) gave clear solutions upon dilution in saline at 40% hydrolysis, reached after 13 hrs at 60°C. For consistency, 50% hydrolysis was used for coatings with both molecular weights of PMM.

Although the 2.8 ppm peak overlaps slightly with the 3.2 ppm peak, the integration is reproducible, giving % hydrolysis values similar to titration (*vide infra*) and accurately measures the degree of hydrolysis of PMM_{100} (100 ± 2%, data not shown).

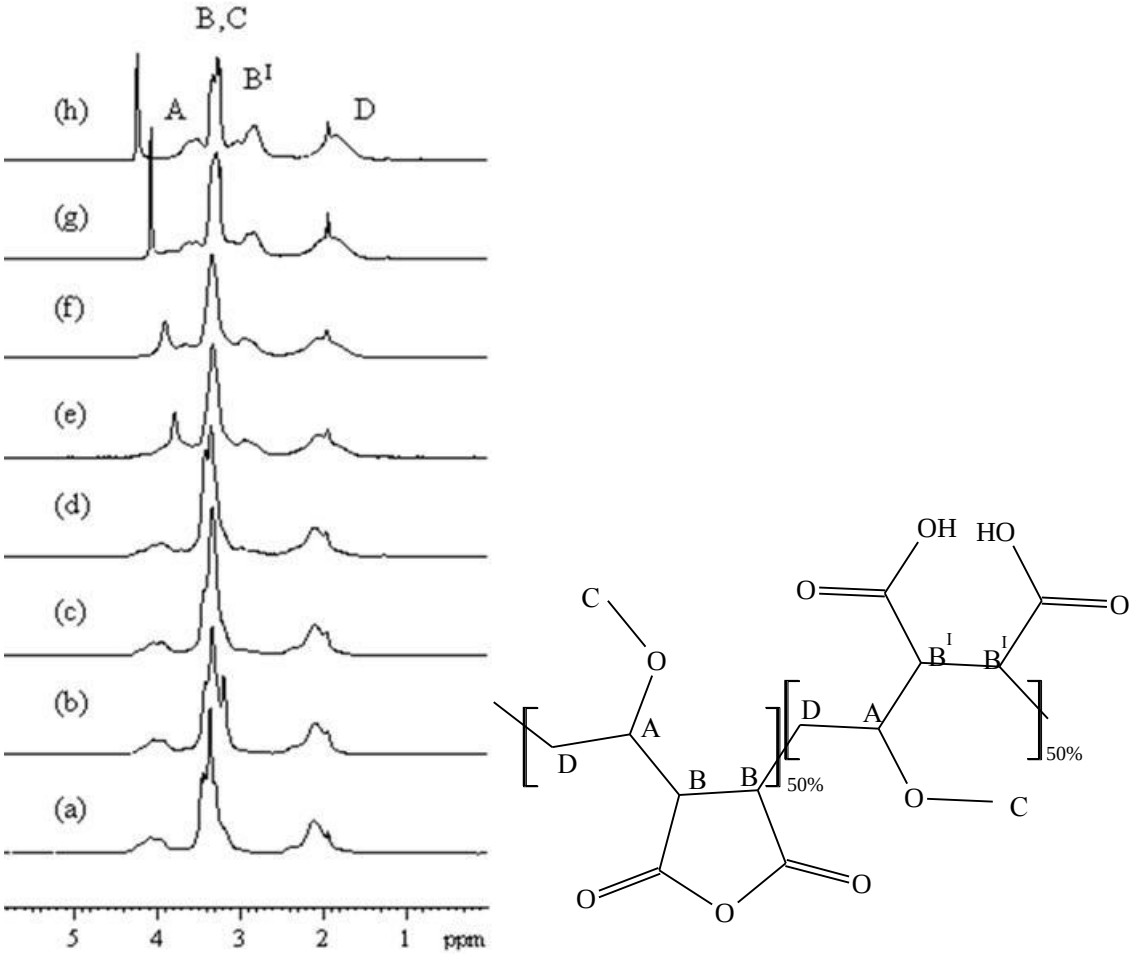

Figure 2.1 *(left) ^1H NMR spectra of a 10% PMM(1080k) solution in ACN-d_3/D_2O, heated at 60°C.* ***(a)*** *in ACN-d_3 prior to addition of D_2O,* ***(b)*** *at t = 0 hrs in a 9/1 mixture of ACNd_3/D_2O,* ***(c)*** *after 3 hrs in a 9/1 ratio,* ***(d)*** *after 6 hrs in a 9/1 ratio,* ***(e)*** *after 17 hrs in a 9/1 ratio,* ***(f)*** *after 23 hrs in a 9/1 ratio,* ***(g)*** *at 30hrs, immediately after adding enough D_2O to give a 3/1 ratio of ACN-d_3 / D_2O,* ***(h)*** *at 52 hrs in a 3/1 ratio. Further heating gave no change in the spectrum (right). Structure of PMM_{50}: 2.1 ppm (CH_{d2}), 2.8 ppm ($CH_{b'}$), 3.2 ppm (CH_b, CH_{c3}), 4.1 ppm (CH_a). The peak for DHO shifts from 3.2 to 3.9 ppm during the hydrolysis.*

PMM hydrolysis in 9/1 ACN-d_3/D_2O is quite slow, and speeds up by several orders of magnitude after dilution in an aqueous buffer to make the coating solution. The rate of hydrolysis of PMM_0 in sodium borate buffered solutions has been measured by Ladaviere[32] by monitoring the pH until it remained constant. They observed that hydrolysis was complete after 80 min at 67°C and pH ~7. However, slow dissolution of PMM_0 in the aqueous medium may have contributed to their apparently slow hydrolysis. Indeed, small-molecule cyclic anhydrides such as succinic anhydride hydrolyze rapidly in aqueous media near pH 7 ($t_{½}$ ~7 min at 20 °C in 28.5% ethanol/water[33] and ~4 min at 25°C in water[34]).

The ACN-d_3/D_2O solution of PMM_{50} was diluted 50-fold in 35 mM HEPES-buffered saline (pH 7.8). HEPES was selected because it is cell compatible and does not react with anhydrides. An initial buffer pH of 7.8 was chosen because it resulted in a coating solution with pH close to 7 after PMM_{50} addition. This 35 mM HEPES buffered saline solution also showed a measurable change in pH during model reactions that allowed determination of the rate of hydrolysis after dilution, going from PMM_{50} towards PMM_{100}. The degree of hydrolysis was determined by monitoring the pH and comparing it with a calibration curve (Figure 2.2a) generated by dissolving PMM_{100} in the buffer in amounts corresponding to the succinic acid concentration present in a 0.2 wt% PMM_x solution at x = 0, 22, 41, 49, 61, 78, and 95.5% hydrolysis. The resulting calibration includes the assumption that the difference in polyelectrolyte effects between PMM_{100} and PMM_x is minor compared to the measured pH change.

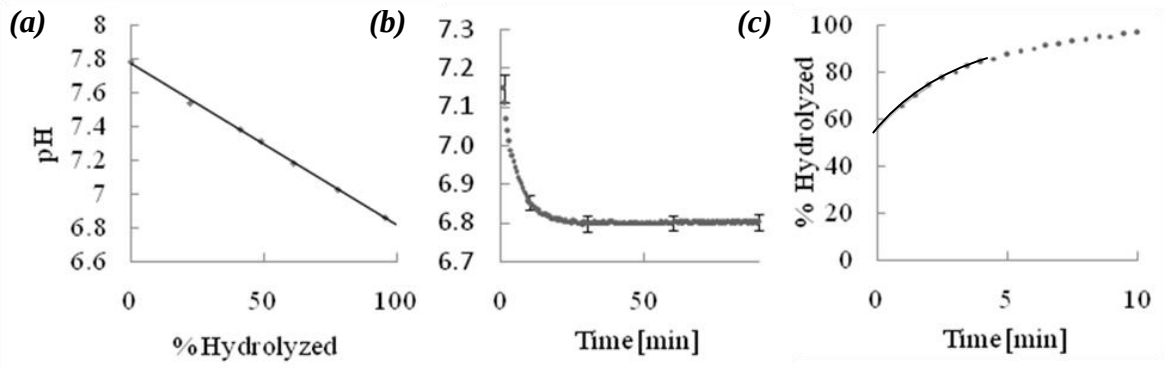

Figure 2.2 (a) *Calibration curve of pH versus amount of PMM_{100} added to 35 mM HEPES pH 7.8 buffered saline;* ***(b)*** *pH change over time, following the addition of a 50% hydrolyzed solution of PMM_{50} (20kDa) (10 wt%) in ACN-d_3 / D_2O (9/1) to a 50 fold excess of 35 mM HEPES pH 7.8 buffered saline at 20°C (only 5 representative error bars are shown for clarity, each representing five replicates)* ***(c)*** *percent hydrolysis of PMM_x following dilution into buffered saline, obtained by combining data in Figures 2.2a and 2.2b. The line, extrapolating to 55% at t = 0, is fitted visually and meant to guide the eye.*

When PMM_{50} was added to the buffer solution the pH dropped rapidly and stabilized at a pH corresponding to PMM_{100}, showing that hydrolysis was complete, within about 30 min (Figure 2.2b). Figure 2.2c combines data from 2.2a and 2.2b to show the degree of hydrolysis versus time in the buffer solution. This reveals that the degree of hydrolysis increases from about 65% to 83% between 1 and 3.5 minutes, corresponding to a half-life time of the anhydride groups of approximately 2.5 min, consistent with the hydrolysis rates observed for succinic anhydride,[33,34] but much faster than that measured for PMM_0.[30] This discrepancy likely reflects the fact that PMM_{50} is fully soluble in the aqueous solution while PMM_0 is not, leading to apparent rates of hydrolysis dominated by the slow rate of dissolution, or etching.

This high rate of hydrolysis of PMM_{50} limits the time available to coat the alginate beads to a few minutes, but also ensures that virtually no reactive anhydride groups remain 30 minutes after the coating process. Thus, it should be possible to produce covalently crosslinked coatings while avoiding covalent binding of proteins during later incubation or implantation.

The two methods used to measure the rate of hydrolysis, ^{1}H NMR and pH change in a buffered solution, agree well with each other. Just prior to dilution in the aqueous buffer solution, the degree of hydrolysis as measured by ^{1}H NMR was 50%. Extrapolating visually back to time zero along the pH versus time curve (Figure 2.2c) gives a degree of hydrolysis of ~55%.

2.4.1 Formation of capsules with crosslinked shells consisting of PLL/PMM

To evaluate the ability of PMM_{50} to form crosslinked shells on PLL-coated calcium alginate beads, a number of A-PLL-PMM_{50} type beads were prepared, using different molecular weights of PLL and PMM_{50}, as shown in Table 2.1.

Name	PLL wt%, MW [kDa]	PMMf_X MW [kDa]
[0]	0.05%, 15-30	PMMf_{100} 1080
[1]	0.05%, 15-30	PMMf_{50} 1080
[2]*	0.05%, 15-30*	PMMf_{50} 1080*
[3]	0.05%, 40-60	PMMf_{50} 1080
[4]	0.25%, 15-30	PMMf_{50} 20
[5]	0.25%, 40-60	PMMf_{50} 20

Table 2.1 *A-PLL-PMMf_X and A-[PLL-PMMf_{50}]$_2$ Microcapsules formed*
*four-layer capsule A[PLL-PMMf_{50}]$_2$.

The microcapsules **[0]** were control capsules prepared using fully hydrolyzed PMMf_{100}[1080 kDa]. As reported recently, ionic interactions alone suffice to form a polyelectrolyte complex shell between PLL and PMM_{100}.[26]

The microcapsules **[1]** were formed by coating calcium alginate beads first with PLL (0.05%, 15-30 kDa) and then with a fluorescently labeled analog to PMM_{50}, $PMMf_{50}$ (1080 kDa). Figures 2.3a and 2.3b show the conventional and confocal fluorescence microscopy images of the resulting A-PLL-$PMMf_{50}$ capsules, **[1]**, described in Table 2.1. The images reveal that this high MW PMM*f* is restricted to the surface of the capsule and that it is homogeneously distributed over the surface.

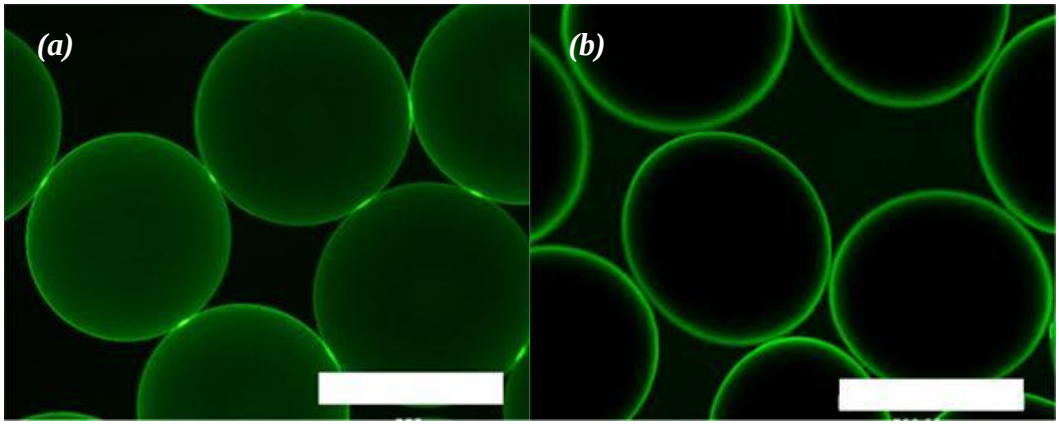

Figure 2.3 (a) *Conventional and* ***(b)*** *confocal fluorescence microscopy image of* ***[1]****. Scale bars are 500 µm.*

To confirm that the present shells involve covalent crosslinking in addition to the electrostatic interactions, the beads **[1]** were exposed in sequence to 1 M sodium citrate to chelate calcium and dissolve the calcium alginate hydrogel core, and to 0.1 M sodium hydroxide to deprotonate PLL and break its electrostatic interactions with the polyanions. This method is based on similar tests reported by Dusseault (2005)[22], and leaves only covalent crosslinks to preserve the structure of the shell.

Figure 2.4 shows fluorescence microscope images (grey scale) during this sequence of citrate and hydroxide challenges**.** Capsules **[0]** coated with $PMMf_{100}$ (a1), the strictly ionic control version, deflate upon extraction of calcium with citrate but still show distinct shells consisting of an A-PLL-$PMMf_{100}$ polyelectrolyte complex (a2). When challenged with 0.1 M NaOH though, the polyelectrolyte complex dissolves entirely (a3).

The second column shows the conversion of A-PLL-$PMMf_{50}$ **[1]** (a1) to hollow shells following treatment with citrate (b2). At this stage the shells may be sustained by ionic crosslinks between PLL and both alginate and PMM, as well as by covalent crosslinks between PLL and PMM. Subsequent exposure to sodium hydroxide reveals the presence of shell fragments, indicating the presence of covalent crosslinking in the shell (b3).

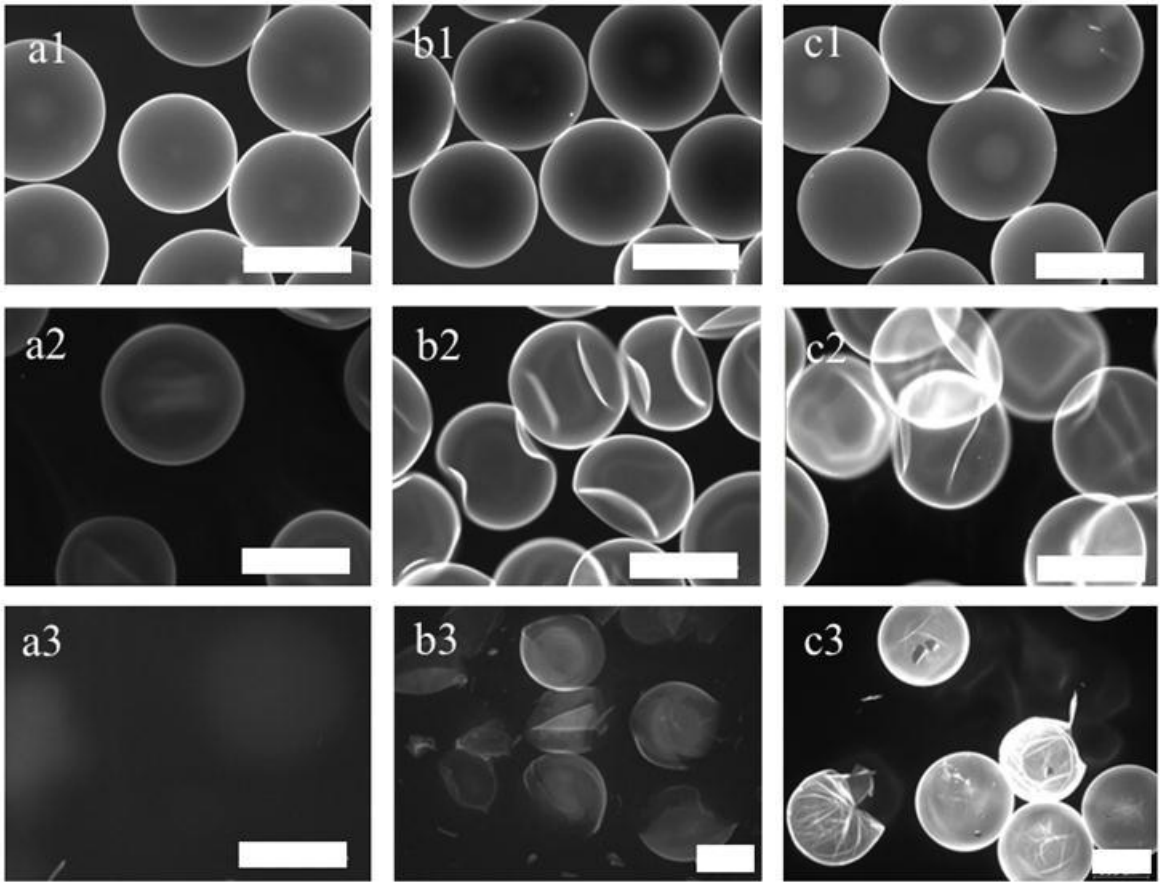

Figure 2.4 *Conventional fluorescence microscopy images of (column a) A-PLL-PMMf_{100} (1080k),* ***[0]****; (column b) A-PLL-PMMf_{50},* ***[1];*** *and (column c) A-[PLL-PMMf_{50}]$_2$,* ***[2]****: as formed (a1, b1, c1), after treatment with 1 M sodium citrate (a2, b2, c2), and after subsequent treatment with 0.1 M sodium hydroxide (a3, b3, c3). Scale bars are 500 µm.*

These results confirmed the presence of crosslinked shells formed by reaction between PLL and partially hydrolyzed PMM_{50}. To improve the strength of the covalently crosslinked shell, the effect of varying the number of coating layers, the coating temperature, the molecular weight and concentrations of PLL, and the molecular weight of PMMf_{50} was examined. The primary aim was to increase the covalent crosslinking between the two polyelectrolytes while maintaining permeability suitable for cell encapsulation and immuno-isolation.

2.4.2 Four-Layer capsules

To augment the covalently crosslinked PLL / PMM_{50} component of the shell the initially formed A-PLL-PMMf_{50} capsules were coated with a second layer of PLL, followed by a second layer of PMMf_{50} (Figure 2.4, c1). In this capsule, crosslinking should occur between all four exterior coatings, provided that some reactive anhydrides remain in the initial PMMf_{50} layer at the time of coating with the second PLL layer. Considering the data in Figure 2.2c, the initial PMM_{50} layer should be almost completely hydrolyzed after six minutes. Thus the coating duration for the initial PMM_{50} coating in these four-layer capsules was reduced to four minutes, and the second PLL coating was applied after a single quick saline wash. The final PMMf_{50} coating was applied as usual. Treatment of these capsules **[2]** (Figure 2.4, c1) with citrate (c2) followed by sodium hydroxide reveals the presence of more pronounced final shells (c3), indicating significantly improved shell strength. Adding additional layers is clearly one promising approach to forming stronger covalently crosslinked capsule shells.

2.4.3 Encapsulation temperature

Most cell encapsulations are carried out at 4-10^{o}C in order to protect the cells by lowering their metabolic rate. Polymer solvation, as well as the rates of hydrolysis and crosslinking are temperature dependent. Hence, coating of A-PLL beads with PMM_{50} was carried out at 10^{o}C, as well as at room temperature. The rate of hydrolysis should be lower at 10^{o}C, allowing more time for coating and crosslinking, as well as leaving more anhydride groups to react with the amine groups of PLL. Measurements for both PMM_{50} of 20 kDa and 1080 kDa indicated that the rate of hydrolysis decreased slightly at 10^{o}C (by about 5%). A-PLL-PMM_{50}(1080 kDa) capsules formed at 10 ^{o}C showed properties indistinguishable from analogs made at room temperature, while A-PLL-PMM_{50}(20 kDa) capsules formed at 10^{o}C showed slightly improved surface smoothness. Therefore, and for better correlation with future cell encapsulations, subsequent coatings were carried out at 10^{o}C.

2.4.4 Effect of PLL molecular weight and concentration on PLL binding

The thickness and density of the crosslinked shells depend on the ability of the two polyelectrolytes to diffuse into the calcium alginate matrix. Lower MW PLL has been shown to diffuse further into calcium alginate-based beads,[27] and would be expected to give rise to thicker crosslinked shells, provided the reactive polyanion PMM_{50} can follow. As a first step, FITC–labeled poly-L-lysine, PLL*f*, of two different molecular weights and at two different concentrations, were coated onto the present calcium alginate beads, and the resulting distributions studied by confocal fluorescence microscopy. Figure 2.5 shows equatorial sections, together with 10 pixel wide intensity profiles that were corrected for the slightly different degrees of labeling of the two polycations used.

The lower MW PLL*f*, 15-30kDa, is shown to be concentrated near the surface at low coating concentration (0.05%, Figure 2.5a), however some PLL*f* is able to penetrate into the core of the present capsules. Higher coating concentration of the same MW PLL*f* (0.25%, Figure 2.5b) enabled further penetration into the beads.

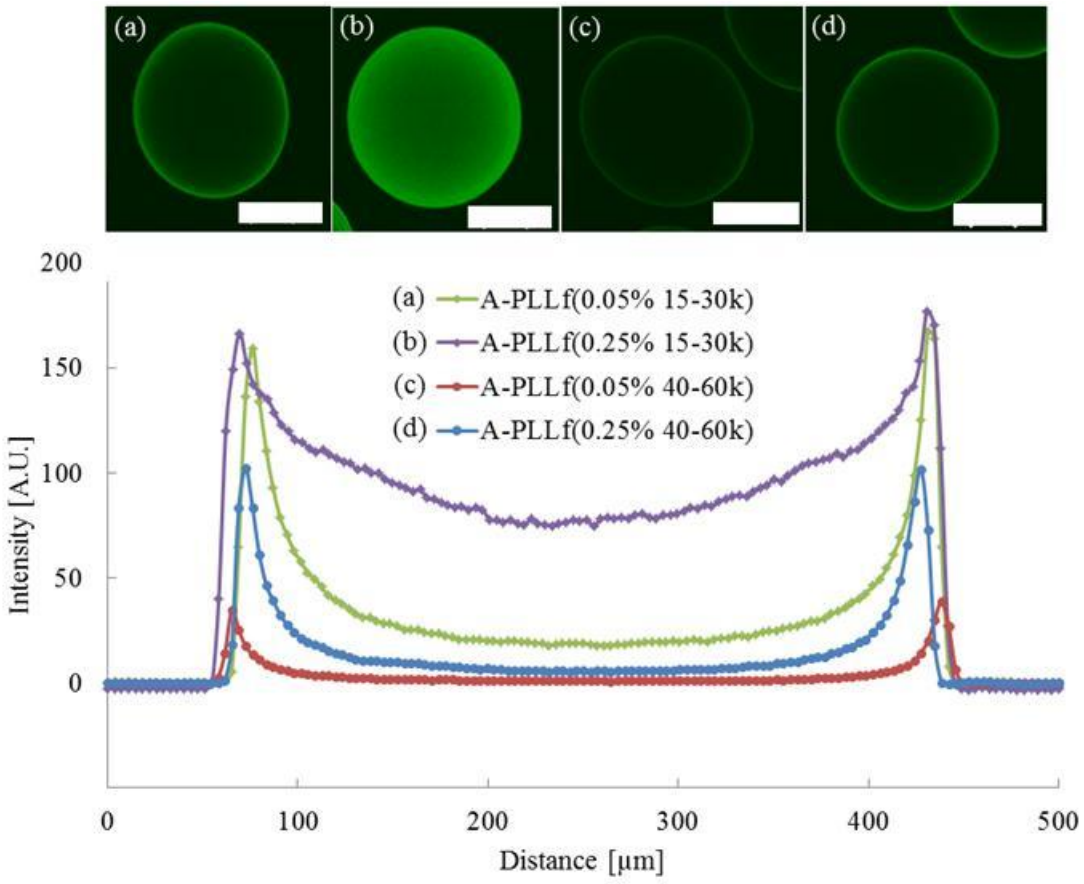

Figure 2.5 *Top: Confocal microscopy images of calcium alginate beads coated with PLLf:* ***(a)*** *15-30 kDa, 0.05%,* ***(b)*** *15-30 kDa, 0.25%.* ***(c)*** *40-60 kDa, 0.05%,* ***(d)*** *40-60 kDa, 0.25% Bottom: line profiles of images a-d. Scale bars are 200µm.*

The higher MW PLL*f* (40-60 kDa) was found to be restricted to the outer shell of the capsules, at either of the two concentrations used (0.05%, Figure 2.5c; and 0.25%, Figure 2.5d) but with a considerably higher concentration of PLL at the surface when the 0.25% concentration was used. The much lower peak height of the 40-60 kDa PLL at 0.05% relative to the 15-30 kDa PLL suggests that the alginate beads have a low binding capacity for this higher MW polycation, possibly due to size exclusion. When the higher concentration of this 40-60 kDa PLL is used higher surficial and interior binding is

observed, both of which are attributed to the lower MW fraction of this polycation sample.

2.4.5 Effect of PMM MW and Concentration on PMM binding

Unlabelled A-PLL beads were next exposed to PMMf_{50} of different MW and concentrations. Figure 2.6 compares the resulting confocal A-PLL-PMMf_{50} profiles with the corresponding A-PLL*f* profiles described above. All profiles are corrected for different degrees of fluorescent labeling, and assuming the same fluorescence efficiencies for labels on both polyelectrolytes.

Considering the anionic nature of both alginate and PMM, the in-diffusion of PMM*f* is assumed to require prior penetration of PLL. Accordingly, MW of either PLL or PMM could limit the depth of penetration of PMM, and hence the depth of covalent crosslinking.

Confocal intensity profiles of the original A-PLL-PMMf_{50}(1080kDa) capsules **[1]**, Figure 2.6a, showed that this high MW PMM cannot easily follow the low MW PLL into the bead. Interestingly, roughly twice as much PMMf_{50}(1080kDa) was bound to the capsules when PLL(40-60kDa) was used (Figure 2.6b) even though much less of this PLL is bound to the capsule surface. It is possible that the higher MW PLL, bound to the alginate surface, has more dangling PLL segments available for binding with PMM.

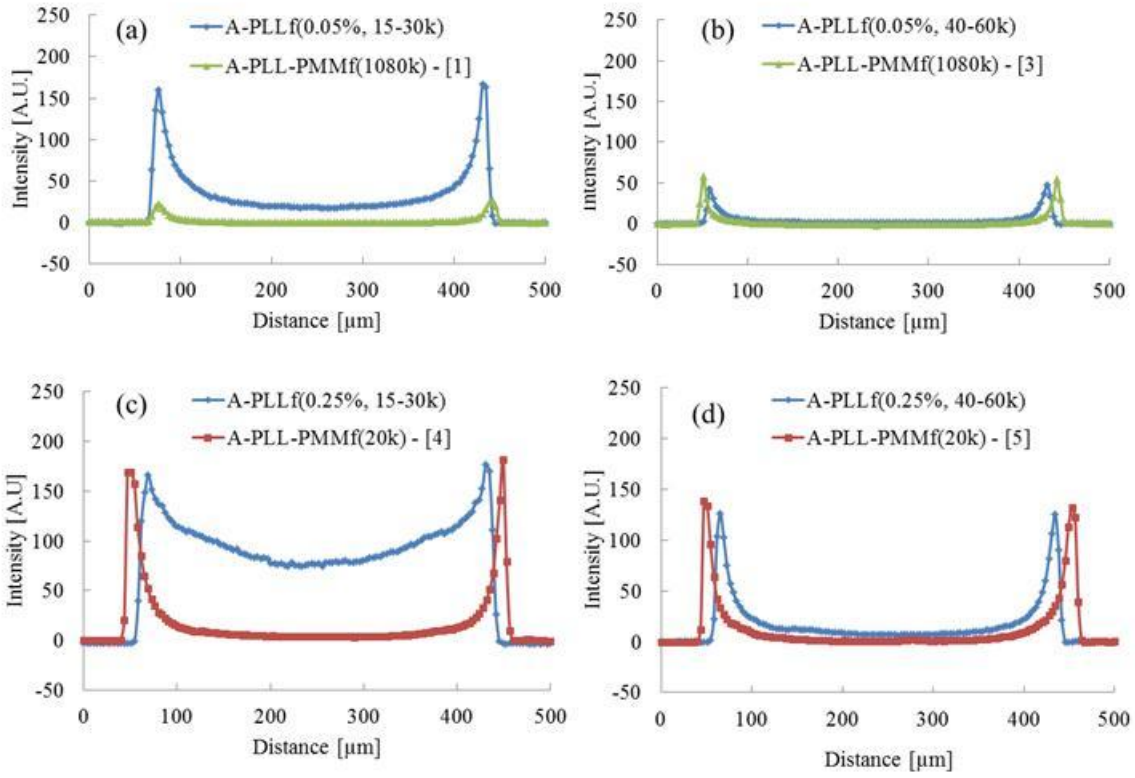

Figure 2.6 *Line profiles from confocal images of* ***(a) [1]*** *and analogous A-PLLf(0.05%, 15-30k)* ***(b) [3]*** *and analogous A-PLLf(0.05%, 40-60k),* ***(c) [4]*** *and analogous A-PLLf(0.25%, 15-30k),* ***(d) [5]*** *and analogous A-PLLf(0.25%, 40-60k). All profiles corrected for degrees of labeling, assuming the same fluorescence efficiencies for labels on both polyelectrolytes.*

In an attempt to prepare crosslinked PLL-PMM shells that were either thicker or denser, capsules were prepared with 15-30k and 40-60k PLL at the higher concentration (0.25%) to increase the PLL loadings, and with a lower MW PMMf_{50} (20 kDa). This lower MW PMMf_{50} (20 kDa) should be better able to access the PLL binding sites near the gel surface, and to diffuse deeper into the gel bead. Confocal analysis of **[4]** (0.25% PLL 15-30k), revealed that these capsules could bind about approximately seven times more PMMf_{50}(20k) than the original capsule **[1]** (0.05% PLL 15-30k), though exclusively near the surface (Figure 2.6c). Capsule **[5]**, surface-saturated with 0.25% of the higher MW PLL (40-60kDa), also binds high amounts of PMMf_{50}(20kDa) (Figure 2.6d). The increased binding of PMM is attributed to both the higher PLL concentration at or near the capsule surface and to better access of PMMf_{50}(20 kDa) to surface and near-surface PLL.

The integrity of the crosslinked shells was probed by sequential exposure to sodium citrate and sodium hydroxide. Figure 2.7 shows grey scale fluorescence images of capsules **[3]**, **[4]** and **[5]** as formed, after extraction of calcium by sodium citrate, and after subsequent exposure to 0.1N sodium hydroxide, respectively. All three capsules form hollow shells after citrate extraction (Figure 2.7; b1, b2, b3). These hollow shells are comprised of electrostatic complexes between PLL and both alginate and PMM, and the covalently crosslinked network formed by amide formation between the PLL and the anhydride groups on the PMM_{50}. Capsules **[4]** feature a thick shell, revealed through their large bending radius and their biconcave disk structure (Figure 2.7, b2), which is attributed to the deep penetration of 15-30 kDa PLL (Figure 2.5b), and its electrostatic complex with alginate. Capsules **[3]** and **[5]** show much thinner shells, reflecting the lower penetration of the higher MW PLL used in these capsules (Figure 2.7, a2 and c2). This sodium citrate test hence supports the confocal analysis, giving good insight into the internal architecture of the capsules.

Subsequent exposure to 0.1 N sodium hydroxide deprotonates the PLL, and thus eliminates all electrostatic contributions to the capsule shells. Capsules **[3]**, **[4]** and **[5]** (Figure 2.7, a3 - c3) all survive this treatment better than the original crosslinked capsule **[1]** (Figure 2.4, b3), indicating their more effective crosslinking. They are all fully re-swollen, likely due to their large net anionic charge density. Of these three, capsules **[4]** and **[5]** appear to be the strongest, with at least 90% of the shells surviving this harsh treatment intact, compared with ~70 % of the capsules **[3]**.

The use of higher PLL(15-30k) concentrations results in thick-walled capsules **[4]** that seem well able to survive calcium loss (Figure 2.7 b2), though it also leads to high concentrations of PLL in the capsule interior. It remains to be seen if the presence of the resulting alginate-PLL complexes in the capsule interior aids in cell attachment, presents a physical barrier to cell proliferation, degrades over time, or perhaps proves cytotoxic to some encapsulated cells. Thus, it may prove to be preferable to restrict PLL to the capsule exterior by using higher MW PLL, such as 40-60kDa as in capsule **[5].** Alternatively, it may be interesting to use PMM_{50} with MW even lower than 20 kDa to allow it to diffuse further into the PLL-rich cores, and to achieve thick, covalently crosslinked shells.

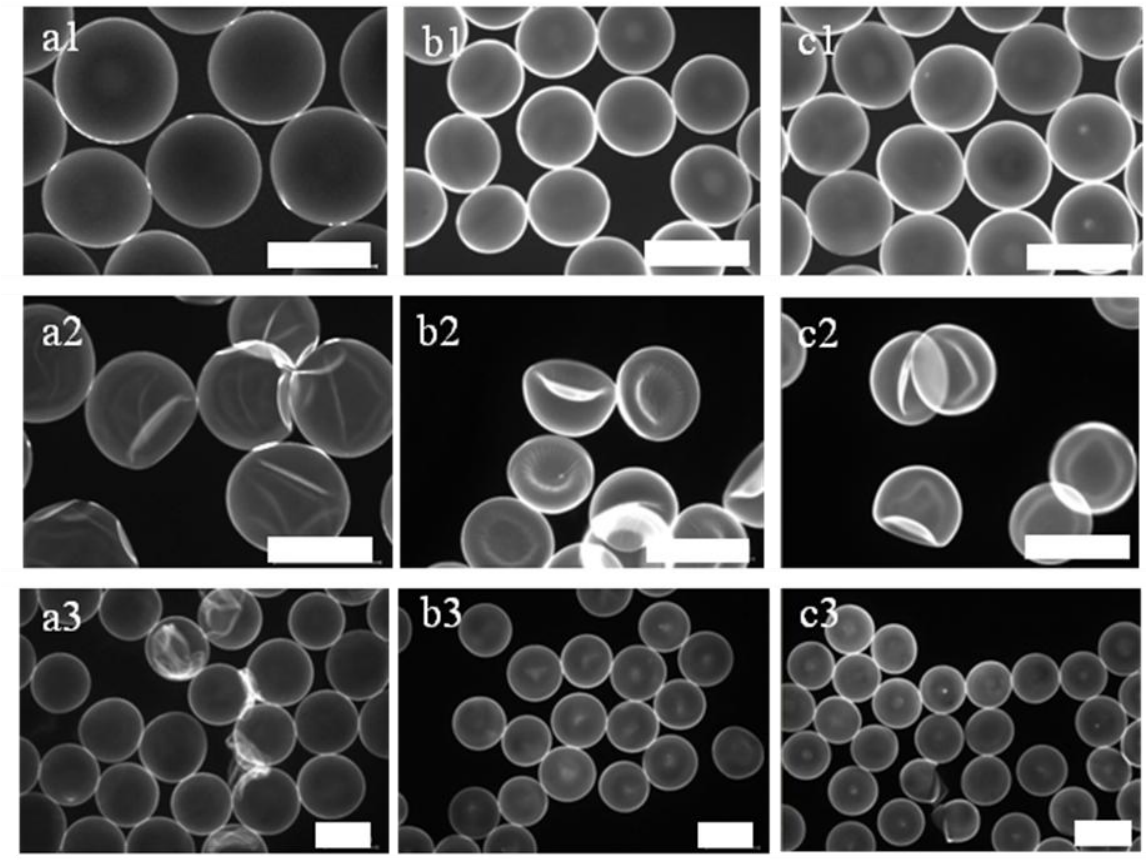

Figure 2.7 *Fluorescence optical microscopy images for (column a)* ***[3],*** *(column b)* ***[4]*** *and (column c)* ***[5]****; as formed (row 1), after the 1M citrate test (row 2), and after the addition of 0.1M sodium hydroxide (row 3). Scale bars are 500 µm.*

2.4.6 Permeability studies on optimized capsule

To confirm that these covalently crosslinked capsules still afford the permeability required for immunoisolation and cell viability, a kinetic permeability test as recently developed[26] was used to measure the rate of in-diffusion of a number of fluorescently labelled dextrans. Figure 2.8 shows that 10 kDa dextran*f* is able to diffuse rapidly into **[3]**, reaching equilibrium within less than 10 minutes, and suggesting that oxygen and small metabolites would rapidly pass through the exterior membrane. These results are comparable to those seen for APA capsules. The 70 and 150 kDa dextran*f* samples diffuse in at a much slower rate, and the 250 and 500 kDa dextrans are essentially excluded from the beads, suggesting that these crosslinked shells combine good permeability for low MW species with exclusion of high MW species, a desirable feature for materials designed for immuno-isolation. Very similar results were observed for other compositions of AP-PMM_{50} capsules. The apparent high rate of in-diffusion of the 150 kDa dextran*f* is

attributed to its extremely broad size distribution, which includes a significant amount of quite low MW chains, as described earlier.[26]

These results were also consistent with permeability measurements involving in-diffusion of dextran*f* measured by confocal fluorescent microscopy after 24 h incubation with dextran*f* solutions (data not shown), as previously described by Vandenbossche (1991)[35] and Stover (2011)[26].

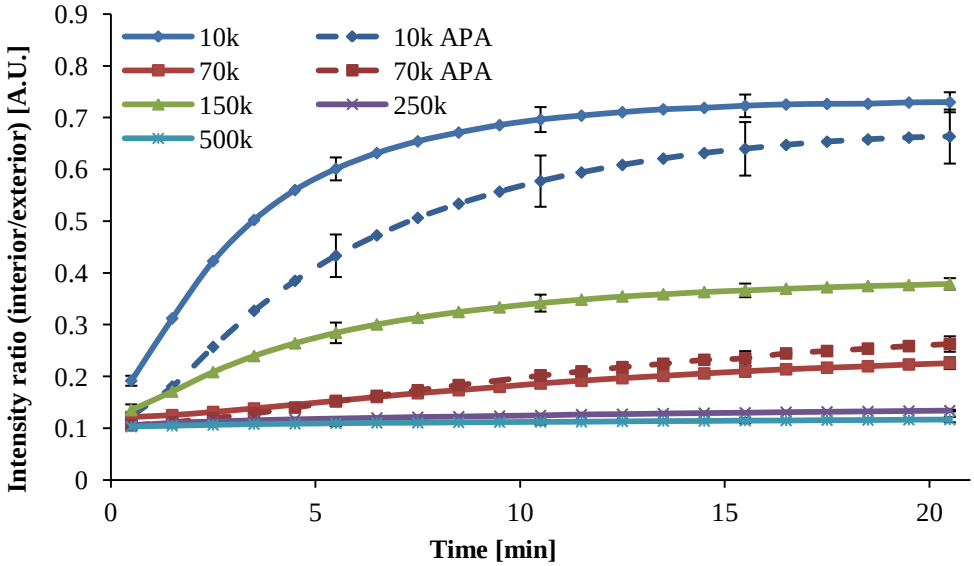

Figure 2.8 *Lateral In-diffusion of dextranf into* ***[3].***

2.4.7 Protein binding study on optimized capsule

One of the design points for the present PMM_{50} type capsules was that the rapid hydrolysis of residual anhydride groups would prevent covalent binding of protein during the incubation step commonly used after cell encapsulation. To test this, A-PLL-PMM_{50} capsules **[3]** were exposed to 0.05% rhodamine-labelled bovine serum albumin (BSA*r)* for 24 hrs, followed by several saline washes. Subsequent confocal microscopy imaging showed no BSA*r* binding to the capsule shells, even with the detector gain set to its maximum. The absence of BSA*r* binding to the crosslinked shell supports the notion that no reactive anhydride groups remain on the capsule surface, and further that the hydrolyzed PMM does not bind BSA*r* electrostatically. The presence of residual reactive groups had been recognized as a potential problem in similar BSA binding studies of capsules prepared using a reactive polyanion containing hydrolytically more stable acetoacetate crosslinking groups.[25] In the present type of temporarily reactive polyanions, any residual reactive groups not only deactivate spontaneously by hydrolysis, but also form additional anionic groups that introduce a very desirable net negative charge to the crosslinked polyelectrolyte complex.

Therefore in the future, the coating properties can be tuned based on cell-viability results. Future work will also explore the mechanical film strength using more direct methods, such as rupture resistance.

2.5 Conclusion

The reactive polyanion PMM_{50} formed by partially hydrolyzing poly(methyl vinyl ether-*alt*-maleic anhydride) (PMM_0) was coated onto calcium alginate-PLL capsules to form permanently crosslinked shells. Integrity of these shells could be improved through proper choice of MW and coating concentrations of PLL and PMM_{50}.

The partial hydrolysis of PMM_0 in ACN-d_3/D_2O was monitored by ^1H NMR. At 50% hydrolysis, PMM_{50} was diluted in a buffered saline solution to 0.2% and immediately used to coat A-PLL beads. The resulting capsule shells withstood challenges with sodium citrate / sodium hydroxide, in contrast to their non-crosslinked analogs.

The amount of PMM bound to the beads correlated with improved shell survival. It was found to increase using multiple PLL-PMM_{50} coatings, higher PLL coating concentrations, higher PLL molecular weight, and lower PMM_{50} molecular weight.

Permeability studies revealed that the covalently crosslinked shell formed on the A-PLL-PMM_{50} capsules allowed for rapid in-diffusion of 10 - 70 kDa dextrans, while excluding larger dextrans. The covalently crosslinked shell did not bind a detectable amount of BSA, confirming that no remaining reactive anhydride groups are present following coating.

2.6 Acknowledgements

The authors would like to acknowledge NSERC and CIHR funding for this research, including an NSERC PGS M held by C.M. Gardner.

2.7 References

[1] M.K. Lee; Y.H. Bae. *Adv. Drug Deliv. Rev*. **2000**, *42*, 103-120.
[2] F. Lim; A.M. Sun. *Science*, **1980**, *210*, 908-910.
[3] A. Hendy; G. Hortelano; G. Tannenbaum; P.L. Chang. *Hum. Gene Ther*. **1995,** *6*, 165-175.
[4] T. Visted; R. Bjerkvig; P.O. Enger. *Neuro. Oncol*. **2003**, *3*, 201-210.
[5] D.F. Emerich; S.R. Winn. *Crit. Rev. Ther. Drug Carrier Syst*. **2001**, *18*, 365-298.
[6] C. Ross; M. Ralph; P.L. Chang. *Hum. Gene Ther*. **1999**, *10*, 49-59.
[7] C.J.D. Ross; L. Bastedo; S.A. Maier; M.S. Sands; P.L. Chang. *Hum. Gene Ther*. **2000,** *11*, 2117–2127.
[8] J.M. Van Raamsdonk; C. Ross; M. Potter; S. Kurachi; K. Kurachi; D. Stafford; P.L. Chang. *J. Lab. Clin. Med.* **2000**, *139*, 35-42.
[9] S. Prakash; T.M.S. Chang. *Nat. Med*. **1996**, *2*, 883-887.
[10] D.A. Cieslinski; H. D. Humes. *Biotechnol. Bioeng.* **1993**, *4*, 291-301.
[11] V. Dixit; G. Gitnick. *J. Biomater. Sc. Polym. Ed.* **1995**, 7, 343-357.
[12] H. Zimmermann; D. Zimmermann; R. Reuss; P.J. Feilen; B. Manz; A. Katsen; M. Weber; F.R. Ihmig; F. Ehrhart; P. Gebner; M. Behringer; A. Sterinback; L.H. Wegner; V.L. Ukhorukov; J.A. Vasquez; S. Schneider; M.M. Weber; F. Volke; R. Wolf; U. Zimmermann. *J. Mater. Sci. Mater. Med.* **2005**, *16*, 491-501.
[13] J. Dusseault; S.K. Tam; M. Ménard; S. Polizu; G. Jourdan; L. Yahia; J.P. Hallé. *J. Biomed. Mater. Res. Part A.* **2006**, *76A*, 243-251.
[14] B. Thu; P. Bruheim; T. Espevik; O. Smidsrod; P. Soon-Shiong; G. Skjåk-Bræk. *Biomaterials* **1996**, *17*, 1069-1079.
[15] H.K. Holme; L. Davidsen; A. Kristiansen; O. Smidsrød. *Carbohydr. Polym.* **2008**, *73*, 656–664.
[16] J. Dusseault; G. Langlois; M.C. Meunier; M. Ménard; C. Perreault; J.P. Hallé. *Biomaterials* **2008**, *29*, 917–924.
[17] I.M. Kung; F.F. Wang; Y.C. Chang. *Biomaterials* **1995**, *16*, 649-655.
[18] A.M. Rokstad; I. Donati; M. Borgogna; J. Oberholzer; B.L. Strand; T. Espevik; G. Skjåk-Bræk. *Biomaterials* **2006**, *27*, 4726–4737.
[19] F. Cellesi; N. Tirelli; J.A. Hubbell. *Macromol. Chem. Phys.* **2002**, *203*, 1466-1472.
[20] M.Z. Lu; H.L. Lan; F.F. Wang; S.J. Chang; Y.J. Wang. *Biotechnol. Bioeng*. **2000**, *70*, 479-483.
[21] Y.J. Wang. *Mat. Sci. Eng.* C. **2000**, *13*, 59-63.
[22] J. Dusseault; F.A. Leblond; R. Robitaille; G. Jourdan; J. Tessier; M. Ménard; N. Henley; J.P. Halle. *Biomaterials* **2005**, 26, 1515–1522.
[23] T. Vermonden; N.E. Fedorovich; D. van Geemen; J. Alblas; C.F. van Nostrum; W.J.A. Dhert; W.E. Hennink. *Biomacromolecules* **2008,** *9*, 919–926.
[24] M.A.J. Mazumder; F. Shen; N.A.D. Burke; M.A. Potter; H.D.H. Stöver. *Biomacromolecules* **2008,** *9*, 2292-2300.
[25] F. Shen; M.A.J. Mazumder; N.A.D. Burke; H.DH. Stöver; M.A. Potter. *J. Biomed. Mater. Res. B Appl. Biomater.* **2009,** *90B*, 350-361.

[26] C.M. Gardner; N.A.D. Burke; T. Chu; F. Shen; M.A. Potter; H.D.H. Stöver. *J. Biomater. Sci. Polym. Ed.* **2011**, *22*, 2127-2145.
[27] M.A.J. Mazumder; N.A.D. Burke; F. Shen; M.A. Potter; H.D.H. Stöver. *Biomacromolecules* **2009**, *10,* 136-73.
[28] A.M. Sun. *Methods Enzymol.* **1988**, 137, 575-580.
[29] N.A. Durgaryan; V.H. Matosyan; S.A. Markarian. *Euro. Polym. J.* **2003**, *39*, 921-925.
[30] C. Ladavière; T. Delair; A. Domard; C. Pichot; B. Mandrand. *Polym. Degrad. Stab*. **1999**, *65*, 231-241.
[31] INCHEM Chemical Safety Information from Intergovernmental Organizations, Environmental Healthy Criteria (EHC) 154, Acetonitrile, 1993, WHO. URL: http://www.inchem.org/documents/ehc/ehc/ehc154.htm
[32] C. Ladavière; T. Delair; A. Domard; C. Pichot; B. Mandrand. *J. Appl. Poly. Sci*. **1999**, *71*, 927-936.
[33] T.C. Bruice; U.K. Pandit. *J. Amer. Chem. Soc.* **1960**, *82*, 5858-5865.
[34] K.R. Davis; J.L. Hogg. *J. Org. Chem.* **1983**, *48*, 1041-1047.
[35] G. Vandenbossche; P. Van Oostveldt; J. Remon. *J. Pharm. Pharmacol*. **1991**, 43, 275-277.

CHAPTER 3: Reactive Polyanions Based on Poly(4,4-dimethyl-2-vinyl-2-oxazoline-5-one-*co*-methacrylic acid)

Casandra M. Gardner, Harald D.H. Stöver

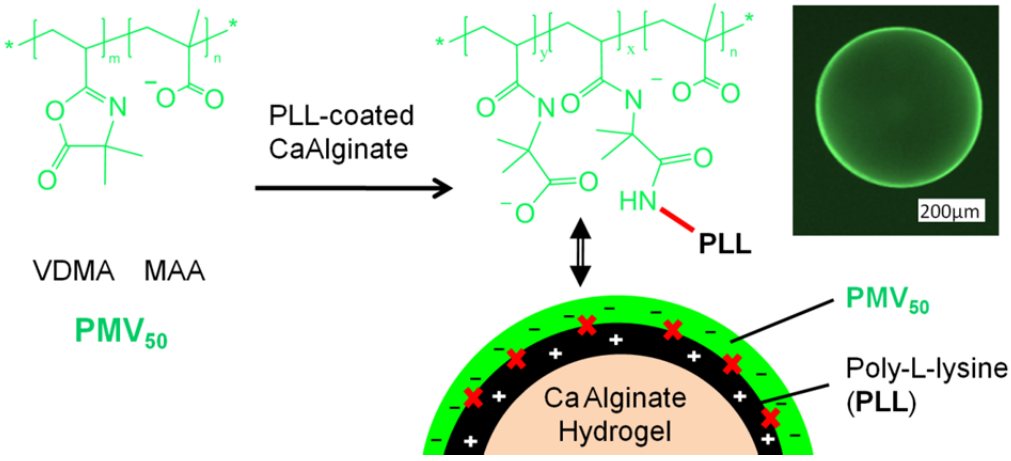

Published in *Macromolecules* **2011**, *44*, 7115-7123.

Contributions:
I performed the following experiments: determination of reactivity ratios, synthesis of PMV_{50} and higher VDMA content copolymers, analysis of the copolymers using ^{1}H NMR, quantitative ^{13}C NMR and GPC, model studies to highlight the transhydration reaction, measurement of PMV_{50}'s hydrolysis in buffer and coating of PMV_{50} onto AP capsules. Dr. Berno helped me set up the saturation-recovery experiment, to measure the T1 values of PMV_{50} for subsequent quantitative ^{13}C NMR analysis. Dr. Kornic performed elemental analysis and FT-IR on my PMV_{50} copolymer. I wrote the manuscript, with edits and guidance from Dr. Stover.

3.1 Abstract

The formation of reactive polyanions by semi-batch copolymerization of 4,4-dimethyl-2-vinyl-2-oxazoline-5-one (VDMA) and methacrylic acid (MAA) by both free radical and photo-induced radical polymerization is described. The reactivity ratios of these two monomers were determined to be 1.36 and 0.41 for r_1(VDMA) and r_2(MAA), respectively, using ^{1}H-NMR spectroscopy. During the free radical copolymerization of a 50:50 VDMA:MAA copolymer (PMV_{50}) in anhydrous DMSO or THF at 60^{o}C, up to 40% of the azlactone groups in the copolymer are hydrolyzed by water formed largely by conversion of methacrylic acid diads into cyclic anhydride. Storage in organic solutions leads to further trans-hydration, while solid PMV_{50} is stable for at least 6 months at room temperature. Increasing the VDMA comonomer content reduces this transhydration, likely through decreasing the incidence of methacrylic acid diads in the backbone. Alternatively, conducting the copolymerization at 20°C using photo-initiation is also effective at suppressing this transhydration. The resulting reactive polyanions bind under physiological conditions to poly-L-lysine-coated calcium-alginate hydrogel beads, and spontaneously crosslink with the polyamine to form covalent networks of interest for long term therapeutic cell encapsulation. This represents the first such use of a VDMA-containing polyanion in aqueous environments. The copolymers were characterized by ^{1}H-NMR, quantitative ^{13}C NMR, ^{13}C DEPT-135 NMR, and FT-IR spectroscopies as well as by elemental analysis.

3.2 Introduction

Polymers with electrophilic groups such as activated esters[1,2] anhydrides,[3] azlactones,[4] and isocyanates[5] are finding increased use in biomaterials, both for cross-linking, and for attaching camouflaging molecules such as poly(ethylene glycol),[4] cell adhesion motifs such as RGD[6], or immune-modulating molecules such as certain anti-inflammatory cytokines[7].

Ideally, these reactive polymers should react spontaneously and quantitatively with polymeric nucleophiles under physiological conditions, without generating potentially cytotoxic small molecule side products. Our group develops water-soluble polyanions containing electrophilic groups, designed to electrostatically bind to poly-amine-coated hydrogel beads, and then spontaneously form covalently crosslinked networks of interest for long-term immuno-protection of encapsulated cells. We recently described a copolymer of methacrylic acid with methacryloylethylacetoacetate (MOEAA) that is able to form both shell-crosslinked[8] and core-crosslinked[9] cell-compatible beads that are stable under physiological conditions for up to four weeks.[10] An analogous reactive polyanion formed by partial hydrolysis of poly(methylvinylether-*alt*-maleic anhydride) forms more permanent networks upon crosslinking with poly-L-lysine coated calcium alginate (AP) beads, due to formation of amide cross-links.[3] Residual anhydride groups not used in crosslinking are rapidly converted into additional anionic carboxylates, considered to promote biocompatibility by shielding the cationic charges on the poly-L-lysine (PLL).

The present work aims to add control over copolymer composition, and reduce the rate of residual electrophile hydrolysis to allow for post-functionalization of the capsules with bioactive molecules, while retaining the advantages of stable amide crosslinks. One electrophilic monomer that has recently attracted interest in this context is 4,4-dimethyl-2-vinyl-2-oxazoline-5-one (VDMA).[11] Azlactones react with amines, alcohols, and thiols in a ring-opening reaction under mild conditions, to form amide, ester and thioester bonds, respectively.[11,12] VDMA is readily polymerized by free radical means or living free radical polymerization (LFRP),[13] and copolymers incorporating azlactone groups have been used to prepare thin films[4,14,15] and to immobilize proteins and other bio-relevant molecules onto polymer supports.[16,17,18,19]

Most of the published work, including the preparations of cross-linked thin films using a layer-by-layer approach,[14] has been carried out in organic media, as the VDMA homopolymer is not soluble in water. VDMA has been shown to incorporate preferentially during copolymerization with methyl methacrylate,[20] *N*,*N*-dimethylacrylamide[21], vinyl pyrrolidone,[22] butyl acrylate and styrene[15] in organic solvents.[18] To date, VDMA has not been copolymerized with an acidic comonomer, or used to form LBL assemblies with polycations in aqueous conditions.

The present work hence describes the preparation and study of VDMA copolymers with methacrylic acid, poly(MAA-*co*-VDMA) or PMV. The key use of these reactive polyanions will be to form covalently cross-linked hydrogels under physiological conditions, typically in the presence of cells.[23] Such hydrogel networks are finding use as long-term biocompatible scaffolds or tissue mimetics for applications including immuno-isolation of transplanted therapeutic cells including islets of Langerhans, and stem cell studies.

Copolymers of VDMA with MAA promise to be water-soluble and able to form polyelectrolyte complexes with polyamines. While the cross-linking reaction is expected to be rapid, hydrolysis of residual VDMA to carboxylates is expected to be slower[3] than for the analogous anhydride-based copolymers, promoting covalent crosslinking while still ensuring conversion of electrophilic groups prior to transplantation.

In principle, VDMA homopolymers may be used for this purpose, as they can be partially hydrolyzed in mixed organic/aqueous solution prior to use. This approach was described recently by Messman (2009),[22] and has been independently used by us to form analogous reactive polyanions from poly(methylvinylether-*alt*-maleic anhydride).[3] The explicit use of an anionic comonomer, MAA, is thought to ensure random distribution of charges and electrophiles along the backbone, minimize extraneous groups resulting from hydrolyzed VDMA, while being more cost effective.

3.3 Experimental

3.3.1 Materials

4,4-Dimethyl-2-vinyl-2-oxazoline-5-one (VDMA) was purchased from TCI America, Portland, OR., methacrylic acid (MAA) 99%, 2,2-dimethoxy-2-phenylacetophenone, 5-

aminofluorescein (AF), HEPES sodium salt, poly(L-lysine hydrobromide) (PLL, 40-60 kDa), anhydrous DMSO, anhydrous THF (inhibitor free), ethylene carbonate 98%, phenethylamine, glutaric acid were purchased from Sigma-Aldrich, Oakville, ON, and used as received. Sodium alginate (Pronova UP MVG, batch no. FP-610-03) was purchased from Novamatrix, Norway. Sodium chloride (Caledon Laboratories Ltd, ON), and calcium chloride (minimum 96% powder, anhydrous, Sigma-Aldrich, ON) were used as received. Sodium hydroxide and hydrochloric acid solutions were prepared from concentrates (Anachemia Chemical, Rouses Point, NY) by diluting to 0.100 M or 1.000 M with deionized water. Azobisisobutyronitrile (AIBN) was obtained from Dupont, Mississauga. Dimethyl sulfoxide-d_6 (99.9 atom% DMSO-d_6) and D_2O (99.9 atom% D) were purchased from Cambridge Isotope Laboratories, Inc. Andover, MA. Poly(methacylic acid) (PMAA) was prepared by free radical polymerization of methacrylic acid as described by Mazumder (2008).[24]

3.3.2 Reactivity ratio determination during free radical copolymerization

Copolymerization was followed in a 5 mm NMR tube by 500 MHz ^{1}H NMR, involving a 50:50 mol% ratio of comonomers at 8 w/v% total monomer loading, 2 mol% AIBN in DMSO-d_6, at 60^{o}C for 4 hr, similar to the protocol described by Aguilar (2002).[25] ^{1}H NMR spectra were taken at increasing time intervals (0, 1, 2, 3, 4, 5, 6, 7, 8, 9, 14, 19, 29, 39, 49, 59, 89, 119, 149, 179, 209, 239, 249 min) and the monomer concentrations were measured by integration of the vinyl MAA peak at 5.55 pm and an average of the two vinyl VDMA peaks at 6.35 ppm and 6.15 ppm. The reactivity ratios were then calculated using both equation 2 and 3 in Aguilar's paper, based on fitting the instantaneous comonomer concentrations to the terminal model of the copolymerization equation.[25] The 95% confidence contour plot was determined using Matlab and the method described by Box (2005).[26]

3.3.3 Semi-batch free radical copolymerization of 2-vinyl-4,4-dimethylazlactone with methacrylic acid

PMV_{50}: Prior to reaction all glassware was heated in an oven at 70^{o}C for two days to remove moisture. A semi-batch copolymerization was performed, starting with a total initial monomer loading of 8 w/v% and an initial comonomer mole ratio of 35: 65 VDMA:MAA, with gradual addition of more VDMA to approximately maintain this comonomer feed ratio. Specifically, in a 100 mL water jacketed round bottom flask VDMA (1.87 g, 13.5 mmol), MAA (2.1 5g, 25 mmol), AIBN (77 mg, 0.469 mmol, 1 mol%) and ethylene carbonate (45 mg, internal standard for ^{1}H NMR), were dissolved in 50 ml of anhydrous DMSO (or THF) to give an 8 wt/v% initial comonomer solution. A stirring bar was added and the system purged with $N_{2\,(g)}$ for 1 hr. The flask was heated to 60^{o}C using a circulating water bath, under $N_{2\,(g)}$ bubbling through a T-junction and an oil-bubbler. After 5 min of heating, t = 0 min, continuous addition of a 0.003 mol/ml solution of VDMA in anhydrous DMSO (or THF) was started. The rate of addition was 3.75 ml/min until t=30 min, and 1.875 ml/hr from there until t=60 min, using an automated

syringe pump. Aliquots of 0.5 ml of the reaction mixture were taken at t = -5, 0, 10, 20, 30, 40, 50 and 60 min, and added to 0.1 ml of DMSO-d_6 for subsequent ^{1}H NMR analysis at 600 MHz.

The reaction was stopped after 1 hr by exposing the system to air and immediately cooling the water jacket with cold water. The reaction solution was then diluted with 50 ml of THF and precipitated into 600 ml of anhydrous diethyl ether under stirring. The resulting dispersion was centrifuged for 20 min at 3500 rpm, the supernatant was removed and the solid precipitate washed with diethyl ether. The resulting product was dried in a vacuum desiccator at room temperature for 1 hr, ground with a mortar and pestle, dried under vacuum for another hour and then redissolved in 20 ml of THF. This solution was re-precipitated into 200 ml of anhydrous diethyl ether, and treated as above, with final drying in the vacuum desiccator for 3 days, to give a white powder, with isolated yields of 43 mol% (44 wt%) in DMSO, and 22 mol% (23 wt%) in THF, with respect to the total amount of monomers added to the reaction (initial VDMA plus VDMA additions).

3.3.4 Synthesis of fluorescently labeled PMV_{50} (PMV_{50}*f*)

PMV_{50}*f* was synthesized as described above, except that 1 mol% of aminofluorescein (89.6 mg, 0.24 mmol) with respect to the total VDMA used in the reaction (3.37 g, 24.2 mmols) was added to the VDMA monomer before this mixture was divided into the initial VDMA reaction mixture and the VDMA feed solution.

3.3.5 Semi-batch synthesis of other PMV compositions

The syntheses of other PMVs with copolymer compositions of 55:45, 65:35, 70:30 and 80:20 VDMA:MAA were carried out in a similar manner as described above, using initial VDMA mol fractions of 0.40, 0.45, 0.60 and 0.72, respectively, as obtained from Figure 3.1b. The same concentration and rate of VDMA addition was used as described above.

3.3.6 Semi-batch photo-copolymerization of 2-vinyl-4,4-dimethylazlactone with methacrylic acid

Two semi-batch photo-copolymerization designed to obtain PMV_{50} and PMV_{70} were performed in a similar manner as described for the free radical polymerization, starting with a total initial monomer loading of 8 w/v% and initial comonomer mole ratios of 35: 65 and 60:40 VDMA:MAA, respectively, with gradual addition of more VDMA to approximately maintain this comonomer feed ratio. The reactions were carried out in a photo-chamber containing 3 black-light bulbs (Microlites Scientific, 350 nm, 8W). A cylindrical reaction vessel (2.5 cm in diameter and 12 cm in height) containing a cold finger running throughout the middle, supplied isolated 22^{o}C tap water during the 1 hr synthesis to minimize heating from the bulbs and the polymerization. The photoinitiator

used was 2,2-dimethoxy-2-phenylacetophenone (0.5 mol% with respect to the total monomer concentration). VDMA solution in DMSO (0.003 mol/ml) was added at 7.5 ml/min until t=30 min, and 3.75 ml/hr from there until t=60 min, to account for the higher rate of photopolymerization. As described above the reaction was monitored by ^{1}H NMR and polymer was isolated.

3.3.7 Covalent layer-by-layer assemblies around calcium-alginate-PLL capsules (AP-PMV$_{50}$ capsules)

Calcium alginate capsules were prepared as described previously.[3] Briefly, a 1 wt% solution of Novamatrix UP MVG sodium alginate in saline was filter sterilized (0.22 μm), and extruded through a flat-tipped 27-gauge needle with a concentric air flow (3.5 L/min) using a modified syringe pump, at a liquid flow rate of 0.5 mL/min, into a 1.1 w/v% $CaCl_2$ gelling bath. The resulting calcium alginate beads were washed once with 1.1 w/v% $CaCl_2$, coated with PLL (filter sterilized (0.22 μm), 0.1% in saline, for 6 min), and washed once each with 1.1 w/v% $CaCl_2$ and saline, to give AP beads. AP-PMV$_{50}$ capsules were formed by coating AP beads with 0.2% filter sterilized PMV$_{50}$*f* solution in 35 mM HEPES buffered saline at pH 7.8 for 10 min, followed by two washes with saline. All washing and coating steps involved a ratio of 1 mL beads to 3.3 mL washing or coating solution.

To confirm covalent crosslinking 1 M sodium citrate was added to 30 capsules on a microscope slide to extract calcium from the core, leaving only the alginate-PLL-PMV$_{50}$ shell. The supernatant was removed and replaced with 0.1 M NaOH to deprotonate the primary amines on PLL, thus eliminating all electrostatic interaction between PLL and both alginate and PMV$_{50}$, leaving only covalent cross-links to maintain shell integrity.

3.3.8 GPC analysis

Molecular weights were determined using PMV that was completely hydrolyzed by reaction in basic (pH ~ 10) distilled deionized water for 3 days, and an aqueous gel permeation chromatography (GPC) system consisting of a Waters 515 HPLC pump, Waters 717 plus Autosampler, three Ultrahydrogel columns (0-3 kDa, 0-50 kDa, 2-300 kDa), and a Waters 2414 refractive index detector. A mobile phase consisting of 0.3 M $NaNO_3$, 0.05 M phosphate buffer (pH 7) at a flow rate of 0.8 ml/min was used for all polymers, and the system was calibrated with narrow-disperse poly(ethylene glycol) standards (Waters, Mississauga, ON).

3.3.9 ^{1}H NMR

(i) Determination of instantaneous monomer feed ratio and the final copolymer composition:

During the free radical and photo- semi-batch copolymerization of PMV_{50} 0.5 ml aliquots were removed from the reaction mixture at -5, 0, 10, 20, 30, 40, 50 and 60 min and added to 0.15 ml of DMSO-d_6 for ^{1}H NMR analysis on a Bruker AV 600. The monomer peaks of VDMA and MAA were integrated at each time point to obtain the instantaneous comonomer feed ratios. The amounts of MAA reacted were determined by tracking the decreasing MAA concentration. The amount of VDMA reacted was determined by subtracting the actual amount of VDMA present in the reaction from the total (initial plus incremental) amount of VDMA, at each time point. The average VDMA content in the PMV_{50} copolymer formed during this hour was determined, based on the amounts of VDMA and MAA consumed during the reaction.

(ii) Analysis of DMSO and/or THF remaining in final product.

The final PMV copolymer was isolated and analyzed by ^{1}H NMR at 600 MHz in DMSO-d_6 to determine the amount of residual solvent (DMSO and/or THF) in the isolated product.

3.3.10 Quantitative ^{13}C NMR to determine the degree of hydrolysis as well as the VDMA:MAA ratio in PMV copolymers

The longitudinal relaxation times, T1, of the ^{13}C nuclei in PMV_{50} were determined using a saturation-recovery experiment (pulse program "satrect1.av_bb"). The T1 times were then used to set up a quantitative ^{13}C NMR experiment using inverse-gated decoupling without NOE enhancement, a 30-degree flip angle, 3000 scans, and a recovery delay time D1 of 10 s. Analyses were performed using 10 wt% solutions of as-formed, and of fully hydrolyzed, PMV_{50}*f* in DMSO-d_6 and D_2O, respectively, on a Bruker AV 600. ^{13}C NMR DEPT-135 experiments were performed to confirm the correct assignment of the carbon peaks.

3.3.11 Elemental analysis to determine the ratio of VDMA:MAA in PMV copolymers

Residual solvents and AF were removed from the polymer by dialysis: 200 mg of PMV_{50}(*f*) was dissolved in 20 ml of 35 mM of pH 7.8 HEPES buffered saline and diluted to 100 ml with distilled water after 2 hr. This solution was then dialyzed against 4 L of distilled deionized water for 1 week, with daily water changes using cellulose dialysis tubing with a molecular weight cut-off of 14 kDa (Membra-cel, Viskase, Darien, IL). This process hydrolyzes all remaining azlactone groups, prior to elemental analysis. The dialyzed solutions were concentrated using a rotary evaporator, followed by precipitation with 1 M HCl. The resulting precipitate was dried in a vacuum oven at 25^{o}C for 3 days. Elemental analysis was performed on a Therm FlashEA 1112 Elemental Analyzer, using the carbon: nitrogen ratio to determine the VDMA to MAA ratio.

3.3.12 UV-Vis determination of AF content in $PMV_{50}f$

The amount of AF bound to the dialyzed $PMV_{50}f$ was determined by UV-Vis spectroscopy on a Varian Cary 50 Bio, using the AF absorbance (λ_{max} ~490 nm) of a 0.10% polymer solution, and the extinction coefficient of free AF of 86,000 $M^{-1}cm^{-1}$at pH 9.[27]

3.3.13 FT-IR analysis

Powder samples of as-formed PMV_{50} and of fully hydrolyzed PMV_{50} were made into KBr pellets with spectrograde KBr and analyzed on a Thermo Scientific Nicolet 6700 FT-IR spectrometer equipped with DTGS detector, extended KBr beam splitter and OMNIC v8 software. Resolution was set to 4 cm^{-1} with 32 scans.

3.3.14 Model studies

To investigate the mechanism of azlactone hydrolysis, model studies were carried out where VDMA monomer alone (control experiment), or VDMA and either MAA, poly(methyacrylic acid) (PMAA), or 1,5-pentanedioic acid (glutaric acid), were dissolved in DMSO-d_6 at a 35: 65 mol ratio of azlactone to carboxylic acid, and heated at 60°C for 1 hr, to mimic the polymerization conditions. The solutions were then stored at room temperature, and the degree of hydrolysis of VDMA was monitored by ^{1}H and ^{13}C quantitative NMR over time.

3.3.15 Potentiometric determination of the rate of hydrolysis of PMV_{50} in aqueous buffer

A Mandel Scientific PC-Titrate automated potentiometric titrator was used to monitor the pH of a 0.2% PMV_{50} solution in pH 8.1, 35 mM HEPES buffered saline. Photo-polymerized PMV_{50} (30 mg) was first dissolved in 1 ml of DMSO-d_6 and a ^{13}C NMR was taken to determine the degree of hydrolysis. This solution was diluted with HEPES buffer to make a 0.2% aqueous PMV_{50} solution.

3.4 Results and Discussion

3.4.1 Synthesis of poly(2-vinyl-4,4-dimethylazlactone-*co*-methacrylic acid), PMV_{50} by free radical polymerization

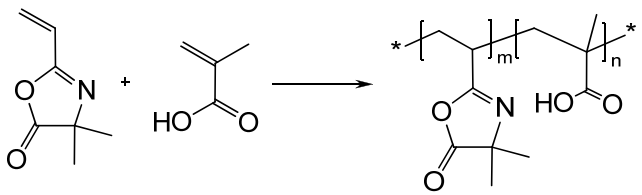

Scheme 3.1 *Free radical solution copolymerization of VDMA with MAA*

Solvent	VDMA:MAA			GPC		Solvent remaining in isolated polymer (after 2 precipitations and 3 days drying under vacuum)
	^{1}H NMR (during reaction)	^{13}C NMR (quantitative)	Elemental analysis	M_n (kDa)	M_w (kDa)	
DMSO	60: 40	50: 50 ± 5	45: 55	100	170	15-30 wt%
THF	60: 40	50: 50 ± 5	45: 55	40	70	8 wt%

Table 3.1 *Summary of PMV_{50} characterization*

Copolymerization of methacrylic acid (MAA) and 2-vinyl-4,4-dimethyl-azlactone (VDMA) has not yet been reported in the literature. Heilmann *et al* (2003)[20] reported the reactivity ratios of VDMA and methyl methacrylate in methyl ethyl ketone as 0.83 and 0.61, respectively, indicating a slightly preferential incorporation of VDMA. VDMA was expected to, and did, behave similarly in the present copolymerization. The calculated reactivity ratios extracted from a ballistic copolymerization of VDMA and MAA starting near a 1:1 molar ratio (Figure 3.1a), were found using the method described by Aguilar (2002)[25] and found to be 1.36 and 0.41 for r_1(VDMA) and r_2(MAA), respectively. The high sensitivity of the 500 MHz NMR instrument used, allowed coverage of large [VDMA]/[MAA] range in a single NMR copolymerization experiment. Figure 3.1b shows the instantaneous copolymer composition graph calculated using these fitted r values, as well as (full circles) the range of comonomer feed ratios and copolymer compositions covered in the NMR experiment. Figure 3.1c shows the 95% joint confidence contours for these r values.

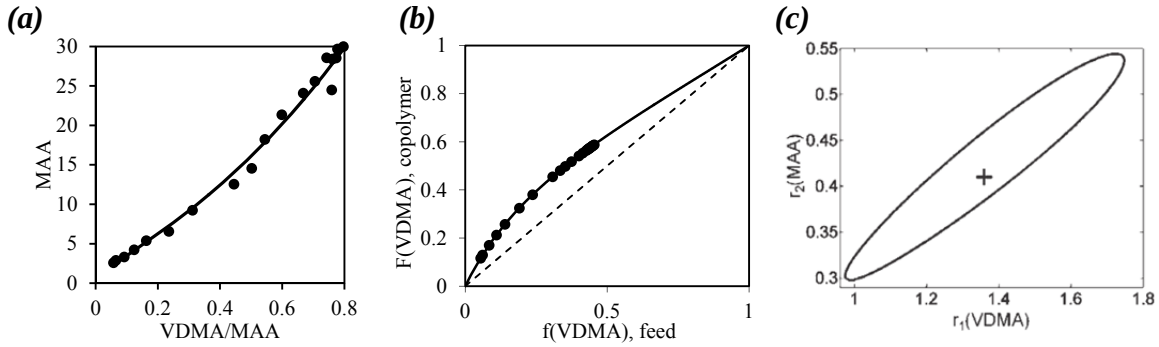

Figure 3.1 (a) *[MAA] versus [VDMA]/[MAA] (arbitrary units) from a copolymerization of VDMA and MAA with an initial mole ratio of about 1:1. Experimental data from ^{1}H NMR: black diamonds; fitted black line calculated using equation 2 of Aguilar's paper.*[25] ***(b)*** *Instantaneous Copolymer Composition curve for VDMA and MAA in DMSO at 60^{o}C, black dots correspond to the experiment data points* ***(c)*** *95% confidence contour for calculated reactivity ratios.*

3.4.2 Transhydration during formation of PMV_{50}

The NMR data revealed the appearance of both monomeric and polymeric hydrolyzed azlactone groups during this copolymerization. Hydrolysis of VDMA monomer is shown by the sharp amide peak at 8.02 ppm as well as by the corresponding vinyl peaks at 6.26, 6.06 and 5.57 ppm (Figure 3.2a and b, respectively). The appearance of a broad amide peak at about 7.7 ppm confirms the presence of hydrolyzed azlactone units in the copolymer (Figure 3.2a), formed either by copolymerization of hydrolyzed monomer or by partial hydrolysis of the copolymer.

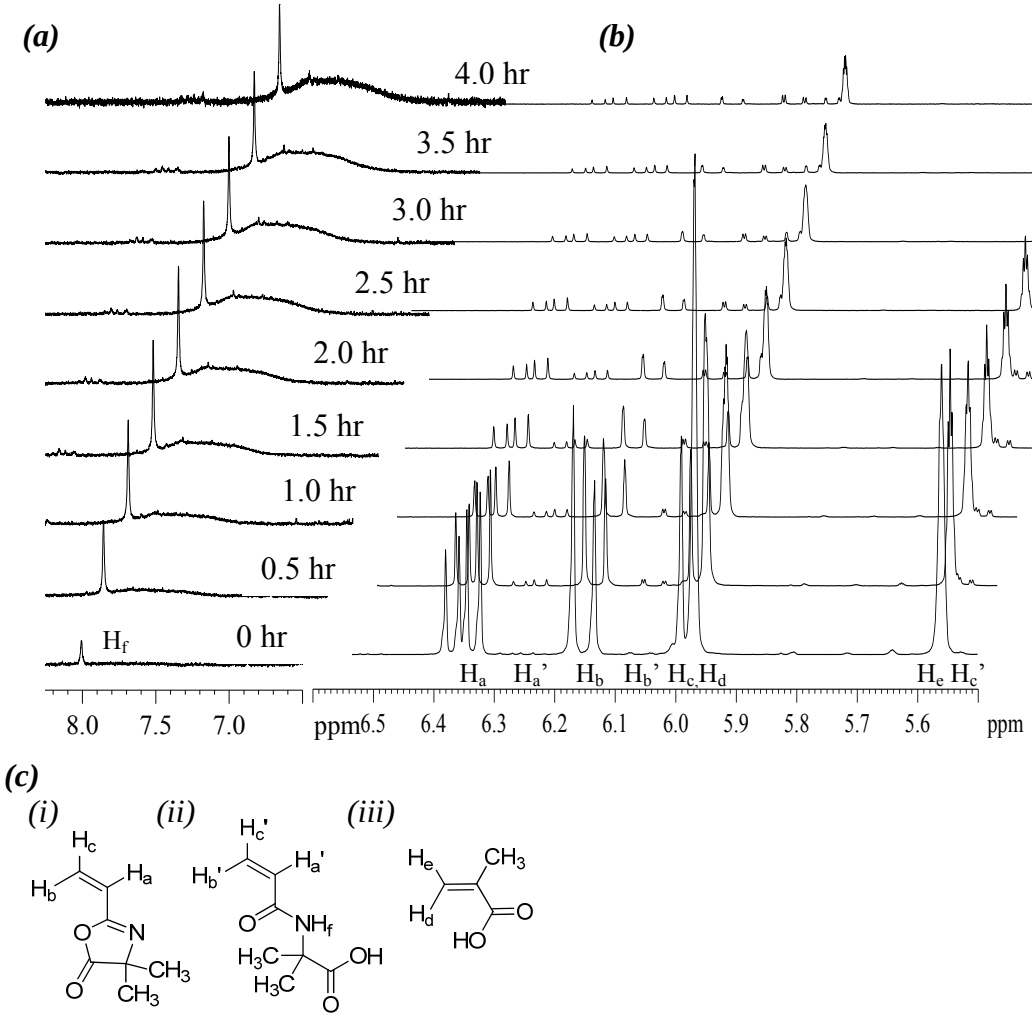

Figure 3.2 *^{1}H NMR (500MHz) spectra over four hours of PMV_{50} synthesis:* ***(a)*** *magnified amide region, showing both a sharp amide signal from hydrolyzed VDMA at 8.0 ppm, and a broad amide signal from partly hydrolyzed PMV_{50} around 7.7 ppm;* ***(b)*** *alkene monomer region, with proton labels under 0 hr referring to monomer structures shown in* ***(c)****;* ***(c)*** *(i) VDMA (ii) hydrolyzed VDMA (iii) MAA with reference to* ***(b)****.*

This complicates the determination of the reactivity ratios, as this system would more accurately be described as a terpolymerization of VDMA, hydrolyzed VDMA and MAA, characterized by six reactivity ratios.[28] A full analysis, though intriguing, is beyond the scope of this thesis. We hence proceeded with the estimation of binary reactivity ratios, accepting that this approach ignores the additional small loss during the copolymerization of VDMA to form hydrolyzed VDMA, and possibly even of MAA to form methacrylic anhydride.

Using the binary reactivity ratios we first aimed for an equimolar VDMA: MMA copolymer in order to balance electrophilic groups with the anionic charges needed for solubility and complexation to polyamines. A semi-batch copolymerization was hence carried out in anhydrous DMSO or THF, starting with an initial VDMA:MAA mol ratio of 35: 65, as interpolated from the instantaneous copolymer composition graph calculated based on the measured reactivity ratios (Figure 3.1b), and adding sufficient VDMA throughout the reaction to maintain this comonomer ratio. ^{1}H NMR spectra were taken every 10 minutes to confirm that the molar comonomer feed ratio of VDMA to MAA remained at roughly 35: 65 (Figure 3.3a) throughout the copolymerization. Figure 3.3b shows the amounts of MAA and VDMA reacted at each of these time points. The comonomer feed ratio drifts just slightly during the copolymerization (Figure 3.3a), with the calculated instantaneous VDMA content of the copolymer increasing from 58% to 63% over the course of the reaction in DMSO, and from 57% to 65% in THF. Averaging over the course of the reaction predicts that about 60% VDMA is incorporated into PMV_{50} in both solvents.

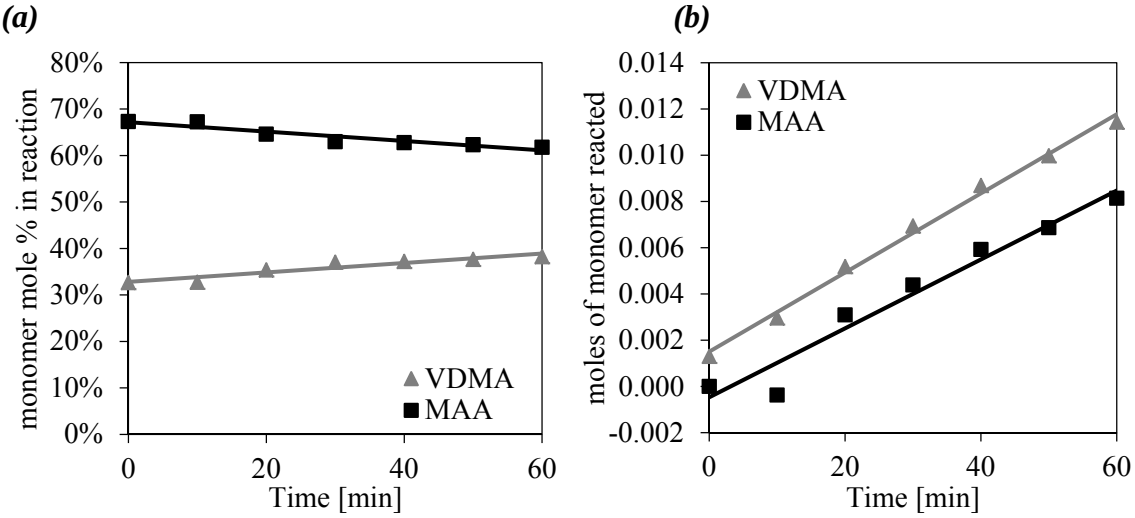

Figure 3.3 *Semi-batch copolymerization in DMSO* ***(a)*** *monomer ratio during the reaction, determined by from* ^{1}*H NMR,* ***(b)*** *moles of monomers reacted, calculated by subtracting moles remaining from the total amount of monomer added.*[a]

[a] This process ignores the minor loss of monomers to hydrolyzed VDMA and anhydride formation.

This VDMA percentage is slightly higher than the actual value determined by ^{13}C NMR and elemental analysis, due to the fact that the VDMA/DMSO solution interfered with smooth piston movement, causing significant backpressure in the automated syringe pump and decreased total injection volumes.

This empirical semi-batch approach was considered sufficient to give near constant copolymer composition throughout the 1 hr copolymerization, obviating the need for explicit analysis and programming of non-linear semi-batch additions.[29]

Copolymerizations carried out in DMSO and THF resulted in very similar compositions, though polymer yields were higher in DMSO at 44 wt%, compared to 23 wt% in (inhibitor-free) THF. ^{1}H NMR analysis of the isolated PMV_{50} polymer revealed that all residual monomer was removed from the polymer. However, residual DMSO proved to be difficult to remove from the isolated polymer: after two precipitations (the second from THF) into diethyl ether and multiple washings, between 15-30 wt% of DMSO and 3wt% THF (determined by ^{1}H NMR analysis taken 3 days after the second precipitation, Table 3.1) still remained with the isolated polymers. A third precipitation from THF reduced the amount of DMSO to 8 wt% and THF to 1wt%, but at the cost of increased hydrolysis of azlactone groups in the polymer. When the analogous copolymerization was performed in THF, two precipitations from THF into diethyl ether led to 8 wt% of THF remaining.[b]

Although small amounts of DMSO are tolerated by cells, THF is thought to be not very cytocompatible, and hence future work will look at removing all of the THF from the isolate polymer. However, recent cell viability studies[23] found no adverse affects arising after coating cell-containing AP capsules with 0.2 wt% PMV_{50}.

GPC analysis on fully hydrolyzed PMV_{50} revealed that PMV_{50} copolymers prepared in DMSO had a higher molecular weight, with average M_n values of 100 kDa and M_w values of 170, compared to the single PMV_{50} prepared in THF which had an M_n value of 40 kDa and M_w of 70 kDa (Table 3.1). The reason for the lower molecular weights of PMV_{50} prepared in THF is not clear, but may at least partly be due to the lower viscosity and higher chain transfer activity of (inhibitor-free) THF.

3.4.3 Determining percentage of VDMA in PMV_{50}

^{1}H NMR spectra of the isolated polymer showed broad, overlapping polymer peaks that could not be accurately quantified, hence quantitative ^{13}C NMR was employed. A ^{13}C DEPT-135 NMR experiment was performed on PMV_{50} to verify the assignment of peaks (Table 3.2). These assignments are in agreement with those of Messman (2009).[22] Subsequently, quantitative ^{13}C NMR spectra were taken of PMV_{50} in DMSO-d_6, and of fully hydrolyzed PMV_{50} in D_2O, both showing that 50 ± 5% VDMA was incorporated

[b] The 8wt% THF remaining is reflective of the polymer being dried under vacuum for 3 days after the final precipitation. ^{1}H NMR spectra collected 2 weeks later (after being stored under vacuum) shows a decrease in THF to 3 wt% (DMSO remains constant).

into PMV_{50}. This copolymer composition was determined by comparing the area of peak C_4' (VDMA) to the average of the areas of the four peaks $C_{7\text{-}10,}$ representing MAA. Averaging equations [1-3] gave a 50:50 copolymer composition.

$$C_{10} = (C_{10} + C_5) - C_4' \quad [1]$$

$$\text{Average of } C_8 \text{ and } C_9 = [(C_8' + C_9 + C_1 + C_3') - 2C_4'] / 2 \quad [2]$$

$$C_7 = (C_2 + C_7') - 2C_4' \quad [3]$$

Elemental analysis of fully hydrolyzed PMV_{50} gave a 45: 55 VDMA:MAA copolymer based on the C: N ratio, in agreement with the ^{13}C NMR data (Table 3.1).

3.4.4 Determining the amount of hydrolysis in as-formed PMV_{50}

Analyses of the quantitative ^{13}C NMR spectra of as-formed, and of fully hydrolyzed PMV_{50}, showed that 39 ± 6% of the VDMA groups in the as-formed PMV_{50} are already hydrolyzed. The amount of hydrolysis of as-formed PMV_{50} was measured in DMSO-d_6 using quantitative ^{13}C NMR, by comparing the integrations of the quaternary carbons C_4 (azlactone, 65 ppm) and C_4' (hydrolyzed azlactone, 55 ppm), Figure 3.4b. Comparing peak areas for C_6 and C_6', and for C_5 and C_5' gave similar results.

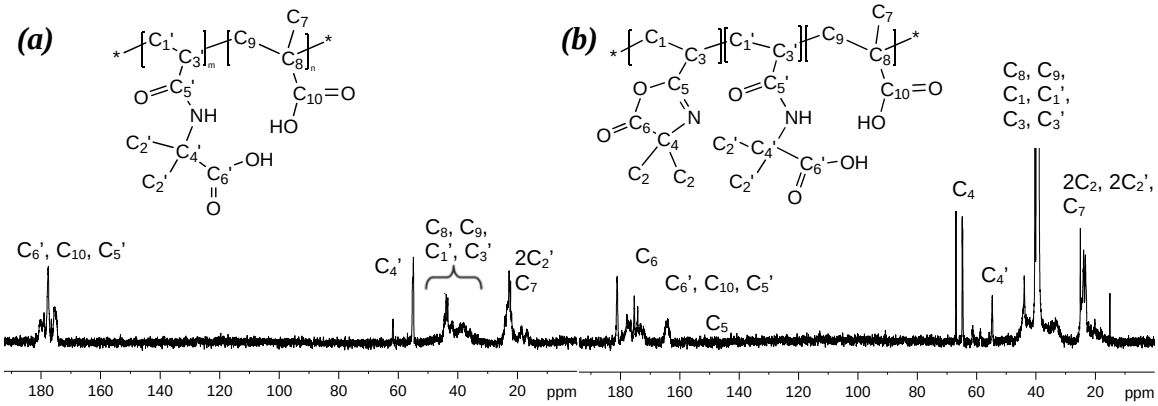

Figure 3.4 *Inverse gated decoupling ^{13}C NMR of* ***(a)*** *dialyzed and hydrolyzed PMV_{50} in D_2O,* ***(b)*** *PMV_{50} (synthesized in DMSO) in DMSO-d_6.*

Carbon	As-formed PMV_{50} [ppm]	Hydrolyzed PMV_{50} [ppm]
1 (CH_2) VDMA	32-37	32-37
2 $(CH_3)_2$ VDMA	15-25	15-25
3 (CH) VDMA	37-46	37-46
4 (C) VDMA	**65**	**55**
5 (O-C=N(C)) VDMA	**165**	**175-182**
6 (O-C=O) VDMA	**182**	**177-180**
7 (CH_3) MAA	15-25	15-25
8 (C) MAA	51-56	51-56
9 (CH_2) MAA	32-37	32-37
10 (COOH) MAA	170-176	170-176

Table 3.2 *^{13}C chemical shifts for as-formed and fully hydrolyzed PMV_{50}, both taken in DMSO-d_6. Peaks for carbons 4, 5 and 6 (bolded) moved significantly upon hydrolysis and were hence used to determine the degree of hydrolysis.*

3.4.5 Model Studies into PMV_{50} Hydrolysis

Further investigation showed that PMV_{50} continued to hydrolyze over time in DMSO-d_6, with the degree of hydrolysis, as measured by quantitative ^{13}C NMR, reaching 94% after 4 months at room temperature (Figure 3.5a). In contrast, a sample of the same PMV_{50} stored in solid form at room temperature proved more stable, with the amount of hydrolysis increasing from an initial level of 33% to reach 40% after 3.3 months, and 43% after 6 months. These findings suggest that the VDMA groups may react with polymeric MAA units, either by directly reacting with single neighboring MAA units, or by reacting with water liberated when MAA diads cyclize to form methacrylic anhydride units, and that this process is accelerated in solution.

To confirm this reaction, mixtures of VDMA and MAA monomers, and of VDMA monomer and PMAA homopolymer, were dissolved in DMSO-d_6 at the same concentration as used in the copolymerizations, and heated at 60°C for 1 hr, to mimic the conditions that occur during synthesis, followed by storage at room temperature over time. The degree of hydrolysis of VDMA was monitored by ^{1}H and ^{13}C quantitative NMR, and after 1 hr of heating at 60°C was found to be 6% for the MAA / VDMA mixture, and 36% for the PMAA / VDMA mixture.[c] After 1 month at room temperature these values had increased to 22% and 97%, respectively (Figure 3.5b). These findings suggest that hydrolysis occurs faster when the MAA units are present in polymeric form,

[c]A control experiment using just VDMA dissolved in DMSO-d_6 revealed only 0.5% hydrolysis after heating for one hour, and only 6% after 1 month at room temperature, indicating that the contributions to hydrolysis from ambient moisture or reaction with DMSO are minimal.

presumably because they can readily form cyclic methacrylic anhydride units by intramolecular dehydration.[30] ^{13}C NMR spectra of PMAA and VDMA in DMSO-d_6 initially and after 1 week at room temperature (92% hydrolysis) shows a decrease of the carboxylic acid peak at 179 ppm and the appearance of a broad anhydride peak at 172 ppm, as well as a broadening of the peaks for the PMAA methyl groups at 16 ppm, the quaternary carbon at 44 ppm, and the methylene carbon at 53 ppm (Figure 3.6).

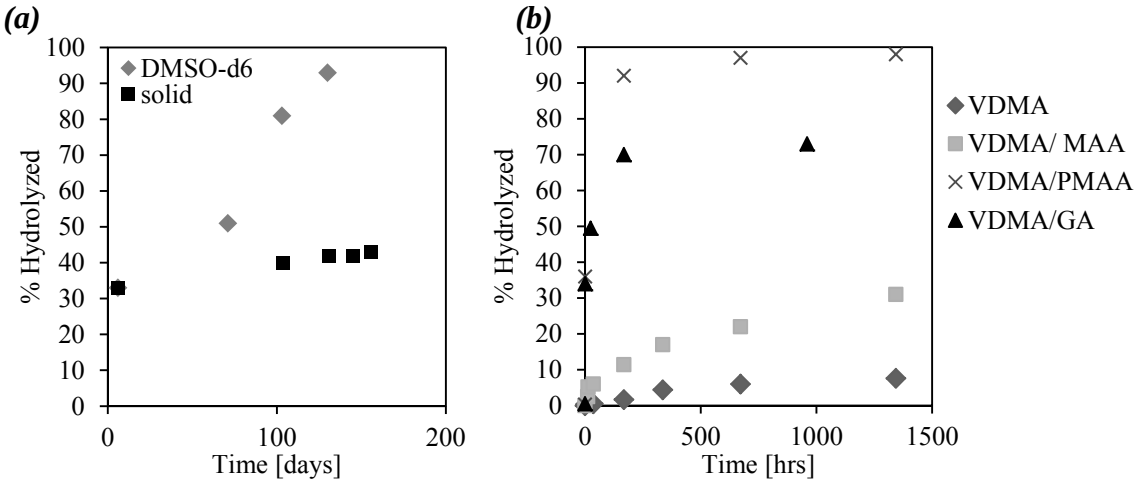

Figure 3.5 *Hydrolysis over time of* ***(a)*** *PMV_{50} in DMSO-d_6 vs. in solid form and* ***(b)*** *monomer model studies in DMSO-d_6.*

It is also interesting to note that VDMA monomer in mixtures with PMAA hydrolyzes faster than the azlactone units in PMV_{50}. This may simply be due to stereo-electronic differences between VDMA monomer and azlactone units in PMV_{50}, but may also be due to the fact that PMV_{50} has fewer MAA diads compared to PMAA.

Additional model studies were carried out using mixtures of VDMA with varying amounts of 1,5-pentanedioic acid (glutaric acid, GA) which is able to form a six membered cyclic anhydride upon dehydration. The rate of VDMA hydrolysis in presence of GA was intermediate between those of VDMA / PMAA and VDMA / MAA mixtures, and varied with the VDMA / GA ratio. Heating a mixture of VDMA and GA (35:65 azlactone:carboxylic acid ratio) in DMSO-d_6 at 60^{o}C for 1 hr led to hydrolysis of 34% of the initial VDMA, and formation of an equivalent amount of cyclic glutaric anhydride. After 1 month in DMSO-d_6 at room temperature, this trans-hydration had reached 70%.

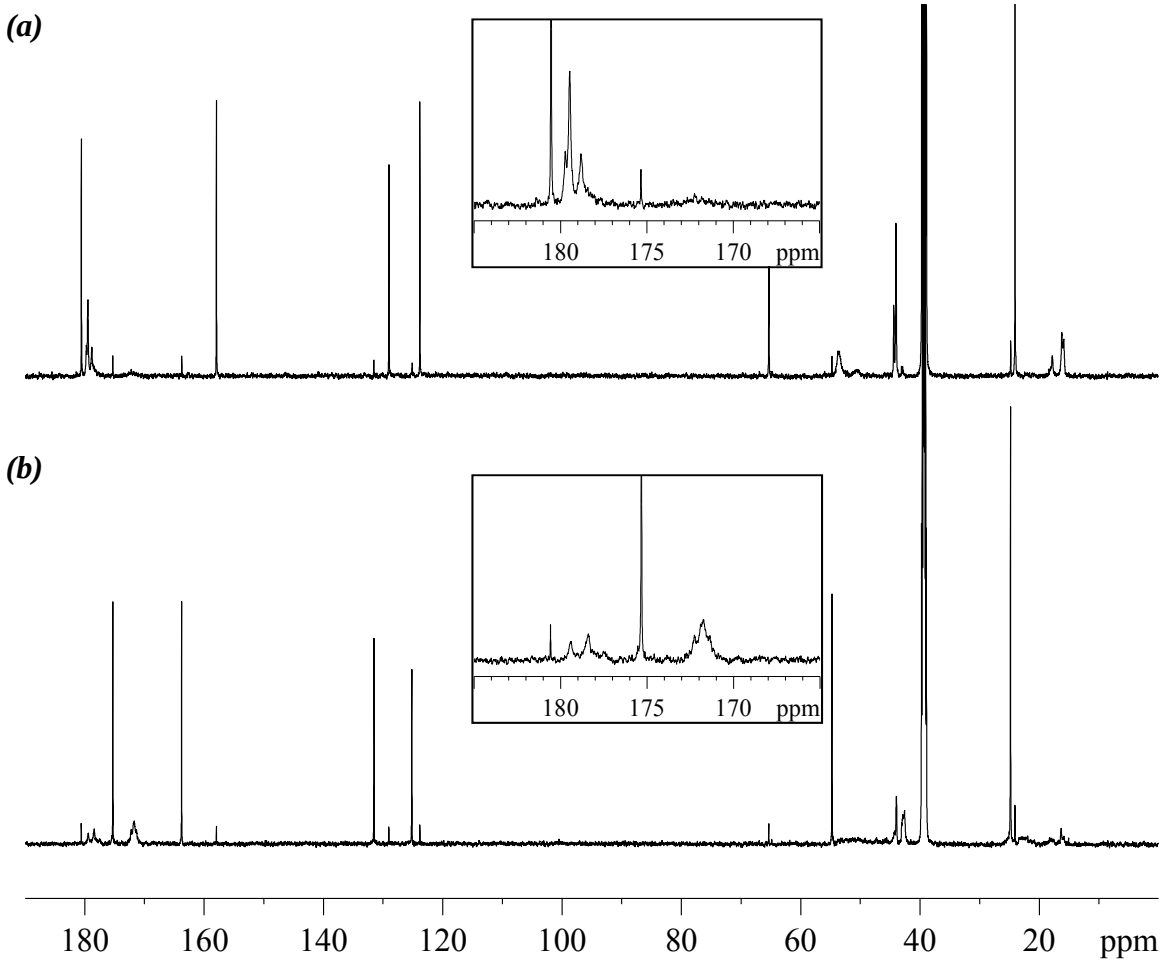

Figure 3.6 *^{13}C NMR spectra of a mixture of PMAA and VDMA in DMSO* ***(a)*** *initially,* ***(b)*** *after 1 week, with insets showing a blown up spectra of the carboxylic acid/anhydride region*

Comparison of the FT-IR spectra of as-formed PMV_{50} and of fully hydrolyzed PMV_{50} (Figure 3.7), shows the disappearance of the C=O stretch absorption corresponding to both the azlactone and the six membered ring anhydride[31] at 1824 cm^{-1}, and the increase of the amide II band at 1539 cm^{-1}.[22] Note that the azlactone C=N band at 1668 cm^{-1} could not be used as it overlaps with the amide C=O band at 1661 cm^{1} of the hydrolyzed azlactone.[15] Similarly, the carboxylic acid C=O band at 1733 cm^{-1} cannot be used as it represents both MAA and hydrolyzed azlactone.

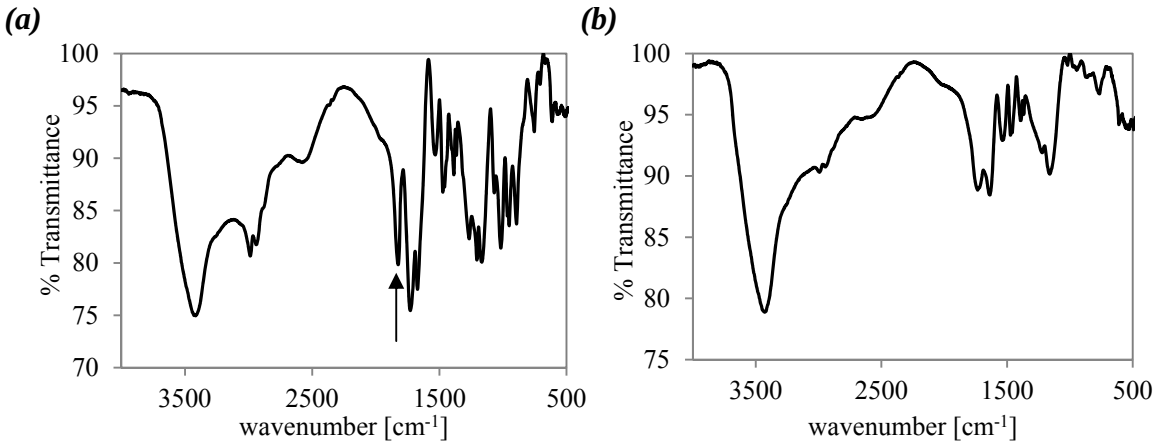

Figure 3.7 *IR spectra (KBr pellets) of* ***(a)*** *as-formed* PMV_{50} *(arrow indicates azlactone/anhydride peak), and* ***(b)*** *fully hydrolyzed* PMV_{50}*.*

3.4.6 Overcoming Transhydration

Two approaches were used to overcome the transhydration reaction. First, the mol ratio of VDMA in the copolymer was increased in order to decrease the probability of MAA diads. Table 3.3 shows how the increase of VDMA content in PMV decreases the amount of trans-hydration. The 70:30 VDMA:MAA PMV copolymer was the highest VDMA content polymer that would instantaneously dissolve in 35 mM HEPES buffered saline (pH 7.8). The 80:20 copolymer took 1 to 2 minutes to completely dissolve.

The second approach to minimize the transhydration reaction was to carry out the copolymerizion at lower temperatures, as it was observed in the model experiments that heating in DMSO accelerated the hydrolysis of azlactone groups. PMV_{50} was hence synthesized by a semi-batch photo-copolymerization at about 20^{o}C, resulting in hydrolysis of only 7% of the azlactone groups in the isolated copolymer.

Free Radical Polymerization (60°C)	
VDMA:MAA (EA and ^{13}C NMR)	**% Hydrolysis (^{13}C NMR)**
45:55	35-45
55:45	9
65: 35	7
70:30	4
80:20	< 1
Free Radical Photo-polymerization (20°C)	
45:55	7
70:30	4

Table 3.3 *Degree of hydrolysis of isolated PMV as function of comonomer ratio and method of copolymerization.*

3.4.7 Rate of hydrolysis of PMV_{50} in aqueous solution

Current literature on the rate of hydrolysis of the corresponding homopolymer, poly(VDMA) is limited, and only states that the polymer is hydrolytically stable in water, as its hydrophobic nature prohibits dissolution.[22] In contrast, the half-life of the VDMA analog 4,4-dimethyl-2-phenyloxazolin-5-one in water has been reported[32] as 36 min at pH 8 and 25°C, which is in agreement with the rates determined for our water-soluble VDMA copolymers. Potentiometric measurements of a 0.2 wt% solution of as-formed photo-polymerized PMV_{50} (7% hydrolyzed) in 35 mM HEPES pH 7.8 buffered saline, revealed that the azlactone hydrolysis is essentially complete after 3 hours, with an approximate half-life of about 30 minutes, Figure 3.8. A rapid initial drop in pH from 8.1 to 7.5 is attributed to the protonation of the free carboxylic acid groups present, and is followed by a more gradual decrease in pH to about 7.25, which is attributed to the hydrolysis of azlactone as well as any anhydride groups present. Similar rates of hydrolysis were observed for the partially hydrolyzed PMV_{50} prepared by copolymerization at 60°C.

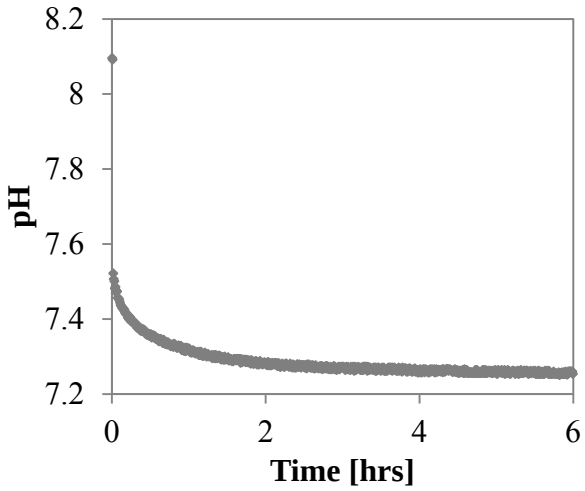

Figure 3.8 *The change in pH over time of PMV_{50} in aqueous medium is measured by dissolving 20 mg of as-formed photo-polymerized PMV_{50}, (7% hydrolyzed after synthesis) in 20 ml of pH 8.1, 35 mM HEPES buffered saline at time 30 s.*

3.4.8 AP-PMV_{50}*f* capsules

Finally, calcium-alginate-PLL (AP) capsules were coated with a 0.2% HEPES buffered PMV_{50}*f* solution for 10 min (Figure 3.9a). Although, some immune-isolation research looks to replace PLL with more bio- and cyto-compatible components,[33] PLL was selected as the polycation for this study, so that subsequent *in-vivo* and *in-vitro* studies[23] would allow for a direct comparison to conventional APA capsules. These studies aim to test whether PMV_{50} is better able to mask the PLL, resulting in improved cell and host compatibility. The PLL and PMV_{50} coating conditions were optimized to allow for sufficient crosslinking between the PLL and PMV_{50}*f* layers, while maintaining good cell viability.[23]

To prove that covalent crosslinking has occurred, AP-PMV_{50}*f* capsules were first treated with 1M sodium citrate to liquefy the calcium-alginate core, leaving only an alginate-PLL-PMV_{50}*f* shell (Figure 3.9b). This shell was then treated with 0.1 M sodium hydroxide (Figure 3.9c), which deprotonates the primary ammonium cations on PLL, eliminating its ionic interactions with the two polyanions. Thus, the only remaining interactions should be the amide crosslinks between PLL and PMV_{50}*f*. If no covalent reaction occurred, the complex would dissolve completely after the addition of sodium hydroxide.

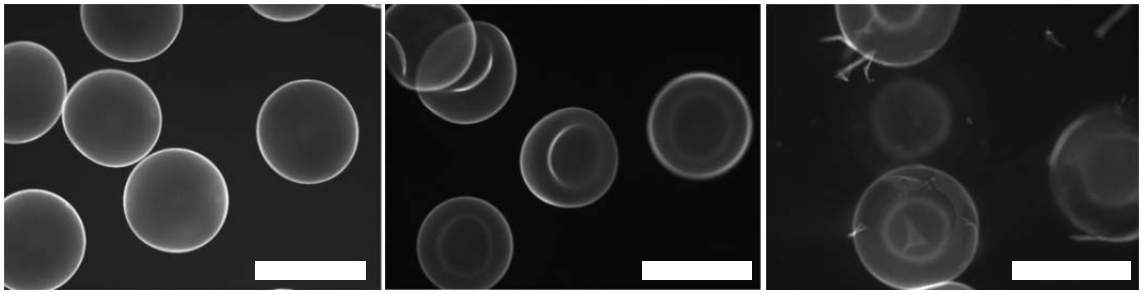

Figure 3.9 (a) *A-PLL-PMV$_{50}$f as seen under the fluorescent optical microscope,* ***(b)*** *after the addition of 1 M sodium citrate,* ***(c)*** *after the addition of 0.1 M sodium hydroxide, the complex remains. Scale bar denotes 500 µm.*

Future work will explore the effect of molecular weight and VDMA/acid ratio on the rate of hydrolysis in aqueous environments, on the polyelectrolyte complexation with polyamines, and on the biophysical properties of the covalent networks formed around AP capsules.

3.5 Conclusions

The reactivity ratios for VDMA and MAA were determined to be 1.36 and 0.41 for r1(VDMA) and r2(MAA), respectively. A copolymer of approximately 50: 50 VDMA:MAA was synthesized by a semi-batch copolymerization carried out at 60°C under anhydrous conditions with a near-constant VDMA:MAA feed ratio of about 35: 65 mol%. Quantitative ^{13}C NMR showed that about 40% of the azlactone groups in the isolated polymer were hydrolyzed during the copolymerization, with concomitant formation of cyclic anhydride from methacrylic acid diads. This trans-hydration side-reaction could be largely suppressed by using higher VDMA:MAA mol ratios, or by use of photo polymerization at 20°C. The half-life of the azlactone groups on PMV$_{50}$ was found to be about 30 min in HEPES buffer, sufficiently long to allow formation of covalently crosslinked shell around AP capsules developed for cell encapsulation. Future work will explore the aqueous hydrolysis, polyelectrolyte complexation and covalent crosslink formation of other VDMA:MAA copolymers, as described above.

3.6 Acknowledgements

The authors would like to thank Dr. Bob Berno for help with the saturation-recovery and quantitative NMR experiments, Dr. Steve Kornic for running elemental analysis and IR samples, and Dr. Randall Dumont for his help with the contour plot. HDHS would like to thank NSERC's discovery program for funding, and CMG would like to acknowledge receiving an NSERC Alexander Graham Bell doctoral scholarship.

3.8 Appendix

A more extensive investigation of the reactivity of the trans-hydrated PMV_{50} polymer with phenethylamine is provided in the supplementary information section.

3.7 References

[1] M.A. Gauthier; M.I. Gibson; H.A. Klok. *Angew. Chem. Int. Ed.* **2009**. *48,* 48-58.
[2] P. Theato. *J. Polym. Sci. A* **2008**, *46,* 6677-6687.
[3] C.M. Gardner; N.A.D. Burke; H.D.H. Stover. *Langmuir* **2010**, *26,* 4916-4924.
[4] M.E. Buck; A.S. Breitbach; S.K. Belgrade; H.E. Blackwell; D.M. Lynn. *Biomacromolecules* **2009**, *10,* 1564-1574.
[5] J.D. Flores; J. Shin; C.E. Hoyle; C.L. McCormick. *Polym. Chem.* **2010**, *1,* 213-220.
[6] U. Freudenberg; A. Hermann; P.B. Welzel; K. Stirl; S.C. Schwarz; M. Grimer; A. Zieris; W. Panyanuwat; S. Zschoche; D. Meinhold; A. Storch; C. Werner. *Biomaterials* **2009**, *30,* 5049-5060.
[7] J. Su; B. Hu; W.L. Lowe Jr.; D.B. Kaufman; P.B. Messersmith. *Biomaterials* **2010**, *21,* 308-314.
[8] F. Shen; M.A.J. Mazumder; N.A.D. Burke; H.D.H. Stöver; M.A. Potter. *J. Biomed. Mat. Res. B Appl. Biomat*. **2009**, *90B,* 350-361.
[9] M.A.J. Mazumder; N.A.D. Burke; F. Shen; M.A. Potter; H.D.H. Stöver. *Biomacromolecules* **2009,** *10,* 1365-1373.
[10] S. Mohajeri; N.A.D. Burke; H.D.H. Stöver. in progress.
[11] S.M. Heilmann; J.K. Rasmussen; L.R. Krepski. *J. Polym. Sci. A* **2001***, 39,* 3655-3677.
[12] B. Sun; Z. Liu; M.E. Buck; D.M. Lynn. *Chem. Commun*. **2010**, *46,* 2016-2018.
[13] D.C. Tully; M.J. Roberts; B.H. Geierstanger. *Macromolecules* **2003**, *36,* 4302-4308.
[14] M.E. Buck; J. Zhang; D.M. Lynn. *Adv. Mater.* **2007**, *19,* 3951-3955.
[15] M.E. Buck; D.M. Lynn. *Langmuir* **2010***, 26,* 16134-16140.
[16] A. Guyomard; D. Fournier; S. Pascual; L. Fontaine; J.F. Bardeau. *Eur. Polym. J.* **2004**, *40,* 2343-2348.
[17] S.M. Heilmann; G.J. Drtina; L.C. Haddad; J.K. Rasmussen; B.N. Gaddam; J.J. Liu; R.T. Fitzsimons; D.D. Fansler; J.R. Vyvyan; Y.N. Yang; T.J. Beauchamp. *J. Mol. Catal. B Enzym.* **2004**, *30,* 33-42.
[18] P.L. Coleman; M.M. Walker; D.S. Milbrath; D.M. Stauffer; J.K. Rasmussen; L.R. Krepski; S.M. Heilmann; *J. Chrom.* **1990**, *512,* 345-363.
[19] J.K. Rasmussen; R.M. Gleason; D.S. Milbrath; R.L. Rasmussen. *Ind. Eng. Chem. Res.* **2005**, *44,* 8554-8559.
[20] L.G. Stanek; S.M. Heilmann; W.B. Gleason. *J. Polym. Sci. A* **2003**, *41,* 3027-3037.
[21] L.G. Stanek; S.M. Heilmann; W.B. Gleason. *Polym. Bull.* **2005**, *55,* 393-402.
[22] J.M. Messman; B.S. Lokitz; J.M. Pickel; S.M. Kilbey II. *Macromolecules* **2009**, *42,* 3933-3941.
[23] C.M. Gardner; M.A. Potter; H.D.H. Stover; *J. Mater. Sci: Mater. Med.* **2012**, *23,* 181-193.

[24] M.A.J. Mazumder; F. Shen; N.A.D. Burke; M.A. Potter; H.D.H. Stover. *Biomacromolecules* **2008**, *9,* 2292-2300.
[25] M.R. Aguilar; A. Gallardo; M.D. Fernánde; J.S. Román. *Macromolecules* **2002**, *35,* 2036-2041.
[26] G.E.P. Box; W.G. Hunter; J.S. Hunter. *Statistics for Experimenters: An Introduction to Design, Data Analysis and Model Building, Second Edition*, John Wiley & Sons: New York, **2005**; p 371.
[27] R.P. Haugland. *Handbook of Fluorescent Probes and Research Products*, *6th Edition*, Molecular Probes, Eugene, OR, **1996**, p 74.
[28] I. Šoljić; A. Jukić; Z. Janović. *Polym. Eng. Sci.* **2010**, *50,* 577-584.
[29] X. Sun; Y. Luo; R. Wang; B.G. Li; B. Liu; S. Zhu. *Macromolecules* **2007**, *40,* 849-859.
[30] M. Lazzari; T. Kitayama; K. Hatada. *Macromolecules* **1998,** *31,* 8075-8082.
[31] A. Asano; M. Eguchi; T. Kurotu. *J. Polym. Sci. Part B: Polym. Phys.* **1999**, *37,* 2007-2012.
[32] J.D. Jersey; B. Zerner. *Biochemistry* **1969**, *8,* 1967-1974.
[33] R. Mahou; C. Wandrey. *Macromolecules* **2010**, *43,* 1371-1378.

3.8 APPENDIX

3.8.1 Reaction of residual azlactone groups in PMV_{50} prepared by free radical copolymerization, with excess phenethylamine

Two 10 wt% PMV_{50} solutions in DMSO-d_6 were prepared. The first sample was used to determine the initial degree of hydrolysis, immediately following dissolution in DMSO-d_6, by quantitative ^{13}C NMR. The second sample was heated for 2 days at 60^oC prior to analysis by quantitative ^{13}C NMR. Both solutions were then separately diluted to 3 wt% using anhydrous DMSO. From each of these solutions, 0.66 mL (0.182 mmol of original azlactone) were taken and reacted with a 5 molar excess of phenethylamine in DMSO for 24 hrs at RT. The remainder of the 3 wt% solutions were diluted with 35 mM HEPES pH 7.8 buffered saline to make 0.2 wt% PMV_{50} solutions. From these solutions, 10 ml aliquots (20mg of PMV_{50}) were taken at 0, 0.25, 0.5, 0.75, 1, 1.5, 2, 3, 5, 7, 24 and 48 hrs after the last dilution, and immediately reacted with phenethylamine (5x molar excess with respect to the amount of azlactone groups present) in HEPES buffer for 24 hrs at RT while rotating at about 4 rpm.

The resulting polymers were precipitated by acidification with 1 M HCl to pH 2, and separated from unreacted phenethylamine by centrifugation for 10 min at 3500 rpm on a Hermle Z323 universal high-speed centrifuge. Subsequently the supernatant was removed and 45 mL alkaline (~pH 12) distilled deionized water was added to re-dissolve the precipitate. This process was repeated 3 times.

The isolated solid was washed twice with water and then dried in a vacuum oven at 60^oC for 3 days. ^1H NMR spectra were taken at 600 MHz in D_2O with 1 drop of 1 M NaOD added. Extent of reaction with phenethylamine was determined by comparing the integrations of the MAA and VDMA-based peaks, with the signal of the phenyl ring (5H) of phenethylamine.

3.8.2 Results and Discussion

Although the azlactone in PMV_{50} is hydrolyzed in this transhydration side reaction, the concurrent formation of anhydride suggests that the overall reactivity of the polymer may not change substantially. To examine this, as-formed PMV_{50} was dissolved in 35 mM pH 7.8 HEPES buffered saline, with aliquots taken at increasing time intervals to 48 hrs and reacted with an excess of phenethylamine to test for total electrophiles present. As well, as-formed PMV_{50} was dissolved in anhydrous DMSO and reacted with phenethylamine under anhydrous conditions. As quantitative ^{13}C NMR had shown that 42% of the VDMA units present in this sample of as-formed PMV_{50} are hydrolyzed, then if no anhydrides were formed in this process we would expect 58% of the original VDMA units on PMV_{50} to react with phenethylamine. However, Figure 3A.1 shows phenethylamine functionalization corresponding to 67% of the original VDMA, and the additional reactivity is attributed to cyclic anhydride units.

As well, a sample of as-formed PMV_{50} was heated in DMSO for two days at 60°C, and showed complete conversion of azlactone to the hydrolyzed azlactone groups by quantitative ^{13}C NMR. Reaction of this sample with phenethylamine still showed phenethylamine binding corresponding to 27% of the original VDMA groups, which is attributed again to reaction of the newly formed cyclic anhydride groups (Figure 3A.1).

However, even though VDMA appears to be hydrolyzed by MAA diacids forming cyclic anhydrides that are still able to react with primary amines such as phenethylamine, the conversion does not appear to be quantitative. Possible reasons for this could involve side reactions of the anhydride with DMSO to give an acyloxymethyl methyl thioether[1] or the gradual incorporation of atmospheric moisture.

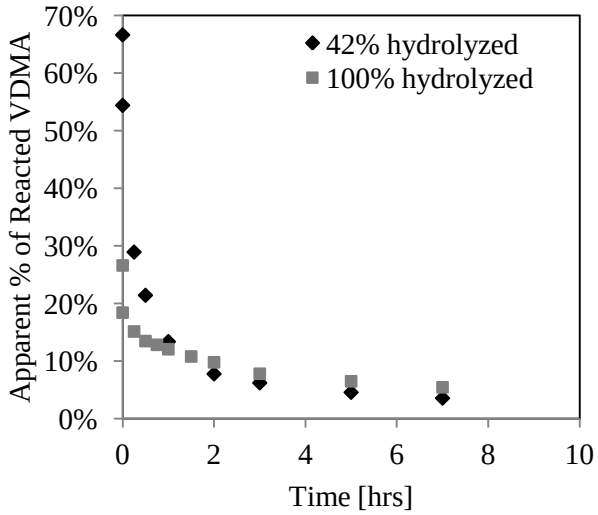

Figure 3A.1 *black diamonds and grey squares show the total electrophile groups as percentage of original azlactone, found using ^{13}C NMR measurement of phenethylamine bound to as-formed and fully transhydrated PMV_{50}, as function of hydrolysis time. The highest point is as-formed PMV_{50} reacted with phenethylamine in DMSO for 24 hrs and the second point is as-formed PMV_{50} reacted with phenethylamine in HEPES buffer for 24 hrs immediately after dissolution (time = 0 hrs).*

The above reactions with phenethylamine also provide some information about the relative rates of hydrolysis of azlactone and anhydrides, starting in HEPES buffer at pH 7.8. Figure 3A.1 shows that as-formed PMV_{50} comprising both azlactones and anhydrides has a half-life of roughly 30 min, whereas PMV_{50} that had been fully transhydrated by reaction in DMSO to contain only anhydride electrophiles, shows a longer half-life of approximately 2 hrs. Although not shown on Figure 3A.1, after 2 days in aqueous environments, no phenethylamine reacts with either as-formed or fully trans-hydrated PMV_{50}.

3.8.3. Reference

[1] N.A. Durgaryan; V.H. Matosyan; S.A. Markarian. *Eur. Polym. J.* **2003**, 39, 921-925.

CHAPTER 4: Improving Covalent Cell Encapsulation with Temporarily Reactive Polyelectrolytes

Casandra M. Gardner, Murray A. Potter, Harald D.H. Stöver

Published in *J Mater Sci. Mater Med*, 2012, 23, 181-193.

Contributions:
Dr. Harald Stöver, Dr. Murray Potter and I designed the experiments presented in this paper. I synthesized the two TRPs, performed *in-vitro* cell viability analysis, cellular overgrowth analysis using optical as well as scanning electron microscope, mechanical strength tests, statistical analysis and wrote the paper. Anna Li performed implantations and explantations of capsules in mice, and both Anna Li and Zahra Isfahani performed flow cytometry on the blood samples. Dr. Harald Stöver and Dr. Murray Potter helped edit the paper.

4.1 Abstract

Calcium alginate / poly-L-lysine beads were coated with either 50% hydrolyzed poly(methyl vinyl ether-*alt*-maleic anhydride) (PMM_{50}), or with poly(vinyl dimethyl azlactone-*co*-methacrylic acid) (50:50, PMV_{50}), to form covalently shell-crosslinked capsules, and compared with analogous capsules coated with sodium alginate. All capsule types were prepared with and without C2C12 murine myoblast cells, and implanted into mice for up to 6 weeks. Cell viability, capsule integrity, fibrotic overgrowth, and mechanical strength of the capsules were assessed, and correlated with inflammatory cytokine marker levels in tail vein blood samples taken at different time points. AP-PMM_{50} capsules displayed the least amount of fibrotic overgrowth, were found to be the strongest, and showed the lowest levels of TNF-α in tail vein serum samples taken at 4 hrs, 24 hrs, 1 week and 6 weeks post transplantation. The results for APA and AP-PMV_{50} capsules were more variable and depended on the presence or absence of encapsulated cells.

4.2 Introduction

Coated calcium-alginate beads are the basis of many encapsulation methods used in pursuit of cell-based enzyme and hormone replacement therapies.[1,2,3,4] The standard alginate - poly-L-lysine - alginate (APA) capsules consist of a calcium-alginate hydrogel core containing cells designed to express a therapeutic product, coated with permeability-controlling poly-L-lysine (PLL, a polycation)[5] followed by an exterior layer of polyanionic alginate. The capsules are typically implanted into the peritoneal cavity of the host where the encapsulated cells receive oxygen and nutrients by passive diffusion from the host and in turn release their therapeutic products. The semi-permeable capsule shell protects the cells from the host's immune system, in particular from cell-based immune attack, and should thus enable cell-based therapies based on allogenic and even xenogenic cells, without use of immune-suppressive drug regimens. As this technique is targeted for treatment of chronic disorders such as diabetes, lysosomal storage disorders, or Parkinson's, the capsules should be biocompatible, but not biodegradable, and provide protection against host immune response as well as mechanical breakdown for at least one year.

Although this approach is promising, the required long term survival of the implanted cells has remained largely elusive as calcium crosslinked APA capsules weaken over time and cause inflammatory responses.[6] An additional issue is that alginate properties vary significantly with source and processing[7] In particular, alginate has been shown to contain variable amounts of allergenic or immunogenic proteins, polyphenols and endotoxins.[8] If present on the exterior of the capsule, as observed by several groups[2,9] these compounds may cause fibrotic overgrowth of the capsule leading to cell asphyxiation.[10,11] As well, alginate has been reported to degrade by redox as well as hydrolytic processes in the body, raising further concerns about its long-term applications.[12]

One potential solution to improve long term performance of such microcapsules is to reinforce the ionic network bonds with a covalent network. In principle, the use of well-defined synthetic polymers may permit tuning of key hydrogel properties, such as strength, permeability, and chemical stability, while avoiding biological impurities found in naturally occurring polymers.

Ideally, covalent crosslinking suitable for cell encapsulation should proceed within minutes in aqueous saline at about 4 °C, without cytotoxic initiators or other small reagents and catalysts, at neutral pH and without producing cytotoxic byproducts or leave behind residual functional groups.

Several approaches to covalent strengthening of microcapsules have been described; these typically involve reactive small molecule crosslinkers or photocrosslinking of natural[13] or synthetic polymers. Some of the best examples of covalent crosslinking include Hubbell's network formation by Michael-type addition between thiol and acrylate-telechelic pleuronics.[14] Wang[15,16] prepared microcapsules that form covalent bonds through photodimerization of modified poly(allylamine) or PLL in the capsular membrane and has also explored the use of reactive poly(vinyl alcohol) to crosslink PLL at the capsule surface.[16] Photo-crosslinking of macromonomers and modified polymers[17] has also become a significant approach, as recent research has shown that polymer-bound radicals are quite cyto-compatible.[18]

In this study we present results of cell encapsulations involving two novel Temporarily Reactive Polyelectrolytes (TPRs) that were designed to replace the final, or 'exterior' alginate layer in conventional APA capsules. TPRs are defined as polyanions that possess reactive electrophilic groups capable of forming stable covalent crosslinks with the underlying polyamine (PLL), but where residual reactive groups subsequently hydrolyze to form innocuous carboxylates.[19]

The basic concept involves replacing the outer alginate layer of APA capsules with TRPs, using the same 'layer-by-layer' coating process already well established in the encapsulation field. The TRPs will electrostatically bind to the PLL present in the outer surface of the hydrogel beads, but then will spontaneously form stable covalent amide crosslinks within minutes of coating. Residual reactive groups will hydrolyze to form carboxylates (Scheme 1), preventing undesired covalent protein binding during incubation or after transplantation. As well, these carboxylate groups will generate additional negative charges at the bead surfaces, which may reduce electrostatic protein binding, and should help suppress inflammatory action arising from the polycation, PLL.[19]

An additional advantage of TPRs over alginate is that their reactive nature permits pre- and/or post- functionalization with bioactive molecules to improve their biocompatibility. For example, functionalization of TRP with short amino-PEGs, anti-inflammatory cytokines or cytokine antagonist peptides[20,21] before or shortly after bead coating could substantially improve the capsules' host-compatibility, as well as the viability of the encapsulated cells.

Results of cell encapsulation and implantations using two different TRPs are presented here and compared to APA capsules: 50% hydrolyzed poly(methyl vinyl ether-*alt*-maleic anhydride), PMM_{50}[19] and poly(methacrylic acid-*co*-2-vinyl-4,4-dimethyl-azlactone) with roughly a 50:50 co-monomer ratio, PMV_{50},[22] Scheme 4.1. These two *TRP*s have hydrolysis half-life times under physiological conditions of 2.5 min (PMM_{50})[19] and about 30 min (PMV_{50}),[22] respectively.

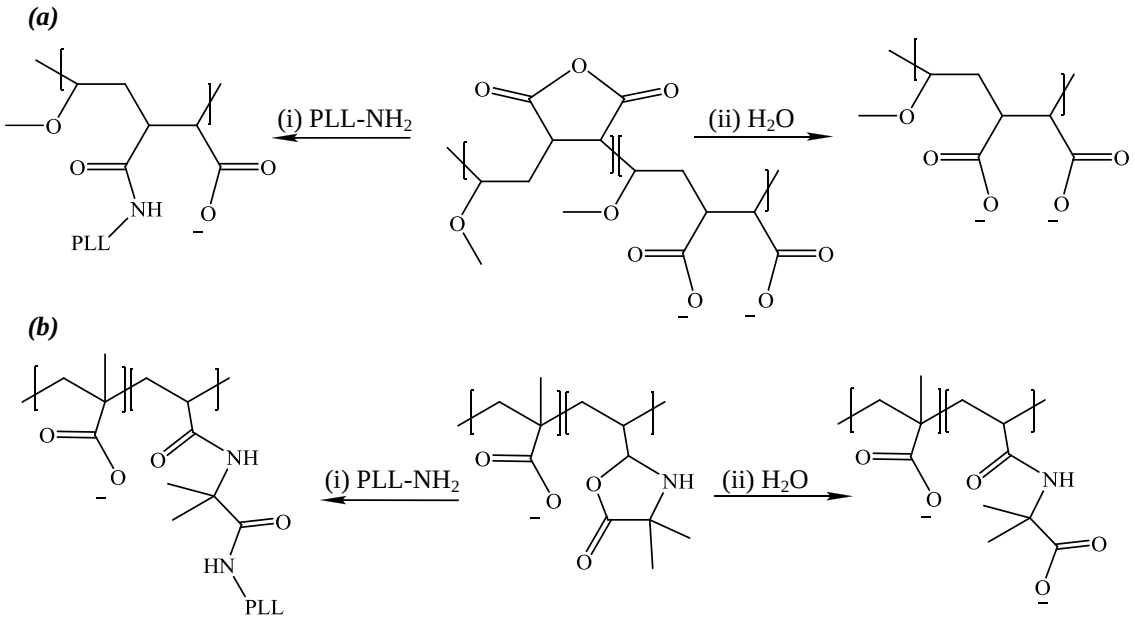

Scheme 4.1 (a) *PMM_{50}* ***(b)*** *PMV_{50}, (i) reaction with the primary amine on PLL, (ii) any remaining reactive groups hydrolysis in water to give carboxylates over time.*

This chapter will explore APA, AP-PMM_{50} and AP-PMV_{50} capsules with and without encapsulated C2C12 cells, in terms of biocompatibility (fibrotic overgrowth as well as serum cytokine analysis), mechanical strength, and both *in vitro* and *in vivo* cell viability over a 6 week time period.

4.3 Experimental

4.3.1 Materials

4,4-Dimethyl-2-vinyl-2-oxazoline-5-one (VDMA) was purchased from TCI America, Portland, OR. Poly(methyl vinyl ether-*alt*-maleic anhydride) (PMM_{100}), 20 kDa was purchased from Scientific Polymer Products, Ontario, and dried in a vacuum oven at 60ºC for 4 days to reform all anhydrides units. Methacrylic acid (MAA) 99%, 5-aminofluorescein (AF), poly(L-lysine hydrobromide) (PLL, 15-30 kDa), tetramethylrhodamine isothiocyanate-conjugated bovine serum albumin, HEPES sodium salt, trypan blue stain (0.4% in 0.81% aqueous NaCl), anhydrous DMSO, anhydrous THF, ethylene carbonate 98%, were purchased from Sigma-Aldrich, Oakville, ON, and

used as received. Azobisisobutyronitrile (AIBN) (Dupont, Mississauga), Sodium alginate (Pronova UP MVG, batch no. FP-610-03) was purchased from Novamatrix, Norway. Sodium chloride (Caledon Laboratories Ltd, ON), and calcium chloride (minimum 96% powder, anhydrous, Sigma-Aldrich, ON) were used as received. Sodium hydroxide and hydrochloric acid solutions were prepared from concentrates (Anachemia Chemical, Rouses Point, NY) by diluting to 0.100 M or 1.000 M with deionized water. Dimethyl Sulfoxide-d_6 (99.9 atom% DMSO-d_6), acetonitrile-d_3 (99.96 atom% D, ACN-d_3), and D_2O (99.9 atom% D) were obtained from Cambridge Isotope Laboratories, Inc. Andover, MA., Dulbecco's Modified Eagle's Medium (DMEM), Lonza serum-free medium 12-725F (Hyclone, VWR, Mississauga ON).

The following reagents were purchased from BD-Bioscience-Pharmingen: FcBlock™ (2.4 G2- purified), Stain buffer (BSA), Fixation buffer, BD Pharm Lyse™ lysing solution. DAPI was obtained from Sigma-Aldrich. Mouse soluble protein master buffer kit for Flex Cytometric Bead Array (CBA) was purchased from BD-Bioscience. The injectable saline (0.9% NaCl) was purchased from Baxter Corporation (Mississauga, ON). It was nonpyrogenic and sterile.

4.3.2 Synthesis of PMM_{50} and PMV_{50}

The syntheses of PMM_{50} [19] and PMV_{50} [22] have been described previously. They involve 50% hydrolysis of the anhydride groups in PMM_{100} (anhydride form) in a 90:10 acetonitrile: water mixture at 60°C for 15 hrs to form PMM_{50}, and the semi-batch copolymerization of VDMA and MAA to form about equimolar copolymers, respectively.

4.3.3 Cell Culture

The C2C12 murine myoblast cell line (American type Culture Collection [ATCC], Rockville, MD; catalog No. CRL- 1772) was maintained in DMEM serum free medium for cell encapsulation in the presence of 5% CO_2 with 100% humidity at 37°C in a water-jacketed incubator.

4.3.4 Cell Viability

The number of viable cells per capsule was determined using the Alamar Blue assay.[23] A total of 100 μL of capsules were loaded into each well of a 24-well plate with 500 μL medium. A 50 μL aliquot of Alamar Blue reagent was added to each sample and the plate was incubated at 37 °C for 4 hr. After incubation, 100 μL of supernatant was taken from each well and placed in a microtiter plate. The fluorescence of each sample was read with a Cytofluor II fluorimeter, with an excitation wavelength of 530 nm and an emission wavelength of 590 nm. The number of viable cells per capsule was determined by comparing the fluorescence intensity with a standard curve generated from a known number of C2C12 cells.

The ratio of live to dead cells in capsules was measured by placing approximately ten capsules on a microscope slide, together with a drop of trypan blue solution (Gibco, Mississauga, Ontario). After removing excess solution, several capsules, each containing approximately 100 cells, were crushed by applying pressure using a glass cover slip, and the released cells were examined for uptake of trypan blue stain. All cells, both dead and live cells, were released from the capsules by this process. At least 300 cells in total were counted for each sample, and the number of live (clear) and dead (blue) cells were used to calculate the percentage of live cells.

4.3.5 Standard Encapsulation procedure

All capsules were prepared by a procedure, derived from Sun[24] that has been described previously.[25] For empty capsules, a solution of 1 wt% MVG Novamatrix alginate in saline was filter sterilized (0.22 μm), and extruded through a flat-tipped 27-gauge needle with a concentric air flow (3.5 L/min) using a modified syringe pump, at a liquid flow rate of 0.5 mL/min, into a 1.1 w/v% $CaCl_2$ bath in a sterile laminar flow hood. For microcapsules containing cells, a C2C12 myoblast cell suspension in saline was mixed with sterile 1.0% w/v alginate solution to a final cell concentration of 2 millions cells/mL of alginate, prior to spraying into the $CaCl_2$ bath as described above. The resulting calcium-alginate beads were washed once with 1.1 w/v% $CaCl_2$, coated with PLL (filter sterilized (0.22 μm), 0.1% in saline for 6 min), and washed once with 1.1 w/v% $CaCl_2$ and once with saline, to give the intermediate AP beads. To form APA capsules, AP beads were coated with 0.03% filter sterilized sodium alginate in saline for 6 min. To form AP-PMM_{50} capsules, AP beads were washed an additional time with saline and then coated with a filter-sterilized 0.2% PMM_{50} solution in 35 mM pH 7.8 HEPES buffered saline for 6 min as described previously.[19] AP-PMV_{50} capsules were prepared by coating AP capsules with a filter-sterilized 0.2% PMV_{50} solution in 35mM pH 7.8 HEPES buffered saline for 6 min (this coating solution is prepared by diluting a 3wt% PMV_{50} solution in DMSO, with a fifteen-fold excess of 35 mM pH 7.8 HEPES buffer). After the final coating the APA, AP-PMM_{50} and AP-PMV_{50} beads were washed twice with saline and once with Lonza serum-free medium 12-725F. All coating and washing steps were performed at 4°C for 2 min and involved a 3:10 volume ratio of concentrated bead suspension to coating or washing solution. The capsules were finally placed in cell-culture dishes in serum free medium for at 2-3 days prior to injection into the mouse. *In-vitro* capsules were maintained in DMEM medium (supplemented with 10% FBS and 1% penicillin/streptomycin) in a tissue culture incubator in the presence of 5% CO_2 at 100% relative humidity and at 37°C for 6 weeks.

4.3.6 Implantation

Animals were treated in accordance with the Canadian Council on Animal Care Guide to the Care and Use of Experimental Animals. Freshly made capsules were kept in the serum free DMEM described above at 37 °C for 3 days before implantation in mice, as described previously.[26] Briefly, the mice were anaesthetized with isoflurane (Anaquest,

Mississauga, ON, Canada) using a small-animal anesthetic machine (Med-Vet, Toronto, ON, Canada). Six mice for each type of capsule APA, AP-PMM_{50}, AP-PMV_{50} with and without cells were implanted with a total of 3 mL of capsules suspended in saline (4 mL total) into the abdominal cavity using an 18 gauge catheter (Angiocath, Mississauga, ON). Microcapsules were recovered 1 week after implantation (1 mouse was sacrificed) and 6 weeks after implantation (5 mice were sacrificed). All mice were euthanized, the peritoneal cavity was opened, and the capsules were scooped out with a spatula. The capsules were washed several times with normal saline before the percent volume of recovered capsules was noted.

Tail vein blood samples were also collected at 4 hr, 24 hr, 1 week and 6 weeks following implantation and frozen at -70^{o}C for 2 months prior to cytokine analysis using flow cytometry.

4.3.7 Microcapsule characterization

Capsules were examined by optical microscopy with an Olympus BX51 optical microscope fitted with a Q-Imaging Retiga EXi digital camera and ImagePro software. The percent of surface overgrowth[27] (overgrown surface area/total surface area) was calculated by manually measuring and averaging the percent surface overgrowth on 200 randomly selected capsules. One mouse was sacrificed after 1 week, and five after six weeks. Capsules were also analyzed by scanning electron microscopy (SEM). To prepare the samples, the capsules were gradually switched from a saline suspension to an ethanol suspension by increasing the ratio of ethanol to water in four steps from 0:100, through 25:75, 50:50, 75:25 to 0:100 water to ethanol, followed by washing four times with ethanol. Optical microscopy showed the capsules shrinking from 500 µm to 300 µm during this process. The capsules were then dried using a critical point dryer from Ladd Research Industries (Williston, VT), where the capsules were observed to shrink further to 150 µm in diameter. The samples were examined using a Tescan Vega II LSU scanning electron microscope (Tescan USA, PA), using a Backscattered Electron (BSE) detector and VEGA UniVac (variable pressure) at 10 kPa which allowed us to examine our capsules in an uncoated state.

4.3.8 Test for Covalent Crosslinking – Na citrate NaOH Test

Capsules (explanted and *in-vitro*) were tested for covalent crosslinking by placing one drop of a concentrated capsule suspension containing about 30 capsules on a microscope slide mounted on a fluorescence microscope. The supernatant was removed and immediately replaced with 2 drops of 1 M sodium citrate, a good calcium chelator, and the capsules were gently mixed. This process was repeated once. Subsequently, the supernatant was replaced with two drops of 0.1 M sodium hydroxide under gentle agitation, and the integrity of any remaining shells assessed qualitatively by optical microscopy.

4.3.9 Flex CBA assay for cytokine detection

BD Cytometric Bead Array (CBA) mouse cytokine Flex Set Master Buffer Kit was employed for simultaneous quantitation of IL-6, IL-10, TNF-α, MCP-1, G-CSF and IL-1a in the serum of C57BL/6 mice. In brief, all lyophilized standard spheres were pooled into one 15 ml conical tube and labelled top standard. Then, top standard was reconstituted with 4 ml of Assay Diluent, generating a stock concentration of 2500 pg/ml for each cytokine. The standard stock was serially diluted in the same buffer to generate 10 points for the standard curve. The 50× concentrated Capture Beads for each cytokine were diluted and mixed together to prepare mixed capture beads. The assay was performed in flow cytometry tubes. Premixed beads (50 µl) coated with target capture antibodies were transferred to each tube and premixed standards or samples (50 µl) were added to each tube containing beads. The tubes were mixed gently and incubated for 1 hour at room temperature. After incubation, the mixed PE detection reagent (50 µl) was added to each tube. The incubation was terminated after 1 hour at room temperature in the dark. After staining, 1 ml Flex CBA array wash buffer was added into each tube, mixed by pipetting, centrifuged (1000 rpm, 5 min at room temperature), the supernatant decanted, and the samples blotted on paper towels. Samples were resuspended in 300 µl Flex CBA wash buffer and run the same day using a FACS LSRII. 3300 events per tube were acquired, and the data analyzed using FCAP array software by the manufacturer.

4.3.10 Statistics

The significance of the data was evaluated by means of single factor ANOVA. A value of $p < 0.05$ was considered statistically significant. A Tukey LSD test was performed on the data that showed statistic differences.

4.4 Results

It has been observed that conventional APA type capsules (when optimized and under specific conditions) work reasonably well in small animals such as mice, but fail in larger animal breeds such as canines.[6] Depending on the alginate source, alginate has different guluronic acid (G): mannuronic acid (M) ratios, different molecular weights and viscosity, and variable amounts of impurities such as polyphenols, proteins and/or endotoxins. It has been pointed out that "there is no reason why alginate should be irreplaceable as the polymer that is used for the outer coating of the microcapsules." [28] Therefore this study explored replacing the exterior coating of alginate on APA capsules with synthetic reactive polyanions that can provide reactive groups capable of forming permanent covalent bonds to improve long term mechanical strength.

APA graft failure has consistently been associated with pericapsular cellular overgrowth leading to thick fibrosis which results in necrosis of encapsulated cells.[29] Capsule overgrowth has been shown to be a typical late-stage foreign body reaction,[27] and is commonly measured by expressing the amount of fibrotic overgrowth in terms of a percentage of surface area overgrowth on the recovered capsules. This type of analysis

was performed in this study and correlated with the pericapsule cellular overgrowth observed using SEM, and with the levels of several cytokines in tail vein serum, at different time points.

All calcium-alginate capsules were coated with 0.1% PLL followed by the exterior polyanion layer. APA, AP-PMM_{50} and AP-PMV_{50} capsules with and without encapsulated cells were then implanted into mice for up to 6 weeks.

AP-PMM_{50} capsules consistently showed the least amount of fibrotic overgrowth for microcapsules with and without encapsulated cells, with 2.5% or less surface overgrowth after 6 weeks (Figure 4.1b, and 4.2a) and 60 ± 5% or greater cell recovery rate, Figure 4.2b (the highest recovery rate seen in this study). Overgrowth is defined here as the average overgrown surface area of at least 200 randomly selected capsules as determined by visible microscopy. It has been reported[27] that severe overgrowth is associated with low recovery rates, whereas higher recovery rates are associated with less peri-capsular overgrowth.

APA capsules with encapsulated cells were found to have 9 ± 3% surface overgrowth after 6 weeks, (statically more overgrowth than AP-PMM_{50}, $p < 0.01$) and a recovery rate of 30 ± 5%, (Figure 4.1a(i) and 4.2). APA capsules without encapsulated cells fared much worse, with 40 ± 40% surface overgrowth and a 25 ± 10% recovery rate after 6 weeks (Figure 4.1a(ii), 4.2), with capsules explanted from two out of the five mice being almost completely overgrown.

AP-PMV_{50} capsules containing cells displayed the most ($p < 0.01$) fibrotic overgrowth, with 70 ± 30% surface overgrowth and a 15 ± 7% recovery rate after 6 weeks (Figure 4.1a(i), 4.2). AP-PMV_{50} capsules containing no cells had substantially less fibrotic overgrowth at 8 ± 3% surface overgrowth and 40 ± 5% recovery rate. At this time it is unclear why AP-PMV_{50} capsules with cells did so poorly. It is most likely not from the nature of PMV_{50} itself, as two pilot studies (unpublished data[a]) with AP-PMV_{50} capsules with and without encapsulated cells showed less than 6 ± 2% and 2% overgrowth, respectively, after 1 week *in-vivo* under identical conditions as in this study (AP-PMM_{50} was also used in this pilot study with results identical to those seen in the present study). Due to the volume of capsules required for this study each type of capsule was prepared in separate batches of 30 mL. Thus, it is possible that some contamination was introduced during the manufacturing of only the AP-PMV_{50} capsules containing cells in this experiment but not in the pilot study or formation of other types of capsules in this study. Supporting this explanation, *in-vitro* AP-PMV_{50} capsules with encapsulated cells were found to be contaminated after week one and had to be discarded.

[a] In the unpublished data, the standard deviation for microcapsules with encapsulated cells reflects calculations of surface overgrowth from five mice. No standard deviation is given for microcapsules without encapsulated cells, as data is reflective of only one mouse.

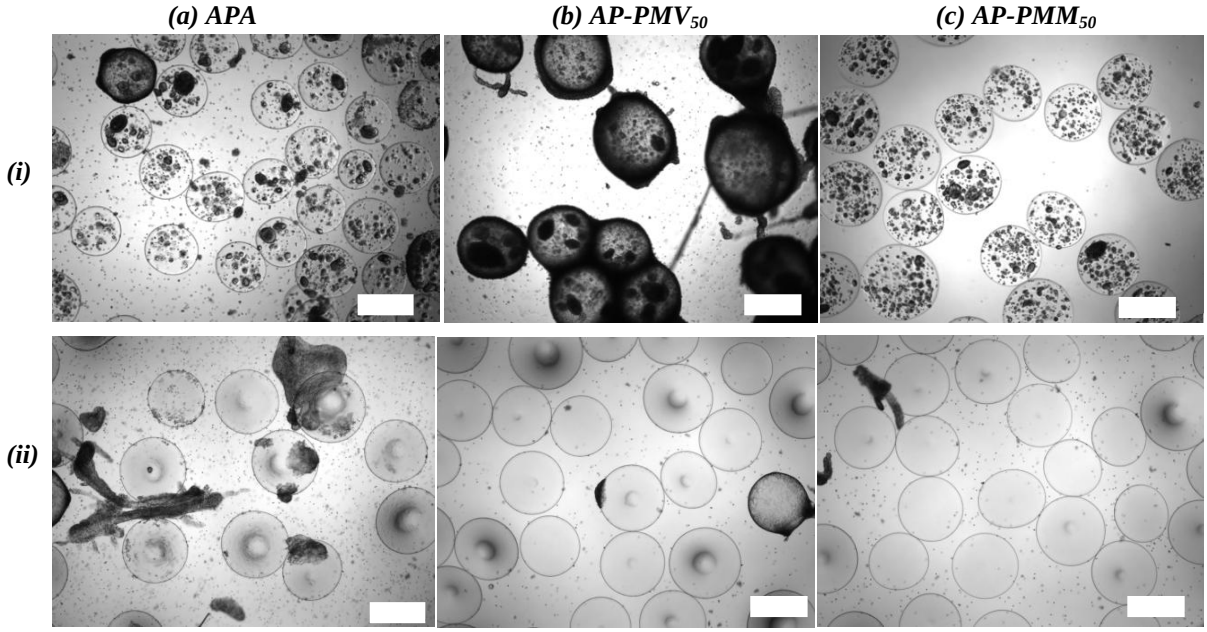

Figure 4.1 (a) *APA,* ***(b)*** *AP-PMV$_{50}$,* ***(c)*** *AP-PMM$_{50}$ microcapsules explanted after 6 weeks* ***(i)*** *with encapsulated cells* ***(ii)*** *without encapsulated cells. *images were selected as representative of the capsules explanted. Scale bar represents 500 µm.*

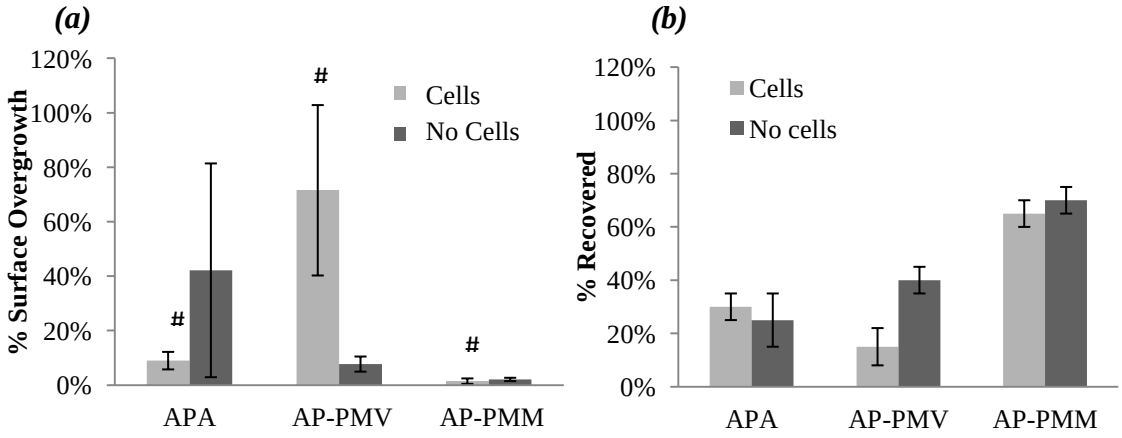

Figure 4.2 *Capsules explanted after 6 weeks,* ***(a)*** *overgrowth comparison* ***(b)*** *% volume of recovered capsules. n=5 mice, # p<0.01, ANOVA.*

The percentage of overgrowth was then correlated with the levels of IL-6, IL-10, TNF-α, MCP-1, G-CSF and IL-1a cytokines in tail vein serum. These cytokines were selected as they had shown the largest spikes in response to peritoneal injection of empty APA capsules or calcium alginate beads, compared with saline control injections.[30]

Cytokine response has not only been connected to cellular overgrowth,[31] but is also important to the encapsulated cells, especially more sensitive cells like islets. Reports as early as 1992 showed that elevated pro-inflammatory cytokine level can reduce

secretion of insulin and progressively damage encapsulated islet cells.[32] More recently, Lin (2009)[20] showed *in-vitro* that a cytokine inhibiting peptide that was covalently grafted to the hydrogel surrounding encapsulated islet cells, increased glucose secretion rates as well as cell viability. While in the future PMM_{50} and PMV_{50} may be similarly covalently modified with anti-inflammatory cytokines to improve long term graft survival, the present chapter aims to assess the cytokine response of unmodified capsules.

Alginate alone, has been shown to activate macrophages (as measured by TNF-α production) generating a pro-inflammatory signal.[33,34] As well, AP microcapsules implanted intraperitoneally have also been shown to increase TNF-α secretion *in-vivo.*[35] It was initially speculated that coating AP capsules with our TRPs, as opposed to alginate, would minimize TNF-α secretion and the subsequent pro-inflammatory response. In the current work, levels of TNF-α peaked at 1 week, with levels for APA capsules with cells being higher than those for AP-PMM_{50} capsules with cells ($p < 0.01$) (Figure 4.3a), and comparable to those measured for AP-PMV_{50} with cells. TNF-α levels at 1 week for empty APA capsules were higher compared to both empty AP-PMV_{50} capsules ($p < 0.01$) and empty AP-PMM_{50} ($p < 0.05$) (Figure 4.3b).

At 6 weeks, APA and AP-PMV_{50} capsules with cells had higher TNF-α levels than AP-PMM_{50} capsules with cells ($p < 0.01$). The high TNF-α levels observed for AP-PMV_{50} is consistent with the 70 ± 30% surface overgrowth seen at 6 weeks. However, APA showed much less surface overgrowth at 6 weeks (9 ± 3%), but had a fairly low capsule recovery percentage at 25 ± 10%. This suggests that the capsules that were not recovered may have been substantially overgrown, thus causing higher TNF-α levels. King (2001)[31] speculated that lower retrieval rates can also be the result of other factors such as capsule instability, which is consistent with the ionic nature of APA capsules.

Generally, AP-PMM_{50} showed the lowest TNF-α levels throughout the 6 week time period. It is also interesting to note that the overall TNF-α levels are similar for capsules with and without encapsulated cells (Figure 4.3a, b).

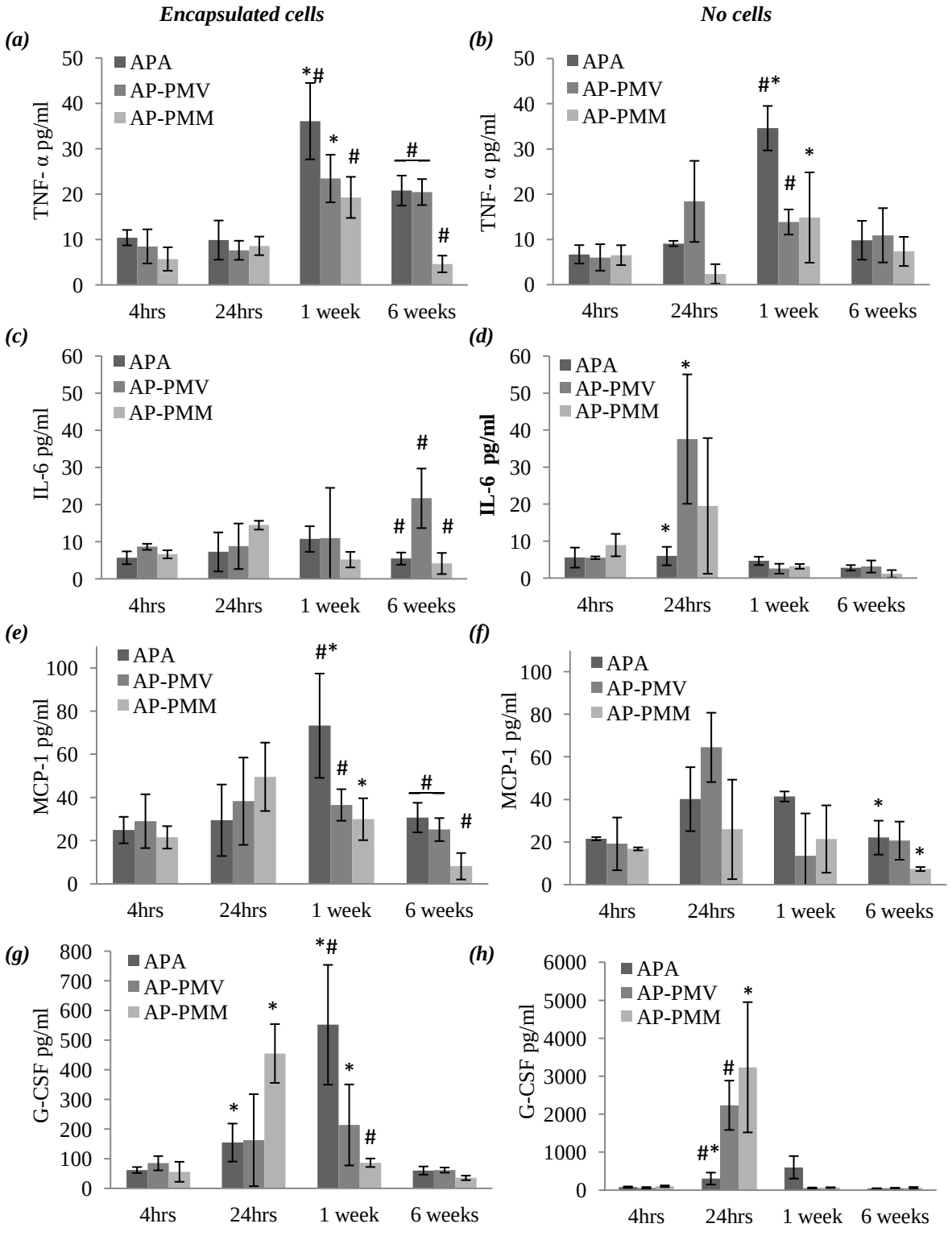

Figure 4.3 (a) *TNF- α levels with encapsulated cells* ***(b)*** *TNF- α levels without cells,* ***(c)*** *IL-6 with encapsulated cells* ***(d)*** *IL-6 without cells,* ***(e)*** *MCP-1 with encapsulated cells* ***(f)*** *MCP-1 without cells,* ***(g)*** *G-CSF with encapsulated cells,* ***(h)*** *G-CSF without cells,*

sampled over the course of 6 weeks from the tail vein serum, and analyzed by flow cytometry.[b] *n=3-5 mice per group, * p<0.05, # p<0.01, ANOVA*

Interleukin-6 (IL-6) can act as both a pro-inflammatory and anti-inflammatory cytokine. However, it often serves as a marker for fibroblast activation. It has also been shown to be important in transitioning between acute and chronic inflammations by recruitment of mononuclear cells to the area of inflammation. Capsules with cells displayed fairly constant IL-6 levels throughout the 6 week study (Figure 4.3c), however at 6 weeks AP-PMV_{50} displayed higher IL-6 levels when compared to both APA and AP-PMM_{50} ($p < 0.01$). This is consistent with the massive amount of overgrowth seen at 6 weeks for empty AP-PMV_{50} capsules, and suggests that the transition between acute to chronic inflammation was occurring. Empty capsules showed peak IL-6 levels at 24 hr (Figure 4.3d). At 24 hr APA IL-6 levels were lower than AP-PMV_{50} ($p < 0.05$), but not AP-PMM_{50} due to its large standard deviation. At 6 weeks, all empty capsules returned back to baseline levels.

In terms of cell encapsulation monocyte chemoattractant protein-1 (MCP-1) has not been studied to the same degree as the previously mentioned cytokines. MCP-1 is produced by both immune and non-immune cells in response to various stimuli including TNF-α.[36] MCP-1 levels peaked between 24 hr and 1 week for both capsules with and without encapsulated cells. For capsules with encapsulated cells the relative values for MCP-1 were identical to TNF- α values for 1 week and 6 weeks, with APA having the highest levels at 1 week ($p < 0.05$, with respect to AP-PMV_{50} and $p < 0.01$, with respect to AP-PMM_{50}). As well APA and AP-PMV_{50} were statistically higher than AP-PMM_{50} at 6 weeks, Figure 4.3e ($p < 0.01$). As stated previously this trend seems to correlate well with the overgrowth data. Empty capsules, on the other hand (Figure 4.3f) displayed large standard deviations, resulting in no statistical variation between all data points with the expectation of AP-PMM_{50} capsules showing lower levels than APA and AP-PMV_{50}, at 6 weeks.

Another less-studied cytokine is granulocyte colony-stimulating factor (G-CSF), which is produced by macrophages to recruit granulocytes as part of the inflammatory response. G-CSF was shown to peak after 24 hrs for both capsules with and without encapsulated cells. Looking at capsules with cells, AP-PMM_{50} levels peaked at 24 hr where as AP-PMV_{50} and APA levels peaked at 1 week, Figure 4.3g. At 24 hr AP-PMM_{50} displayed higher G-CSF levels than APA ($p < 0.05$), however at 1 week APA was statistically higher than both AP-PMV_{50} ($p < 0.05$) and AP-PMM_{50} ($p < 0.01$) levels, Figure 4.3g. G-CSF levels returned to baseline for all three types of capsules after 6 weeks. A similar trend was observed for capsules without cells, Figure 4.3h. G-CSF

[b] Four outlying values (that were 9 times or greater than the average of the other data points in the group) were removed from this analysis, as measurement errors were suspected. These outlying values were removed from 1 week or 6 weeks where there was 5 and 4 data points respectively, thus leaving 4 or 3 data points to determine SD.

levels peaked at 24 hr for AP-PMM_{50} and AP-PMV_{50} and 1 week for APA capsules. However, AP-PMM_{50} and AP-PMV_{50} were both found to have extremely high levels of G-CSF at 24 hr ($p < 0.05$ and $p < 0.01$, respectively, when compared to APA capsules). At this point it is unclear why the synthetic polymers elicit such high G-CSF levels at 24 hr. However, at 1 week levels returned to baseline and remained there until 6 weeks, indicating that these initial high levels resolve themselves.

IL-1α and IL-10 showed no statistical difference between all types of capsules and at each time point in this study, therefore no conclusions could be drawn. All IL-1α values averaged around 75 ± 45 pg/ml whereas IL-10 values were all barely above baseline, averaging about 1.8 ± 1.4 pg/ml.

The encapsulated C2C12 cell viability was also assessed throughout the 6 week time period *in-vitro*, using the Alamar blue assay to determine the number of viable cells/capsule, as well as using Trypan blue staining to determine the percentage of live cells to dead cells in each capsule. These methods do not allow screening of explanted capsules as fibrotic overgrowth would give large false positives.

Initially (the day of implantation, following 2-3 days incubation in serum-free medium[c]) the Alamar blue test revealed that AP-PMV_{50} and AP-PMM_{50} capsules contained approximately 200 viable cells/capsule, whereas APA capsules contained approximately 100 viable cells/capsule (Figure 4.4). Analysis with trypan blue showed that a similar percentage (approximately 75%) of the cells were alive in all three types of capsules, which suggests that the encapsulated cells are not negatively affected by PMV_{50} and PMM_{50} coating. The initial difference in the amount of viable cells/capsule in APA *vs.* AP-PMM_{50} and AP-PMV_{50} is the result of variations between each batch of capsules made, and not from an increase in proliferation in AP-PMV_{50} and AP-PMM_{50} capsules, as the same percentage of alive cells was found in each capsule type. The viability of all encapsulated cells and the percentage of live cells to dead cells was maintained over the course of 1 week *in-vitro*, ($p > 0.05$).[d] This is consistent with previous results seen in our mouse pilot study (unpublished data) where the cellular viability of AP-PMM_{50} and AP-PMV_{50} encapsulated cells did not change over the course of 1 week *in-vitro*, with 87 ± 6 and 50 ± 10 cells/capsule, respectively and > 85% alive cells for both capsule types.

[c] Capsules are incubated in serum-free medium to avoid transfer of serum proteins from the cell culture medium to the mouse when the capsules are implanted.
[d] Due to contamination issues after 1 week, the 6 week data points could not be reliably presented.

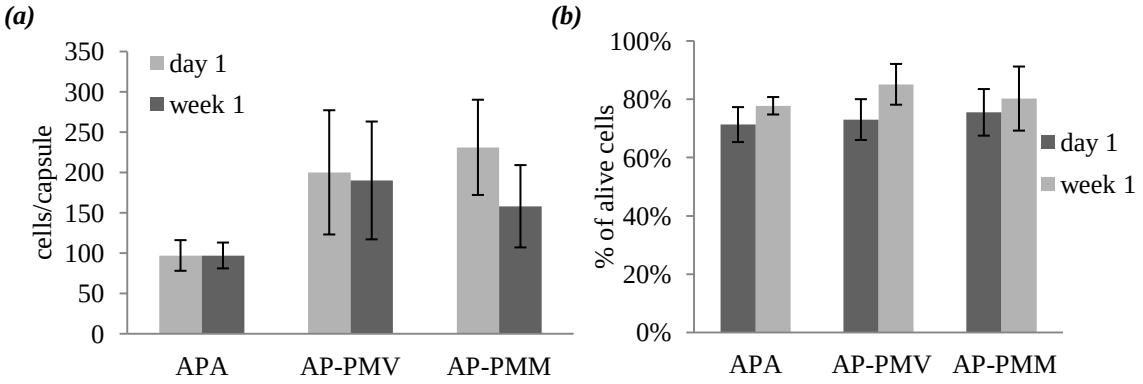

Figure 4.4 *Viability tests on in-vitro capsules* ***(a)*** *alamar blue test* ***(b)*** *trypan blue test for microcapsules with encapsulated cells showing the number (based on metabolic activity) and the percent of alive encapsulated cells, respectively.*

However, it was noted that there was a significant difference in cell proliferation between *in-vitro* and *in-vivo* samples, with much more cell proliferation occurring *in-vivo*. Figure 4.5a, shows APA capsules after 6 weeks *in-vitro* compared to APA and AP-PMM_{50} capsules after 6 weeks *in-vivo*, Figure 4.5b and 4.5c, respectively. It is clear that the cells inside capsules extracted from mice (*in-vivo)* have divided/proliferated to a greater extent, when compared to cells in capsules that were kept in growth medium (*in-vitro*). This can be seen by the larger dark clusters of cells in Figure 4.5b and c compared to the much smaller clusters seen in the APA *in-vitro* capsules. Similar results for encapsulated C2C12 cells were observed by Li (2006).[37] Therefore, it is important to note that testing *in-vitro* cell viability may not accurately reflect the *in-vivo* situation. Future mice studies will use genetically engineered cells that secret a specific enzyme that can be quantified following explantation to give a better indication of *in-vivo* cellular viability and activity.

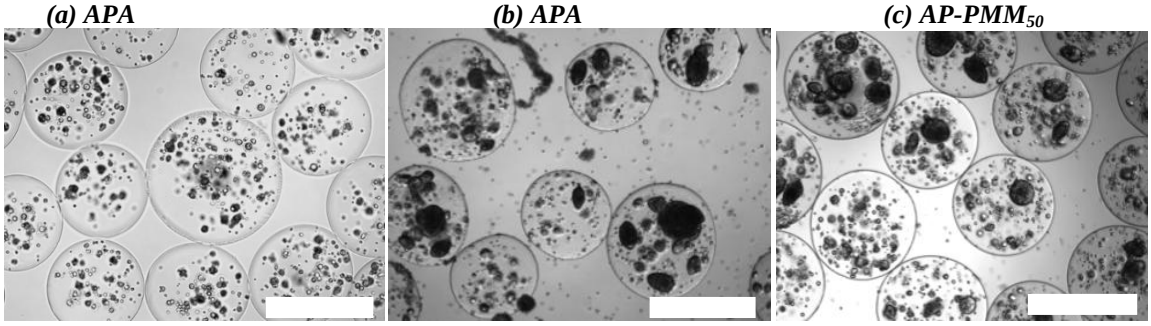

Figure 4.5 (a) *APA capsules in-vitro for 6 weeks,* ***(b)*** *APA capsules in-vivo for 6 weeks* ***(c)*** *AP-PMM_{50} capsules in-vivo for 6 weeks. Scale bar represents 500 µm.*

As long-term integrity is a key requirement for therapeutic cell capsules, we compared the resistance of all three types of capsules to chelators and sodium hydroxide

at different stages, in particular to assess the effect of the covalently crosslinked AP-PMM_{50} and AP-PMV_{50} capsules to the ionically crosslinked APA capsules.

The sodium citrate / sodium hydroxide test[19] is designed to test for covalent cross-linking. After liquefying the calcium-alginate core with sodium citrate, a strong Ca^{2+} chelator, 0.1 M NaOH is added to the capsules to deprotonate the primary amines on PLL, removing all electrostatic interactions. Ionically crosslinked capsules should hence completely dissolve after sodium hydroxide addition, and this was indeed observed for APA capsules (Figure 4.6a). For covalently crosslinked capsules the shell or shell fragments should persist after the addition of NaOH, as seen in Figure 4.6b for AP-PMM_{50} capsules. The number of intact capsules (full shells) is counted after NaOH addition, in order to get an idea of the crosslink density of the capsules (i.e. higher crosslink density should give completely intact shells, whereas lower crosslink density would give more shell fragments, Figure 4.6c).

When this test was performed on AP-PMM_{50} capsules both *in-vitro* and *in-vivo* after week 1 and 6, 100% of the capsules remained intact indicating a high crosslink density around the capsule that did not weaken over time. For AP-PMV_{50} 70% of the capsules remained intact for *in-vitro* capsules after 1 and 6 weeks, where as *in-vivo* capsules explanted after 1 week were slightly weaker having 60% remaining (Figure 4.6c). However after 6 weeks *in-vivo* 100% of the capsules were found to be intact. These results were identical for capsules with and without encapsulated cells.

APA capsules behaved as expected, completely dissolving after the NaOH addition for all *in-vitro* samples and for the capsules explanted after the first week, (Figure 4.6a). However after 6 weeks, *in-vivo* capsules no longer dissolved (Figure 4.6d). This was seen both for APA capsules with and without encapsulated cells.

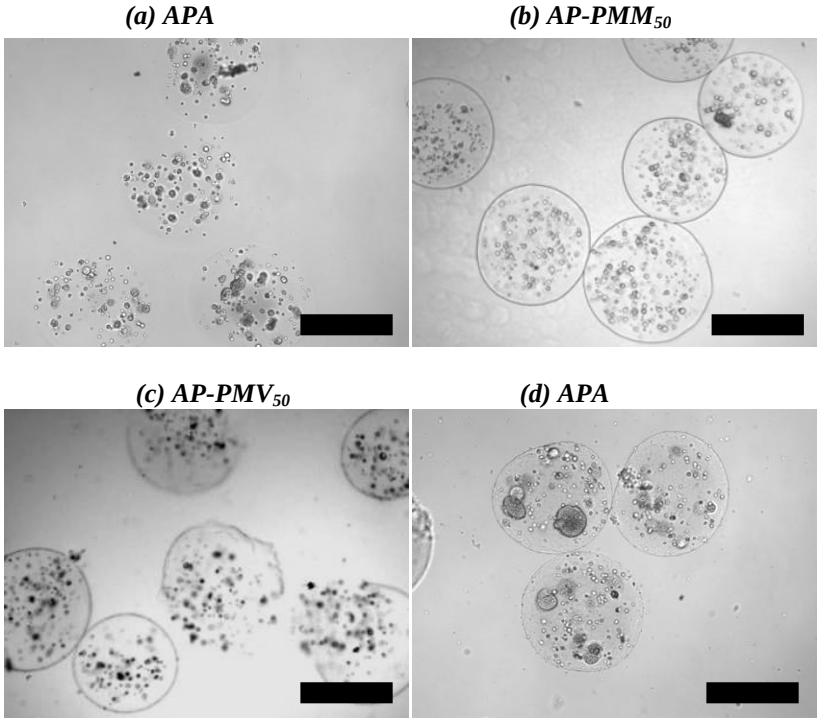

Figure 4.6 *Microcapsules with encapsulated cells after the Na-citrate NaOH test* ***(a)*** *APA 6 weeks in-vitro shells completely dissolved* ***(b)*** *AP-PMM$_{50}$ 6 weeks in-vitro remained intact,* ***(c)*** *AP-PMV$_{50}$ capsules explanted after 1 week in-vivo* ***(d)*** *APA 6 weeks in-vivo remain intact. Scale bar represents 500 µm.*

This apparent increase in capsule strength seen for AP-PMV$_{50}$ and APA capsules after 6 weeks *in-vivo* is most likely due to protein and/or host cell deposition on the surface of the capsules, forming an alkaline-resistant coating. To further investigate this hypothesis scanning electron microscopy (SEM) images were taken of explanted capsules and compared to *in-vitro* capsules.

Figure 4.7 and 4.8 show the three *in-vitro* capsules as well as their counterparts that were explanted after 1 week and 6 weeks, with and without encapsulated cells, respectively. The capsules shrink approximately 3 fold in diameter during sample preparation, leading to surface wrinkling as well as protrusion of encapsulated cells (Figure 4.7). Figure 4.7(iii) and 4.8(iii) shows capsules explanted after 6 weeks *in-vivo*, in which you can clearly see small cells deposited on the surface of most capsules. It was noted that more cellular deposition was seen for APA capsules compared to other capsule types, with the exception of AP-PMV$_{50}$ capsules with encapsulated cells, which were completely covered with fibrotic overgrowth forming a fibrotic "bag" surrounding the microcapsule, as seen in Figure 4.7c(iii)). If this cellular deposition includes macrophages, this would correlate well to the elevated TNF-α levels seen for APA capsules (Figure 4.3a,b), even though not much visible fibrotic overgrowth was seen using optical microscopy, (Figure 4.1a). The small amount of cellular overgrowth seen

for AP-PMM_{50} capsules after 6 weeks also correlates well to AP-PMM_{50}'s low TNF-α levels.

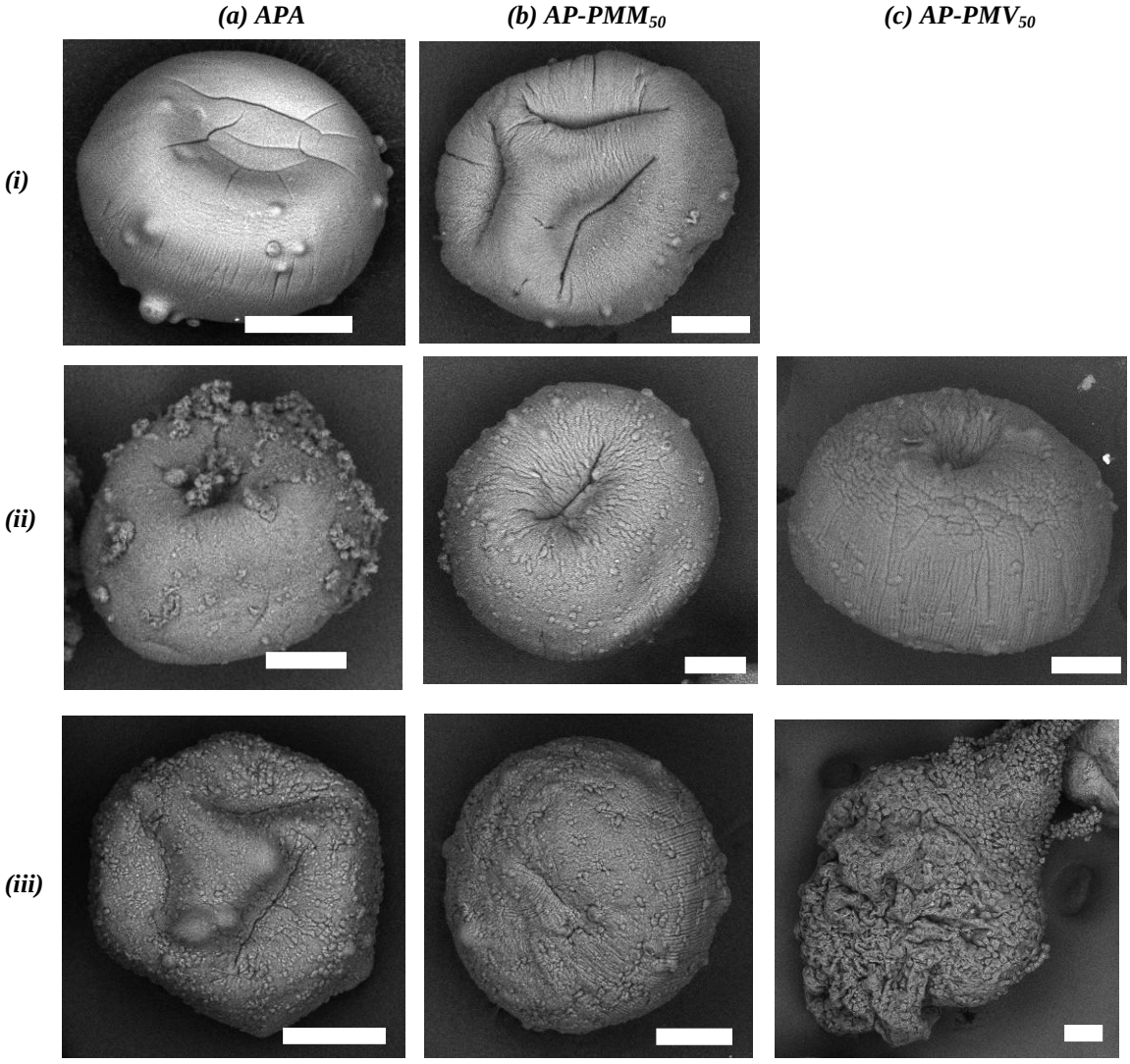

Figure 4.7 *SEM images of fibrotic overgrowth on microcapsules with encapsulated cells,* ***(a)*** *APA,* ***(b)*** *AP-PMM_{50},* ***(c)*** *AP-PMV_{50},* ***(i)*** *6 weeks in-vitro,* ***(ii)*** *explanted after 1 week,* ***(iii)*** *explanted after 6 weeks. Scale bar represents 50 µm. Capsule images are representative of each sample.*

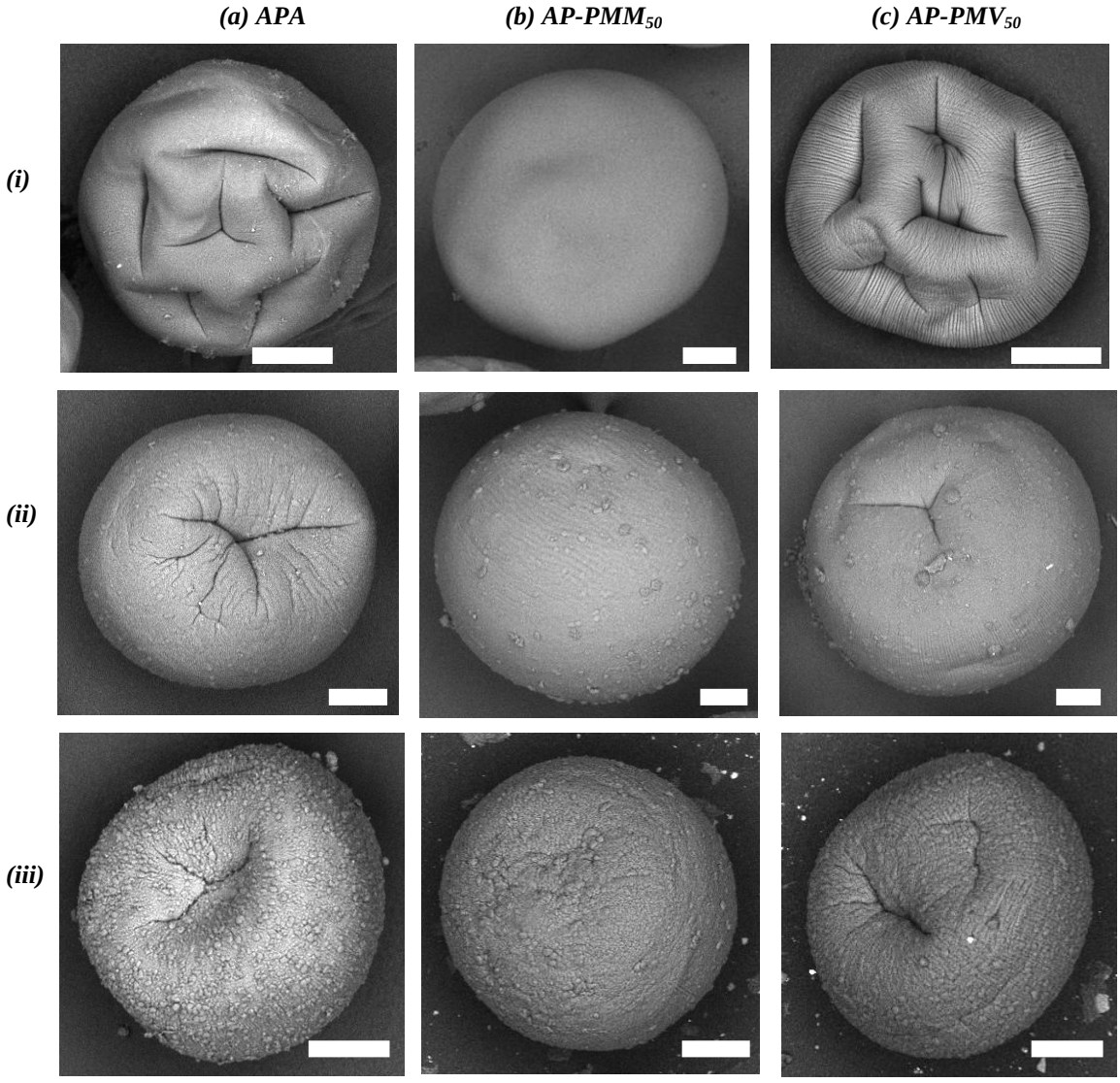

Figure 4.8 *SEM images of fibrotic overgrowth on microcapsules* ***without*** *encapsulated cells,* ***(a)*** *APA,* ***(b)*** *AP-PMM$_{50}$,* ***(c)*** *AP-PMV$_{50}$,* ***(i)*** *6 weeks in-vitro,* ***(ii)*** *explanted after 1 week,* ***(iii)*** *explanted after 6 weeks. Scale bar represents 50 µm. Capsule images are representative of each sample.*

Comparing images from explanted capsules at 6 weeks to capsules explanted after 1 week, it is clear that much more cellular disposition has occurred after 6 weeks (Figure 4.7 and 4.8 (iii) compared to (ii)). The difference between week 1 and 6 is probably most noticeable in Figure 4.8, without encapsulated cells. Note that SEM images also show larger cells and cell clusters (most likely fibroblasts, fibrocytes, giant cells and collagen deposition as seen in other encapsulation studies[27]) covering the surface of the APA capsule in Figure 4.7a(ii), which can also be observed under the optical microscope (Figure 4.1a(ii)).

The apparent increase in mechanical strength of APA capsules (seen in the sodium citrate sodium hydroxide test), resulting from the thin layer of cellular deposit around the capsules after 6 weeks in mice was not expected, as APA capsules have been shown to lose strength overtime *in-vivo*. It is speculated that the thin cellular and/or protein coating around APA capsules is the body's response to the APA capsule surface, and most likely reflects a heightened inflammatory response as evident from the higher TNF-α levels. Comparatively, the smaller cellular deposits seen for AP-PMM_{50} and AP-PMV_{50} capsule (latter without encapsulated cells) at 6 weeks, as well as the lower TNF-α levels, suggest the host's innate immune system is less stimulated by these synthetic polymers. Alternatively, these synthetic polymers might be able to "hide" PLL better from the innate immune system, by interacting more strongly with it through both ionic and covalent interactions.

4.5 Conclusions

APA, AP-PMM_{50} and AP-PMV_{50} capsules (with and without encapsulated C2C12 cells) were implanted into mice for up to 6 weeks and compared in terms of their fibrotic overgrowth and mechanical strength, as well as serum cytokine levels in the hosts. AP-PMM_{50} capsules were shown to have the least amount of overgrowth 2.5% or less) whereas AP-PMV_{50} and APA capsules showed more and varied overgrowth, depending on if the capsules contained encapsulated cells or not. A good correlation was observed between the amount of overgrowth around the capsules and the levels of TNF-α and MCP-1 in the serum, with APA showing the highest cytokine levels, and AP-PMM_{50} the lowest levels, especially at 6 weeks. IL-6, G-CSF, IL-1a and IL-10 showed weaker or no correlations to capsule overgrowth.

The *in-vitro* viability of encapsulated cells was assessed with the Alamar blue assay and using trypan blue staining. The alamar blue assay showed that the encapsulated cells were not initially affected by the TRP coating process and remained viable for 1 week *in-vitro*. Trypan blue staining showed that >75% of the encapsulated cells were alive for all capsule types and did not change over the course of 1 week *in-vitro*.

The mechanical resilience was also observed to differ at 6 weeks for *in-vivo* vs. *in-vitro* capsules, especially for APA capsules. Using SEM this apparent increase in strength of *in-vivo* capsules after 6 weeks was attributed to a cellular coating on the surface of APA capsules and to a lesser extent on AP-PMM_{50} and AP-PMV_{50} capsules. Future work will explore how mechanical strength of covalently crosslinked capsules and ionically crosslinked capsules differ in larger bread animals.

Future work will also look at optimizing PMV_{50} TRPs, to try to improve its mechanical resilience and consistency. As well both PMM_{50} and PMV_{50} will be covalently grafted with bioactive peptides, in an attempt to further decrease the capsules inflammatory response.

4.6 References

[1] H. Zimmermann; S. Shirley; U. Zimmermann. *Curr. Diab. Rep*. **2007**, *7*, 314-320.
[2] P. De Vos; M.M. Faas; B. Strand; R. Calafiore. *Biomaterials* **2006**, *27*, 5603-5617.
[3] S. Poncea; G. Orive; R. Hernandez; A.R. Gascon; J.L. Pedraza; B.J. de Haan; M.M. Marijke Faas; H.J. Mathieu; P. de Vos. *Biomaterials* **2006**, *27*, 4831-4839.
[4] J.T. Wilson; E.L. Chaikov. *Adv Drug Deliv. Rev*. **2008**, *60*, 124-145.
[5] M. De Castro; G. Orive; R.M. Hernández; A.R. Gascón; J.L. Pedraz. *J. Microencapsul*. **2005**, *22*, 303–315.
[6] M.A. Peirone; K. Delaney; J. Kwiecin; A. Fletch; P.L. Chang. *Hum. Gene Ther*. **1998**, *9*, 195–206.
[7] H. Zimmermann; D. Zimmermann; R. Reuss; P.J. Feilen; B. Manz; A. Katsen; M. Weber; F.R. Ihmig; F. Ehrhart; P. Gebner; M. Behringer; A. Sterinback; L.H. Wegner; V.L. Sukhorukov; J.A. Vasquez; S. Schneider; M.M.Weber; F. Volke; R. Wolf; U. Zimmermann. *J. Mater. Sci: Mater. Med.* **2005**, *16*, 491-501.
[8] J. Dusseault; S.K. Tam; M. Ménard; S. Polizu; G. Jourdan; L. Yahia; J.P. Hallé. *J. Biomed. Mater. Res. A*. **2006**, *75A*, 243-251.
[9] G. Orive; S.K. Tam; J.L. Pedraz; J.P. Hallé. *Biomaterials* **2006**, *27*, 3691–3700.
[10] M.Y. Fan; Z.P. Lum; X.W. Fu; L. Levesque; I.T. Tai; A.M. Sun. *Diabetes* **1990**, *39*, 519-522.
[11] M.F.A. Goosen; G.M. O'Shea; H.M. Charapetian; S. Chou; A.M. Sun. *Biotechnol. Bioeng.* **1984**, *27*, 146-150.
[12] H.K. Holme; L. Davidsen; A. Kristiansen; O Smidsrød. *Carbohydr. Polym*. **2008**, **73**, 656–664.
[13] A.M. Rokstad; I. Donati; M. Borgogna; J. Oberholzer; B.L. Strand; T. Espevik; G. Skjåk-Bræk. *Biomaterials* **2006**, *27*, 4726–4737.
[14] F. Cellesi; N. Tirelli; J.A. Hubbell. *Macromol. Chem. Phys*. **2002**, *203*, 1466-1472.
[15] M.Z. Lu; H.L. Lan; F.F. Wang; S.J. Chang; Y.J. Wang. *Biotechnol. Bioeng.* **2000**, *70*, 479-483.
[16] Y.J. Wang. *Mat. Sci. Eng. C.* **2000**, *13*, 59-63.
[17] J. Dusseault; F.A. Leblond; R. Robitaille; G. Jourdan; J. Tessier; M. Ménard; N. Henley; J.P. Hallé. *Biomaterials* **2005**, *26*, 1515–1522.
[18] T. Vermonden; N.E. Fedorovich; D. van Geemen; J. Alblas; C.F. van Nostrum; W.J.A. Dhert; W.E. Hennink. *Biomacromolecules* **2008**, *9*, 919–926.
[19] C.M. Gardner; N.A.D. Burke; H.D.H. Stover. *Langmuir* **2010**, *26*, 4916-4924.
[20] C-C. Lin; A.T. Metters; K.S. Anseth. *Biomaterials* **2009**, *30*, 4907-4914.
[21] J. Su; B-H. Hu; W.L. Jr Lowe; D.B. Kaufman; P.B. Messersmith. *Biomaterials* **2010**, *31*, 308-314.
[22] C.M. Gardner; H.D.H. Stover. *Macromolecules* **2011**, *44*, 7115-7123.
[23] A.A. Li; N.C. McDonald; P.L. Chang. *J. Biomater. Sci. Polym. Ed.* **2003**, *14*, 533–549.
[24] A.M. Sun. *Methods Enzymol*. **1988**, 137, 575-580.
[25] F. Shen; M.A.J. Mazumder; N.A.D. Burke; H.D.H. Stöver; M.A. Potter. *J. Biomed. Mater. Res. B: Appl. Biomater.* **2009**, *90B*, 350-361.

[26] F. Shen; A.A. Li; Y-K. Gong; S. Somers; M.A. Potter; F.M. Winnik; P.L. Chang. *Hum. Gene. Ther*. **2005**, *16*, 971–984.
[27] W.M. Fritschy; R. deVos; H. Groen; F.A. Klatter; A. Pasma; G.H.J. Wolters; R. van Schilfgaarde. *Transpl. Int.* **1994**, *7*, 264-271.
[28] G. Langlois; J. Dusseault; S. Bilodeau; S.K. Tam; D. Magassouba; J.P. Hallé. *Acta Biomater*. **2009**, *5*, 3433-2440.
[29] J. Wijsman; P. Atkison; R. Mazaheri; B. Garcia; T. Paul; J. Vose; G. O'Shea; C. Stiller. *Transplantation* **1992**, *54*, 588-5492.
[30] Z.G. Isfahani. *In-vivo* Characterization of Murine Innate Immune Response to Alginate-Poly-L-Lysine – Alginate Microcapsules. Thesis, (MSc). McMaster University.
[31] A. King; S. Sandler; A. Andersson. *J. Biomed. Mater. Res*. **2001**, *57*, 374-383.
[32] D.R. Cole; M. Waterfall; M. McIntyre; J.D. Bair. *Diabetologia* **1992**, *35*, 231-237.
[33] A. Thomas; K.G. Harding; K. Moore. *Biomaterials* **2000**, *21*, 1797-1802.
[34] M. Otterlei; A. Sundan; G. Skjåk-Bræk; L. Ryan; O. Smidsrod; T. Espevik. *Infect Immun.* **1993**, *61*, 1917-25.
[35] R. Robitaille; J. Dusseault; N. Henely; K. Desbien; N. Labrecque; J.P Hallé. *Biomaterials* **2005**, 26, 4119-4127.
[36] S.W. Chensue; K.S. Warmington; J.H. Ruth; P.S. Sanghi; P. Lincoln; S.L. Kunkel. *J. Immunol*. **1996**, *157*, 4602-4608.
[37] A.A. Li; F. Shen; T. Zhang; P. Cirone; M.A. Potter; P.L. Chang. *J. Biomed. Mater. Res. B.* **2006**, *77*, 296-306.

CHAPTER 5: Synthesis and Properties of Azlactone Copolymers

Casandra M. Gardner, Carla Brown, Harald D.H. Stöver*

Accepted in *J. Polym. Sci. A Polym. Chem.*

Contributions: I designed and performed all experiments except for elemental analysis of the VDMA copolymers. Experiments I performed include: reactivity ratio determination, synthesis and characterization of all VDMA copolymers using GPC, ^{1}H NMR and quantitative ^{13}C NMR and measurements of the VDMA copolymer's hydrolysis. I also wrote the manuscript with edits and guidance from Dr. Stover. Carla Brown initially developed the pH titration program that I used to perform the hydrolysis measurements.

5.1 Abstract

Preparation and study of a series of copolymers incorporating the electrophilic monomer 2-vinyl-4,4-dimethylazlactone (VDMA) is reported. The reactivity ratios for photo-initiated free radical copolymerization of VDMA with methacrylic acid (MAA), acrylic acid (AA), acrylamide (AAm), dimethylacrylamide (DMAA), hydroxyethyl methacrylate (HEMA), methoxy poly(ethylene glycol) methacrylate ($MPEG_{300}MA$), and 2-methacryloyloxyethyl phosphorylcholine (MPC), were determined by fitting comonomer conversion data obtained by *in-situ* ^{1}H-NMR to a terminal copolymerization equation. These reactivity ratios were used to design semi-batch photo-copolymerizations to synthesize the corresponding VDMA copolymers of constant composition. Their solubility and dissolution behaviour in water, as well as their hydrolysis half-lifes at physiological pH, were determined by pH-stat potentiometric measurements. P(VDMA-*co*-MAA) copolymers having between 52 and 93% VDMA content showed decreasing initial solubility and increasing hydrolysis half-lifes with increasing VDMA content, especially at high VDMA content. VDMA copolymers with non-ionic monomers AAm and DMAA were water soluble only at VDMA contents of 41 and 22 mol% or less, respectively, and showed longer hydrolysis half-lifes than comparable MAA copolymers. VDMA copolymers with HEMA and $MPEG_{300}MA$ were found to crosslink during storage, so their hydrolysis half-lifes were not determined. VDMA copolymers with 18% zwitterionic MPC showed a much longer half-life and superior initial solubility compared to analogous p(VDMA-*co*-MAA), identifying this copolymer as a promising candidate for macromolecular crosslinkers in e.g. aqueous layer-by-layer co-depositions with polyamines.

5.2 Introduction

Reactive polymers are increasingly used in biomedical research, for applications including drug and gene delivery, biosensing, biomolecule immobilization, immunodiagnostics, immuno-isolation, as well as for directing cell function.[1,2,3,4,5] Some of these applications involve attachment to, or immobilization within, reactive polymers based on 2-vinyl-4,4-dimethylazlactone (VDMA). VDMA contains the electrophilic azlactone ring that can rapidly react with amines, alcohols, and thiols in a ring-opening reaction under mild conditions, to form amide, ester and thioester bonds, respectively,[6] without formation of any small molecule by-products. VDMA is readily polymerized by both conventional and controlled free radical polymerizations,[7] incorporating preferentially during copolymerization with methacrylic acid (MAA),[8] methyl methacrylate,[9] *N*,*N*-dimethylacrylamide,[10] vinyl pyrrolidone,[11] butyl acrylate and styrene.[6]

The majority of VDMA based polymers have been used to prepare thin films[12,13] and to immobilize proteins and other bio-relevant molecules onto solid polymer supports.[14,15] Generally, these reactions are carried out either in organic medium, or in aqueous medium between a VDMA-containing solid phase and aqueous phase nucleophiles.

Our group is interested in developing water-soluble VDMA copolymers that can form covalently crosslinked networks and immobilize biomolecules in the presence of living cells. We recently showed that p(VDMA-*co*-MAA) 50:50 copolymers can be deposited onto poly-L-lysine-coated calcium-alginate beads to form crosslinked hydrogel shells, without affecting the viability of encapsulated C2C12 murine cells.[3] A critical element in this process is the competition between the amide bond formation, azlactone reacting with polyamines, and azlactone hydrolysis to carboxylic acid. While the hydrolysis of residual azlactones helps avoid immunogenic protein binding, hydrolysis half-lifes that are too short can limit the extent of crosslinking achievable. Our previously reported, p(VDMA-*co*-MAA) 50:50 copolymer had an hydrolysis half-life of about 30 minutes in HEPES buffered saline at about pH 7.4.[8] That work also showed that photo-initiated copolymerization at room temperature could be used to suppress undesirable side-reactions between the azlactone and methacrylic acid groups on the copolymers.

The present work was in part motivated by a desire to develop water soluble VDMA copolymers with higher azlactone content and longer hydrolysis half-lifes, in order to maximize crosslinking in aqueous phase reactions with polyamines. In this context it was noted that the VDMA homopolymer can be hydrolytically stable for up to a year, presumably because its hydrophobic nature prohibits dissolution.[11]

We first determined the reactivity ratios for photo-initiated copolymerization of VDMA with several types of comonomers: methacrylic acid (MAA), acrylic acid (AA), anionic monomers; acrylamide (AAm), dimethylacrylamide (DMAA), hydroxyethyl methacrylate (HEMA) and methoxy poly(ethylene glycol) methacrylate ($MPEG_{300}MA$), polar uncharged monomers; and 2-methacryloyloxyethyl phosphorylcholine (MPC), a zwitterionic monomer.

Semi-batch photo-initiated copolymerizations were then used to prepare analogous VDMA copolymers without compositional drift. Copolymer compositions (VDMA content) were selected so that they would allow for instantaneous or near-instantaneous solubility in water under physiological conditions, upon dispersion from 3% solutions in DMSO.

The dissolution behaviour in water, as well as the subsequent hydrolysis half-lifes of these copolymers were determined, to assess their ability to serve as network formers in future reactions with polyamines under physiological conditions in the presence of live cells.

5.3 Experimental

5.3.1 Materials

2-vinyl-4,4-dimethylazlactone (VDMA)**,** was purchased from Angene International Limited, Hong Kong. 2-Methacryloyloxyethyl phosphorylcholine (MPC) was purchased from Wonda Science, Montreal, QC. Methacrylic acid (MAA) 99%, methoxy poly(ethylene glycol) methacrylate (average PEG M_n 300), acrylamide (99+%), *N*,*N*-dimethylacrylamide (99%), 2-hydroxyethyl methacrylate (97%), acrylic acid

anhydrous (99%), 2,2-dimethoxy-2-phenylacetophenone, anhydrous DMSO, anhydrous THF (inhibitor free), ethylene carbonate (98%), were purchased from Sigma-Aldrich, Oakville, ON, and used as received. Azobisisobutyronitrile (AIBN) was obtained from Dupont, Mississauga. Dimethyl sulfoxide-d_6 (D, 99.9%) and methanol-d_4 (D, 99.8%) were purchased from Cambridge Isotope Laboratories, Inc. Andover, MA.

5.3.2 Determination of Reactivity Ratios for Photo-Initiated Copolymerizations

Photo-initiated copolymerizations were carried out at room temperature in 5 mm NMR tubes placed in a photo-reactor fitted with one black-light bulb (350 nm, Ushio F8T5BL, 8 watts), using 10 wt% total monomer, 1 mol% 2,2-dimethoxy-2-phenylacetophenone with respect to total monomer, and 2 mol% of ethylene carbonate as internal standard in 1 g of a DMSO-d_6.[a] Three different initial molar feed ratios were used for each comonomer pair, e.g., VDMA:MPC copolymerizations were carried out at 46:54, 68:32, and 27:73 mol ratios (see Appendix 5.8) for the specifics of other copolymerizations). Monomer conversions were determined by 600 MHz ^{1}H NMR at time intervals chosen to cover a wide range of conversion, e.g. at 0, 1, 3, 6, 11, 18, 21 and 28 min irradiation for VDMA/MPC copolymerizations. The monomer concentrations were measured by integration of the corresponding monomer vinyl peaks. The reactivity ratios were then calculated using both equations (2 and 3) in Aguilar's paper[16] (equation [1] and [2] in this paper). The data from the three monomer feed ratios were fitted to a common set of reactivity ratios, using both a shift factor as described by Aguilar (2002), and by treating the shift factor as a variable during curve fitting, with very similar results. MATLAB was then used to obtain 95% confidence contour plots of r_1 and r_2, using the method described by Box (2005).[17]

5.3.3 Semi-batch free radical photo-copolymerizations

Semi-batch photo-copolymerizations were carried out in a 100 mL glass reaction vessel equipped with a cold finger circulating tap water at ~10^{o}C. Most copolymerizations involved 8 wt% total monomer in 50 mL of anhydrous DMSO, with VDMA:comonomer ratios chosen to produce the targeted copolymer compositions (Table 5.1). VDMA-MPC copolymerizations used 10 wt% total monomer in a mixture of 48 ml DMSO and 2 ml methanol which enabled MPC to dissolve. Photo initiator (2,2-dimethyloxy-2-phenylacetophenone, 0.3 mol% with respect to total monomer) and internal standard (ethylene carbonate, 2 mol%) were added, and the solutions were stirred and purged with $N_{2\,(g)}$ for 1 hr prior to polymerization. Photo initiation was carried out as described above. The reaction was allowed to proceed for 5 min without addition of further VDMA, to account for an induction delay due to residual inhibitors. After 5 min (t = 0 min), addition of VDMA in anhydrous DMSO was added at a rate chosen to approximately maintain the initial comonomer feed ratio. The VDMA feed was added in

[a] VDMA:MPC copolymerization was performed in DMSO-d_6: methanol-d_4 (9:2 v/v), in order to keep both monomers, and copolymer, in solution.

numerous small aliquots by manual addition, averaging to rates reported in Table 5.1. The rate of monomer addition was decreased by 50% after 30 min. Aliquots of 0.5 ml of the reaction mixture were taken at t = -5, 0, 10, 20, 30, 40, 50 and 60 minutes, and added to 0.2 ml of DMSO-d_6 for subsequent ^{1}H NMR analysis at 600 MHz (data not shown).

Comonomer % in copolymer[a]	Initial comono-mer % (mmoles)	[VDMA] in feed (mol/ml)[b]	VDMA feed rate 1st 30 min (ml/hr)	VDMA% by:			^{13}C NMR % VDMA gone[c]	% azlact-one[d]	M_n, M_w (kDa, GPC)
				^{1}H NMR	^{13}C NMR	EA			
MAA 48	65 (25)	0.0015	7.5	54	58	45	7	48	27, 60
MAA 42	55 (20)	0.0017	7.5	63	58	57	4	55	35, 63
MAA 28	42 (15)	0.0017	7.5	81	73	70	0	72	47, 85
MAA 16	21 (7)	0.0017	7.5	89	85	83	0	84	60, 93
MAA 7	6 (1.8)	0.0018	7.5	96	94	91	0	93	64, 101
AAm 59	80 (40)	0.0015	3	52	41	40	0	41	33, 70
DMAA 78	90 (35)	0.001	3	27	22	21	0	22	20, 37
MPC 18	21 (6)	0.001	6	88	81	82	7	76	61, 110
MPC 8	8 (2.5)	0.001	6	98	90	93	3	89	62, 103
HEMA 86	90 (35)	0.0015	3	23	14	--	0	14	--
$MPEG_{300}MA$ 37	50 (9)	0.0017	7.5	71	63	--	25	47	73, 123
p(VDMA)	100 (43.1)	0	0/0	--	100	99	0	100	30, 44

Table 5.1 *Summary of VDMA copolymer synthesis and characterization*
[a] Reported values are the average of ^{13}C NMR and EA results. ^{1}H NMR results were not included as they have been shown previously to overestimate the amount of VDMA incorporated into the copolymer.[8]
[b] Rate of addition was reduced to 50% for second 30 minutes.
[c] Azlactone disappearance is attributed to residual side reactions with comonomer[8] *and/or solvent.*
[d] Calculated based on the average VDMA% (a) and the amount of azlactone gone (b).

The reactions were stopped after 1 hr and the reaction mixtures (except for MPC copolymerizations) diluted with 50 ml of THF and precipitated into 600 ml of anhydrous diethyl ether under stirring. In the MPC copolymerization the reaction mixtures were diluted with 50 ml of DMSO and precipitated into a mixture of 600 ml anhydrous diethyl ether and 100 ml of methanol, to help remove unreacted MPC.

The resulting dispersions were centrifuged for 10-20 min at 3500-4500 rpm, the supernatants were removed and the solid precipitates washed with diethyl ether. The resulting products were redissolved in THF (DMSO for p(VDMA-*co*-MPC)) and re-

precipitated into 200 ml of anhydrous diethyl ether, and treated as above. The products were then dried under vacuum at room temperature for 1-3 days.

5.3.4 Homopolymerization of VDMA

P(VDMA) was synthesized by both photo-initiated polymerization (as described above, but without comonomers or VDMA feed), as well as thermally initiated polymerization. The hydrolysis data presented here are from the polymer formed by thermal polymerization, carried out by placing 75 mL of a THF solution containing 8 mol% VDMA and 1 mol% AIBN (relative to VDMA), in a 250 ml water jacketted round bottom flask. The flask was purged with $N_{2(g)}$ for 30 min prior to the reaction. The water circulating in the jacket was heated to 60^{o}C, and the reaction allowed to proceed for four hours. P(VDMA) was isolated as described for the VDMA copolymers above. Yield of the isolated polymer was 90 %.

5.3.5 GPC analysis

Molecular weights were determined for VDMA copolymers or homopolymer that were completely hydrolyzed by reaction in basic (pH ~ 9) distilled deionized water for 1-3 days. An aqueous gel permeation chromatography (GPC) system consisting of a Waters 515 HPLC pump, Waters 717 plus Autosampler, three Ultrahydrogel columns (0-3 kDa, 0-50 kDa, 2-300 kDa), and a Waters 2414 refractive index detector was used. A mobile phase consisting of 0.3 M $NaNO_3$, 0.05 M phosphate buffer (pH 7) at a flow rate of 0.8 ml/min was used for all polymers, and the system was calibrated with narrow-disperse poly(ethylene glycol) standards (Waters, Mississauga, ON).

5.3.6 ^{1}H NMR

(i) Determination of instantaneous monomer feed ratio and final copolymer composition

During the semi-batch photo-polymerization of VDMA and comonomers, 0.5 ml aliquots were removed from the reaction mixtures at -5, 0, 10, 20, 30, 40, 50 and 60 min and added to 0.2 ml of DMSO-d_6 for ^{1}H NMR analysis using a Bruker AV 600. The monomer peaks of VDMA and comonomer were integrated at each time interval to determine the instantaneous comonomer feed ratios. For all copolymers reported here the instantaneous comonomer feed ratio did not change more than 7%, and on average changed less than 3% throughout the course of the polymerization. The average VDMA content in the VDMA copolymers formed during this hour was estimated, based on the amounts of VDMA and comonomer added and consumed during the reaction (Table 5.1).

(ii) Analysis of solvent remaining in final product

The final copolymer was isolated and analyzed by ^{1}H NMR at 600 MHz in DMSO-d_6 to determine the amount of residual solvent (DMSO, THF and/or methanol for MPC) in the isolated product.

5.3.7 Quantitative ^{13}C NMR: Determination of final copolymer compositions, and degree of side reactions

The longitudinal relaxation times, T_1, of the ^{13}C nuclei in the copolymers were determined using a saturation-recovery experiment (pulse program "satrect1.av_bb"). The obtained T_1 values were then used to set up a quantitative ^{13}C NMR experiment using inverse-gated decoupling without NOE enhancement, using a 30-degree flip angle, 3000 scans, and a recovery delay time of 10 s. Analyses were performed using 10 wt% solution of polymer in DMSO-d_6, on a Bruker AV 600.

5.3.8 Elemental analysis to determine the total VDMA incorporation

Residual solvents were removed from the polymers by dialysis: 200 mg of each VDMA copolymer was dissolved in a small amount of water at pH ~10. After one day this solution was diluted to 100 ml with distilled water. This solution was then dialyzed against 4 L of distilled deionized water for one week, with daily water changes, using cellulose dialysis tubing with a molecular weight cut-off of 14 kDa (Membra-cel, Viskase, Darien, IL). This process ensures hydrolysis of all remaining azlactone groups. The dialyzed solutions of p(VDMA-*co*-MAA), p(VDMA-*co*-AAm), and p(VDMA-*co*-DMAA) were concentrated using a rotary evaporator, and precipitated with 1M HCl. The resulting solids were dried in a vacuum oven at 25^{o}C for 3 days. The dialysed solutions for p(VDMA-*co*-MPC) were freeze-dried using a Leybold Trivac D4A pump at room temperature for one day. Elemental analysis was performed on a Therm FlashEA 1112 Elemental Analyzer, using the carbon: nitrogen ratio to determine the VDMA content in the copolymers.

5.3.9 Potentiometric determination of the rate of hydrolysis of VDMA copolymers at pH 7.4

A Mandel Scientific PC-Titrate automated potentiometric titrator was used to determine the rate of hydrolysis of VDMA copolymers and p(VDMA), in triplicates. The VDMA copolymers were first dissolved in DMSO as 3.0 wt% solutions. A small amount (1.6 ml for p(VDMA-*co*-DMAA) and 0.46 - 0.80 ml for all other (co)polymers) of this solution was added to 10 ml of saline in the titrator vessel so as to form hydrolysis solutions containing 1.0 x 10^{-4} mol of azlactone groups. Given the different VDMA contents, this led to polymer concentrations in the final saline solutions of 0.49 wt% (p(VDMA-*co*-DMAA)) and 0.14 - 0.24 wt% (other (co)polymers). The pH of the hydrolysis solutions decreased upon addition of the polymer, and a titration program was

used to quickly bring the pH of the solutions back up to 7.4 and maintain it there throughout the hydrolysis, using small injections (0.005 - 0.1 ml) of 0.1 M NaOH.

The amount of 0.1 M NaOH injected over time to maintain the pH at 7.4 was taken to reflect the rate of acid produced by hydrolysis of azlactone. The total amount of 0.1 N NaOH added for all neutral copolymer hydrolyses was 1.05 ± 0.05 ml, consistent with the $1x10^{-4}$ moles of azlactone present in each (co)polymer solution. For p(VDMA-*co*-MAA) copolymers, more 0.1 N NaOH was required to neutralize the MAA units, reflective in the more rapid initial pH drop. Here, 0.1N NaOH additions ranged from 1.8 ± 0.1 ml to 1.08 ± 0.05 ml for p(VDMA-*co*-MAA) 52% to 97% VDMA. Therefore the endpoint of hydrolysis was taken to be the last addition of 0.1 N NaOH (the titration program requires a minimum pH decrease of 0.05 for further NaOH addition).

The rates are shown in a first order plot, as $\ln([A]_o/[A])$ *vs.* time. The resulting curves show strong deviation from linearity, likely due to a complex combination of polymer phase separation and neighbouring group effects along the polymer backbone. A full analysis of the kinetics of hydrolysis is beyond the scope of this paper. As a practical measure, the first order plot was divided into four equal quarters, taking the final time (end of the hydrolysis) to be when the last aliquot of 0.1N NaOH was added, seen in Figure 5.5 as the beginning of the levelled off slope at $1.03\ x10^{-4}$ moles. The slopes of the first three quarters are reported and compared here. The last quarter corresponds to smaller amounts of azlactone hydrolyzing, and thus is associated with more error.

5.4 Results and Discussion

While VDMA-based polymers are used to immobilize biomolecules onto solid supports, their rate of hydrolysis in water has not been studied explicitly, even though hydrolysis can compete with immobilization. Our group is interested in crosslinked hydrogels formed by reactions between VDMA-based copolymers and polyamines in saline. A good understanding of the solubility of these VDMA copolymers in water, and of the competition between crosslinking and hydrolysis, is hence required. The effect of copolymer composition on these issues is complicated by the preference of VDMA to incorporate preferentially into its copolymers. This requires semi-batch copolymerizations to avoid drift in the instantaneous copolymer composition. Hence, reactivity ratios were determined to help choose feed rates for the semi-batch copolymerizations. Photo-initiated copolymerization near room temperature was used in order to suppress side reactions between VDMA and functional groups in the forming copolymer.[8]

5.4.1 Reactivity Ratios

	r_1(VDMA)	r_2(comonomer)
MAA	1.45	0.57
AA	3.10	0.20
AAm	5.82	0.19
DMAA	2.13	0.17
HEMA	1.21	0.54
$MPEG_{300}MA$	1.12	0.45
MPC	1.55	0.74

Table 5.2 *Reactivity ratios using equation [1] and the fraction correction factor to combine the three different feed ratio polymerizations, as described by Aguilar* (2002).[16]

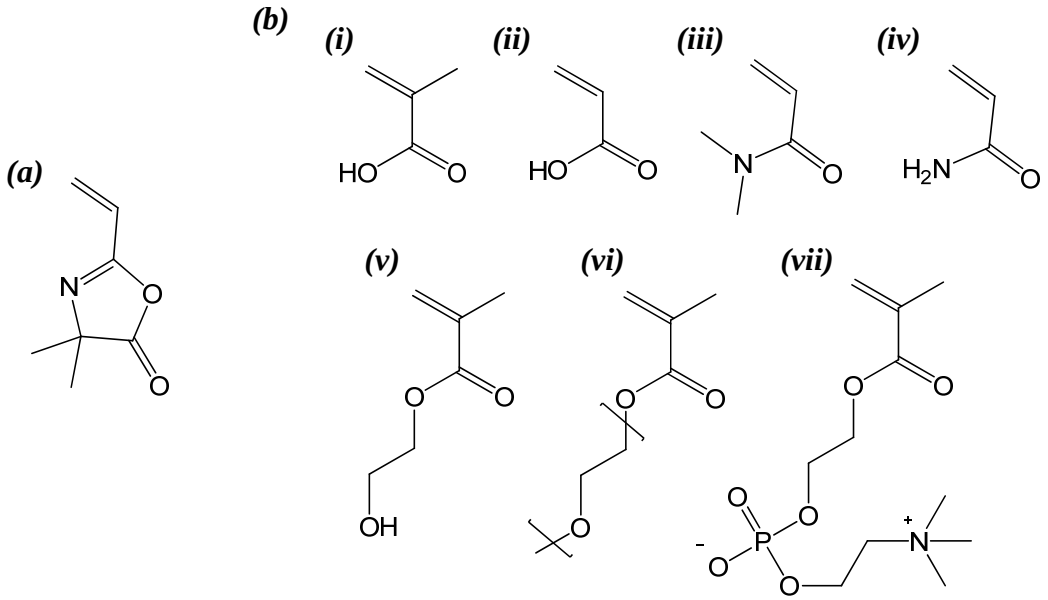

Scheme 5.1 (a) *VDMA,* ***(b)*** *copolymers* ***(i)*** *MAA,* ***(ii)*** *AA,* ***(iii)*** *DMAA,* ***(iv)*** *AAm,* ***(v)*** *HEMA,* ***(vi)*** *$MPEG_{300}MA$,* ***(vii)*** *MPC*

The reactivity ratios for seven different VDMA-comonomer pairs (Scheme 5.1) were determined using Aguilar's approach, using least-squares fitting of *in-situ* monomer conversion data to a solution for the differential copolymer equation for Mayo and Lewis's terminal model of copolymerization.[16] The reactivity ratios were estimated using both equation [1] and [2] (referred to as equations 2 and 3 in Aguilar's paper, respectively).

$$[M_2] = [M_{20}]\left(\frac{\frac{[M_1]}{[M_2]}}{\frac{[M_{10}]}{[M_{20}]}}\right)^{\frac{r_2}{(1-r_2)}}\left(\frac{1-r_2+(r_1-1)\frac{[M_1]}{[M_2]}}{1-r_2+(r_1-1)\frac{[M_{10}]}{[M_{20}]}}\right)^{\frac{(r_1r_2-1)}{[(1-r_1)(1-r_2)]}} \quad [1]$$

where $[M_1]$ and $[M_2]$ are the monomer concentrations at a given time in the copolymerization and $[M_{10}]$ and $[M_{20}]$ are the initial monomer concentrations.

$$[M_2] = k\left(\frac{[M_1]}{[M_2]}\right)^{\frac{r_2}{(1-r_2)}}\left(1-r_2+(r_1-1)\frac{[M_1]}{[M_2]}\right)^{\frac{(r_1r_2-1)}{[(1-r_1)(1-r_2)]}} \quad [2]$$

where

$$k = [M_{20}]\left(\frac{1}{\frac{[M_{10}]}{[M_{20}]}}\right)^{\frac{r_2}{(1-r_2)}}\left(\frac{1}{1-r_2+(r_1-1)\frac{[M_{10}]}{[M_{20}]}}\right)^{\frac{(r_1r_2-1)}{[(1-r_1)(1-r_2)]}} \quad [3]$$

and is *k* a constant that includes the initial conditions, and is used as the third variable in the nonlinear fitting. While Aguilar (2002) preferred equation [2] as it can correct for measurement errors of the initial conditions, we found it required very good initial estimates for r_1 and r_2 values to avoid converging on local minima. Typically, estimates obtained from equation [1] were needed to allow equation [2] to converge on the global minimum, with very little overall improvement. Thus, the reactivity ratios presented here are calculated using equation [1]. NMR analysis was performed on high field, 600 MHz NMR spectrometer, to help ensure accurate quantification even at high conversion.

For each comonomer pair three different initial molar feed ratios were used to cover a broad range of comonomer ratios (Figure 5.1a, b). The three data sets were then combined using shift factors as described by Aguilar (2002) (Figure 5.2a, b), as well as by treating the shift factor as a variable during curve fitting. The results for both of these methods were very similar (see Appendix 5.8). MATLAB was used to produce the 95% confidence contour plots for p(VDMA-*co*-MPC) and p(VDMA-*co*-DMAA) (Figure 5.3, 5.4c) and the other comonomer pairs (see Appendix 5.8).

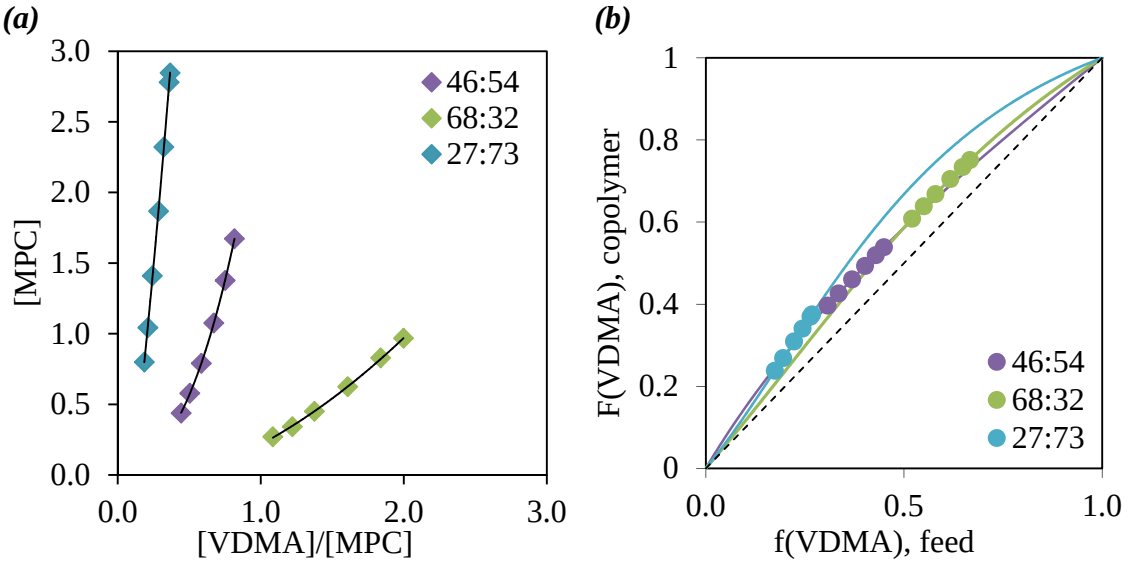

Figure 5.1 (a) *[MPC] vs. [VDMA]/[MPC] from ^{1}H NMR analysis of three copolymerizations with VDMA:MPC initial feed molar ratios of 46:54, 68:32 and 27:73. The black lines show the fitted data of calculated [MPC]'s using equation [1], and coloured diamonds represent experimental data.* ***(b)*** *Copolymer composition diagram showing (lines) separate fits to the data (circles) of three reactions with VDMA:MPC initial molar ratios of 46:54, 68:32 and 27:73.*

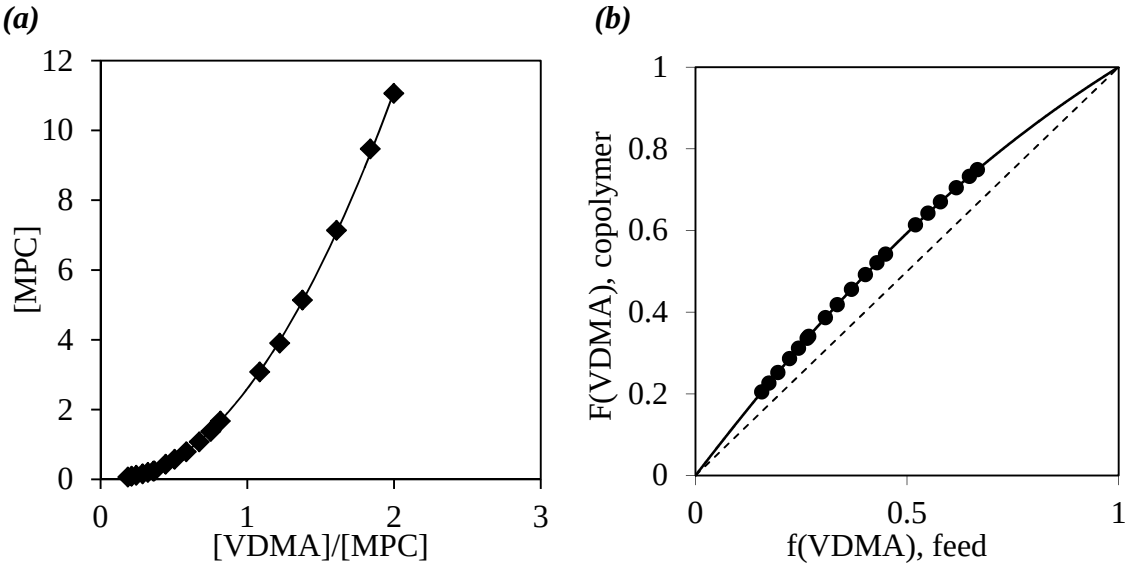

Figure 5.2 (a) *Corrected global [MPC] vs. [VDMA]/[MPC] as described by Aguilar (2002) The black line shows the fitted data of calculated [MPC]'s using equation [1]. Black diamonds represent experimental data.* ***(b)*** *Composition diagram obtained with the reactivity ratios determined using equation [1] and the corrected global data (a). The black line shows a fit to the data, the full black circles show the individual experimental data points.*

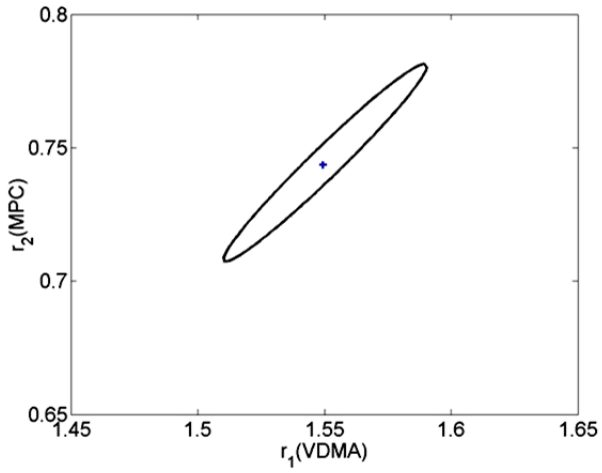

Figure 5.3 *95% confidence contour for r_1(VDMA) and r_2(MPC) determined using equation [1].*

It was found the VDMA is preferentially incorporated into the copolymer for all seven comonomer pairs (Table 5.2). This is consistent with current literature[6,9,10] that reports preferential incorporation of VDMA with DMAA, methyl methacrylate (MMA), butyl acrylate (BA) and styrene.

The reactivity ratios of VDMA and MAA measured here for photo-initiated polymerization at ~10°C in DMSO (r_1(VDMA) = 1.45 and r_2(MAA) = 0.57) are in good agreement with our previously reported values (r_1(VDMA) = 1.36 and r_2(MAA) = 0.41),[8] obtained using the same analysis method but thermally initiated polymerization at 60°C with AIBN, also in DMSO.

Our three initial feed molar compositions for VDMA and DMAA (Figure 5.4a) gave overlapping composition curves (Figure 5.4b), reflecting very similar r_1 and r_2 values (see Appendix 5.8 for separate r values). The resulting combined reactivity ratios (r_1(VDMA) = 2.13 and r_2(DMAA) = 0.17) differ from the values reported by Stanek (2005). (r_2(VDMA) ~0.7 and r_2(DMAA) ~0.3),[10] and do not point to the azeotropic behaviour that was observed by Stanek (2005) at a VDMA mol fraction 0.78. Stanek (2005) used thermally initiated polymerization in methylethylketone at 70°C, while we used room temperature photo-polymerization in DMSO and *in-situ* tracking of monomer conversion by ^{1}H-NMR. Reasons for the discrepancy may hence include the differences in temperature and solvent, as well as the likely higher accuracy of measuring monomer rather than copolymer signals by ^{1}H NMR.

Compared to the VDMA-DMAA system, the VDMA-AA system showed a slightly stronger preference for VDMA homo propagation, r_1(VDMA) = 3.10 and r_2(AA) = 0.20, while the VDMA-AAm system, with r_1(VDMA) = 5.82 and r_2(AAm) = 0.19, showed an even stronger preference for VDMA homo propagation. Interestingly, DMAA,

AA and AAm showed comparable preferences for cross propagation, leading to significant preferential incorporation of VDMA in all three systems.

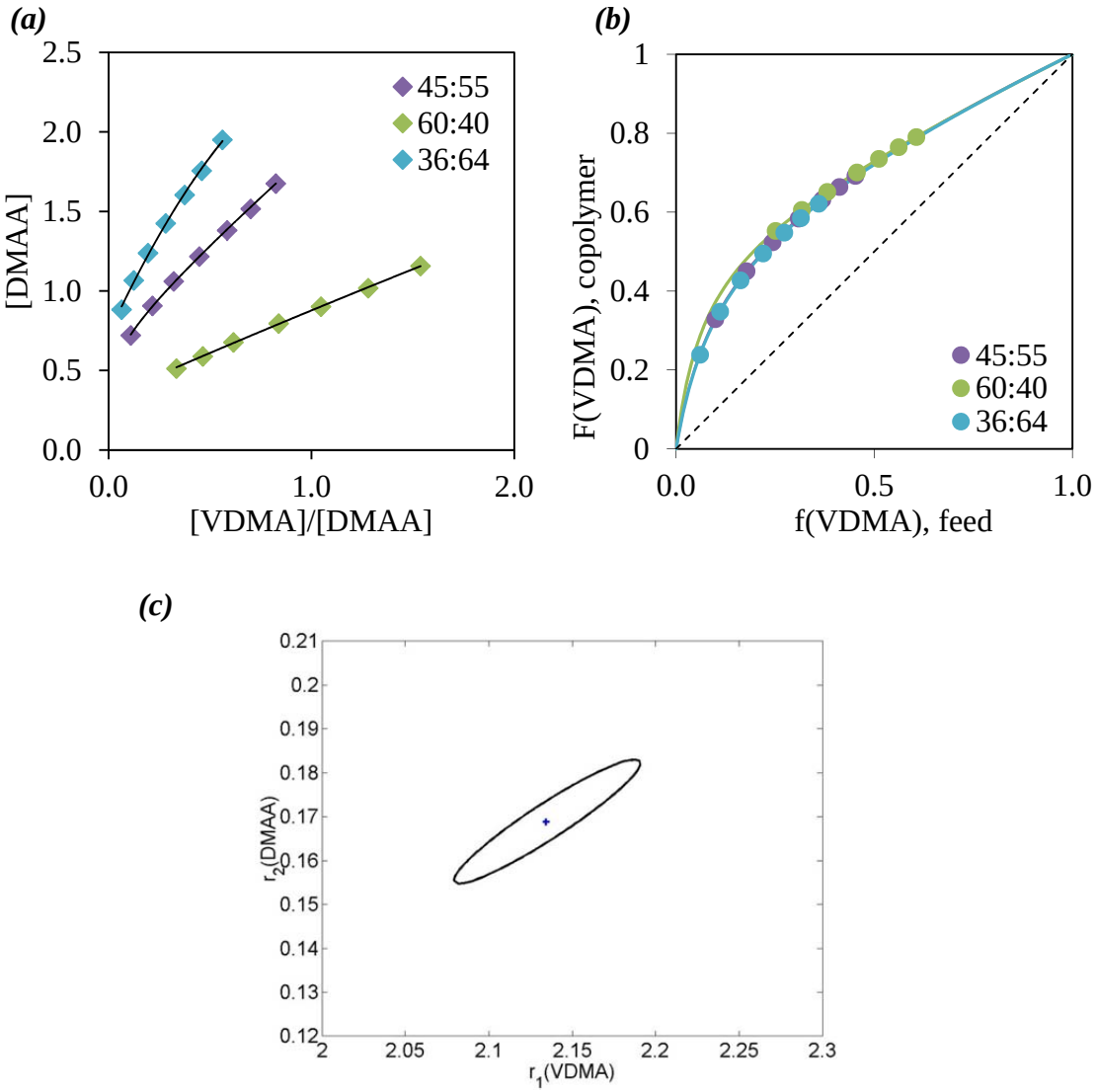

Figure 5.4 (a) *[DMAA] vs. [VDMA]/[DMAA] from ^{1}H NMR analysis of three copolymerizations with VDMA:DMAA initial molar feed ratios of 45:55, 60:40 and 36:64. The black lines show the fitted data of calculated [DMAA]'s using equation [1], and coloured diamonds represent experimental data.* ***(b)*** *Copolymer composition diagram showing separate fits (lines) to the data (circles) of three VDMA:DMAA initial ratios of 45:55, 60:40 and 36:64.* ***(c)*** *95% confidence contour for r_1(VDMA) and r_2(DMAA) obtained by fitting equation [1] to the combined data set.*

The reactivity ratio of r_2(MPC) = 0.74, was the highest of all the comonomer reactivity ratios determined here. As r_1(VDMA) = 1.55 is also fairly close to unity, their

ballistic copolymerization accordingly showed the least compositional drift. MPC's reactivity ratio is close to that of MMA, r_2(MMA) = 0.61, for its copolymerization with VDMA as reported by Stanek (2003)[9] This is not surprising given their similar structure. Note that the reactivity ratios of other methacrylates reported here, HEMA and $MPEG_{300}MA$, are also fairly close to 1.

5.4.2 Synthesis and General Properties of VDMA copolymers

Semi-batch photo-polymerizations were carried out to prepare a series of uniform composition (no-drift) VDMA copolymers. P(VDMA-*co*-MAA) polymers were prepared with 48 – 100 mol% VDMA. For copolymers with lower VDMA content a small amount of transhydration was observed as reported previously,[8] attributed to reaction between azlactone and methacrylic acid groups (Table 5.1).

While p(VDMA-*co*-AA) seems like an interesting candidate due to expected higher water solubility compared to analogous p(VDMA-*co*-MAA) copolymers, it is known that poly(acrylic acid) easily forms cyclic anhydrides by dehydration of adjacent acid units.[18] Recent copolymerizations in our lab between AA and electrophilic comonomers in fact indicated significant dehydration of AA units even during photo-polymerization at room temperature,[19] in a manner analogous to that seen in low VDMA content p(VDMA-*co*-MAA) copolymers.[8]

P(VDMA-*co*-HEMA) copolymers were prepared as HEMA is a neutral monomer used extensively in biomedical applications.[20,21] The copolymerization of VDMA and HEMA in 55:45 and 86:14 mol ratios did not show any apparent crosslinking, despite the presence of the HEMA hydroxy groups. However, quantitative ^{13}C NMR showed a slow decrease of azlactone groups during storage over the next couple of weeks, and after 4 weeks the solid copolymer was no longer soluble in aqueous or organic solvents. This suggests that the azlactone groups can crosslink with the HEMA groups during storage in the solid state, and therefore the hydrolysis of these copolymers were not studied.

P(VDMA-*co*-$MPEG_{300}MA$) copolymers are of interest as they combine PEG's non-fouling properties with the azlactone groups' electrophilicity. Although these copolymers were water-soluble for $MPEG_{300}MA$ mol fractions as low as 37%, it was noted that immediately after their synthesis 25% of the azlactone groups had reacted (Table 5.1). Quantitative ^{13}C NMR again showed a gradual decrease of azlactone content over several weeks of storage, with the polymer eventually becoming insoluble in any solvent. ^{1}H NMR, and previous analysis[22], indicated that the $MPEG_{300}MA$ monomer contained no detectable amounts of hydroxy terminal $PEG_{300}MA$ groups that might be responsible for crosslinking. At this time the mechanism behind the loss of azlactone and the crosslinking during storage is not clear.

P(VDMA-*co*-MPC) copolymers are of interest due to the anti-fouling, nonthrombogenic properties of MPC.[23,24] Despite initial preparative challenges, these copolymers proved to be very hydrophilic, and good candidates for network formation.

As MPC is not soluble in DMSO, alternate solvent systems had to be explored for its copolymerization with VDMA. Mixtures of acetic acid with acetic anhydride could dissolve both monomers, but a side reaction was noted by NMR, indicating a decrease of azlactone groups. Chloroform also dissolved both monomers, but the forming polymer precipitated early during the polymerization, creating a two-phase system that could cause compositional drift through the bootstrap effect. Acetonitrile/t-butanol and DMSO/t-butanol mixtures required high levels of t-butanol which led to rapid reaction with azlactone. DMSO/methanol mixtures turned out to be the most appropriate solvent system.

Initially, a 50:50 VDMA:MPC copolymer was synthesized in a 42:10 ml mixture of DMSO:methanol, reflecting the least amount of methanol required for MPC solubility. However, residual methanol could not be removed from the isolated copolymer by precipitation in diethyl ether or vacuum, and slowly reacted with the azlactone groups during storage as observed by ^{1}H NMR and quantitative ^{13}C NMR. On the other hand, copolymers containing 82% and 92% VDMA could be prepared in 50:2 ml mixtures of DMSO:methanol. Here, all of the methanol could be removed by precipitation in diethyl ether followed by vacuum drying. Quantitative ^{13}C NMR showed that only 7% and 3% of the azlactones groups, respectively, had reacted during synthesis and work-up, presumably with methanol.

5.4.3 Initial Solubilities and Rate of Hydrolysis of VDMA Copolymers

A key aim of this project is to develop reactive copolymers that can form covalent crosslinks with amines and polyamines under physiological conditions. Specific applications include encapsulation of therapeutic cells within immuno-isolating crosslinked hydrogels. Such applications require water-soluble polymer containing electrophilic groups that can rapidly form amide crosslinks with polyamines, such as poly-L-lysine, before residual electrophiles hydrolyze to form innocuous carboxylate anions.

A key issue here is the hydrolysis half-life, i.e. the time required for half of the azlactone groups to hydrolyze in saline at pH 7.4 and room temperature. This half-life is expected to govern the total time available for dissolution of the reactive polymer and its deposition onto amine-functional substrates, before crosslinking starts to cease due to azlactone hydrolysis.

Increasing the VDMA content for a given copolymer should increase its half-life, due to increasing hydrophobicity. Of course, increasing the VDMA content will slow down, and eventually prevent, dissolution in aqueous media. Even for soluble copolymers, increasing the VDMA content will weaken the polymer-water interactions and cause chain collapse in solution, and possibly formation of simple coacervates. At the same time, the ongoing hydrolysis of azlactone groups to anionic carboxylates will increase the polymers' hydrophilicity, adding a dynamic element.

An example of the effect of composition on rate of hydrolysis is the drastic difference between p(VDMA) (homopolymer), which was reported to lose only 19% of its azlactone groups after storage in water for one year,[11] and our p(VDMA-*co*-MAA) 50:50 copolymer which is water soluble and has a hydrolysis half-life of about 30 min.[8] To our knowledge the only other investigation into the rate of hydrolysis of VDMA copolymers involves Stanek's[25] preparation of poly(MMA-*co*-VDMA) microspheres by aqueous emulsion copolymerization, with the implication that copolymerization was faster than azlactone hydrolysis.

To determine the rates of hydrolysis in this study, all copolymers were first dissolved at 3 wt% in DMSO. A small amount of this solution (0.46 - 1.6 ml) was then dispersed into 10 ml of saline to form aqueous solutions containing 1.0 x 10^{-4} moles of VDMA units. Polymer loading ranged from 0.14 to 0.49 wt%, depending on VDMA/comonomer ratio. The results match those obtained in preliminary trials (data not shown) using 0.2 wt% copolymer solutions.

Addition of the DMSO solutions[b] to the aqueous saline led to a rapid initial drop in pH. A titration program was used to quickly bring the pH back to 7.4, and keep it there, using injections of variable volumes of 0.1 N NaOH. An example of a resulting plot of moles of NaOH consumed over time is shown in Figure 5.5, and is taken to correspond to the rate of acid produced by hydrolysis of azlactone groups. Time zero corresponds to when the (co)polymer/DMSO solution was added to saline, however the rate of 0.1 N NaOH addition used to calculate acid formation did not start until the pH was brought back up to 7.4 (in Figure 5.5, this would be about 0.1x10^{-4} moles of NaOH).

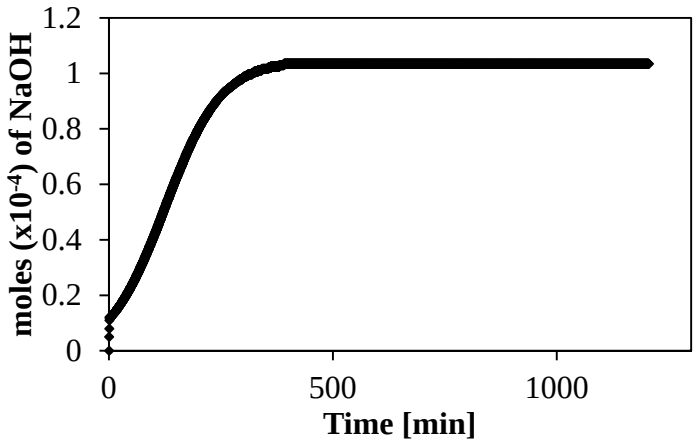

Figure 5.5 *NaOH [0.1N] added over time for the titration of p(VDMA-co-MPC) 82:18.*

Hydrolysis of small molecule azlactones in excess water should follow classic pseudo-first order kinetics, with a linear relationship between $\ln([A]_0 / [A])$ and time. Not

[b] Use of DMSO solutions was chosen to facilitate dispersion of the copolymers in the aqueous saline phase, and remove effects of particle size and porosity on dissolution. It is recognized that the efficiency of dispersion of these DMSO solutions in water can depend on polymer properties.

surprisingly, most of the copolymers studied did not show simple first order kinetics, which can be attributed to a variety of factors, including both changes in neighbouring group effects and solvation, as well as composition and degree of hydrolysis. A full analysis of this system is beyond the scope of this study. To compare rates of hydrolysis, or half-lifes, between different copolymers we found it sufficient to divide the first order plots into four equal 'time' quarters, analyze each quarter according to first order kinetics, and report the half-lifes for the first three quarters. Figure 5.6a,b,c shows the first order plots for hydrolysis of p(VDMA-*co*-MAA) 58:42, 84:16, 93:7, respectively. Figure 5.6c shows an example of the best-fit lines and R^2 values for the first three quarters. The half-lifes ($t_{1/2}$) are obtained by dividing ln(2) by the slopes of these linear fits, which represent the quasi-first order rate constant *k*. Figure 5.6a reveals that hydrolysis of the lower VDMA content copolymer actually seems to follow first order kinetics quite closely. Increasing VDMA content leads to increasing deviation from linearity, attributed partly to the lower degree of hydration of the copolymers (Figure 5.6b,c).

The initial rate of hydrolysis, represented by the slope of the first quarter, decreases with increasing VDMA content as might be expected from the increasing initial hydrophobicity of these copolymers. The corresponding plot for the p(VDMA) homopolymer (Figure 5.6d) shows an initial linear rate of hydrolysis about an order of magnitude lower than that of the 93% VDMA copolymer (Figure 5.6c). The fact that this homopolymer hydrolyses at all on this timescale is remarkable, and is attributed to the process of depositing it into aqueous saline from DMSO, which leads to formation of very fine, partially solvated particles that slowly dissolve by surface hydrolysis (etching, see below for further discussion).

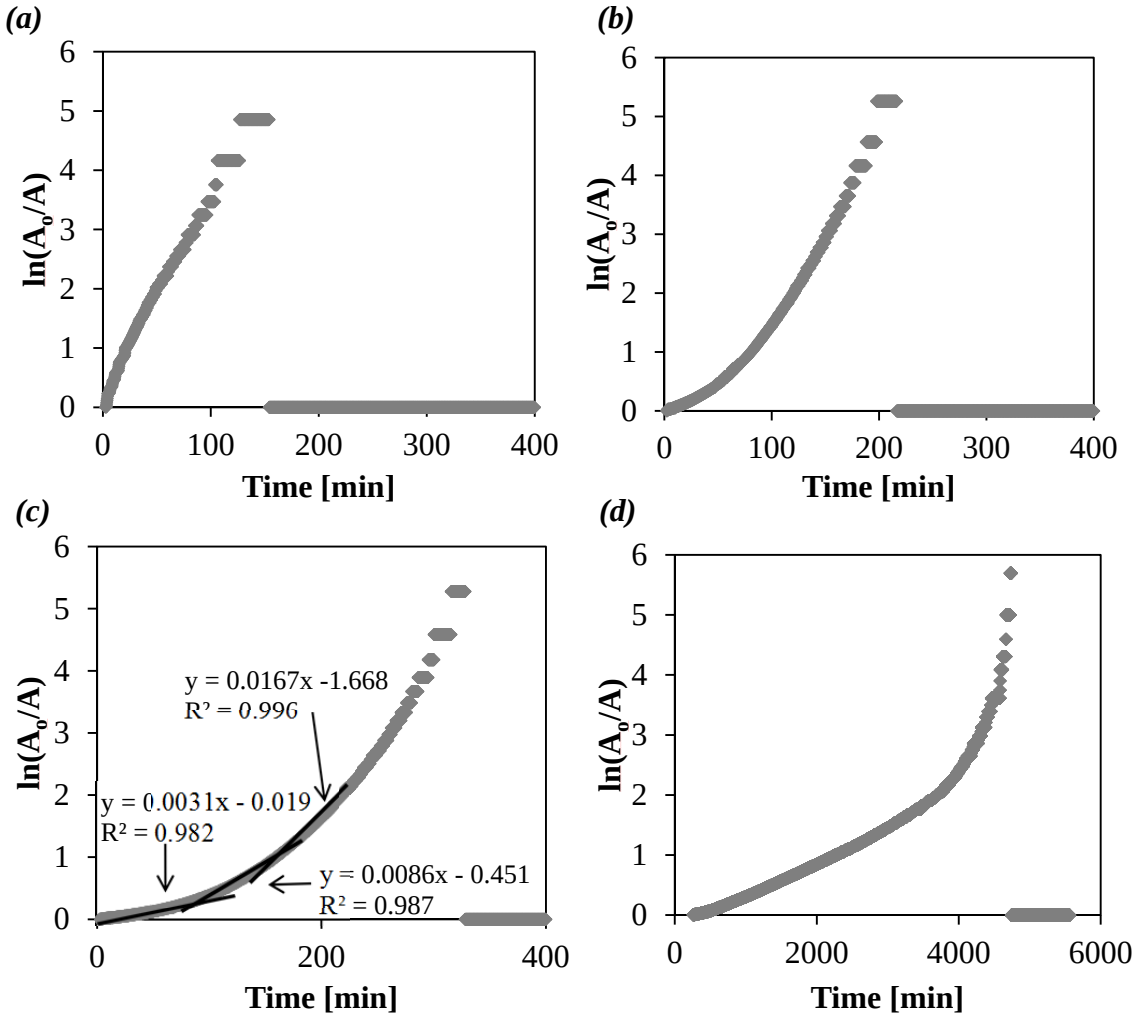

Figure 5.6 *First order plots for p(VDMA-co-MAA) with VDMA:MAA ratios of:* ***(a)*** *58:42* ***(b)*** *84:16* ***(c)*** *93:7 (slopes and R^2 values of the first three quarters)* ***(d)*** *100:0 (VDMA homopolymer).*

Figure 5.7 compares the half-lifes obtained for all p(VDMA-*co*-MAA) copolymers. The time in boxes above each copolymer indicates the time it takes for the copolymer to completely dissolve, e.g. where no detectable particles could be seen in a droplet sampled and observed by optical microscopy under 20x magnification.

The first three lower VDMA content p(VDMA-*co*-MAA) copolymers dissolve completely within 10 min and showed near-linear first order hydrolysis kinetics, with all half-lifes under 35 min.

The two higher VDMA content copolymers have much longer first quarter half-lifes of 76 ± 3 and 250 ± 20 min, respectively, which matches the 80 min and 180 min they needed to completely dissolve. Interestingly, their 2nd and 3rd quarter half-lifes

decrease, approaching the half-lifes of the lower VDMA copolymers. These results indicate a direct correlation between solubility and the rate of hydrolysis of these copolymers. This may simply be attributed to increasing hydration of the backbone, and possibly due to the catalytic action of the generated carboxylic groups (hydrolyzed VDMA).

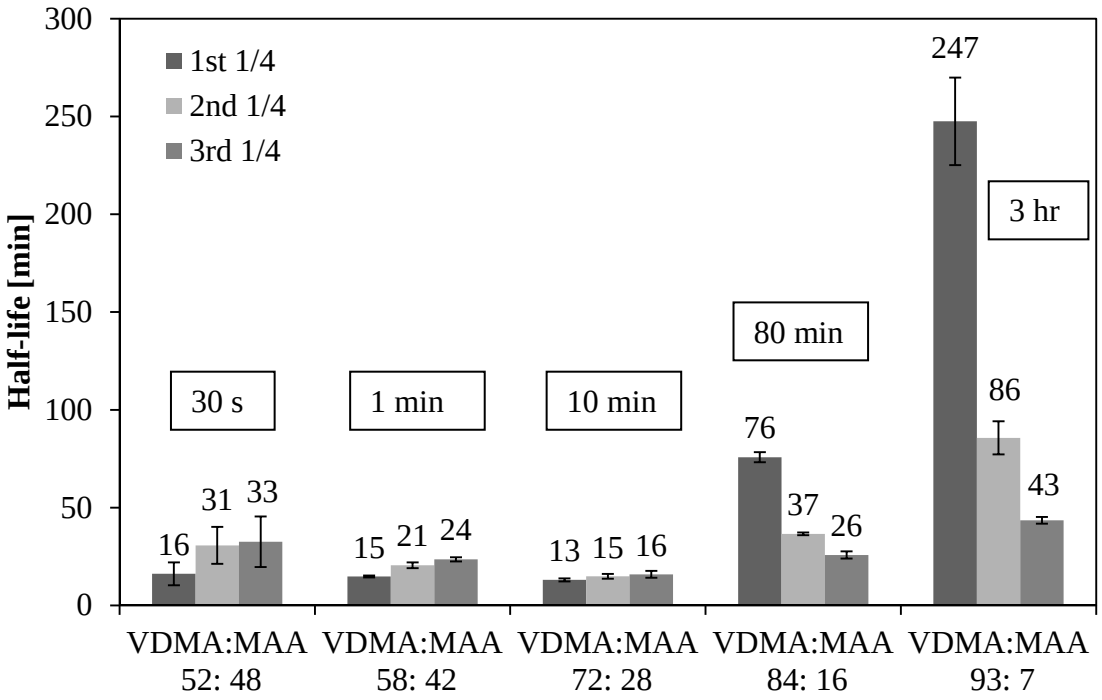

Figure 5.7 *Hydrolysis half-lifes for the first three quarters for p(VDMA-co-MAA) copolymers. The time above each copolymer indicates how long its aqueous dispersion took to become clear.*

As interesting is the comparison of the hydrolyses of p(VDMA-*co*-MAA) 93:7 and p(VDMA) (Table 5.3, Figure 5.6c,d). Using the same method of dispersing the polymers from 3 wt% DMSO into aqueous saline, it took 19 hrs for the initially formed aqueous p(VDMA) dispersion to form a clear solution, with a first quarter half-life of 1300 ± 100 min (22 hrs). The 1st quarter half-life of p(VDMA) is hence over five times longer than that of p(VDMA-*co*-MAA) 93:7, while its 2nd and 3rd quarter half-lifes are 1000 ± 100 min and 900 ± 70, respectively, 12 and 21 times longer than those of p(VDMA-*co*-MAA)'s 93:7 2nd and 3rd quarter half-lifes.

This remarkable effect of the presence of a small percentage of MAA in the 93:7 copolymer is attributed to the excellent solvation provided by this small anionic comonomer. Dispersion of the DMSO solutions of p(VDMA) and p(VDMA-co-MAA) 93:7 into aqueous saline led to cloudy suspensions of small polymer particles. The

hydrophobic p(VDMA) particles can only hydrolyze by surface etching. In contrast, the small amount of MAA present in the copolymer is thought to help swell these particles and thus additionally enable bulk hydrolysis. Only at high degrees of hydration does the hydrolysis of p(VDMA) speed up, which may be attributed to increasing hydration of all portions of this polymer due to the formation of carboxylic groups, and possibly also to catalytic action of the carboxylic groups being formed.

Comonomer % in copolymer	VDMA%[a]	Azlact-one%[b]	Polymer weight%	1st ¼ $t_{1/2}$ [min]	2nd ¼ $t_{1/2}$ [min]	3rd ¼ $t_{1/2}$ [min]
MAA 48	52	48	0.23	16 ± 6	30 ± 10	30 ± 10
MAA 42	58	56	0.20	15 ± 1	21 ± 1	24 ± 1
MAA 28	72	72	0.17	13 ± 1	15 ± 1	16 ± 2
MAA 16	84	84	0.15	76 ± 3	37 ± 1	26 ± 2
MAA 7	93	93	0.14	250 ± 20	86 ± 8	43 ± 2
PVDMA	100	100	0.14	1300 ± 100	1000 ± 100	900 ± 70
MPC 18	82	76	0.21	180 ± 10	80 ± 10	49 ± 6
MPC 8	92	89	0.17	110 ± 20	61 ± 8	46 ± 8
AAm 59	41	41	0.24	55 ± 5	80 ± 8	100 ± 20
DMAA 78	22	22	0.49	134 ± 7	270 ± 30	300 ± 30

Table 5.3 *Half-lifes of VDMA copolymers and p(VDMA).*
[a] Reported values are the average of ^{13}C NMR and EA results. ^{1}H NMR results were not included as they have been shown previously to overestimate the amount of VDMA incorporated into the copolymer.[8]
[b] Calculated based on the average VDMA% (a) and the amount of azlactone gone as seen from ^{1}H NMR (column 8 Table 5.1).

Comparison of the hydrolysis half-lifes of p(VDMA-*co*-MAA) with those of the DMAA, AAm and MPC copolymers also showed significant differences (Table 5.3). P(VDMA-*co*-DMAA) 22:78 formed a clear solution immediately upon dispersion from DMSO into saline, while the analogous 37: 63 copolymer dispersion took about 10 min to become clear. Due the more hydrophilic nature of AAm, p(VDMA-*co*-AAm) 59:41 formed a clear solution upon dispersion from DMSO solution into saline, while the analogous 71:29 copolymer took 2 hrs to become clear.

P(VDMA-*co*-DMAA) 22:78 and p(VDMA-*co*-AAm) 41:59 (Figure 5.8) showed much longer half-lives compared to p(VDMA-*co*-MAA) 52:48. As these three copolymers all form clear solutions within a minute or less, and are thus considered fully

hydrated, the significant differences in their rate of hydrolysis may hence be due to catalytic action of carboxylic groups on p(VDMA-*co*-MAA). These three copolymers are unique in that their hydrolyses get slower with increasing conversion (Figure 5.8), in contrast to all other copolymers studied. The cause of this behaviour is not clear at this time.

The p(VDMA-*co*-MPC) 82:18 copolymer instantly dissolves in saline. Despite this high initial solubility, this copolymer shows a long first quarter half-life of about 3 hrs (Figure 5.8). Its 92:8 analog takes 30 minutes to form a clear solution yet has a shorter first quarter half-life. This suggests that while MPC helps dissolve the copolymer, its amphiphilic nature may also shield the hydrophobic azlactone from hydrolysis.

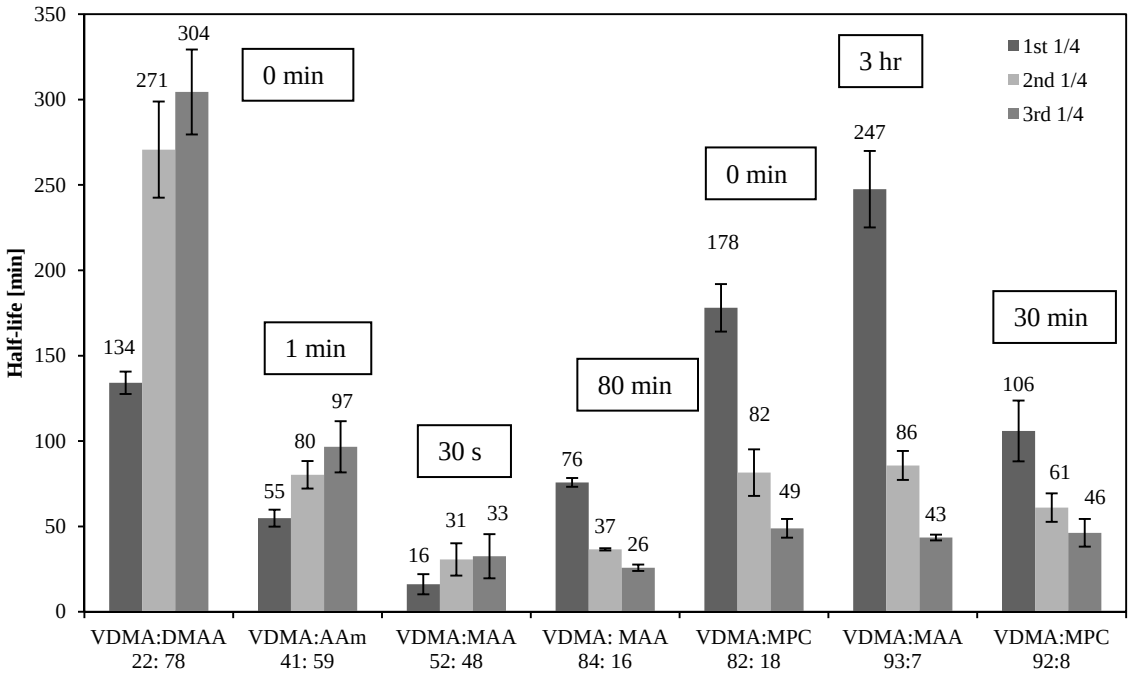

Figure 5.8 *Comparison of the half-lifes for the first three quarters of VDMA copolymers. The time above each copolymer indicates how long its aqueous dispersion took to become clear.*

Also interesting to note is that while the two p(VDMA-*co*-MPC) copolymers are both more water-soluble than their p(VDMA-*co*-MAA) counterparts with comparable VDMA content (Figure 5.8), the first quarter half-life of p(VDMA-*co*-MPC) 82:18 is much longer than that of p(VDMA-*co*-MAA) 84:16, while the p(VDMA-*co*-MPC) 92:8 has a shorter first quarter half-life compared to p(VDMA-*co*-MAA) 93:7. It is possible that the positive charge on the zwitterionic MPC interacts with the negatively charged carboxylates of the hydrolyzed VDMA, reducing the hydrophilicity of the carboxylate and possibly negating its ability to catalyze further hydrolysis.

These findings make p(VDMA-co-MPC) 82:18 an intriguing lead candidate for the formation of biomedical hydrogels from aqueous solutions: it combines high azlactone content and hence high crosslinking ability, with instant solubility under physiological conditions, and a low rate of hydrolysis. This combination of features promises a long working time in aqueous conditions to perform crosslinking reactions and/or immobilize biomolecules, and will be the starting point of further study.

5.5 Conclusions

The reactivity ratios of several VDMA/comonomer pairs using photo-initiated copolymerization at room temperature were determined by fitting comonomer conversions obtained by *in-situ* ^{1}H NMR to the copolymer equation. VDMA was found to be preferentially incorporated in all cases studied. Corresponding no-drift copolymers were subsequently prepared using semi-batch photo-initiated copolymerization. Their ability to form clear aqueous solutions upon dispersion from DMSO solution into saline, and their rates of hydrolysis, were determined. P(VDMA-*co*-MAA) copolymers showed decreasing initial solubility and rate of hydrolysis, with increasing VDMA content. Even 7% MAA comonomer increased both the rate of clarification and the rate of hydration by an order of magnitude, compared to the VDMA homopolymer. P(VDMA-*co*-DMAA) 22:78 and p(VDMA-*co*-AAm) 41:59 showed lower rates of hydrolysis than corresponding p(VDMA-*co*-MAA) copolymers, suggesting possible catalysis of azlactone hydrolysis by neighboring MAA groups. The hydrolysis of p(VDMA-*co*-HEMA) and p(VDMA-*co*-MPEG$_{300}$MA) was not investigated as these polymers self-crosslinked during storage.

The most interesting copolymer studied was the zwitterionic p(VDMA-*co*-MPC). P(VDMA-*co*-MPC) 82:18 had a much longer first quarter half-life and better solubility compared to an analogous p(VDMA-*co*-MAA) copolymer. The high VDMA content, solubility and slow rate of hydrolysis, and possible anti-fouling properties of p(VDMA-MPC) 82:18 make this copolymer appealing for use in future cell-encapsulation studies.

5.6 Acknowledgments

The authors would like to thank Dr. Steve Kornic for elemental analyses, and Dr. Bob Berno for help with the saturation-recovery and quantitative NMR experiments. HDHS would like to thank NSERC's Discovery Grant program for funding, and CMG would like to acknowledge receiving an NSERC Alexander Graham Bell doctoral scholarship.

5.7 References

[1] J. Jagur-Grodzinski. *React. Funct. Poly*. **1999**, *39*, 99-138.
[2] W.H. Binder; R. Sachsenhofer. *Macromol. Rapid Commun*. **2007**, *28*, 15-54.
[3] C.M. Gardner; M.A. Potter; H.D.H. Stöver. *J. Mater. Sci. Mater. Med.* **2012**, 23, 181-193.
[4] A.H. Broderick; S.M. Azarin; M.E. Buck; S.P. Palecek; D.M. Lynn. *Biomacromolecules* **2011**, *12*, 1998-2007.
[5] B. Sun; Z. Liu; M.E. Buck; D.M. Lynn. *Chem. Commun*. **2010**, *46*, 2016-2018.
[6] S.M. Heilmann; J.K. Rasmussen; L.R. Krepski. *J. Polym. Sci. A* **2001**, *39*, 3655-3677.
[7] D.C. Tully; M.J. Roberts; B.H. Geierstanger. *Macromolecules* **2003**, *36*, 4302-4308.
[8] C.M. Gardner; D.H.D. Stöver. *Macromolecules* **2011**, *44*, 7115–23.
[9] L.G. Stanek; S.M. Heilmann; W.B. Gleason. *J. Polym. Sci. A* **2003**, 41, 3027-3037.
[10] L.G. Stanek; S.M. Heilmann; W.B. Gleason. *Polym. Bull.* **2005**, *55*, 393-402.
[11] J.M. Messman; B.S. Lokitz; J.M. Pickel; S.M. Kilbey. *Macromolecules 42*, **2009**, 3933-3941.
[12] M.E. Buck; J. Zhang; D.M. Lynn. *Adv. Mater.* **2007**, 19, 3951-3955.
[13] M.E. Buck; D.M. Lynn. *Langmuir* **2010**, *26*, 16134-40.
[14] J.E. Barringer; J.M. Messman; A.L. Banaszek; H.M. Meyer; S.M. Kilbey. *Langmuir* **2009**, *25*, 262-268.
[15] A. Guyomard; D. Fournier; S. Pascual; L. Fontaine; J.F. Bardeau. *Eur. Polym. J.* **2004**, *40*, 2343-2348.
[16] M.R. Aguilar; A. Gallardo; M. del Mar Fernánde; J.S. Román. *Macromolecules* 35, **2002**, 2036-41
[17] G.E.P. Box; W.G. Hunter; J.S. Hunter. *Statistics for Experimenters: An Introduction to Design, Data Analysis and Model Building*, 2nd Ed.; John Wiley & Sons: New York, 2005; p 371.
[18] A. Eisenber; T. Yokoyama; E. Sambalido. *J. Polym. Sci. A* **1969**, *7*, 1717-1728
[19] P. Foley. Development of Reactive Polyanions for Encapsulation of Live Yeast Cells within Polymer Hydrogel Films. Thesis, (MSc). McMaster University.
[20] R. Jeyanthi; R. Rao. *Biomaterials* **1990**, *11*, 238-243.
[21] K. Kejilová; J. Labský; D. Jírová; H. Bendová. *Toxicology in Vitro*, **2005**, *19*, 957-962.
[22] M.M. Ali; H.D.H. Stöver. *Macromolecules* **2003**, *36*, 1793-01801
[23] M. Gong; Y.B. Wang; M. Li; B.H. Hu; Y.K. Gong. *Colloids Surf. B* **2011**, *85*, 48-55.
[24] S. Monge; B. Canniccioni; A. Graillot; J.J. Robin. *Biomacromolecules* **2011**, *12*, 1973-1982.
[25] L.G. Stanek; S.M. Heilmann; W.B. Gleason. *Colloid Polym. Sci.* **2006**, *284*, 586-595.

5.8 Appendix

5.8.1 VDMA:MAA

For VDMA:MAA copolymerization a 45:55, 65:35 and 20:80 initial feed molar compositions were used. The reaction was stopped at 0, 2, 4, 7, 12, 19, 30 min and analyzed by 600 MHz ^{1}H NMR.

	Equation [1]		Equation [2]		
	r_1(VDMA)	**r_2(MAA)**	**r_1(VDMA)**	**r_2(MAA)**	**k**
45:55	2.297	0.689	1.085	0.317	58.34
65:35	1.918	1.023	1.905	1.023	56.95
20:80	7.291	0.683	1.141	0.334	56.34
Aguilar fraction	1.446	0.569	1.086	0.312	61.38
Sliding fraction	1.339	0.420	1.051	0.201	60.68

Table 5A.1 *Calculated reactivity ratios using various methods*

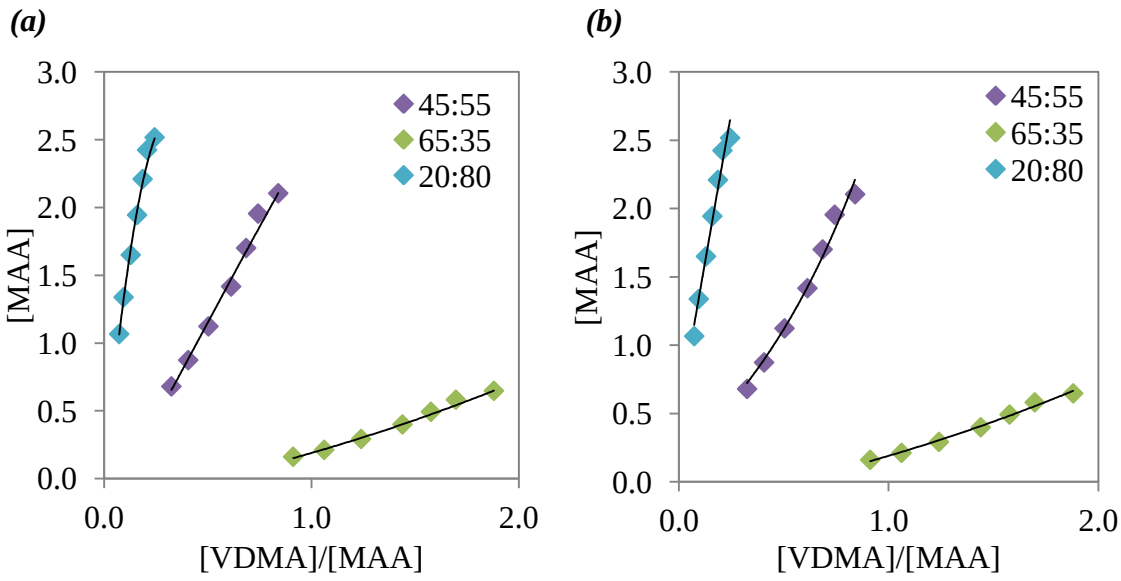

Figure 5A.1 *[MAA] vs. [VDMA]/[MAA] from ^{1}H NMR analysis of three copolymerizations with VDMA:MAA initial feed ratios of 45:55, 65:35 and 20:80. The black lines show the fitted data of calculated [MAA]'s using* ***(a)*** *equation [1] and* ***(b)*** *equation [2], and colored diamonds represent experimental data.*

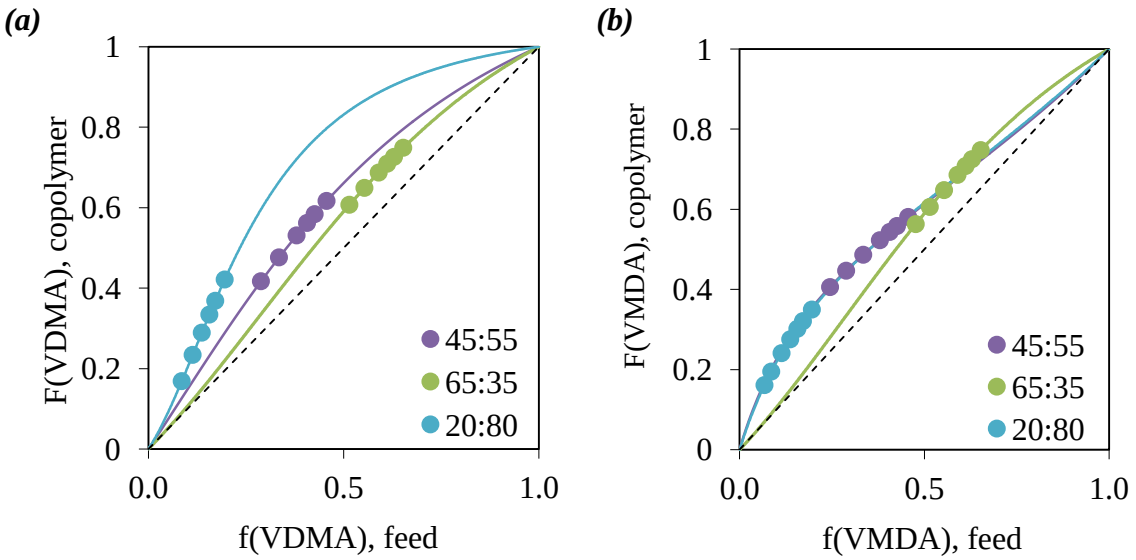

Figure 5A.2 *Copolymer composition diagrams showing (lines) separate fits to the data (circles) of three reactions with VDMA:MAA initial molar ratios of 45:55, 65:35 and 20:80, using* ***(a)*** *equation [1],* ***(b)*** *equation [2].*

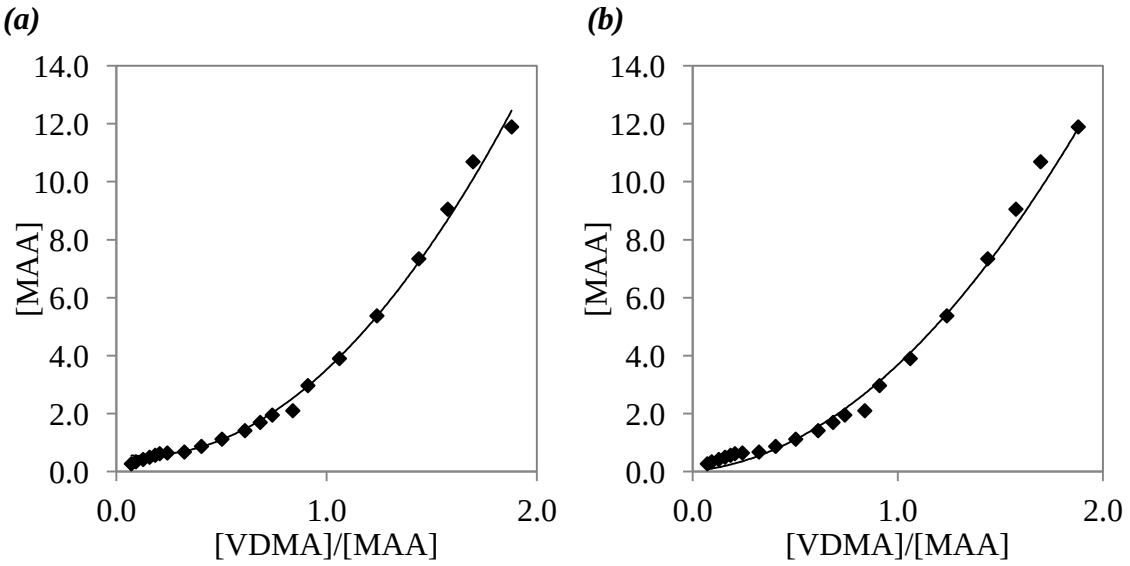

Figure 5A.3 *Corrected global [MAA] vs. [VDMA]/[MAA] as described by Aguilar. The black lines show the fitted data of calculated [MAA]'s using* ***(a)*** *equation [1] and* ***(b)*** *equation [2]. Black diamonds represent experimental data.*

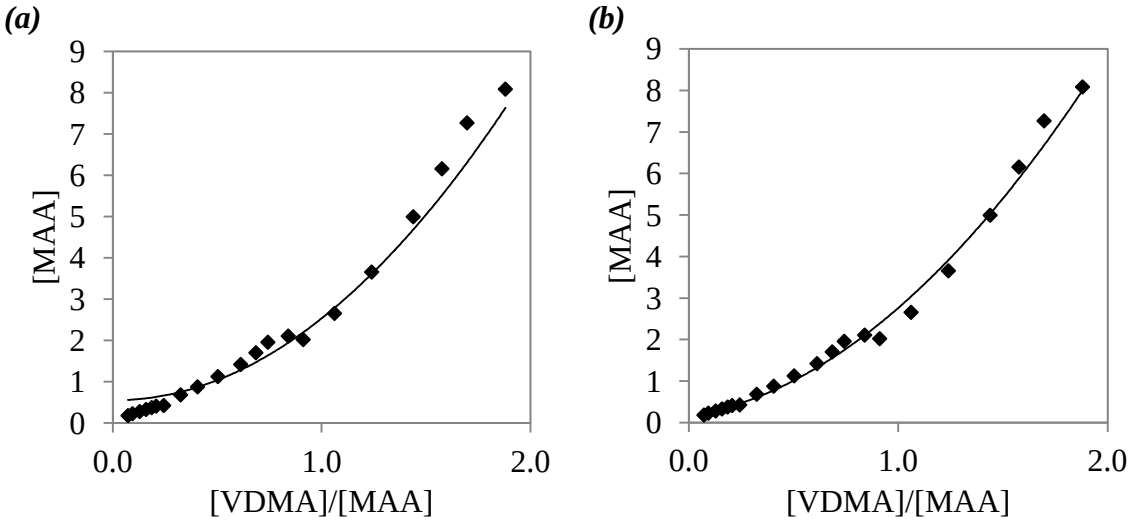

Figure 5A.4 *Corrected global [MAA] vs. [VDMA]/[MAA] calculated using a sliding fraction via EXCEL solver. The black lines show the fitted data of calculated [MAA]'s using* ***(a)*** *equation [1] and* ***(b)*** *equation [2]. Black diamonds represent experimental data.*

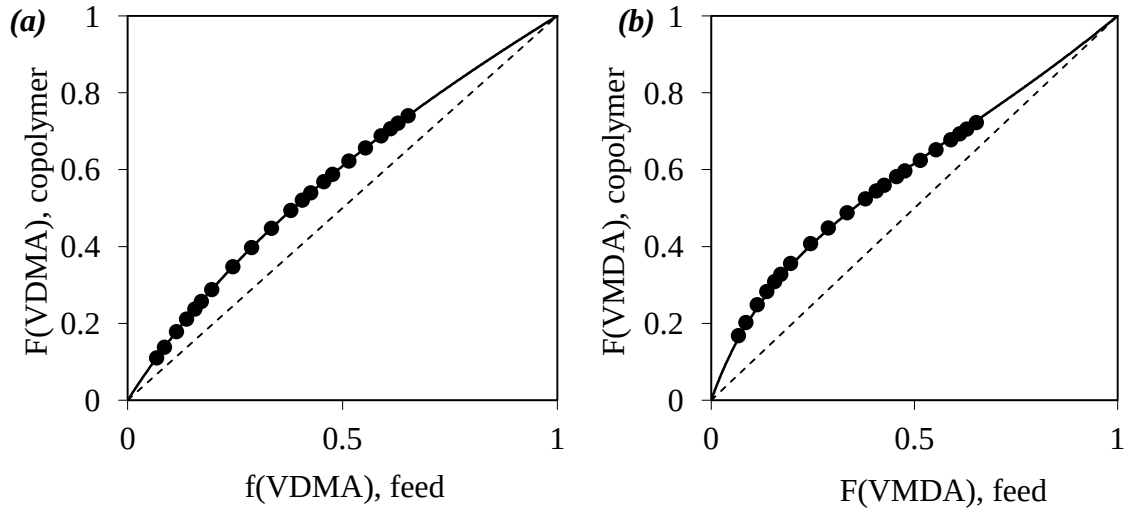

Figure 5A.5 *Composition diagrams obtained with the reactivity ratios determined using* ***(a)*** *equation [1],* ***(b)*** *equation [2] and the corrected global data using Aguliar's fraction method (Figure 5A.3). The black lines show a fit to the data, the full black circles show the individual experimental data points.*

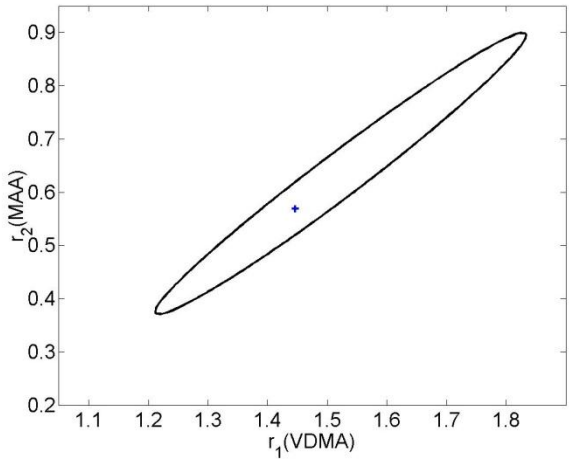

Figure 5A.6 *95% confidence contour for r_1(VDMA) and r_2(MAA) using equation [1].*

5.8.2 VDMA:AA

For VDMA:AA copolymerization a 45:55, 65:35 and 28:71 initial feed molar compositions were used. The reaction was stopped at 0, 2, 4, 6, 8, 11, 15 and 20 min and analyzed by 600 MHz ^{1}H NMR.

	Equation [1]		Equation [2]		
	r_1(VDMA)	**r_1(AA)**	**r_1(VDMA)**	**r_1(AA)**	**k**
45:55	3.086	0.208	3.283	0.219	1.88
65:35	2.860	0.132	4.321	0.478	2.18
28:71	2.925	0.216	3.011	0.216	3.00
Aguilar fraction	3.104	0.202	3.233	0.212	1.86
sliding fraction	3.132	0.213	3.267	0.22	1.89

Table 5A.2 *Calculated reactivity ratios using various methods*

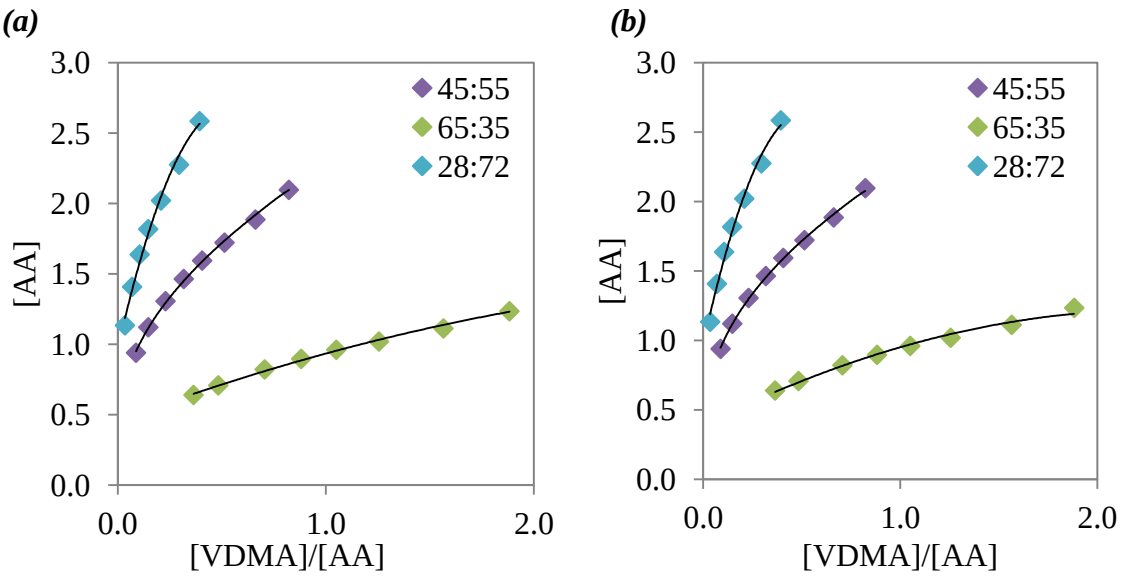

Figure 5A.7 *[AA] vs. [VDMA]/[AA] from ^{1}H NMR analysis of three copolymerizations with VDMA:AA initial feed ratios of 45:55, 65:35 and 28:72. The black lines show the fitted data of calculated [AA]'s using* ***(a)*** *equation [1] and* ***(b)*** *equation [2], and colored diamonds represent experimental data.*

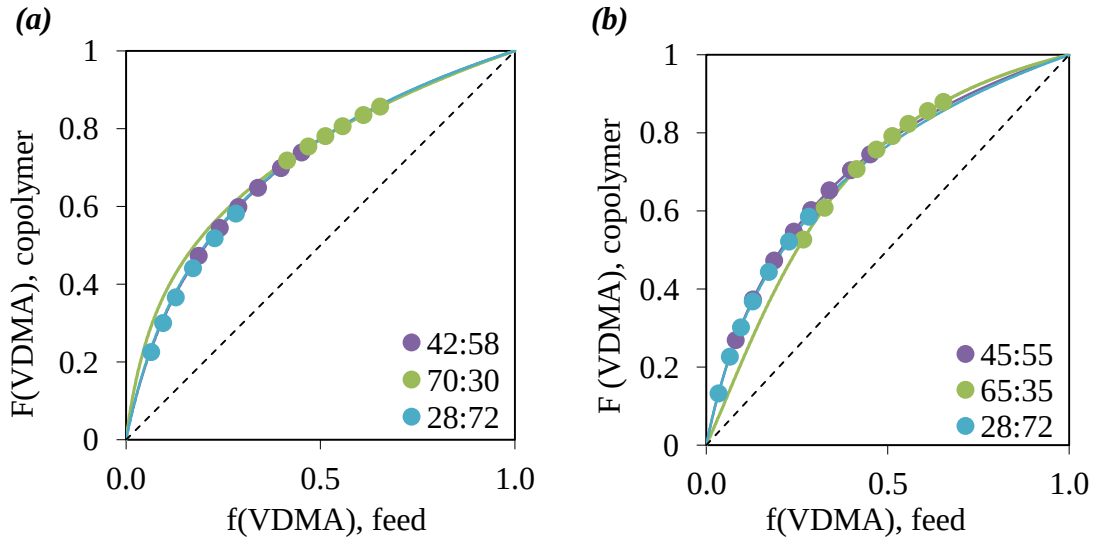

Figure 5A.8 *Copolymer composition diagrams showing (lines) separate fits to the data (circles) of three reactions with VDMA:AA initial molar ratios of 45:55, 65:35 and 28:72, using* ***(a)*** *equation [1],* ***(b)*** *equation [2].*

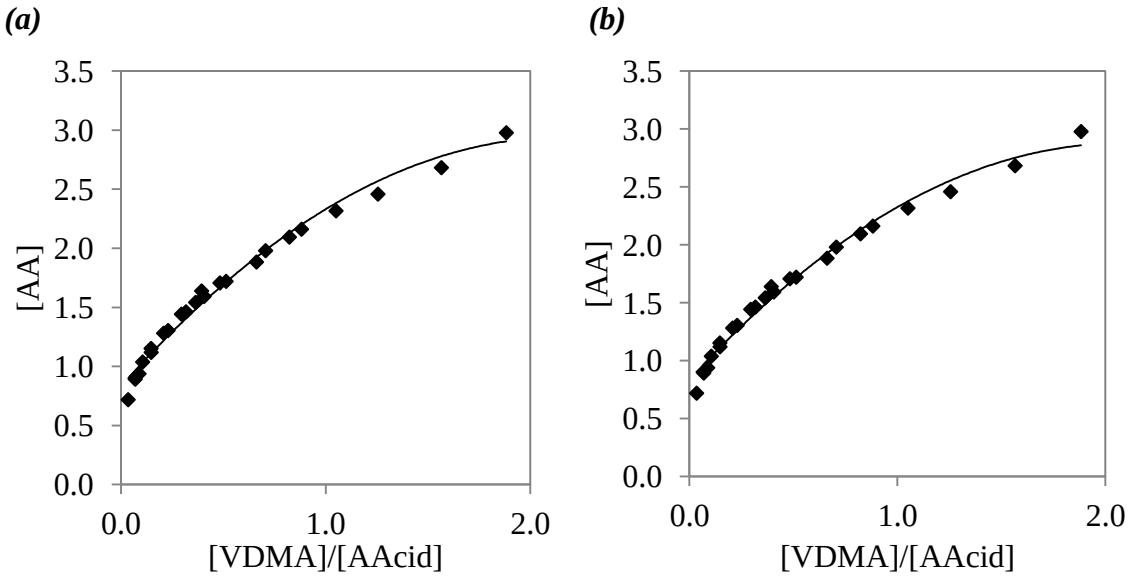

Figure 5A.9 *Corrected global [AA] vs. [VDMA]/[AA] as described by Aguilar. The black lines show the fitted data of calculated [AA]'s using* ***(a)*** *equation [1] and* ***(b)*** *equation [2]. Black diamonds represent experimental data.*

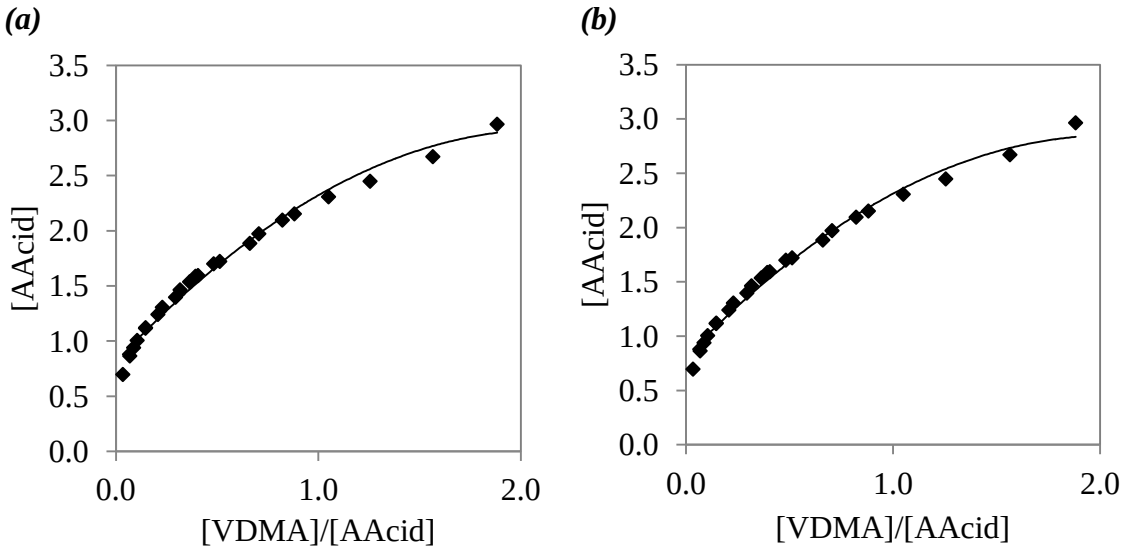

Figure 5A.10 *Corrected global [AA] vs. [VDMA]/[AA] calculated using a sliding fraction via EXCEL solver. The black lines show the fitted data of calculated [AA]'s using* ***(a)*** *equation [1] and* ***(b)*** *equation [2]. Black diamonds represent experimental data.*

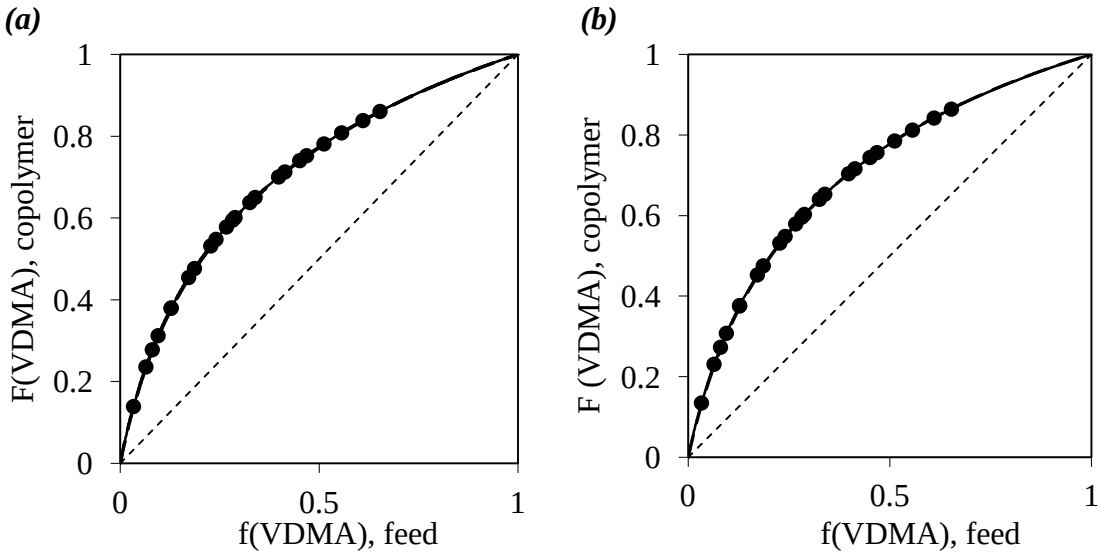

Figure 5A.11 *Composition diagrams obtained with the reactivity ratios determined using* ***(a)*** *equation [1],* ***(b)*** *equation [2] and the corrected global data using Aguliar's fraction method (Figure 5A.9). The black lines show a fit to the data, the full black circles show the individual experimental data points.*

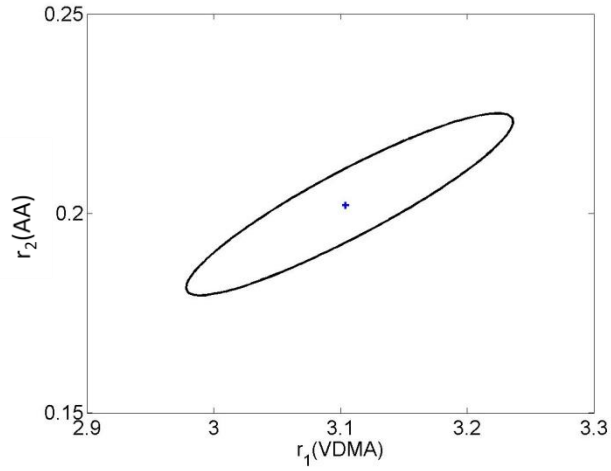

Figure 5A.12 *95% confidence contour for r_1(VDMA) and r_2(AA) using equation [1].*

5.8.3 VDMA:AAm

For VDMA:AAm copolymerization a 46:54, 72:28 and 23:77 initial feed molar compositions were used. The reaction was stopped at 0, 1, 2, 4, 6, 11, 16, 21 and 31 min and analyzed by 600 MHz ^{1}H NMR.

	Equation [1]		Equation [2]		
	r_1(VDMA)	r_2(AAm)	r_1(VDMA)	r_2(AAm)	k
46: 54	15.991	0.752	8.368	0.325	2.39
72: 28	7.000	0.300	6.594	0.520	5.11
23: 77	9.370	0.144	7.091	0.130	4.79
Aguilar fraction	5.820	0.191	5.059	0.147	1.05
sliding fraction	5.627	0.147	4.854	0.107	0.96

Table 5A.3 *Calculated reactivity ratios using various methods*

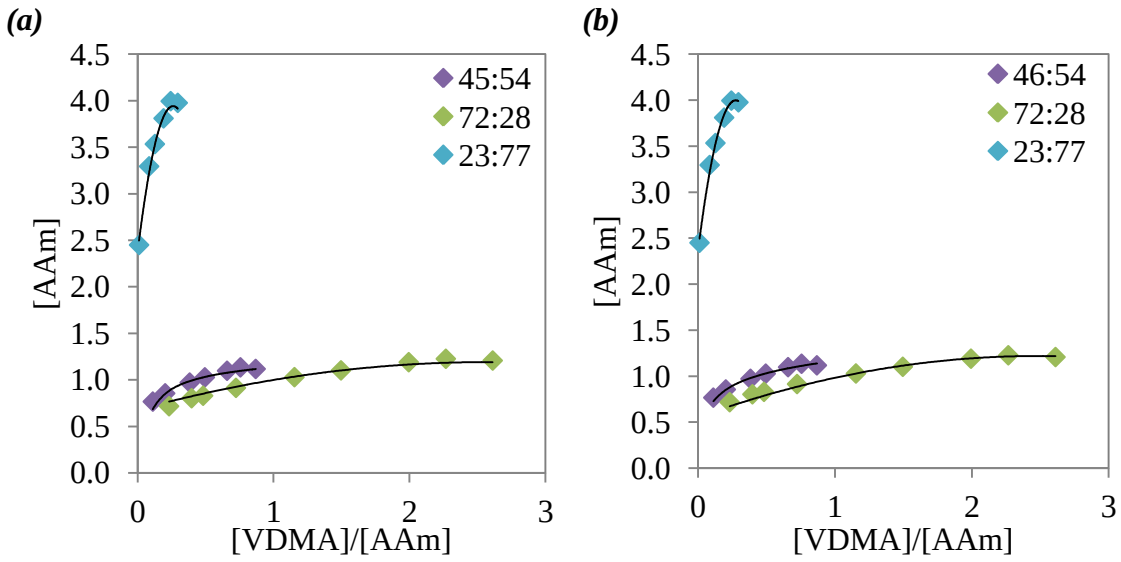

Figure 5A.13 *[AAm] vs. [VDMA]/[AAm] from ^{1}H NMR analysis of three copolymerizations with VDMA:AAm initial feed ratios of 46:54, 72:28 and 23:77. The black lines show the fitted data of calculated [AAm]'s using* ***(a)*** *equation [1] and* ***(b)*** *equation [2], and colored diamonds represent experimental data.*

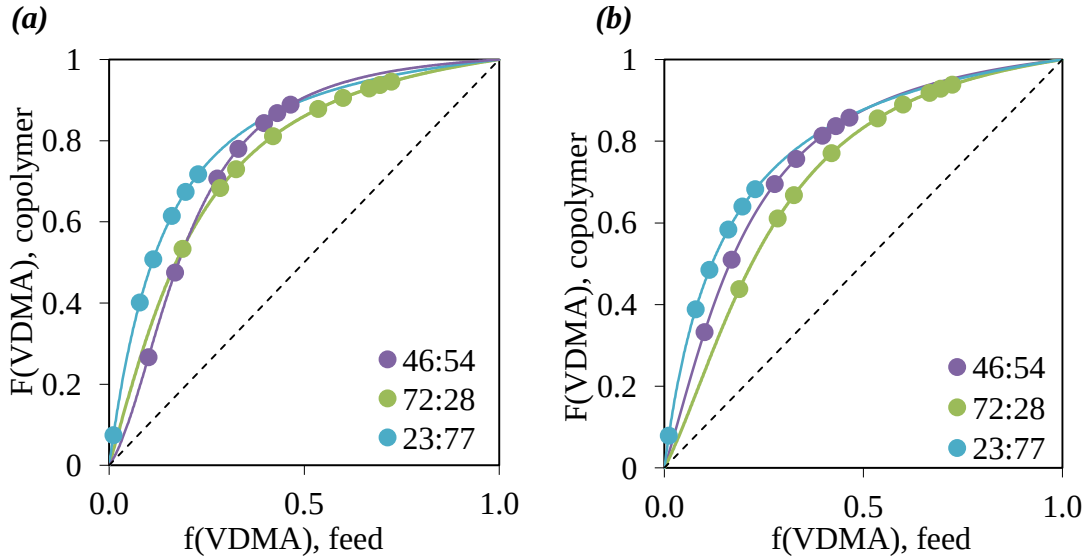

Figure 5A.14 *Copolymer composition diagrams showing (lines) separate fits to the data (circles) of three reactions with VDMA:AAm initial molar ratios of 46:54, 72:28 and 23:77, using* ***(a)*** *equation [1],* ***(b)*** *equation [2].*

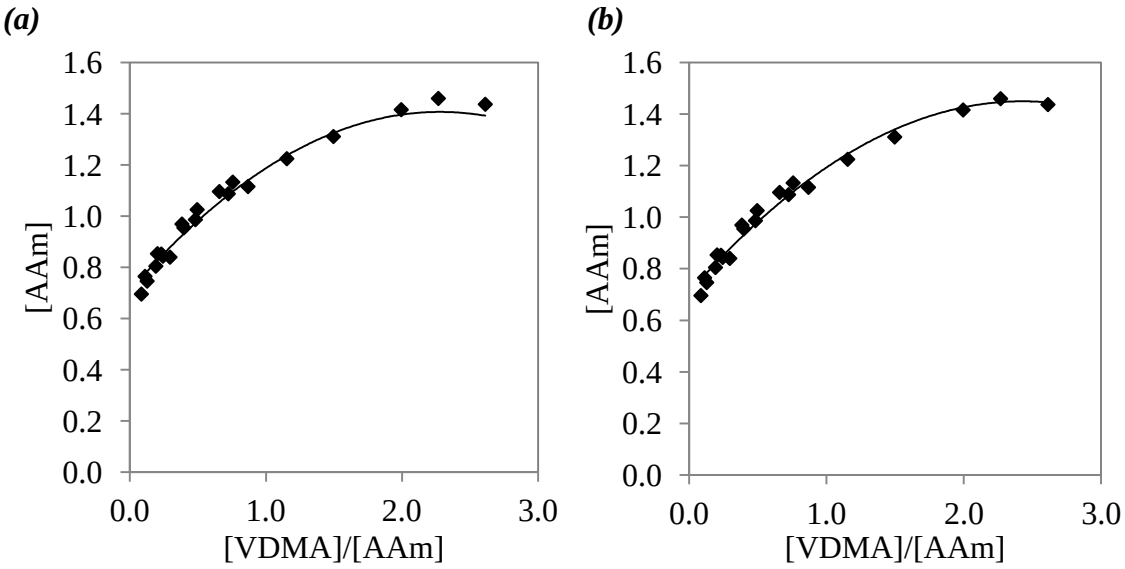

Figure 5A.15 *Corrected global [AAm] vs. [VDMA]/[AAm] as described by Aguilar. The black lines show the fitted data of calculated [AAm]'s using* ***(a)*** *equation [1] and* ***(b)*** *equation [2]. Black diamonds represent experimental data.*

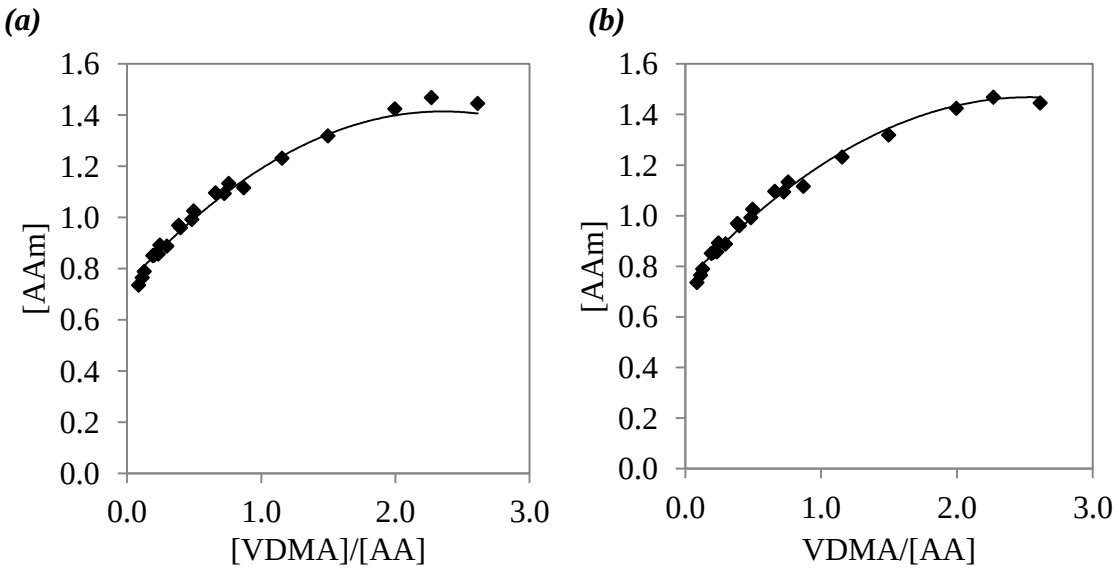

Figure 5A.16 *Corrected global [AAm] vs. [VDMA]/[AAm] calculated using a sliding fraction via EXCEL solver. The black lines show the fitted data of calculated [AAm]'s using* ***(a)*** *equation [1] and* ***(b)*** *equation [2]. Black diamonds represent experimental data.*

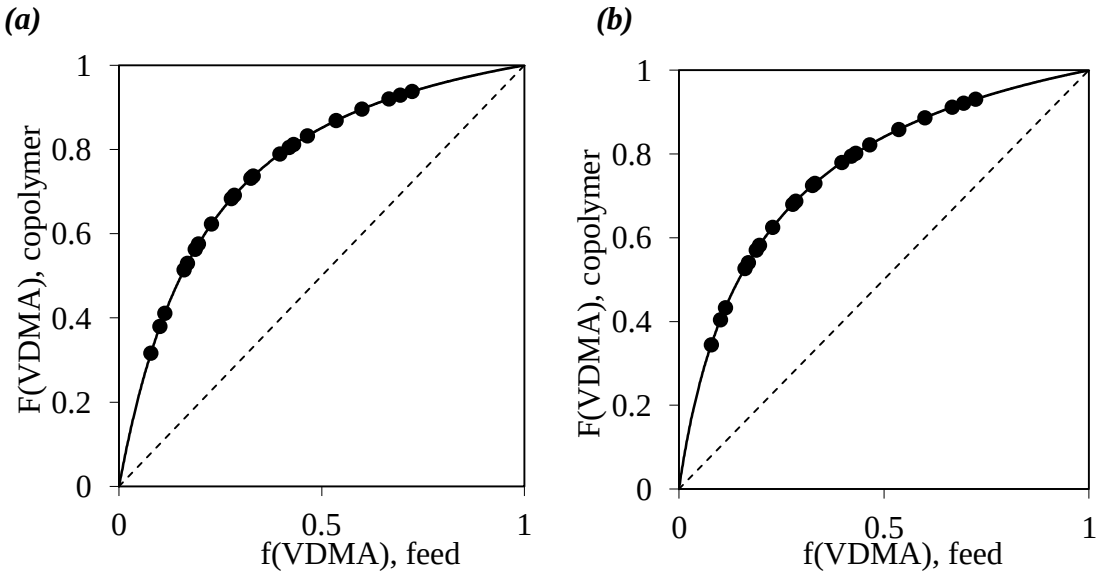

Figure 5A.17 *Composition diagrams obtained with the reactivity ratios determined using* ***(a)*** *equation [1],* ***(b)*** *equation [2] and the corrected global data using Aguliar's fraction method (Figure 5A.15). The black lines show a fit to the data, the full black circles show the individual experimental data points.*

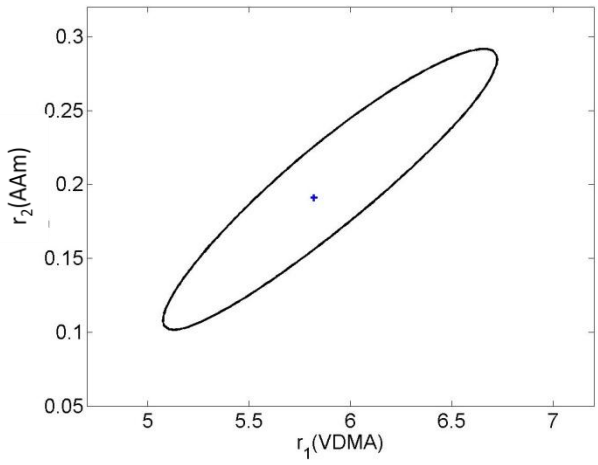

Figure 5A.18 *95% confidence contour for r_1(VDMA) and r_2(AAm) using equation [1].*

5.8.4 VDMA:DMAA

For VDMA:DMAA copolymerization a 45: 5, 60:40 and 36:64 initial feed molar compositions were used. The reaction was stopped at 0, 2, 4, 7, 11, 16, and 26 min and analyzed by 600 MHz ^{1}H NMR.

	Equation 2		Equation 3		
	r_1(VDMA)	**r_2(DMAA)**	**r_1(VDMA)**	**r_2(DMAA)**	**k**
54:55	2.051	0.164	2.118	0.170	1.18
60:40	1.989	0.117	2.182	0.182	0.57
36:64	2.013	0.168	2.062	0.171	1.69
Aguilar fraction	2.134	0.169	2.167	0.173	1.20
sliding fraction	2.144	0.173	2.175	0.177	1.20

Table 5A.4 *Calculated reactivity ratios using various methods*

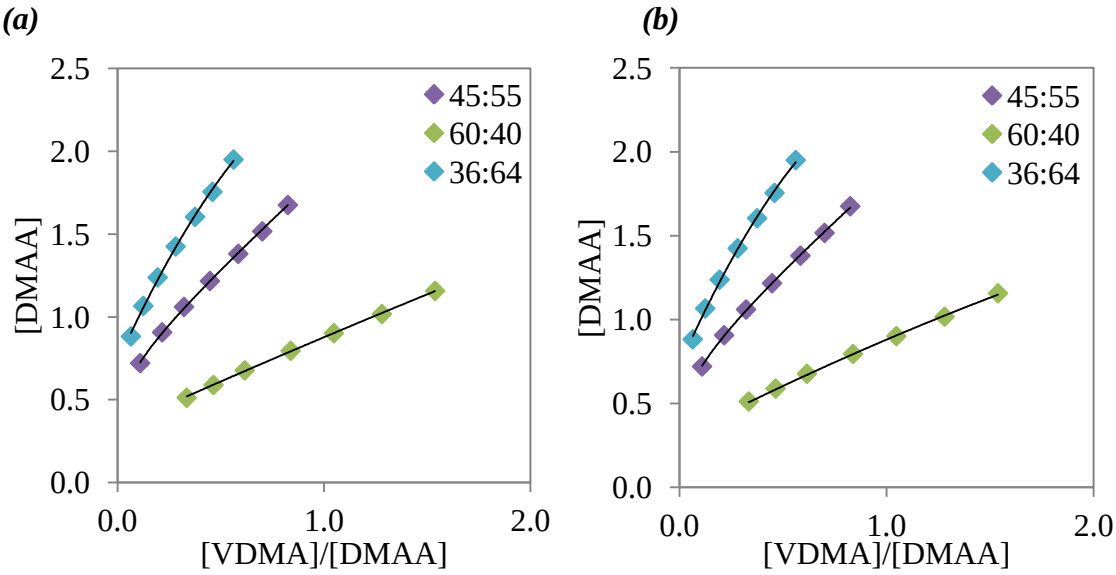

Figure 5A.19 *[DMAA] vs. [VDMA]/[DMAA] from ^{1}H NMR analysis of three copolymerizations with VDMA:DMAA initial feed ratios of 45:55, 60:40 and 36:64. The black lines show the fitted data of calculated [DMAA]'s using* ***(a)*** *equation [1] and* ***(b)*** *equation [2], and colored diamonds represent experimental data.*

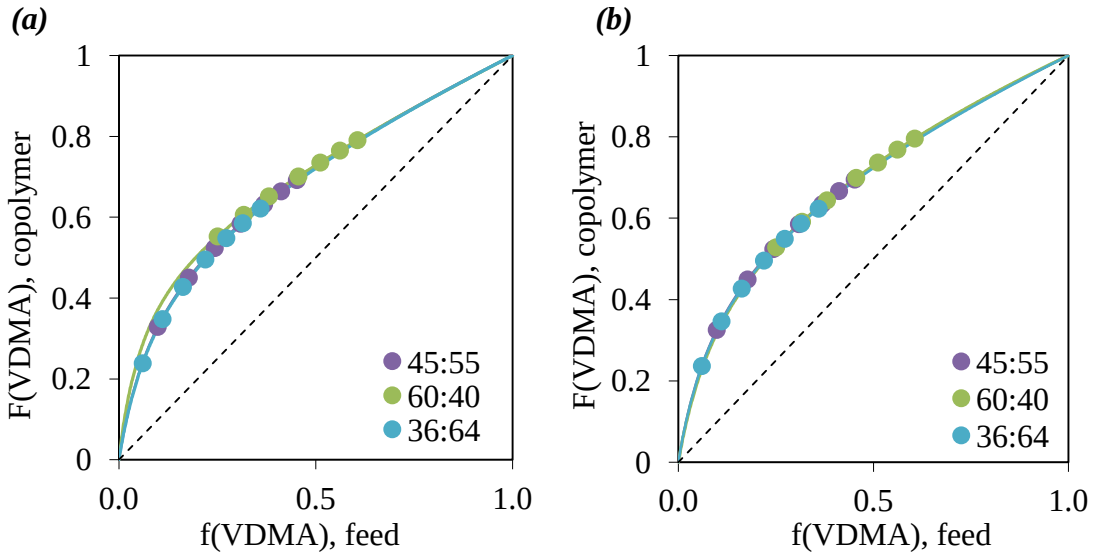

Figure 5A.20 *Copolymer composition diagrams showing (lines) separate fits to the data (circles) of three reactions with VDMA:DMAA initial molar ratios of 45:55, 60:40 and 36:64, using* ***(a)*** *equation [1],* ***(b)*** *equation [2].*

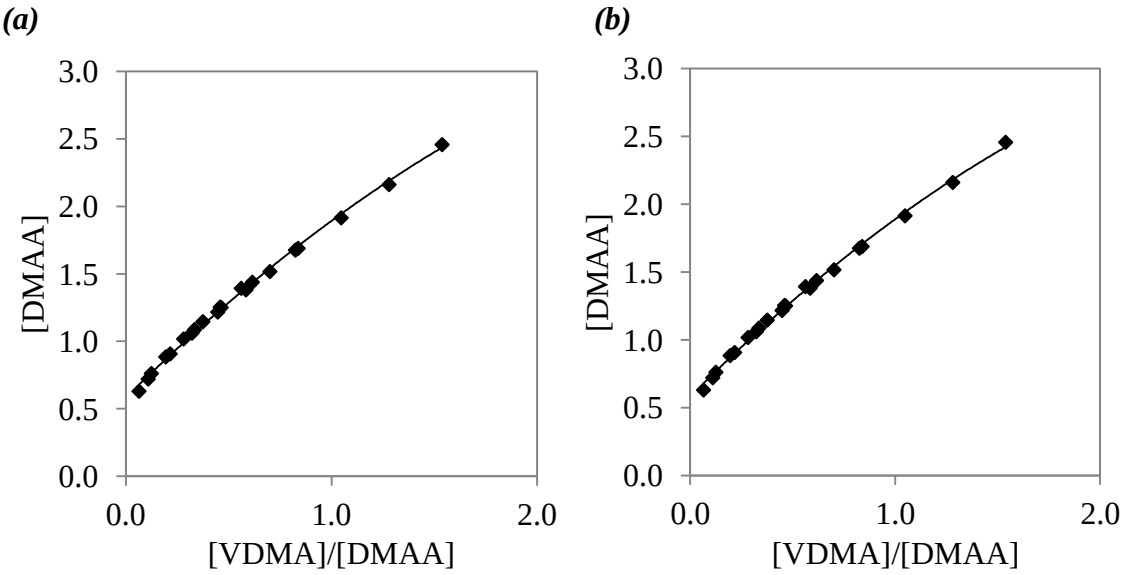

Figure 5A.21 *Corrected global [DMAA] vs. [VDMA]/[DMAA] as described by Aguilar. The black lines show the fitted data of calculated [DMAA]'s using* ***(a)*** *equation [1] and* ***(b)*** *equation [2]. Black diamonds represent experimental data.*

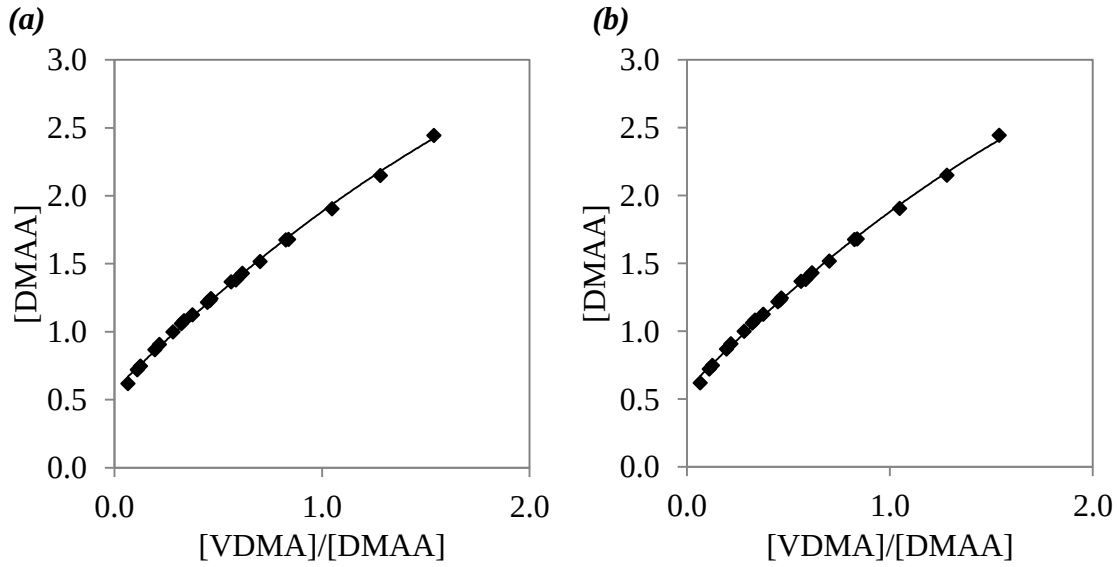

Figure 5A.22 *Corrected global [DMAA] vs. [VDMA]/[DMAA] calculated using a sliding fraction via EXCEL solver. The black lines show the fitted data of calculated [DMAA]'s using* ***(a)*** *equation [1] and* ***(b)*** *equation [2]. Black diamonds represent experimental data.*

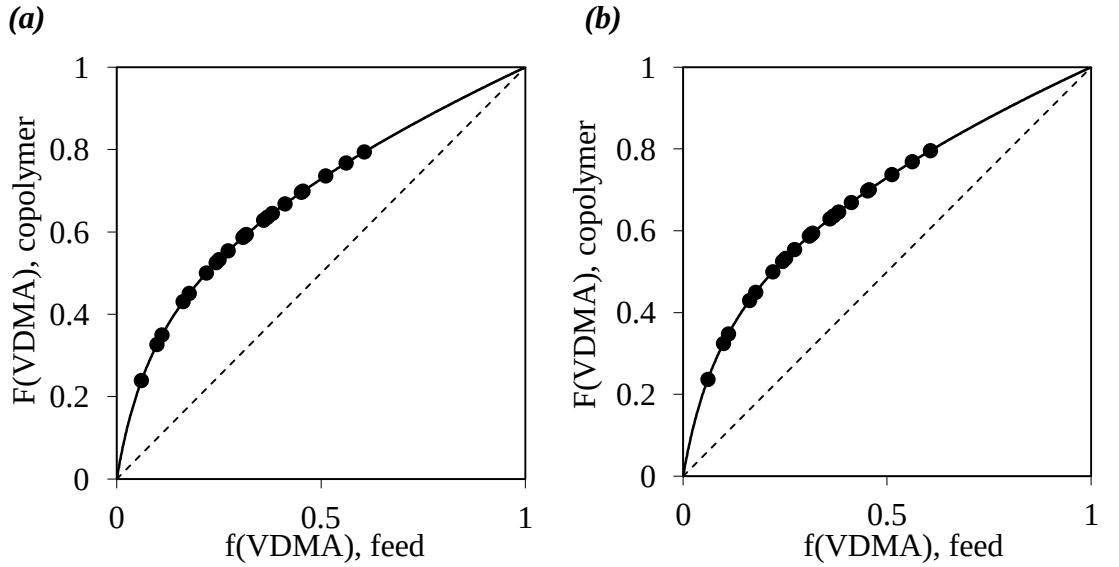

Figure 5A.23 *Composition diagrams obtained with the reactivity ratios determined using* ***(a)*** *equation [1],* ***(b)*** *equation [2] and the corrected global data using Aguliar's fraction method (Figure 5A.21). The black lines show a fit to the data, the full black circles show the individual experimental data points.*

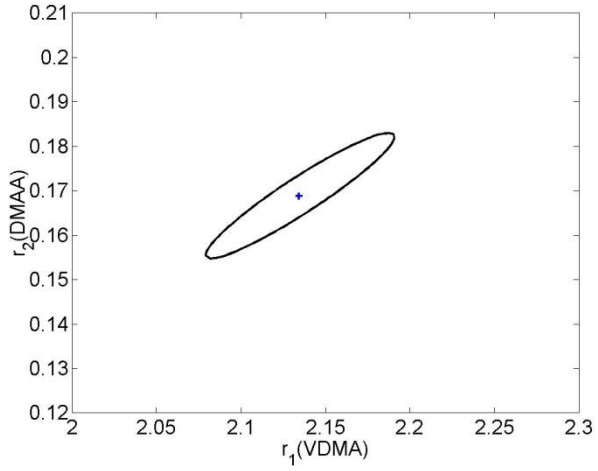

Figure 5A.24 *95% confidence contour for r_1(VDMA) and r_2(DMAA) using equation [1].*

5.8.5 VDMA:HEMA

For VDMA:HEMA copolymerization a 45:55, 69: 31 and 27:73 initial feed molar compositions were used. The reaction was stopped at 0, 1, 3, 5, 8, 13, 20, and 31 min and analyzed by 600 MHz ^{1}H NMR.

	Equation [1]		Equation [2]		
	r_1(VDMA)	**r_2(HEMA)**	**r_1(VDMA)**	**r_2(HEMA)**	**k**
45:55	1.285	0.571	1.145	0.516	58.40
69:31	1.199	0.520	1.054	0.340	55.83
27:73	1.710	0.623	1.246	0.549	56.70
Aguilar fraction	1.212	0.539	1.210	0.538	15.98
sliding fraction	1.214	0.542	1.210	0.538	15.99

Table 5A.5 *Calculated reactivity ratios using various methods*

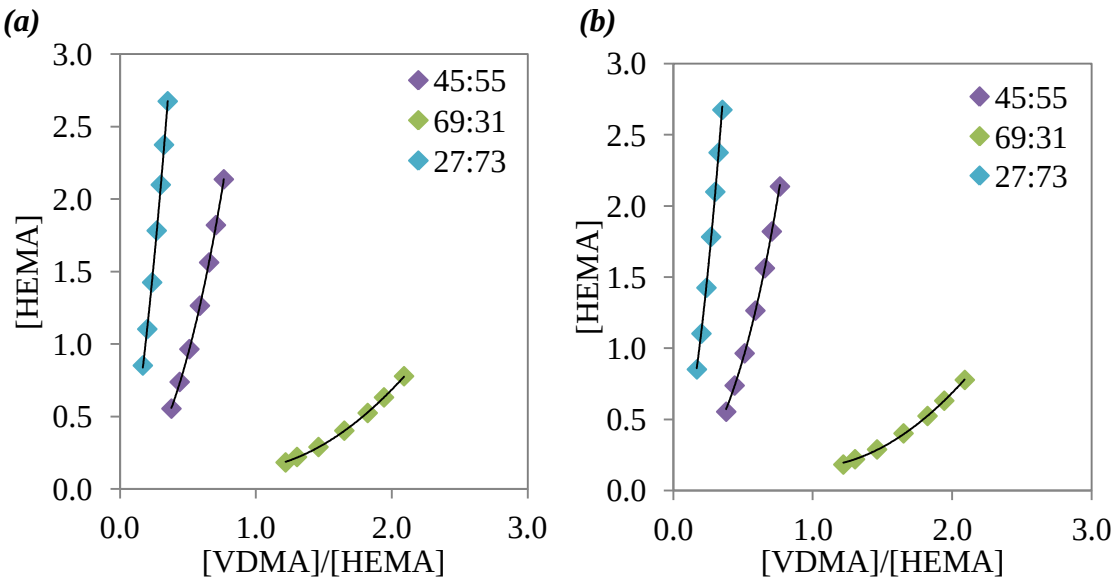

Figure 5A.25 *[HEMA] vs. [VDMA]/[HEMA] from ^{1}H NMR analysis of three copolymerizations with VDMA:HEMA initial feed ratios of 45:55, 69:31 and 27:73. The black lines show the fitted data of calculated [HEMA]'s using* ***(a)*** *equation [1] and* ***(b)*** *equation [2], and colored diamonds represent experimental data.*

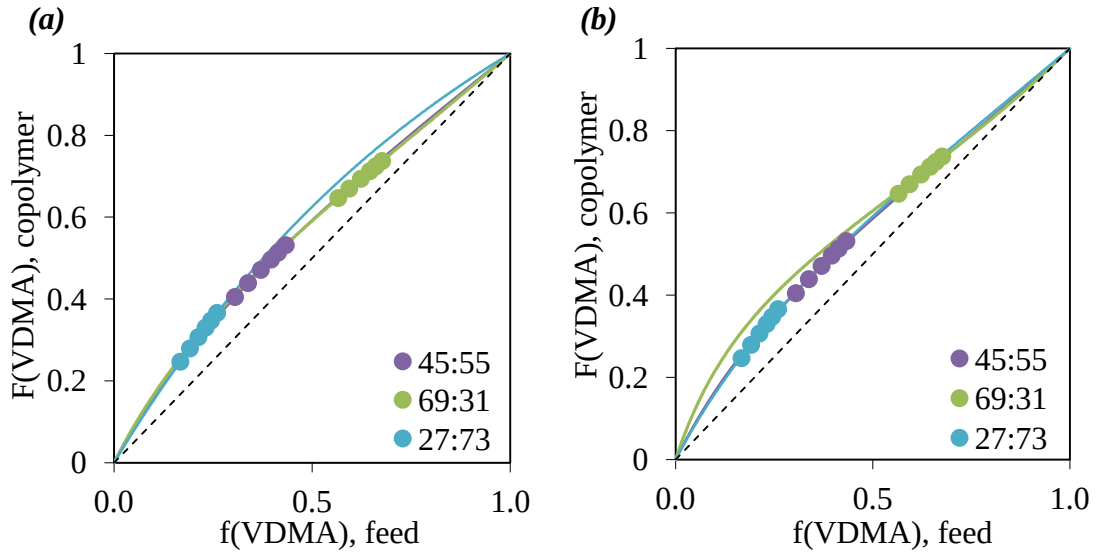

Figure 5A.26 *Copolymer composition diagrams showing (lines) separate fits to the data (circles) of three reactions with VDMA:MAA initial molar ratios of 45:55, 69:31 and 27:73, using* ***(a)*** *equation [1],* ***(b)*** *equation [2].*

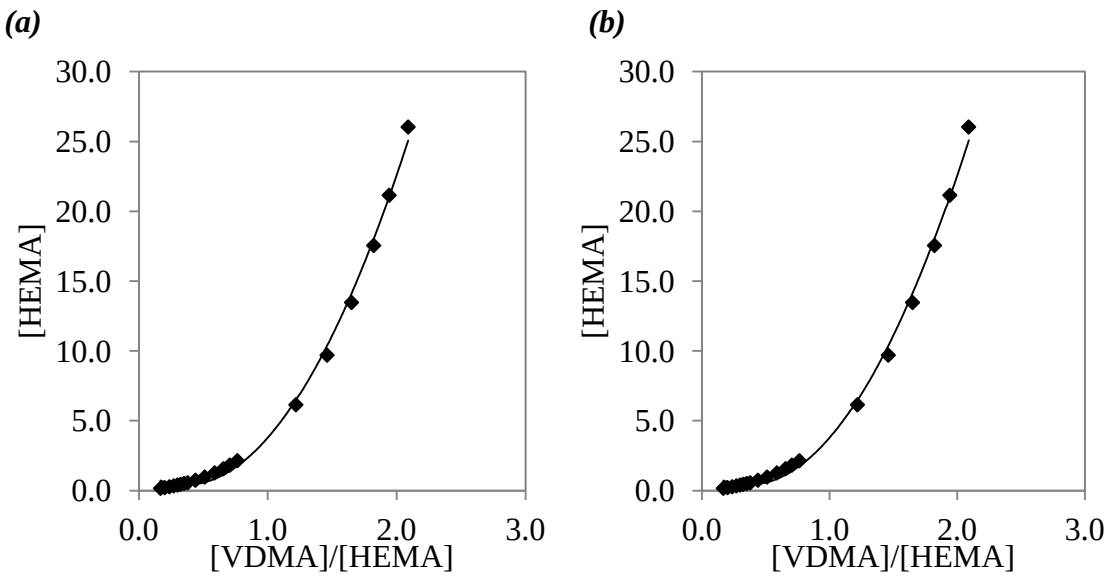

Figure 5A.27 *Corrected global [HEMA] vs. [VDMA]/[HEMA] as described by Aguilar. The black lines show the fitted data of calculated [HEMA]'s using* ***(a)*** *equation [1] and* ***(b)*** *equation [2]. Black diamonds represent experimental data.*

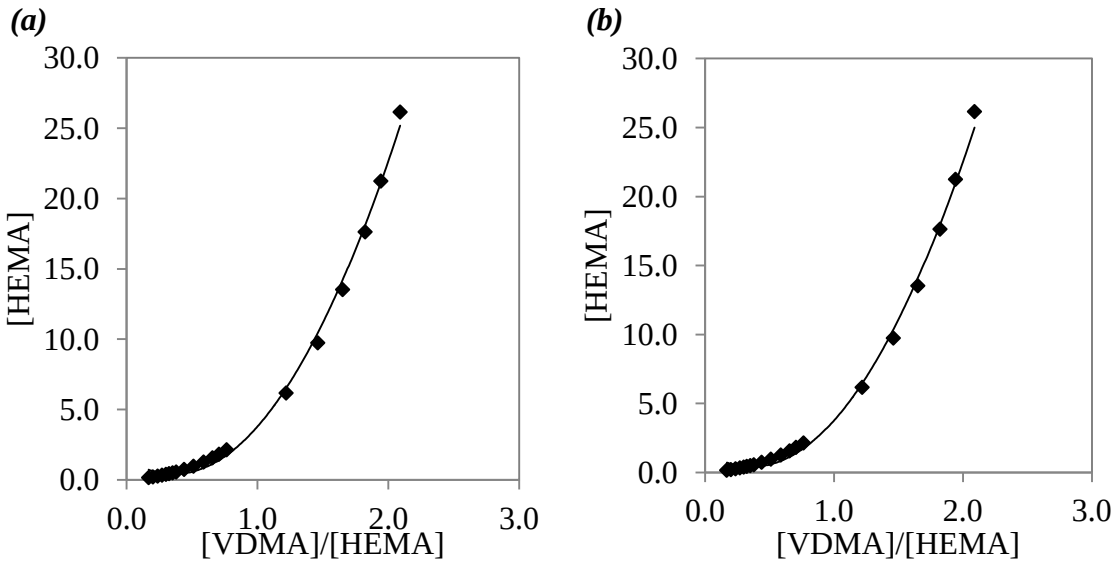

Figure 5A.28 *Corrected global [HEMA] vs. [VDMA]/[HEMA] calculated using a sliding fraction via EXCEL solver. The black lines show the fitted data of calculated [HEMA]'s using* ***(a)*** *equation [1] and* ***(b)*** *equation [2]. Black diamonds represent experimental data.*

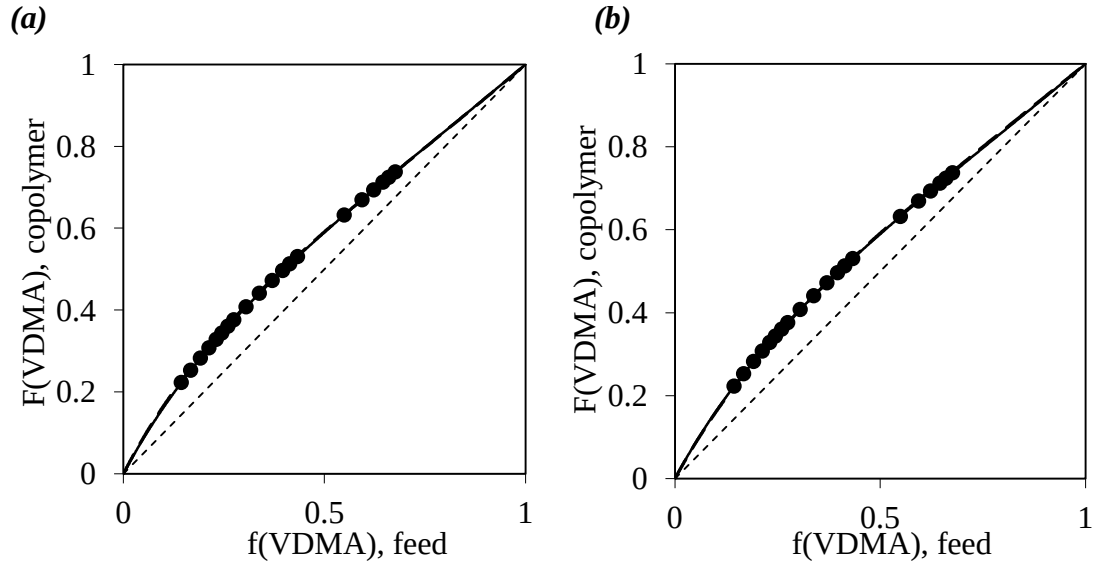

Figure 5A.29 *Composition diagrams obtained with the reactivity ratios determined using* ***(a)*** *equation [1],* ***(b)*** *equation [2] and the corrected global data using Aguliar's fraction method (Figure 5A.27). The black lines show a fit to the data, the full black circles show the individual experimental data points.*

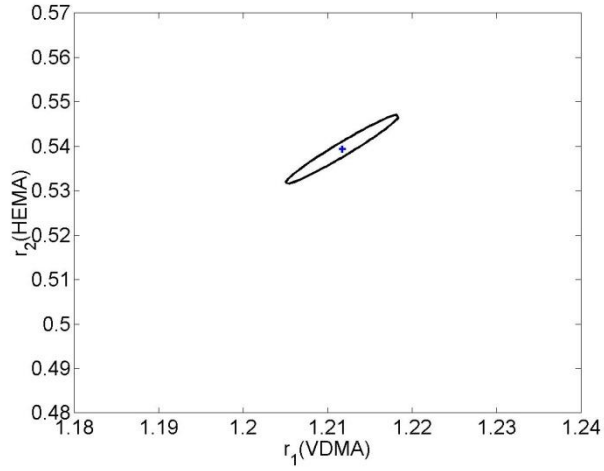

Figure 5A.30 *95% confidence contour for r_1(VDMA) and r_2(HEMA) using equation [1].*

5.8.6 VDMA:MPEG$_{300}$MA

For VDMA:MPEG$_{300}$MA copolymerization a 47: 53, 63:37 and 27:73 initial feed molar compositions were used. The reaction was stopped at 0, 2, 4, 6, 9, 14 and 24 min and analyzed by 600 MHz ^{1}H NMR.

	Equation [1]		Equation [2]		
	r_1(VDMA)	**r_2(MPEG$_{300}$MA)**	**r_1(VDMA)**	**r_1(MPEG$_{300}$MA)**	**k**
47:53	1.384	0.609	1.132	0.501	58.24
63:37	1.068	0.415	1.794	1.075	56.98
27:73	0.121	0.358	1.266	0.540	56.45
Aguilar fraction	1.124	0.454	1.124	0.451	43.27
sliding fraction	1.141	0.484	1.133	0.475	43.15

Table 5A.6 *Calculated reactivity ratios using various methods*

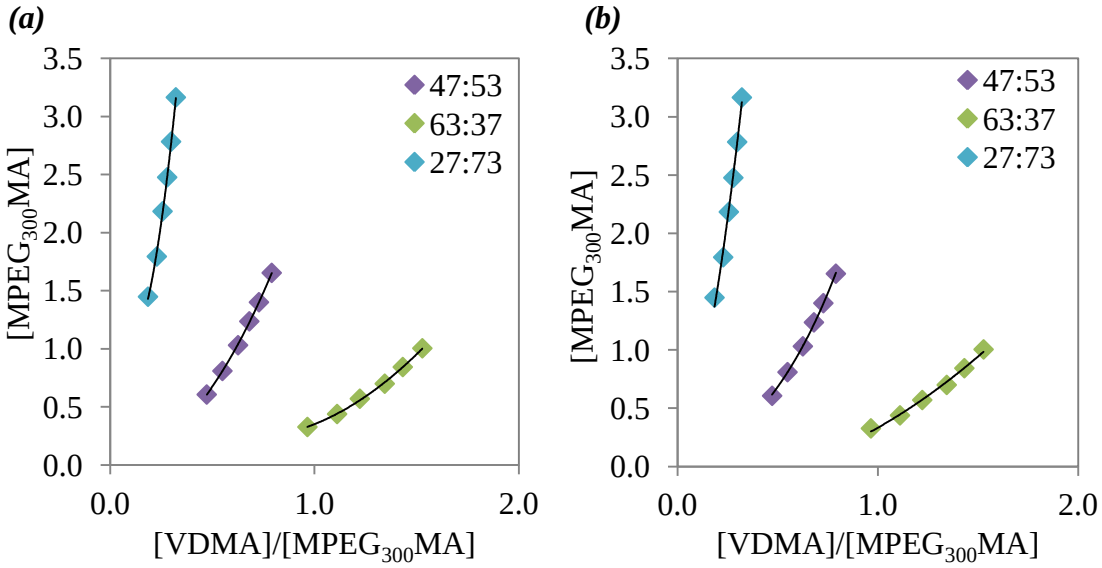

Figure 5A.31 *[MPEG$_{300}$MA] vs. [VDMA]/[MPEG$_{300}$MA] from ^{1}H NMR analysis of three copolymerizations with VDMA:MPEG$_{300}$MA initial feed ratios of 47:53, 63:37 and 27:73. The black lines show the fitted data of calculated [MPEG$_{300}$MA]'s using* ***(a)*** *equation [1] and* ***(b)*** *equation [2], and colored diamonds represent experimental data.*

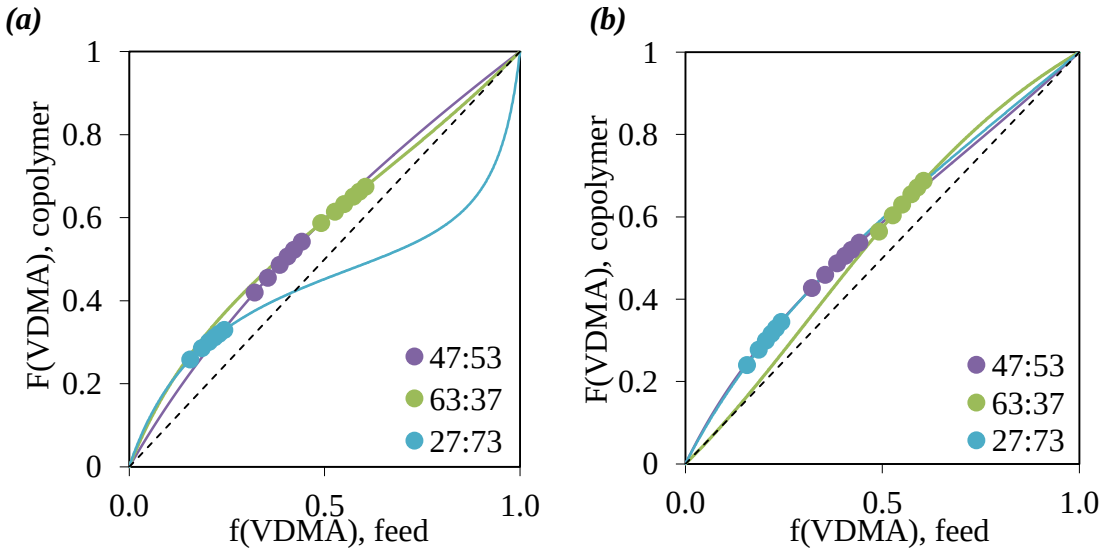

Figure 5A.32 *Copolymer composition diagrams showing (lines) separate fits to the data (circles) of three reactions with VDMA:MPEG$_{300}$MA initial molar ratios of 47:53, 63:37 and 27:73, using* ***(a)*** *equation [1],* ***(b)*** *equation [2].*

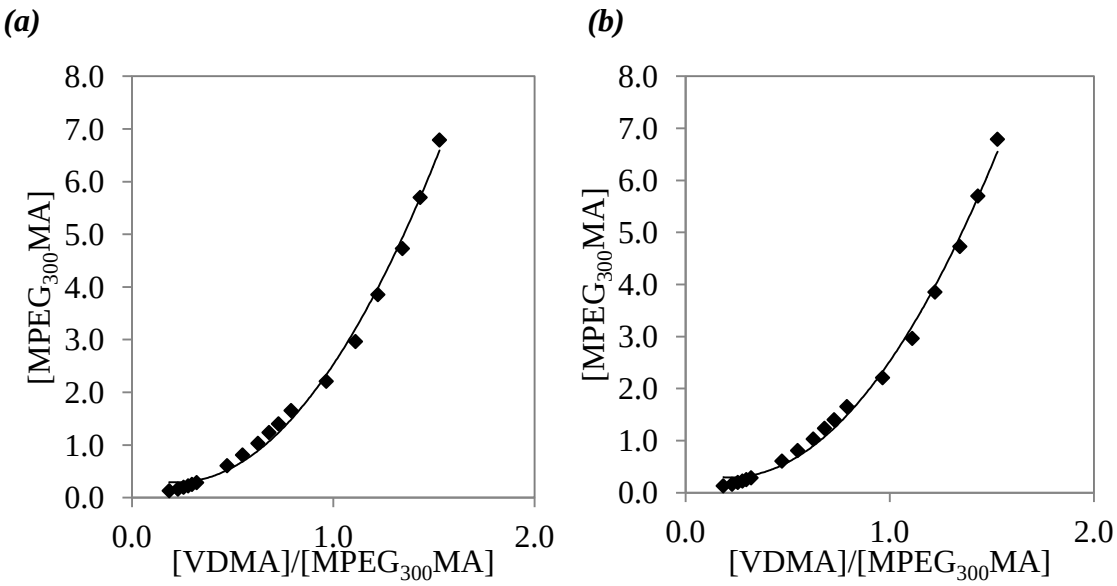

Figure 5A.33 *Corrected global [MPEG$_{300}$MA] vs. [VDMA]/[MPEG$_{300}$MA] as described by Aguilar. The black lines show the fitted data of calculated [MPEG$_{300}$MA]'s using* ***(a)*** *equation [1] and* ***(b)*** *equation [2]. Black diamonds represent experimental data.*

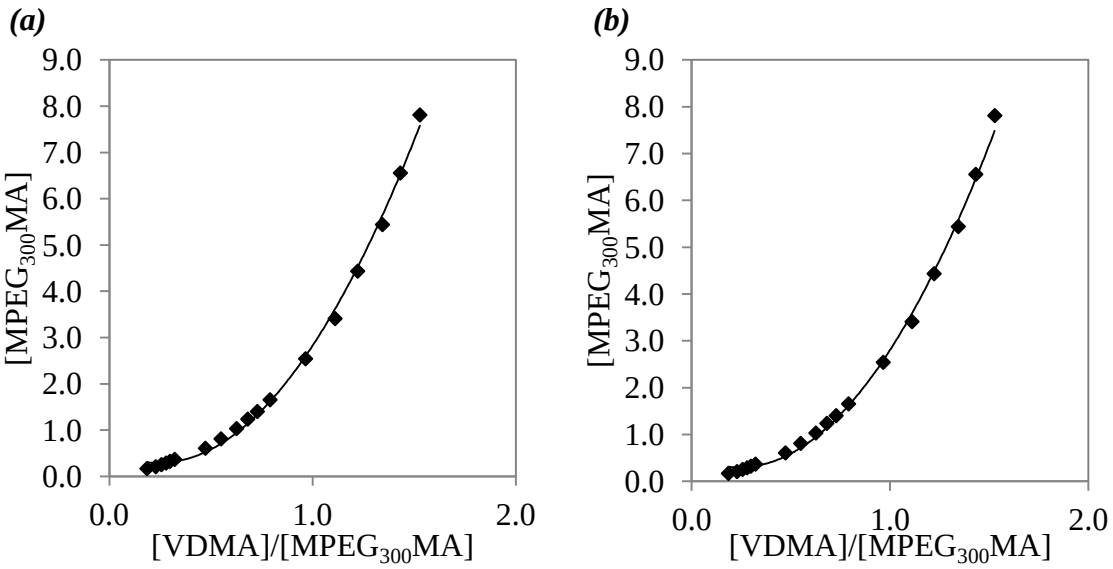

Figure 5A.34 *Corrected global [$MPEG_{300}MA$] vs. [VDMA]/[$MPEG_{300}MA$] calculated using a sliding fraction via EXCEL solver. The black lines show the fitted data of calculated [$MPEG_{300}MA$]'s using* ***(a)*** *equation [1] and* ***(b)*** *equation [2]. Black diamonds represent experimental data.*

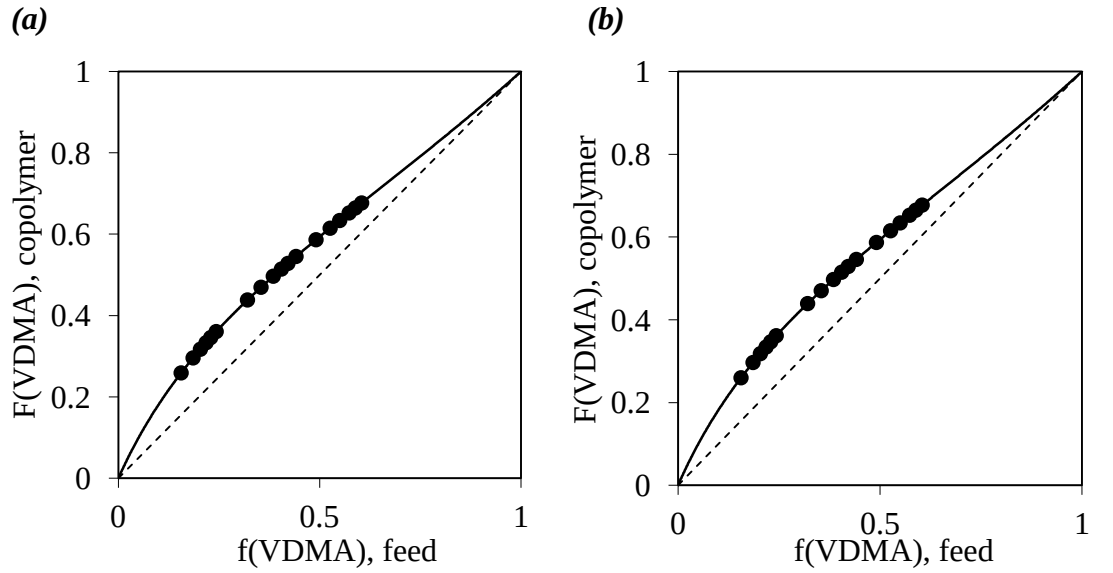

Figure 5A.35 *Composition diagrams obtained with the reactivity ratios determined using* ***(a)*** *equation [1],* ***(b)*** *equation [2] and the corrected global data using Aguliar's fraction method (Figure 5A.33). The black lines show a fit to the data, the full black circles show the individual experimental data points.*

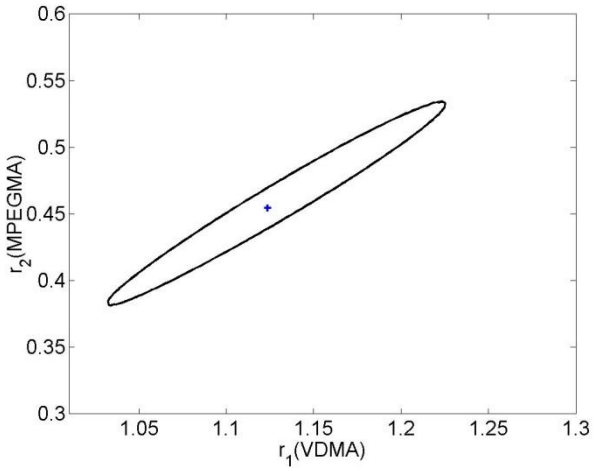

Figure 5A.36 *95% confidence contour for r_1(VDMA) and r_2(MPEG$_{300}$MA) using equation [1].*

5.8.7 VDMA:MPC

For VDMA: MPC copolymerization a 46: 54, 68: 32 and 27:73 initial feed molar compositions were used. The reaction was stopped at 0, 1, 3, 6, 11, 18 and 28 min and analyzed by 600 MHz ^{1}H NMR.

	Equation [1]		Equation [2]		
	r_1(VDMA)	**r_2(MPC)**	**r_1(VDMA)**	**r_2(MPC)**	**k**
46: 54	1.286	0.615	1.143	0.551	58.31
68: 32	1.689	0.895	1.833	1.048	56.93
27:73	2.726	0.852	1.271	0.592	56.90
Aguilar fraction	1.549	0.744	1.532	0.732	2.15
sliding fraction	1.556	0.751	1.533	0.733	2.14

Table 5A.7 *Calculated reactivity ratios using various methods*

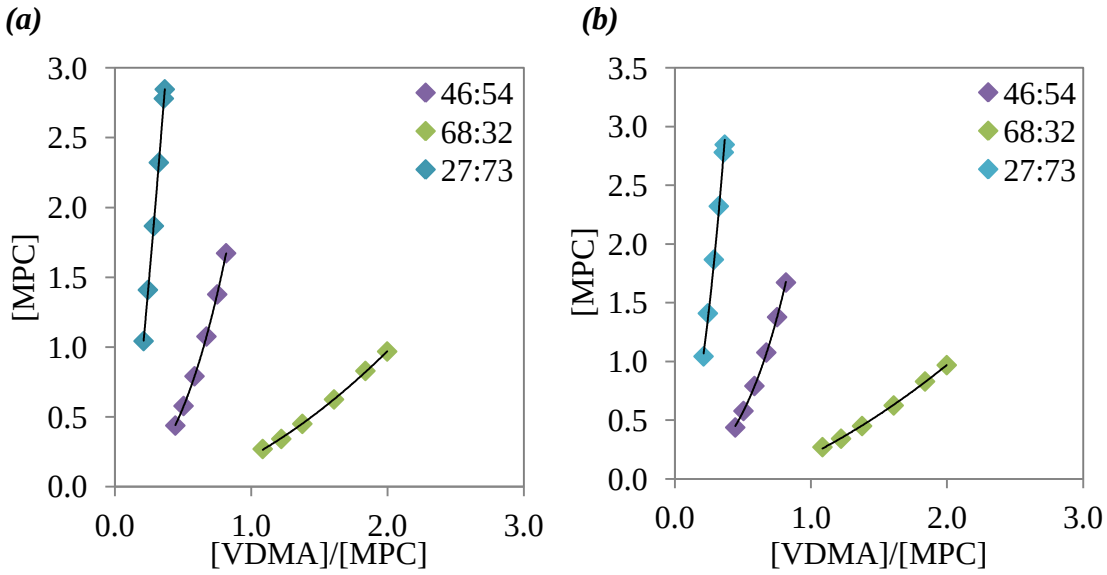

Figure 5A.37 *[MPC] vs. [VDMA]/[MPC] from ^{1}H NMR analysis of three copolymerizations with VDMA:MPC initial feed ratios of 46:54, 68:32 and 27:73. The black lines show the fitted data of calculated [MPC]'s using* ***(a)*** *equation [1] and* ***(b)*** *equation [2], and colored diamonds represent experimental data.*

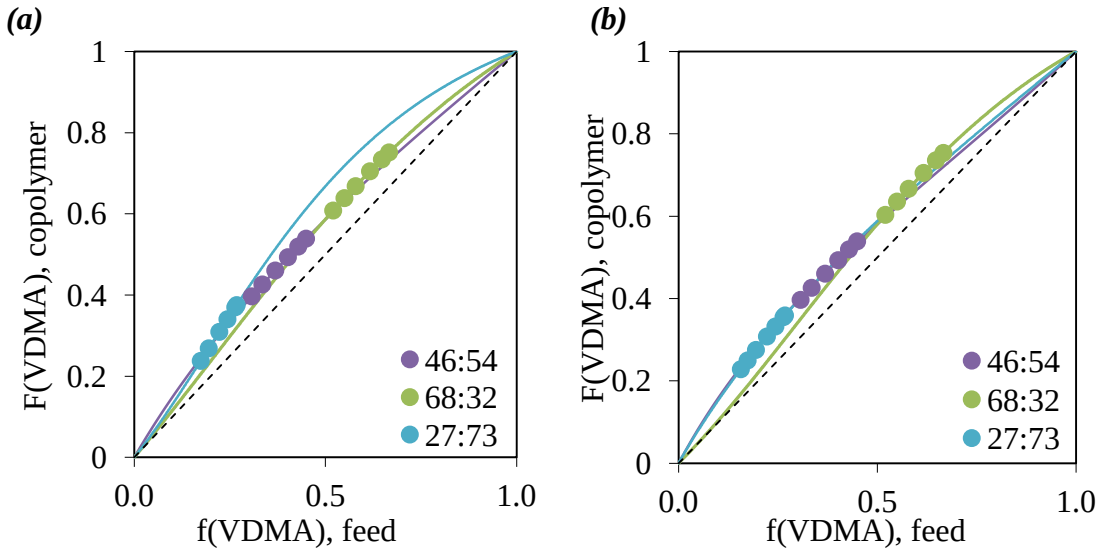

Figure 5A.38 *Copolymer composition diagrams showing (lines) separate fits to the data (circles) of three reactions with VDMA:MPC initial molar ratios of 46:54, 68:32 and 27:73, using* ***(a)*** *equation [1],* ***(b)*** *equation [2].*

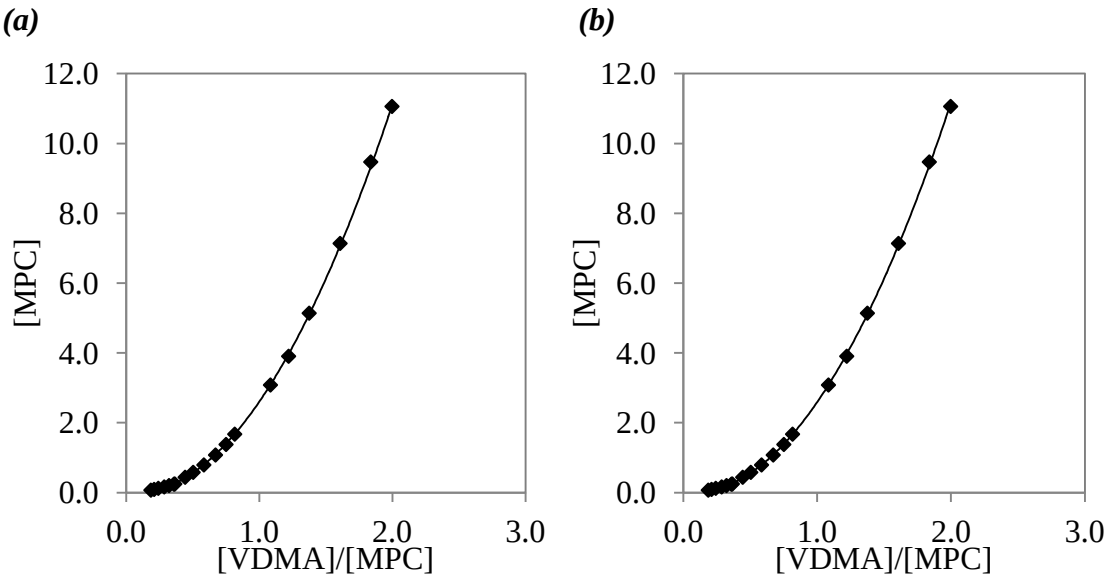

Figure 5A.39 *Corrected global [MPC] vs. [VDMA]/[MPC] as described by Aguilar. The black lines show the fitted data of calculated [MPC]'s using* ***(a)*** *equation [1] and* ***(b)*** *equation [2]. Black diamonds represent experimental data.*

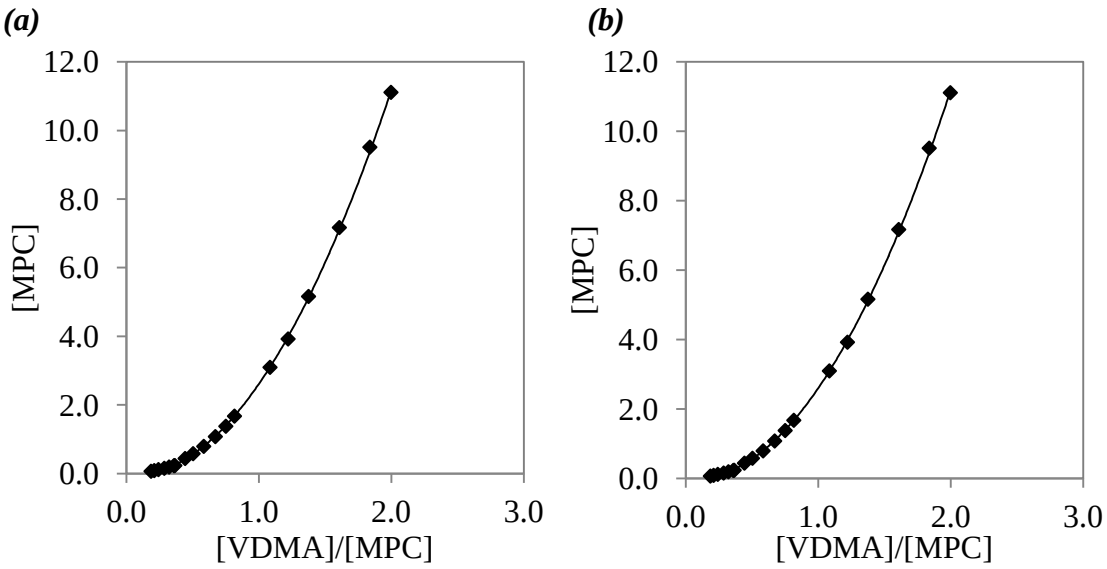

Figure 5A.40 *Corrected global [MPC] vs. [VDMA]/[MPC] calculated using a sliding fraction via EXCEL solver. The black lines show the fitted data of calculated [MPC]'s using* ***(a)*** *equation [1] and* ***(b)*** *equation [2]. Black diamonds represent experimental data.*

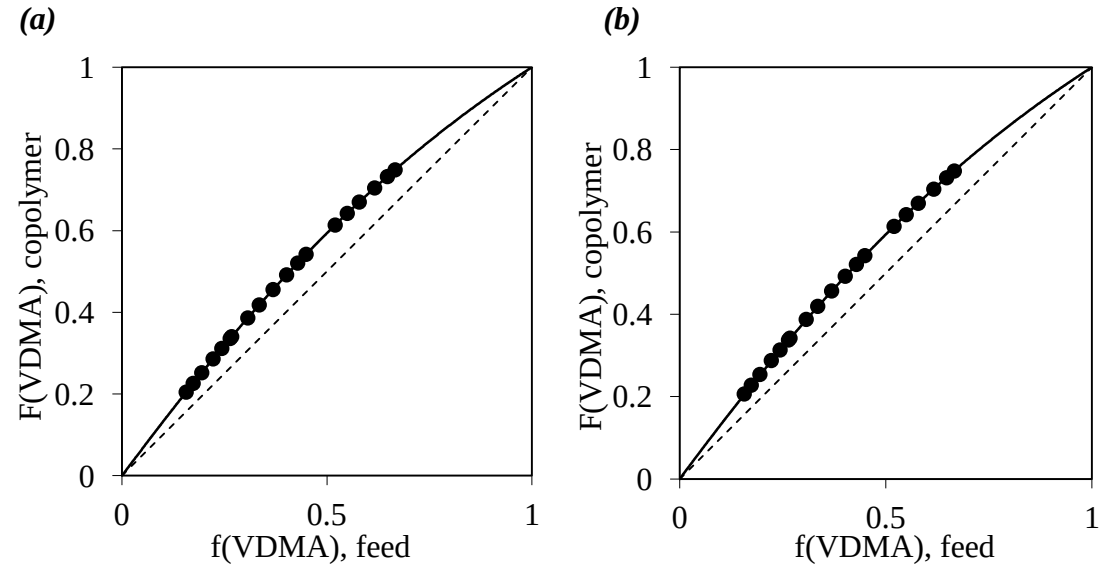

Figure 5A.41 *Composition diagrams obtained with the reactivity ratios determined using* ***(a)*** *equation [1],* ***(b)*** *equation [2] and the corrected global data using Aguliar's fraction method (Figure 5A.39). The black lines show a fit to the data, the full black circles show the individual experimental data points.*

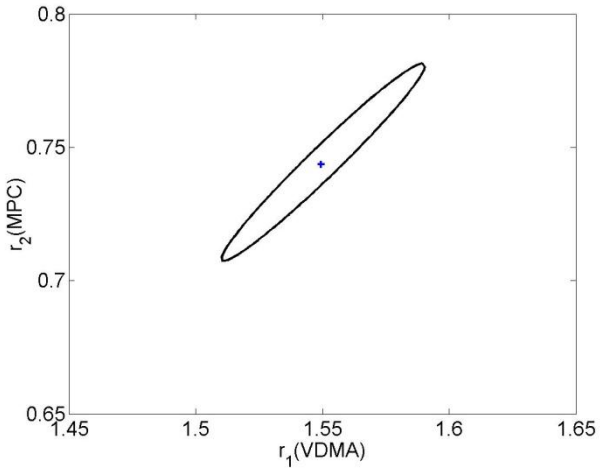

Figure 5A.42 *95% confidence contour for r_1(VDMA) and r_2(MPC) using equation [1].*

Chapter 6: Summary and Future Work

6.1 Summary

APA capsules are the basis of many encapsulation methods used in pursuit of cell-based enzyme and hormone replacement therapies. APA capsules consist of a calcium-alginate hydrogel core containing cells designed to express the therapeutic product, coated with permeability controlling PLL (a polycation), followed by an exterior layer of polyanionic alginate. Such capsules may be implanted into the body (e.g., peritoneal cavity or portal vein) where they should remain undetected by the immune system for about a year. Therapeutic cell capsules should work in a symbiotic relationship with the host, where the encapsulated cells secrete the enzyme or hormone that the host is lacking, and receive nutrients and oxygen from the host to maintain the encapsulated cells viability.

While the alginate capsule system has shown enough potential to warrant a few clinical trials, it has serious inherent limitations. For example, calcium and barium alginate capsules without polycation coating tend to be host compatible but weak, while capsules coated with e.g., poly-L-lysine are physically stronger but also attract a stronger immune response, attributable to both the hydrophobic nature of the polyelectrolyte complex, and to the presence of cationic charges near the surface. It has been pointed out that "there is no reason why alginate should be irreplaceable as the polymer that is used for the outer coating of the microcapsules[1]."

This thesis explored replacing the outer alginate layer of APA capsules with Temporarily Reactive Polyelectrolytes (TRPs). This approach leads to a covalently crosslinked outer shell with improved chemo-mechanical properties for long term encapsulation. It also improves the host compatibility of the capsules by converting positively charged amines to amide crosslinks, by the absence of biocontaminates, and by the liberation of carboxylates at the capsule surface through hydrolysis of residual electrophiles. In principle, the use of defined synthetic polymers permits tuning of hydrogel properties such as strength, permeability, and chemical stability. The reactive nature of the TRPs also allows for functionalization with bioactive molecules to further improve the capsules biocompatibility.

The following summarizes the results presented in this thesis:

6.1.1 CHAPTER 2

The first TRP (PMM_{50}) was synthesized by partially hydrolyzing poly(methyl vinyl ether-*alt*-maleic anhydride) (PMM_0). The partial hydrolysis of PMM_0 was carried out in organic medium (ACN-d_3/D_2O) and monitored by ^1H NMR. At 50% hydrolysis, PMM_{50} was diluted in a buffered saline solution to 0.2 wt% and immediately used to coat AP capsules. Monitoring the pH of the 0.2 wt% PMM_{50} solution over time, showed that

PMM_{50} has a half-life of roughly 2.5 min under these conditions, and that hydrolysis was complete in less than 30 min.

AP-PMM_{50} capsules proved to be covalently crosslinked as determined by resistance to sodium citrate/sodium hydroxide exposure, in contrast to their non-crosslinked analogs AP-PMM_{100} and APA capsules. The chemical resistance and physical integrity of these shells could be improved by varying the MW and coating concentrations of PLL and PMM_{50}. Confocal fluorescent microscopy of AP-PMM_{50} capsules, using either fluorescently labeled PLL or PMM_{50}, showed correlation between the amount of PMM_{50} bound to the capsules and their chemical resistance as determined from the sodium citrate/sodium hydroxide test. The amount of PMM_{50} bound was found to increase using multiple PLL-PMM_{50} coatings, higher PLL coating concentrations, higher PLL molecular weights, and lower PMM_{50} molecular weights.

Permeability studies on AP-PMM_{50} capsules revealed that the covalently crosslinked shell still allowed for rapid in-diffusion of 10 - 70 kDa dextrans, while excluding larger dextrans. Initial protein binding tests involving incubation of the capsules in fluorescently labeled bovine serum albumin (BSA) solutions showed no detectable amounts of protein binding, indicating absence of residual anhydride groups following coating.

6.1.2 CHAPTER 3

Development of the second TRP (PMV_{50}) started with determining the reactivity ratios for VDMA and MAA using in-*situ* ^{1}H NMR technique. The results showed preferred incorporation of VDMA, with $r_{VDMA} = 1.36$ and $r_{MAA} = 0.41$. A semi-batch copolymerization process was thus developed to prepare no-drift PMV_{50} at 60°C in DMSO under anhydrous conditions while maintaining a constant VDMA: MAA feed ratio of 35: 65 mol%, aiming for a 50: 50 VDMA:MAA mol% copolymer. However, quantitative ^{13}C NMR of this isolated copolymer showed that about 40% of the azlactone groups were hydrolyzed, with concomitant formation of cyclic anhydride from adjacent MAA units. This trans-hydration side-reaction could be suppressed to 7% by using photo-polymerization at 20^{o}C, or alternatively by using higher VDMA:MAA mol ratios.

Monitoring the pH of a 0.2 wt% PMV_{50} solution in buffered saline showed that the half-life of the azlactone groups was about 30 min. This was substantially less than the homopolymer of VDMA which is hydrolytically stable in water for up to a year, largely reflecting their differences in hydrophilicity. Capsules were made by coating a 0.2 wt% solution of PMV_{50} onto AP capsules, and covalent crosslinks were confirmed through the sodium citrate/sodium hydroxide test.

6.1.3 CHAPTER 4

This chapter presents the results from a 6 week *in-vivo* study comparing APA to AP-PMM_{50} and AP-PMV_{50}, both with and without encapsulated C2C12 cells. The capsules were compared in terms of their fibrotic overgrowth, mechanical strength, and effects on mouse tail vein serum cytokine levels. AP-PMM_{50} capsules, with and without encapsulated cells, showed the least amount of overgrowth at 2.5% or less of total capsule area. APA and AP-PMV_{50} capsules showed variable overgrowth, depending on presence and absence of encapsulated cells.

AP-PMV_{50} capsules without cells had very little surface overgrowth (8 ± 3%), however suspected contamination resulted in substantial overgrowth for capsules containing cells (70 ± 30%). Contamination is supported by the fact that the *in-vitro* AP-PMV_{50} capsules were found to be terminally contaminated after 1 week. As well, preliminary studies involving implanting AP-PMV_{50} capsules with cells into mice for 1 week showed very little surface overgrowth (6 ± 2%), comparable to AP-PMM_{50} capsules also studied here.

APA capsules without cells showed substantial surface overgrowth (40 ± 40%), whereas much less was observed for APA capsules containing cells (9 ± 3%). Although APA capsules containing cells showed little surface overgrowth when viewed under the optical microscope, scanning electron microscopy (SEM) revealed a denser cell coating than AP-PMM_{50} and AP-PMV_{50} (without cells). The presence of this cellular and perhaps protein coating was highlighted when performing the test for covalent crosslinking (sodium citrate/sodium hydroxide test). Six week *in-vitro* and 1 week *in-vivo* APA capsules dissolved, however after 6 weeks *in-vivo* this protein/cellular coating prevented these ionically crosslinked capsules from dissolving. Additionally, high and persistent TNF-α and MCP-1 levels in serum samples at 1 and 6 weeks of APA capsules, suggests a heightened immune response. AP-PMM_{50} capsules showed the lowest cytokine levels.

In-vitro viability measurements of AP-PMM_{50} and AP-PMV_{50} capsules containing encapsulated cells showed that the cells were not affected by the TRP coating process and remained viable for 1 week *in-vitro*. As well, the chemical resilience of these covalently crosslinked capsules was observed to be unaffected after 6 weeks in a mouse's peritoneal cavity (seen by sodium citrate/sodium hydroxide test).

6.1.4 CHAPTER 5

In Chapter 3, it was discovered that PMV_{50} had a shorter half-life in water of 30 min compared to the VDMA homopolymer, which is hydrolytically stable in water for up to 1 year. This led to the investigation of how the comonomer identity affects the rate of hydrolysis of reactive azlactone groups under physiological conditions, in hopes of finding alternative temporarily reactive polymers.

Several ionic, non-ionic and zwitterionic comonomers were selected, their reactivity ratios with VDMA determined, and no-drift copolymers prepared by semi-batch photo-initiated copolymerizations.

First, the large difference between the half-life of PMV_{50} and p(VDMA) was analyzed by studying a series of PMV copolymers with VDMA content ranging from 52 to 100%. Analysis of these PMV copolymers under physiological conditions showed that as the percentage of VDMA in the copolymer increased the solubility and rate of hydrolysis decreased. However, a very large difference between PMV_{93} (93% VDMA) and p(VDMA) was still observed, indicating that even small amounts of MAA can help hydrate the copolymer.

HEMA and $MPEG_{300}MA$ comonomers showed intermolecular crosslinking during preparation and workup and were hence not studied further. DMAA and AAm displayed lower rates of hydrolysis compared to PMV, but required higher comonomer contents to maintain solubility in water. This might place an upper limit on the crosslink density attainable with these copolymers.

The most interesting copolymer identified was the zwitterionic p(VDMA-*co*-MPC). This copolymer was instantly water soluble up to 82 mol% VDMA content. At the same time, this p(VDMA-*co*-MPC) with 82% VDMA had a much slower rate of hydrolysis in water than comparable p(VDMA-*co*-MAA)'s. Even more interestingly, the opposite trend was observed for p(VDMA-*co*-MPC) with 92% VDMA. It displayed much higher rates of hydrolysis than p(VDMA-*co*-MAA) with comparable composition, and p(VDMA-*co*-MPC) with less VDMA (82%). This suggests that interactions between VDMA and MPC may be responsible for the slower hydrolysis of the lower VDMA content p(VDMA-*co*-MPC) copolymer compared to the higher one. Along with its high reactive group content, superior solubility and longer half-life, MPCs' reported biomimetic and anti-fouling properties makes this zwitterionic copolymer very appealing for use in cell-encapsulation systems, and a key candidate for future studies.

6.2 Future work

6.2.1 Large animal *in-vivo* studies with AP-PMM_{50} and AP-PMV_{50}

As AP-TRP and APA capsules showed similar mechanical properties in the 6 week mouse study (Chapter 4), future work will look at performing longer term *in-vivo* studies on AP-PMM_{50} and AP-PMV_{50} capsules, in larger animal models. The hope here is to confirm the host compatibility of these capsules in larger animal models, as well to differentiate between APA capsules and AP-TRP capsules in terms of mechanical strength. The poor mechanical strength of the APA capsules should become more apparent in larger, more active animals.

6.2.2 Functionalization of PMM_{50} and PMV_{50} with anti-inflammatory cytokines

It is now becoming more apparent that immunoisolation of cells requires more than just a physical barrier between encapsulated cells and host tissue. Although semi-permeable hydrogels used for encapsulation are able to protect encapsulated cells from large immunoglobulins and antibodies (> 75 kDa), the permeability required for rapid influx of oxygen and metabolites to the encapsulated cells also allows low molecular pro-inflammatory cytokines to diffuse into and out of the microcapsule. This can elicit an immune response and decrease the encapsulated cells' viability. Amoli (2006)[2] proposed that blocking cytokines would improve the outcome of pancreatic islet transplantation. Anseth (2009),[3] went on to incorporate a peptide binding sequence into the hydrogel that was capable of sequestering the pro-inflammatory cytokine, TNFα. Later, Messersmith (2010)[4] grafted an inhibitory peptide sequence for islet cell surface IL-1 receptor, which improved the viability and productivity of the encapsulated islet cells.

The idea to utilize key cytokines in biomaterials was explored by Reichert (2009),[5] in a paper that looked at developing immune evasive biomaterials based on biomimetic strategies employed by viruses and bacteria. The anti-inflammatory cytokines IL-10 and pro-inflammatory receptor antagonist IL-1ra are both used by bacteria and viruses to help them hide from the immune system, and are new and promising candidates to be incorporated into AP-TRP capsules for future cell encapsulation studies.

Both IL-10 and IL-1a are currently being used for treatment of a number of inflammatory diseases such as colitis and rheumatoid arthritis.[6,7,8] IL-10 is suggested because of its enormous potential to modulate the immune response, by inhibiting the synthesis of pro-inflammatory cytokines IL-1, IL-2, IL-6, IL-12, IFN-γ, TNF-α and immunoglobulins, deactivating macrophages and down-regulating cellular immunity and the presentation of class II major histocompatibility complex antigens.[9] To the best of my knowledge, to date, IL-10 has not been immobilized on a biomaterial surface. IL-1ra has been explored in great detail in the biomaterial literature.[10] IL-1ra binding to IL-1 receptor type I, prevents IL-1α and IL-1β from binding to it, which in turn blocks the cascade of events leading to transcription of inflammatory and immunogenic genes.

TRPs provide the perfect platform to incorporate such bioactive molecules onto the surface of AP-TRP capsules. Bioactive molecules could be incorporated by pre-functionalization (covalent immobilization of bioactive molecules onto TRP prior to coating AP capsules), concurrent-functionalization (adding both bioactive molecule and TRP to an aqueous solution containing AP capsules), or post-functionalization (covalently immobilizing bioactive molecules onto AP-TRP surfaces). Pre-functionalization is probably the most cost effect method; however some bioactive molecules may not be soluble, or lose bioactivity, in organic solvents used for pre-functionalization. As well, covalently immobilizing bioactive groups onto the TRP prior to coating may interfere with the polyelectrolyte complexation and subsequent covalent crosslinking of the functionalized TRP around AP capsules. This has been observed when high MW PEG was covalently immobilized onto PMM_{100} prior to coating.[11]

Preliminary experiments were performed on pre-, concurrent- and post-functionalization [6.4 Appendix] for the two TRP's investigated in this thesis. These results showed that after pre-functionalizing PMM_{50} and PMV_{50} with a fluorescently labeled amino-PEG (3.5 kDa), the resulting functionalized TRPs could then be coated onto AP capsules and still form covalent crosslinks. When amino-PEG was coated concurrently with the PMM_{50} around AP capsules, again the fluorescently labeled amino-PEG was successfully immobilized onto the surface of the capsules, as seen by confocal microscopy. However, when amino-PEG was concurrently coated with PMV_{50} around AP capsules no detectable amount of PEG is found on the surface of the resulting capsules. Finally, when AP-PMV_{50} capsules were exposed to amino-PEG*f* during attempted post-functionalization, no fluorescently labeled PEG is observed on the surface. It is suspected that azlactone reaction with amines is slower compared to that of anhydride, and hence does not form covalent bonds with PMV_{50} during the 6-10 min coating time. Post-functionalization of AP-PMM_{50} capsules showed no immobilized PEG on the surface, although here, it is thought that PMM_{50}'s quick hydrolysis is responsible [6.4 Appendix].

Future work will explore pre-functionalizing the TRPs with anti-inflammatory cytokines IL-10 and/or IL-1ra and/or the peptide binding sequence capable of sequestering TNFα as described by Anseth (2009).[3] The most cost-effective technique for immobilizing anti-inflammatory cytokines is to synthesize their active peptide sequence. This method provides the additional advantage in that each end of the peptide can be tailored to facilitate covalent immobilization to the capsule. For PMM_{50} and PMV_{50} the reactive anhydride and azlactone functionality respectively, is most suitable for reactions with thiol and/or amine terminated peptide sequences.

Analysis of these functionalized TRPs will focus on *in-vitro* and *in-vivo* responses when coated onto AP capsules. The affect of sequestering anti-inflammatory cytokines onto the surface of the capsules will be examined for the encapsulated cell viability and function, as well as the host's innate inflammatory response to the material, through measurements of serum cytokine levels and fibrotic overgrowth around capsules. The cytokine analysis of AP-PMM_{50} and AP-PMV_{50} capsules performed in Chapter 4 will provide a good comparison for anti-inflammatory cytokine functionalized AP-TRP capsules.

6.2.3 P(VDMA-*co*-MPC) Copolymer

In Chapter 5, the unique properties of p(VDMA-*co*-MPC) (82% VDMA) were highlighted. Features such as high VDMA content, excellent initial water solubility, lower rates of hydrolysis under physiological conditions, and reported anti-fouling properties of MPC make this VDMA copolymer an appealing biomaterial for cell encapsulation.

Some preliminary experiments (data not shown) show that p(VDMA-*co*-MPC) (82% VDMA) is able to coat onto AP capsules composed of high MW PLL (40-60 kDa), but not when lower MW PLL is used (15-30 kDa). Additionally, when PLL is added over

time to a hydrolyzing p(VDMA-*co*-MPC) solution, it was found that the polyelectrolyte complexation with PLL gets weaker and weaker throughout the course of the hydrolysis until eventually at the end no complexation between PLL and p(VDMA-*co*-MPC) is observed. This is the opposite trend for what is observed for other TRPs such as PMV_{50}, and needs to be explored further.

Due to the slightly hydrophobic nature of p(VDMA-*co*-MPC), a fluorescently labeled p(VDMA-*co*-MPC) was also shown to coat onto calcium-alginate capsules (without PLL present). These p(VDMA-*co*-MPC)-coated alginate capsules could then be covalently crosslinked with an external layer of PLL. These A-p(VDMA-*co*-MPC)-PLL capsules would not be ideal for cell encapsulation due to the external PLL layer. However, variations to this, such as forming A-p(VDMA-*co*-MPC) capsules and then crosslinking them with a diamino-PEG, may be more suitable, and will be explored in future work. Also of interest are A-p(VDMA-*co*-MPC)-polyamine-p(VDMA-*co*-MPC) capsules, as they may show less opportunity for undesirable polyamine-cell interactions. Future work will also study the driving force for the A-p(VDMA-*co*-MPC) complexation.

Preliminary experiments showed that composite capsules composed of a 1:1 weight ratio of alginate: p(VDMA-*co*-MPC) could be made and coated with PLL to get a covalently crosslinked core (using low MW PLL that can diffuse into the capsules) or a covalently crosslinked shell (using high MW PLL that is restricted to the surface of the capsules). A close examination under the optical microscope of the alginate-p(VMDA-MPC)*f* solution used to make these capsules showed that tiny coacervates of p(VDMA-MPC)*f* are formed in the alginate. Again future work will explore this complexation in more detail, and see if it can be harvested for use in cell encapsulation.

6.3 References

[1]G. Langlois; J. Dusseault; S. Bilodeau; S.K. Tam; D. Magassouba; J.P. Hallé JP. *Acta Biomater.* **2009**, *5*, 3433-3440.
[2] M.M. Amoli; B. Larijani. *Med. Hypotheses* **2006**, 66, 816-819.
[3] C. Lin; A.T. Metters; K.S. Anseth. *Biomaterials* **2009**, *30*, 4907-4914.
[4] J. Su; B.H. Hu; W.L. Lowe Jr; D.B. Kaufman; P.B. Messersmith. *Biomaterials* **2010**, *31*, 308-314.
[5] M.T. Novak; J.D. Bryers; W.M. Reichert. *Biomaterials* **2009**, *30*, 1989-2005.
[6] L. Steidler; W. Hans; L Schotte; S. Neirynck; F. Obermeier; W. Falk; W. Fiers; E. Remaut. *Science* **2000**, *289*, 1352-1355.
[7] K. Asadullah; W. Sterry; H.D. Volk. *Pharmacol. Rev.* **2003**, *55*, 241-269.
[8] B. Brenihan. *Ann. Rheum. Dis.* **1999**, 58, 196-198.
[9] S. Pestka; C.D. Krause; D. Sarkar; M.R. Walter; Y. Shi; P.B. Fisher. *Annu. Rev. Immunol.* **2004**, *22*, 929–979.
[10] D.H. Kim; J.T. Smith; A. Chilkoti; W.M. Reichert. *Biomaterials* **2007**, *28*, 33-69-3377.
[11] C.M. Gardner; N.A.D. Burke; T. Chu; F. Shen; M.A. Potter; H.D.H. Stover. *J. Biomater. Sci.* **2011**, *22*, 2127-2145.

6.4 APPENDIX

Preliminary work has been done to test if AP-PMM$_{50}$ and AP-PMV$_{50}$ capsules can be pre-, post- or concurrently functionalized with amine based molecules or small polymers (used as model compounds for future work). To date aminofluoresceine (AF) and fluorescently labeled amino-PEG*f* (3.5 kDa) have been explored.

Pre-functionalization with amino-PEG*f* and separately AF has been successfully completed for PMM$_{50}$ and PMV$_{50}$. For PMM$_{50}$ both reactions were performed in acetonitrile during the initial 50% hydrolysis in organic medium. The PMM-PEG*f* or PMM*f* organic solution was then diluted with 35 mM pH 7.8 HEPES buffered saline and successfully coated onto and crosslinked around AP capsules (Figure 6A.1a shows a confocal profile of an AP capsule that has been pre-grafted with amino-PEG*f*, and Figure 6A.2a shows the sodium citrate sodium hydroxide test confirming covalent crosslinking). For PMV$_{50,}$ these reactions were performed after PMV$_{50}$ synthesis in DMSO, where the organic solution is diluted with buffer and coated onto AP capsules (Figure 6A.1b). Figure 6A.2b confirms that these capsules are also crosslinked. Note that any unreacted amino-PEG*f* or AF is still in the coating solution while coating AP capsules. This may or may not be required to be removed prior to coating.

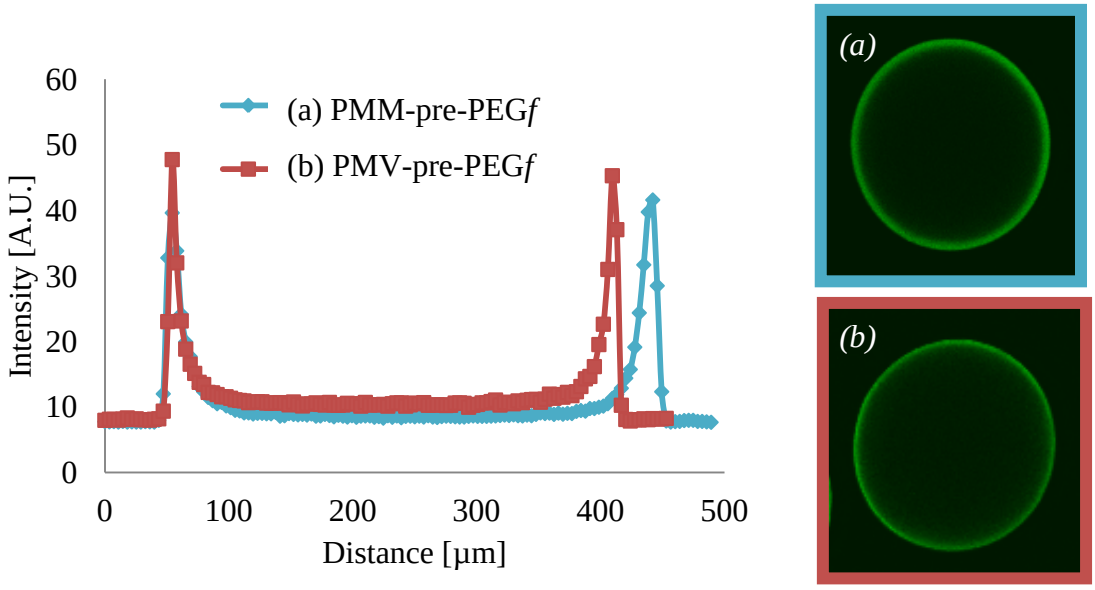

Figure 6A.1 *Graph shows a confocal profile of* ***(a)*** *AP-PMM- and* ***(b)*** *AP-PMV- pre-functionalized with amino-PEGf. Images show the confocal microscopy images of corresponding TRP.*

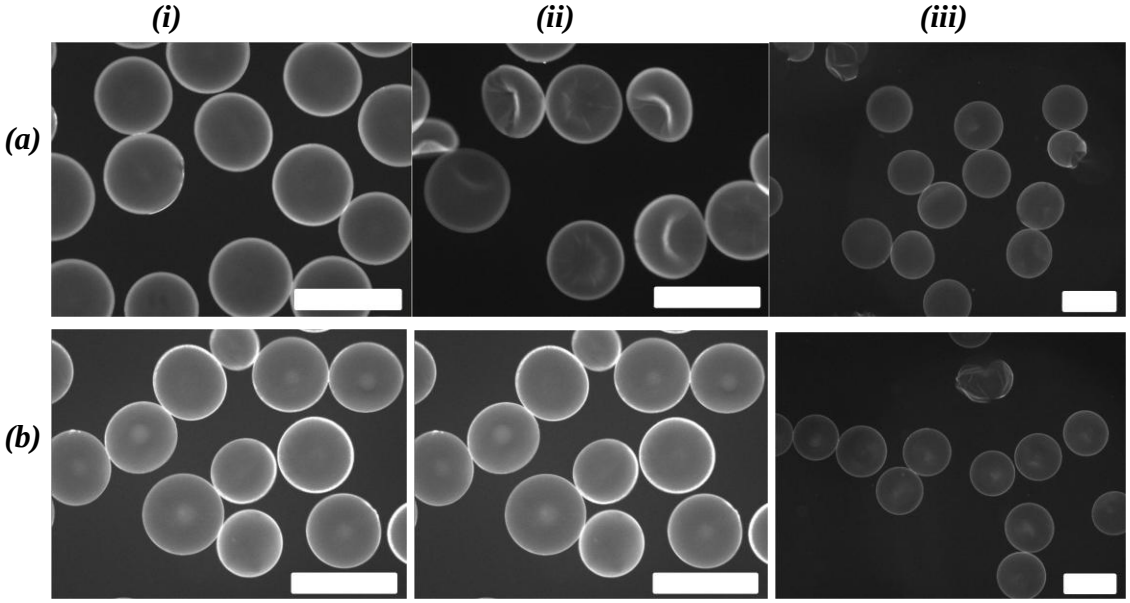

Figure 6A.2 *Covalent crosslinking test* ***(a)*** *AP-PMM_{50}- and* ***(b)*** *AP-PMV_{50}- pre-functionalized with amino-PEG*f*.* ***(i)*** *shows original capsules viewed under the optical microscope,* ***(ii)*** *shows capsules after 1 M sodium citrate* ***(iii)*** *shows capsules after 0.1 M NaOH addition. Scale bar is 500 µm.*

Next, AP capsules were concurrently coated with TRP and amino-PEG*f* for normal coating times (6-10 min). Figure 6A.3b shows that while fluorescently labeled amino-PEG*f* was able to bind to the surface of AP-PMM_{50} capsules; it did not for AP-PMV_{50} capsules. It is speculated that the ring opening azlactone reaction with primary amines is much slower than the anhydride's reaction with the primary amines. This speculation consistent with the fact that PMV_{50} hydrolyzes slower in water compared to PMM_{50}. Based on this hypothesis, it is not that PMV_{50} has no remaining reactive groups; it is that the reaction with primary amines is too slow to occur in the 10 minute coating time without the help of the polyelectrolyte effect which aids in PMV_{50}'s binding to surface PLL.

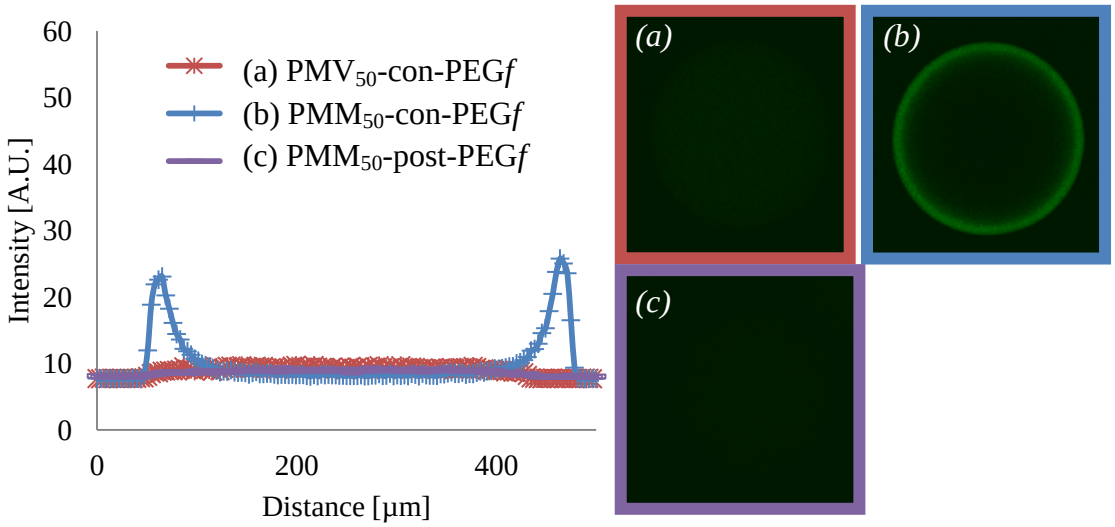

Figure 6A.3 *Graph shows a confocal profile of* ***(a)*** *AP-PMV$_{50}$- and* ***(b)*** *AP-PMM$_{50}$-concurrently-functionalized with amino-PEGf, and* ***(c)*** *AP-PMM$_{50}$-post-functionalize with amino-PEGf. Images show the confocal microscopy images of corresponding TRP.*

Post-functionalization was then attempted for AP-PMM$_{50}$ and AP-PMV$_{50}$ capsules. As seen in Figure 6.3c, post-functionalization was not possible for AP-PMM$_{50}$ capsules, which was expected as all reactive groups are gone after about 30 min under physiological conditions (post-functionalization requires PMM$_{50}$ to first be coated onto AP capsules for 6 minutes, ideally washed for about 5 minutes and then coated with amino-PEG*f*).

Currently, AP-PMV$_{50}$ capsules have not been able to be post-functionalized either. When AP-PMV$_{50}$ capsules were coated with 0.2% amino-PEG*f* at room temperature for 10 minutes, no visible fluorescence could be seen. When amino-PEG*f* coating solution was allowed to coat for 24 hr at 40^{o}C a small amount of fluorescence could be seen on the surface of capsules, however at this point it is unclear if this attachment is due to a radical reaction with the heated PEG or covalent attachment with the primary amine. Much more work in this area has to be done to see if conditions can be optimized to a point in which fluorescently labeled primary amines can bind to the surface of AP-PMV$_{50}$ capsules.

Several factors can be examined in the future:

(1) Increasing the amount of surface bound PMV$_{50}$ on AP capsules by increasing the coating solution concentration and/or increasing the coating time of PMV$_{50}$, also exploring the use of higher ionic strength in coating solution.[1] It has been observed that more PMV$_{50}$*f* binds to the surface of the capsules when coated for 10 min as opposed to 6 min. Preliminary ionic strength studies show that higher ionic strength does not increase the amount of PMV$_{50}$ bound, however addition of $CaCl_2$ in the PMV$_{50}$ coating solution increases the amount of bound PMV$_{50}$. The mechanism for this is still not clear.

(2) Increasing the concentration and/or coating time of fluorescently labeled primary amine. This has to be done within reason to prevent damage to encapsulated cells.

(3) Using a different fluorescently labeled primary amine such as dansyl cadaverine which has been used for post-functionalization of PVMDA in $DMSO^2$ or green fluorescent protein (GFP).

6.4.1 References

[1] J.K. Rasmussen; R.M. Gleason; D.S. Milbrath; R.L. *Ind. Eng. Chem. Res.* **2005**, *44*, 8554-8559.
[2] M.E. Buck; D.M. Buck. *Langmuir* **2010**, *19*, 16134-16140.